Impact Assessment on Watershed Hydrology and Soil Erosion under Land Use Land Cover and Climate Change Scenarios in Rib and Gumara Watersheds, Ethiopia

Thesis submitted in partial fulfillment of the requirements

for the award of the degree of

DOCTOR OF PHILOSOPHY

in

Civil Engineering

by

Lewoye Tsegaye

(Roll No. 166104045)

Under the Supervision of

Dr. Rishikesh Bharti

DEPARTMENT OF CIVIL ENGINEERING
INDIAN INSTITUTE OF TECHNOLOGY GUWAHATI
GUWAHAT-781039, INDIA
MAY, 2021

Statement of the author

The work contained in this thesis entitled "Impact Assessment on Watershed Hydrology and Soil Erosion under Land Use Land Cover and Climate Change Scenarios in Rib and Gumara Watersheds, Ethiopia" has been carried out by me under the supervision of Dr. Rishikesh Bharti, Department of Civil Engineering, Indian Institute of Technology Guwahati. I affirm that this thesis is my bonafide work and all sources of materials used for it have been duly acknowledged. I declare that this thesis is not submitted to any other university or institute for the award of any academic degree.

Date

20-10-2020

Lewoye Tsegaye Ayalew

DEPARTMENT OF CIVIL ENGINEERING
INDIAN INSTITUTE OF TECHNOLOGY GUWAHATI
GUWAHAT-781039, INDIA

Dr. Rishikesh Bharti
+91-361-258-3340
rbharti@iitg.ac.in

Certificate

This is to certify that the thesis entitled "Impact Assessment on Watershed Hydrology and Soil Erosion Under Land Use Land Cover and Climate Change Scenarios in Rib and Gumara Watersheds, Ethiopia" submitted by Lewoye Tsegaye, in partial fulfillment of the requirements for the award of the degree of Doctor of Philosophy, to the Indian Institute of Technology Guwahati, Assam, India, is a record of the bonafide research work carried out by him under my guidance and supervision at the department of civil engineering, Indian Institute of Technology Guwahati, Assam, India. To the best of my knowledge, this thesis is not submitted to any other university or institute for the award of any academic degree.

Date: May 5, 2021
Place: IIT Guwahati

Rishikesh Bharti
05-05-2021

Dr. Rishikesh Bharti

Dedication

I dedicate my thesis to my wife, Alemfrie Derese. I also dedicate the thesis to my families and friends for their support and encouragement.

Acknowledgment

I would like to give my deep sense of gratitude and sincere thanks to my enthusiastic supervisor Dr. Rishikesh Bharti, for his consistent support, and sincere, faithful and immense advice and guidance for the completion of the work. This thesis would not have been completed like this without his aforementioned contributions. Thank you very much, Sir. I express my deep feelings and gratitude to the Doctoral Committee Members; Prof. Bimlesh Kumar (Chairman), Dr. Archana M Nair, and Dr. Amit Kumar for their constrictive comments, valuable suggestions, and kind support throughout the period of the research work.

I would also like to express my gratitude to the Ministry of Education of Ethiopian (MoE) and Bahir Dar University for awarding me a scholarship to pursue my Ph.D. I am thankful to the Ethiopian Meteorological Agency (EMA) and the Ministry of Water Resource of Ethiopia for providing the necessary meteorological and hydrological data during the research work. I am greatly appreciating Alemayehu Abate and shiferaw Eromo for sharing their SWAT model expertise during the study.

Most importantly, I would like to forward loving thanks to my family especially my wife Alemfrie Derese. Frye, this is my special gratitude and respect for your energetic support and encouragement from the inception to the completion of the Ph.D. program. You took every job and responsibility and suffered all the bitterness while I was through the tight Ph.D. program. The success belongs to both of us Frye.

I am thankful to the Indian Institute of Technology Guwahati for providing the opportunity to carry out my research work.

Lastly, I want to thank My God for his blessings and his gift of endurance to overcome the challenges through the Ph.D study.

Abstract

Currently, watersheds are the focus of environmental conservation for sustainable development. Watershed-scale hydrology and soil erosion are the main environmental components that are greatly affected by climate and environmental perturbations. The aim of this study is to assess the impacts of Land Use and Land Cover (LULC) and climate changes on hydrology and sediment at the watershed-scale and to understand the relationships between hydrologic components and sediment yield with climate and land-use scenarios. An approach of modelling was used to examine the impacts of LULC and climate change scenarios on hydrology and sediment. The empirical LULC change model, Dynamic Conversion of Land Use and its Effects (Dyna-CLUE), and a hydrologic model, Soil and Water Assessment Tool (SWAT) were employed to assess the impacts of LULC and climate changes on soil erosion and sedimentation in Rib and Gumara watersheds, North-western Highlands of Ethiopia. The Dyna-CLUE model was calibrated with 1984 LULC map and validated with the simulated and reality LULC maps of 2016 to predict the LULC until 2049. The regional climate model (RCM) REMO and RACMO22T model outputs were analysed to assess climate changes. The REMO is from the driving model of ECHAM5 based on the IPCC SRES-AR4 A1B emission scenario. The RACMO22T model is from the driving model of the Hadley Global Environment Model 2-Earth System (HadGEM2-ES) in CORDEX-Africa under emission scenarios of RCP2.6, RCP4.5, and RCP8.5. These climate models were bias-corrected and the future climate of 2025-2099 with three-time slices (2030s, 2060s, and 2090s) was predicted. After flow and sediment calibration and validation, sub-watershed level sediment yield host spots were identified and four sediment management scenarios were simulated and compared with the baseline scenario. It is found that implementing filter strip and stone/soil bund management scenarios have a significant impact on reducing erosion and sediment yield. Analysis of the LULC change indicated that there has been a high increase in cultivated land at the expense of mixed forest and shrublands and a low and gradual increase in plantation and urban lands between 1984 and 2049.

The climate change prediction result indicated that generally, there will be a decrease in precipitation in all SRES A1B, RCP 2.6, 4.5, and 8.5 scenarios except in the Bega (dry) season and an increase in minimum and maximum temperatures in all of the scenarios. The increase in temperature will be highest in the Belg season (intermediate season). The analysis of LULC and climate change prediction indicated that there will be an increase in runoff and

a decrease in groundwater flow in Rib watershed. On the other hand, in Gumara watershed the general trend shows that there will be a decrease in runoff and groundwater flow. The consistent increase in temperature in the climate scenarios will have an increasing impact on the projected ET in both watersheds. The increase in cultivated land and a decrease in forest and shrubland give rise to an increase of sediment in most scenario periods.

This study also examines the soil loss and sediment yield of Anjeb watershed, in the North-western Highlands of Ethiopia, employing RUSLE integrated with GIS and Remote sensing techniques. The average annual soil loss was 17.3 t ha^{-1} yr^{-1}. From a total of 20125.5 tons of soil, 2254.5 tons of sediment was delivered to the stream channels annually in the watershed.

Because of the continual increase in the population, there has been a frequent LULC change mainly the expansion of croplands. The climate prediction shows that the climate of the area is changing due to the impact of the global increase of atmospheric greenhouse gasses and the changing LULCs. All these phenomena give rise to the increase of soil erosion and changes in surface and groundwater flow in the study watersheds. High erosion and land degradation has been reducing crop yield which is the main source of livelihood of the area. Therefore, short and long-term watershed-scale resource management activities have to be designed and implemented to curb soil erosion facing at present and in the long-run. Soil and water conservation works effective and adaptable to the slopes have to be planned and implemented to minimize erosion through reducing surface flow, sheet erosion, and slope lengths which increase infiltration and groundwater recharge. Among the various conservation measures filter strips and stone/soil bunds with appropriate spacing could be implemented since they significantly reduce soil erosion. In the long-run vegetation covers mainly forestation programs have to be implemented along steeper slopes where crop cultivation is prohibited because they have a function to reduce erosion and moderating the local climate.

Contents

List of tables

List of figures

List of abbreviations and acronyms

A1, A1B, A2, B1, B2 A1FI and A1T	IPCC SRES emission scenarios
AGNPS	Agricultural Nonpoint Source Pollution Model
ALPHA_BF	Base flow alpha factor
amsl	above mean sea level
EUROSEM	European Soil Erosion Model
AQ	Aquifer Recharge
AR4,5	4^{th} and 5^{th} IPCC Assessment Report
ArcGIS	Suit consisting of Geographical Information System software
ArcSWAT	ArcGIS Integrated SWAT Hydrological Model
ASCII	American Standard Code for Information Interchange
BMP	Best Management Practice
BoEPLAU	Bureau of Environmental Planning & Land Administration Authority
CANMX	Maximum Canopy Storage
C-factor	Land cover factor
CH_COV2	Channel cover factor
CH_ERODMO	Channel erodebility factor
CH_K2	Main channel effective hydraulic conductivity
CLUE-S	Conversion of land use and its Effects-S
CN2	SCS runoff curve number for moisture condition II
CO_2	Carbon dioxide
CMIP5	Coupled model inter-comparison project phase fifth
CORDEX-Africa	Coordinated Regional Climate Downscaling Experiment–Africa
CREAMS	Chemicals, Runoff, Erosion from Agricultural Management System
CSA	Central Statistics Agency
DEM	Digital Elevation Model
Dyna- CLUE	Dynamic conversion of land use and its effects
ECHAM	European Centre Hamburg Model
ECHAM5	European Centre Hamburg Model Fifth Generation
EI30	Storm kinematic energy and maximum rainfall intensity in 30 min

ENMA	Ethiopian National Mapping Agency
EPCO	Plant evaporation compensation factor
ESCO	Soil evaporation compensation factor
ET	Evapotranspiration
ETM	Enhanced Thematic Mapper
FILTERW	Width of filter strip
FAO	Food and Agriculture Organization
Fore-SCE	FOREcasting SCEnarios of Land-use Change modeling framework
GCM	General Circulation Model
GCP	Ground Control Point
GERICS	Climate Service Center Germany
GHG	Greenhouse gas
GIS	Geographic Information System
GLUE	Generalized Likelihood Uncertainty Estimation
GPS	Global Positioning System
GW_DELAY	Groundwater delay
GW_REVAP	Groundwater “revap” coefficient
GWQMN	Threshold depth of water in the shallow aquifer for return flow
HadCM3	Hadley Centre Climate Model
HadGEM2-ES	Hadley Global Environment Model version 2-Earth System
HEC_Geo HMS	Geospatial Hydrologic Modeling Extension
HRU_SLP	Average slope steepness
HRU	Hydrologic Response Unit
HSPF	Hydrologic Simulation Program Fortran
IPCC	Intergovernmental Panel on Climate Change
SPSS	Statistical Package for Social Sciences
IDW	Inverse Distance Weighting
IPCC-TGCIA	Intergovernmental Panel for Climate Change Task Group on Data and Scenario Support for Impact and Climate Analysis
IWMI	International Water Management Institute
K-factor	Soil erodibility factor

KHisto	Kappa history
‘KLoc	Kappa location
LULC	Land Use and Land Cover
LANDSAT 5, 7, & 8	LANDSAT fifth, seventh and eighth mission
LH-OAT	Latin Hypercube One-factor-At-a-Time
LS-factor	Slope steepness factor
M^3/s	Cubic meter per second
MCK	Map Comparison Kit
MCMC	Mark chain Monte Carlo
Mg/l	milligram per litter
MoWR	Ministry of Water Resource
NSE	NashSutclif Efficiency
NRCS	Natural Resource Conservation Service
OLI	Operational Land Imager
OV_N	Manning's "n" value for overland flow
P/km^2	persons per square kilometer
PBIAS	Percent Bias
ParaSol	Parameter Solution
P-factor	Land management practices factor
ppm	parts per million
PSO	Particle Swarm Optimization
R^2	Coefficient of determination
RACMO22T	a regional climate model
RCHRG_DP	Deep aquifer percolation fraction
RCM	Regional Climate Model
RCP	Representative Concentration pathways
RCP 2.6, 4.5 and 8.5	Representative Concentration Pathway of Radiative Forcing Levels 2.6, 4.5 and 8.5 W/m^2 by the year 2100
REMO	REgional MOdel
REVAPMN	Threshold depth of water in shallow aquifer for ‘revap’
R-factor	Rainfall erosivity factor

RMSE	Root Mean Square Error
ROC	Receiver Operating Characteristics
RSR	Ratio of root mean square error & Standard deviation of Observation
RUSLE	Revised Universal Soil Loss Equation
SCS	Soil Conservation Service
SDR	Sediment Delivery Ratio
SLEUTH	Slope, Land use, Exclusion, Urban, Transportation, and Hill-shade
SLSUBBSN	Slope steepness
SOL_AWC	Available water capacity of the soil layer
SOL_BD	Soil bulk density
SOL_K	Saturated hydraulic conductivity
SPCON	Linear re-entrained factor parameter for channel sediment routing
SPEXP	Exponent of re- entrainment parameter for channel sediment routing
SRC	Sediment Rating Curve
SRES	Special report on Emission Scenario
SRTM- DEM	Shuttle Radar Topographic Mission Digital Elevation Model
SUFI-2	Sequential Uncertainty Fitting version 2
SURLAG	Surface runoff lags time
SWAT	Soil and Water Assessment Tool
SWATCUP	SWAT Calibration and Uncertainty Program
SY	Sediment yield
TM	Thematic mapper
UNESCO	United Nations Educational, Scientific and Cultural Organization
USDA-ARS	US Department of Agriculture, Agriculture Research Service
USLE_C	Minimum value of USLE C factor applicable to the land cover
USLE_P	USLE support practice parameter
W/m^2	watt per square meter
WCRP	World Climate Research Programme
WGS84UTM	World Geodetic System 84 Universal Transverse Mercator
WYLD	total water yield

Chapter 1 : Introduction

1.1 General

Soil erosion is a natural geomorphic process that can be accelerated under improper land use and management practices. Apart from reducing the water storage capacity, sediment delivered into water bodies may also be a source of contamination, which adversely impacts the aquatic biota (Hurni, 1989). Sediment delivery to river channels is probably the most problematic off-site consequence of soil erosion. The input of sediment by erosion processes into rivers, reservoirs, and ponds results in high sediment deposition rates and frequent dredging.

The soil depth of more than 34 % of the land area is already less than 35 cm in Ethiopia. The country loses about 1.3 billion metric tons of fertile soil every year and the degradation of land through soil erosion is increasing at a high rate (Hurni, 1989; Tsighe, 1995). A review of soil erosion and conservation in Ethiopia by Haregeweyn et al. (2015) reported that soil loss rates caused by sheet and rill erosion at plot and catchment scales indicate that soil degradation process varies strongly spatially, with a mean soil loss of 29.9 t ha^{-1} yr^{-1}. According to this report, the highest rates were observed in Anjeni (110 t ha^{-1} yr^{-1}) and Chemoga (102 t ha^{-1} yr^{-1}) of the Upper Blue Nile Basin. Though the highlands of the country are among the highest agricultural potentials in Africa, they contain one of the largest areas of ecological degradation in Africa and in the world. A study made in the highlands revealed that 50% of the highlands are significantly eroded, 25% seriously eroded while 4% had reached a point of no economic return (FAO, 1984).

Studies indicated that the causes of high soil erosion in Ethiopia especially in the Northwestern highland parts of the country are the LULC changes (reduction of vegetation and expansion of agricultural lands), climate change (torrential rains) and rugged terrain among others. Climate change alters the frequency and intensity of precipitation which affects soil detachment and erosion processes. The effect of climate change on the rate and extent of soil erosion processes has been predicted by several researchers (Mullan et al., 2012; Nearing et al., 2005; Nunes et al., 2013; Zhang, 2007; Zhang and Nearing, 2005; Ayele et al., 2017, Nadew et al., 2018). The LULC changes and land degradation are strongly related (Gete and Hurni, 2001). A number of studies conducted at different spatial and

temporal scales revealed that LULC change has a significant impact on soil erosion and sediment transport rates (Van Rompaey et al., 2005; Jordan et al., 2005; Nearing et al., 2005; Cebecauer and Hofierka, 2008; Yang et al., 2003; Ito, 2007; Siyuan et al., 2007). It is crucial to understand the potential impacts of climate and LULC changes on runoff and erosion in basins for the long term water resource planning and management activities. In particular, effective water resource and sediment management require reliable information about flows under different scenarios of changing conditions of land use and climate (Mango et al., 2011). Studies on the separate impacts of climate and LULC changes on the hydrology and sediments of watersheds has great importance for the planning of land use and water resource (Wang et al., 2012). The hydrology of a basin is influenced by a complex of processes that complicate the separation of the impacts of LULC and climate change on stream flows (Tang, 2011), and still a challenge to differentiate their separate impacts (Lioubimtseva, 2005).

Still there is a very limited understanding of the separate as well as combined impacts of LULC and climate changes on regional water and energy cycles, and therefore more in-depth research is needed, especially in the arid and semiarid regions (Mango et al., 2011). Research outputs and data generated about runoff, sediment transport and accumulation using current data on LULC, climate, soil, hydrology, topography, and properly projected land use and climate data at the watershed-level is essential to design watershed-level resource management systems and development plans.

1.2 Statement of the Problem

Lake Tana, the source of The Blue Nile River and the UNESCO Biosphere Reserve, is affected by land degradation, soil erosion, and sediment deposition due to the impacts of frequent land use and land cover change, climate change, deforestation, and overgrazing. The basin is affected by the hydrological processes and sediment transported from the watersheds of Rib and Gumara which are experiencing frequent LULC changes, overpopulation combined with low land management methods. In addition, the topography of these catchments is rugged that accelerates the rate of soil erosion and transportation of sediments to their mouth, Lake Tana. The lake ecosystem is largely affected by agro-chemical sediments from the surrounding highlands transported using these major rivers. Climate and LULC changes are amongst the greatest global environmental pressures resulting from anthropogenic activities, both of which greatly impact the hydrological cycle (Mango et al., 2011). The hydrological response of watersheds to climate and LULC changes and the

potential impacts of LULC change on the hydrological cycle must be considered by water resource managers (Mango et al., 2011; Steegen et al., 2001).

Lack of decision support tools and limitation of research outputs concerning the changing LULC, climate and alternative land management practices are factors that significantly hinder development options in the study area. The lack of watershed-scale researches on hydrology, erosion, and sediment yield using physically-based models and varieties of data including the changing LULC and climate have a determining impact on the proper resource management and the productivity of the area (Dile et al., 2013). Therefore, the hydrology and sediment processes of the watersheds needed to be studied by considering the necessary data of climate and LULC changes for the better management of the soil and water resources of the study watersheds.

1.3 Significance of the Research

Land degradation has become more evident in the Ethiopian highlands (Hurni, 1989) with increasing changes in land use, and this is clearly observed within the area of the present study, Rib and Gumara watersheds. It is necessary to spatially assess the current and future hydrology and erosion responses at the sub-watershed levels to assist in identifying and prioritizing areas that require appropriate and immediate conservation measures (Dile et al., 2013). To improve water resource development, land productivity, and achieve sustainable land use in Rib and Gumara watersheds, an integrated catchment management approach is significant. Research outputs and data generated about the current and future hydrology and sediment conditions is essential to design short and long-term watershed level resource management systems to enhances productivity and improve the livelihood of the population. Agricultural sediments of the watersheds cause siltation and expansion of water hyacinth in the Lake Tana which degrades its size and the productivity of fish. Therefore, the result of the study is crucial input for the management of the Lake Tana ecosystem. The study is vital for the local farmers to implement proper soil and water conservation practice to enhance land productivity. The study is also important for district, regional and national level resource managers and decision-makers for example Amhara National Regional State Bureau of Agriculture and Natural Resource Management, South Gondar Zone Bureau of Agriculture and Natural Resource Management, and the Abbay Basin Authority to plan and practice long term watershed and sub-watershed level eco-friendly and efficient conservation measures so as to improve crop productivity in the watersheds and reduce the risk of sedimentation and

spreed of water hyacinth in the Lake Tana. The study could be an input for the conservation plan of Anjeb watershed.

1.4 Aim of the Study

It is important to account for LULC change along with climate change when predicting long term patterns in hydrological response and soil erosion processes at a watershed-scale.

Potential impacts of future climate and land-use change can be quantified for a specific watershed by using an integrated hydrological model with a downscaled climate derived from Global Climate Models (GCM) and land-use projections. The main aim of this research is to assess the long term patterns of hydrological response and soil erosion in the Rib and Gumara watersheds under LULC and climate change scenarios. The impact of LULC and climate change projected scenarios on hydrology, erosion, and sediment yield in the watersheds will be examined. The study will also estimate soil erosion and sediment yield of Anjeb ungauged watershed using the RUSLE model and remote sensing data integrated with the GIS interface.

1.4.1 Specific objectives

- To predict the land use and land cover (LULC) change scenario of Rib and Gumara watersheds
- To examine the climate changes of Rib and Gumara watersheds under the SRES and RCP scenarios
- To estimate soil loss and sediment yield of Anjeb watershed
- To investigate the impacts of LULC and climate change scenarios on the hydrology and sediment yield in Rib and Gumara watersheds.

1.5 Organization of the Thesis

The thesis is organized into nine chapters. The contents of each chapter are presented as follows:

Chapter 1 is the general introduction of the thesis which includes the statement of the problem, significance of the study, and research objectives (main and specific objectives).

Chapter 2 is the literature review which discusses about the LULC prediction and modelling, climate change prediction and the GCM/RCM models, the representative concentration pathways (RCP) of the Fifth Assessment Report (AR5), hydrology and erosion modeling, agricultural management practices and soil erosion, and impacts of LULC and climate changes on watershed hydrology and sediment.

Chapter 3 deals about LULC modelling of Rib and Gumara watersheds which include description of the study area, data (including the LULC classification accuracy assessment), and the Dyna-CLUE model used to predict the LULC scenario of the watersheds. Detail description has presented about the driving factors of LULC change, the LULC demand, the conversion elasticity of the LULCs, land-use type specific conversion settings or sequences and the model validation (the ROC values with the Logit model and comparison of the simulated and reality maps).

Chapter 4 is about predicting future climate change of Rib and Gumara watersheds. It discusses about the special report on emission scenarios (SRES) of A1B and RCP (2.6, 4.5 and 8.5) scenarios used for the climate change study. It focused on the RACMO22T RCM model from the driving model of Hadley Global Environment Model 2-Earth System (HadGEM2-ES) in CORDEX-Africa for the Representative Concentration Pathways and the REMO RCM from the driving model of ECHAM5 from the Max-Planck-Institute for Meteorology for the SRES A1B scenario. The chapter also discusses about the delta change method for correcting the bias on GCM/RCM rainfall and temperature data.

Chapter 5 explains about the ArcSWAT hydrologic model and spatial and weather input data sets. The identified sensitive parameters of flow and sediment for the SWAT model calibration and validation were presented in this chapter. The statistical model performance evaluation criteria (coefficient of determination (R^2), Nash and Sutcliffe simulation efficiency (NSE), RMSE-observations standard deviation ratio (RSR) and Percept bias (Pbias) used for the SWAT performance evaluation were discussed. Hydrograph and scatter graph analysis made for the visual comparison between simulated and measured data to identify differences in time and magnitude of low and peak discharge of flow and sediment in calibration and validation periods were presented in this chapter.

Chapter 6 is about the agricultural management practices simulated in agricultural HRUs, all slopes and soil types to reduce the sediment yield in both watersheds. The amount of sediment yield under the current condition of the watersheds is presented for comparison purposes. The agricultural management scenarios (grass filter strips with strip width of 1 meter (scenario 1) and 5 meter (scenario 2) and soil bunds with the determining parameters of CN2, USLE_C and SLSUBBSN having two scenarios (scenario3 and scenario 4) were discussed together with the resulting sediment yield per sub-watershed scales in both watersheds.

Chapter 7 deals about soil loss and sediment yield estimation of the Anjeb watershed. The location of study area, the RUSLE input parameters, sediment delivery ratio and sediment yield were discussed. The spatial soil loss, the SDR of channels and the sediment yield of the watershed were analysed and presented in the chapter.

Chapter 8 discusses about the impacts of LULC and climate change scenarios in Rib and Gumara watersheds. The current status and projected changes in the hydrologic components and sediment yield in both watersheds were analysed and presented. The major hydrological processes of surface runoff, groundwater flow, lateral flow, actual evapotranspiration (ET), total water yield (WYLD) and sediment yield have been analysed using a calibrated ArcSWAT model for the present condition and future periods under the CMIP5 RCM model with SRES A1B and RCP (2.6, 4.5 and 8.5) scenarios with time slices of 2030s, 2060s and 2090s. The major hydrologic components were analysed with two sets of scenarios (the current LULC and predicted climate and predicted LULC and climate) and compared with the watersheds existing condition in order to differentiate the separate as well as the combined impacts of LULC and climate changes in annual and monthly basis.

In **chapter 9** conclusions and recommendation of the study is presented. Recommendations for future works were given based on the results obtained in the study. Supporting data of tables, figures, and photos taken from the study areas were presented in the section of the appendices.

2.1 Motivation of the research

The study watersheds share a significant portion of the Lake Tana Basin, part of the Upper Blue Nile Basin, which covers the lion's share of the Nile waters. The Blue Nile River is from the Lake Tana sub-basin, Lake Tana, and contributes around 48 billion m^3 or 86% of water per year (Abtew and Melesse, 2014) to the Nile River which has been supporting around 250 million populations. The landform of Highland Ethiopia is mountainous and rugged (1500–4620m a.s.l) which has been exposed to millennia of erosion due to its topography and longtime agricultural activities (Haregeweyn, 2015). The Rib and Gumara watersheds are part of the Lake Tana Basin with diverse topography and exposed to soil erosion and land degradation due to excessive crop cultivation to steepest slopes and limited land management practices. There has been extensive soil degradation in the upstream of the watersheds and frequent flooding in downstream areas due to frequent LULC and climate changes and limited land management practices (Dile et al., 2013). Because of this, the watersheds discharge a significant amount of sediment to Lake Tana that has been threatening the reservoir which is the source of livelihood for a large number of people. Reports have shown that land productivity has been declining due to erosion which threatening the food security of the local farmers. On the other hand, the downstream of the watersheds have been frequently affected by flooding mainly due to the blockage of river channels by sediment from the upstream. Lake Tana which is among the largest lakes in Africa is facing a reduction of fish stock due to agricultural sediments (chemicals) from these watersheds (Bires and Raj, 2019). These chemicals currently create a suitable environment for the spread of water hyacinth which degrades the productivity of fish and reducing the size of the lake. This has been threatening the people whose livelihood is depending on fishing and also affecting the larger population who depend on fish products in the region. In this study topographic, LULC, climate, hydrology, and sediment data sets has been organized and processed to investigate the current and future states of hydrologic components and sediment of the watersheds so as to provide land management and policy inputs for land managers and decision-makers. The study helps to identify critical sub-watersheds affected by erosion and examines alternative soil conservation practices to mitigate erosion and increase the land productivity of farmers. The sediments upstream of the watersheds clog the river channels so that downstream areas were frequently affected by flooding. The land management

practices that will be suggested in this study helps to reduce the soil erosion from the upstream and sediment deposition downstream including the reservoir, Lake Tana, which helps to improve the livelihood of the catchments and the surrounding population. The study is also significant for the local and regional land managers to implement selected soil and water conservation measures so as to mitigate erosion and is also a stepping stone for further studies related to watershed hydrology and soil erosion.

2.2 Land Use and Land Cover Modeling and Prediction

Land-use change is an important issue for the environmentalists and hydrologists, since it is one of the main causes of environmental problems, such as global temperature change, biodiversity loss, and soil erosion among others (Agarwal et al., 2002; Murray-Rust et al., 2014). Land-use planning is therefore an important issue for sustainable exploitation and management of natural resources. The purpose of land use modelling is to provide effective decision support tools for environmental, economic, and social development policies (Verburg et al., 2002).

Land-use and land cover patterns over a period of time are determined by demographic, economic, and environmental driving factors (Castella and Verburg, 2007) both at a national and global scale. Land-use and cover changes are widespread and accelerated environmental processes (Rawat and Kumar, 2015) and is among the most sensitive environmental issues of global concern (Guan et al., 2011; Veldkamp and Lambin, 2001) which is considered as the main driver of global change with its interactions to climate, ecosystem, biogeochemical cycles, biodiversity, and human activities.

Analyzing the past and modelling the future LULC provides knowledge about the locations where the LULC change occurs, and to estimate the rates of changes (Lambin, 1997). Modelling of LULCs at a local and regional scale has been conducted in different parts of the world (Ruelland et al., 2010; Teferi et al., 2013; Li et al., 2014; Lima et al., 2015). Models of land-use change basically demonstrate the relationship between the land-use change and the land-use drivers. Examples of LULC models developed include the SLEUTH model (Dietzel et al., 2007), CLUE-S (Verburg et al., 2002), Fore-SCE (Sohl et al., 2007), Dyna- CLUE 2.0 (Verburg and Overmars, 2009).

Dyna-CLUE model is an empirical and dynamic spatial land-use prediction model which can

integrate current and historical land-uses, socio-economic conditions and biophysical land use drivers at various spatial scales. The model has two separate modules which are the spatially explicit land-use allocation module and the demand (non-spatial) module. Each land-use demand for each simulated year is determined using the non-spatial module. The spatial module allocates at the pre-determined land use demands of each land-use at suitable locations using an iteration procedure. Dyna-CLUE model is a combination of spatial, empirical and dynamic modelling characteristics (Verburg and Overmars, 2009). Dyna-CLUE is spatially explicit and grid-based land-use change model (Verburg et al. 2002). The empirical analysis in the model helps determine the relation between the immediate driving factors that govern the spatial distribution of land use and the specific land uses. A competition between land uses for a particular location is simulated considering the competitive advantage of each land use.

2.3 Climate Change Prediction and General Circulation Models (GCM)

Climate simulations from GCM could be an input for hydrological models, which used to evaluate the hydrological and water resource effects of climate changes. GCMs representing physical processes in the atmosphere, ocean, and land surface are the only credible tools currently available for simulating the response of the global climate system to the increasing greenhouse gas concentrations (Carter et al., 1999). GCMs suggest that rising concentrations of greenhouse gases will have significant implications for climate at global and regional scales. GCMs are limited in their usefulness for local impact studies because of their coarse spatial resolution and inability to differentiate important sub-grid scale features such as clouds and topography (Wilby and Dawson, 2007). Many of the processes which control local climate, e.g., topography, vegetation, and hydrology, are not included in coarse resolution GCMs. The development of statistical relationships between the local scales and large scales may include some of these processes implicitly. Thus, it is important to downscale the large scale GCMs to regional and local scale levels (Wilby and Dawson, 2007). Downscaling is the general name for a procedure to take information known at large scales to make predictions at local scales. The two main approaches to downscaling climate information are dynamical and statistical methods (Wilby and Dawson, 2007).

In dynamical downscaling a high resolution RCM is forced to use GCM output (Murphy, 1999) rather than using mathematical equations. The RCM, a high resolution climate model, is driven by the boundary conditions of GCMs to produce finer spatial scale climatic ariables (Schmidli et al., 2007). The greater advantage of the RCMs is providing small-scale

atmospheric features than their host GCMs and their drawback is demanding substantial computing resources and expensiveness (Abdo et al., 2009, Wilby and Dawson, 2007). The downscaled RCM/GCM outputs have been an important climate data sources for studying the regional climate changes because of global warming. Global warming is evident because of the emissions of greenhouse gases since the industrial revolution (Ramaswamy et al., 2001). Global warming is increasing because of the concentration of greenhouse gasses mainly carbon dioxide. The concentration of CO_2 in the atmospheric has increased to 368 ppm in 2000 compared to the 280 ppm in 1750 (IPCC, 2001). This figure has accelerated to 400 ppm in 2015 (WMO, 2016) and will expected to rise 445–640 ppm in 2050 and 540–970 ppm in 2100 (IPCC, 2001).

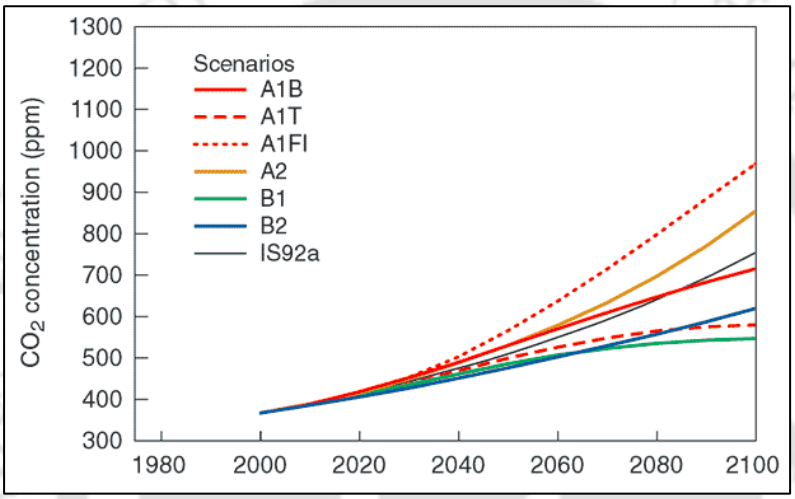

Figure 2-1 Projected changes in CO_2 concentration in the atmosphere (IPPC, 2001)

Scientific evidence indicates that increased greenhouse gas emissions will cause an increase in the average temperature of the earth up to 1.4–5.8^{o}C by the end of the 21st century (Ramaswamy et al., 2001). The world average temperatures show increasing (Unganai, 1996; New et al., 2006; IPCC, 2014; Loukas et al., 2015) which result for melting of glaciers, rising of sea levels and change in patterns of atmospheric circulation which affects precipitation, availability of water, and prevalence of droughts and floods.

In the prediction of the future climate change the IPCC has set climate scenarios by considering future trends in energy demand, emissions of greenhouse gases, land-use change as well as assumptions about the behavior of the climate system over long time scales (IPCC, 2007). According to the IPCC description, climate scenarios are plausible representations of the future that are consistent with assumptions about future emissions of greenhouse gas and other pollutants and the effect of increased atmospheric concentrations of these gases on the

global climate.

The IPCC (2007) summarized future emission of greenhouse gases on four emission scenarios called storylines which are labeled as A1, A2, B1, and B2. The A1 scenario family is categorized into three groups that describe alternative directions of technological change in the energy system: fossil intensive (A1FI), non-fossil energy (A1T) and a balance of all energy sources (A1B). These storylines describe the relationship between the forces driving aerosol and greenhouse gas emissions and their evolution in the 21st century. The scenarios of the SRES represent different social-economic, demographic, technological, and environmental developments. Climate projections in the different SRES scenarios showed the increase of average global temperature and rising of sea levels (Figure 2-2 & Table 2-1).

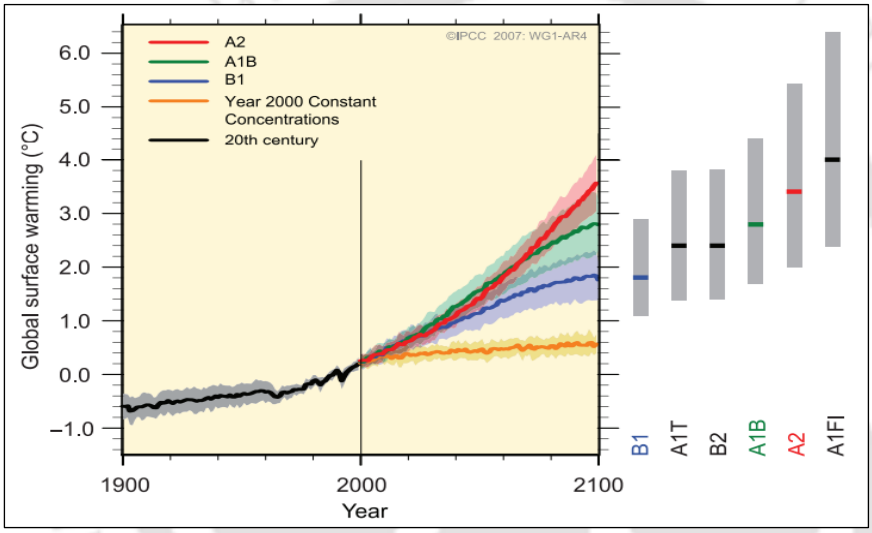

Figure 2-2 Multi-model of ranges for surface warming with SRES scenarios (IPCC, 2007)

Table 2-1 Projected global average surface warming and sea level rise at the end of the 21st century (IPCC, 2007).

Temperature Change (°C) (at 2090-2099 relative to 1980-1999)		Sea Level Rise (m) (at 2090-2099 relative to 1980-1999)	
Case	Best estimate	Likely range	Model-based range excluding future rapid dynamical changes in ice flow
Constant year 2000	0.6	0.3-0.9	Not available
B1 scenario	1.8	1.1-2.9	0.18-0.38
A1T scenario	2.4	1.4-3.8	0.20-0.45
B2 scenario	2.4	1.4-3.8	0.20-0.43
A1B scenario	2.8	1.7-4.4	0.21-0.48
A2 scenario	3.4	2.0-5.4	0.23-0.51
A1FI scenario	4.0	2.4-6.4	0.26-0.59

2.3.1 The representative concentration pathways of the fifth assessment report (AR5)

The AR5 introduces a new scenario, representative concentration pathways **(**RCPs) (IPCC, 2014). The RCPs aim to denote the atmospheric concentration of GHG emissions and they are consistent with a range of expected changes in emission of these gases because of anthropogenic of impacts. Its findings have based on a new set of scenarios that replace the Special Report on Emission Scenarios (SRES) standards. There are four pathways: RCP8.5 (long term change), RCP6.0 (mid-term change), RCP4.5 (mid-short term change), and RCP2.6 (short-term change). The numbers refer to radiative forcing for each RCPs (IPCC, 2014*)*. The RCPs describe a set of possible developments in emissions and land use, based on consistent scenarios representative of current literature (IPCC, 2014). In the RCP scenarios it is projected that the concentration of carbon dioxide (CO_2) will increase and peaks in the RCP8.5. According to the report of IPCC (2014), in the RCP 2.6 CO_2 emissions start declining by 2020 and close to zero by 2100. The CO_2 emissions start declining approximately by 2045 to reach roughly half of the levels of 2050 by 2100 in the RCP4.5, and in the RCP 8.5 scenario emission CO_2 continue to rise throughout the 21st century (Figure 2-3)

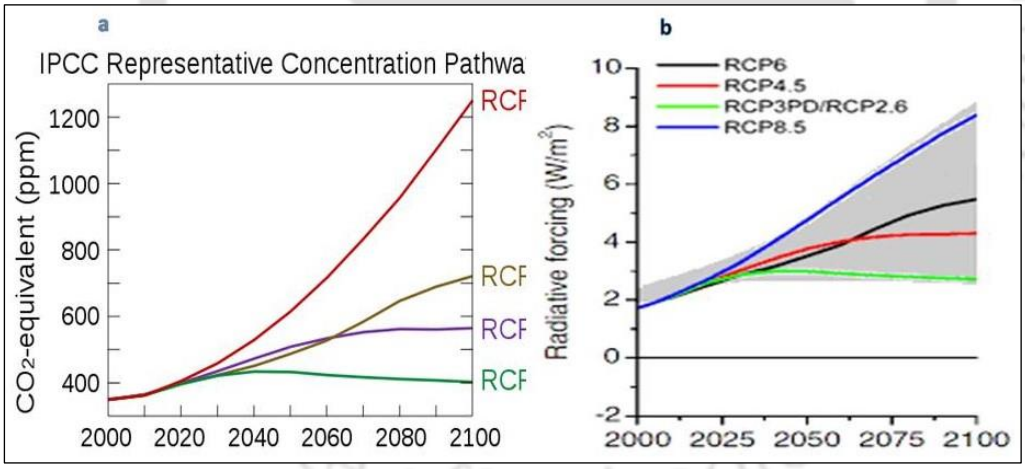

Figure 2-3 The CO_2 concentration (a) and radiative forcing (b) in the atmosphere with RCPs

As it is reported in IPCC (2014), increase in global average temperature, changes in patterns of local precipitation, and rising sea levels are the scientific evidence for the changing global climate. During 2046-2100, global mean temperature will increase between 0.4 to 1.7 in RCP2.6, 0.9 to 2.6 in RCP4.5, 0.8 to 3.1 in RCP6,0 and 1.4 to 4.8 in RCP8.5 (IPPC 2014) (Table 2-2). At the end of the 21st century in RCPs the average global temperature and sea level is projected to increase between 0.3 to 4.8 °C and 0.26 to 0.82 m respectively (IPCC, 2014) (Table 2-2).

Table 2-2 Global temperature increase (°C) and mean sea level increase (m) (IPCC, 2014)

	Global warming increase (°C)		Global mean sea level increase (m)	
	2046–2065	2081–2100	2046–2065	2081–2100
Scenario	Mean and likely range	Mean and likely range	Mean and likely range	Mean and likely range
RCP2.6	1.0 (0.4 to 1.6)	1.0 (0.3 to 1.7)	0.24 (0.17 to 0.32)	0.40 (0.26 to 0.55)
RCP4.5	1.4 (0.9 to 2.0)	1.8 (1.1 to 2.6)	0.26 (0.19 to 0.33)	0.47 (0.32 to 0.63)
RCP6.0	1.3 (0.8 to 1.8)	2.2 (1.4 to 3.1)	0.25 (0.18 to 0.32)	0.48 (0.33 to 0.63)
RCP8.5	2.0 (1.4 to 2.6)	3.7 (2.6 to 4.8)	0.30 (0.22 to 0.38)	0.63 (0.45 to 0.82)

2.4 Hydrology and Erosion Modeling

Simulation programs implemented at watershed hydrology are important tools for watershed management. There are several empirical and physically-based hydrology and erosion models. Empirical models are based on defining important factors through field observation, measurement, experiments, and statistical methods (Pilesjoe, 1992). They are useful in predicting the hydrology or soil erosion, but are site-specific and require long term data (Elirehema, 2001). Physically-based models are based on knowledge of the fundamental physical processes and incorporate the laws of conservation of mass and energy (Pilesjoe, 1992). They consider the spatial and temporal changes of different factors. Physically-based distributed watershed models play a major role in analyzing the impact of land management practices on water, sediment, and agro-chemical yields in large and complex watersheds. These hydrological and soil erosion models are designed to describe the hydrology, erosion, and sedimentation processes. They describe the physical processes controlling the transformation of precipitation to runoff, and detachment and transport of sediments. There are different hydrological models designed and applied to simulate the rainfall-runoff relationship under different temporal and spatial dimensions. The focus of these models is to establish a relationship between various hydrological components such as precipitation, evapotranspiration, surface runoff, groundwater flow, and infiltration (Pilesjoe, 1992). Models vary considerably in their objectives, time, and spatial scales involved. Many of the models share a common base in their attempt to incorporate the heterogeneity of the watershed and spatial distribution of topography, vegetation, land use, soil characteristics, rainfall and evaporation (Pilesjoe, 1992). Some of the watershed models developed in the last two decades were CREAMS (Chemicals, Runoff, and Erosion from Agricultural

Management Systems) (Knisel, 1980), EPIC (Erosion Productivity Impact Calculator) (Williams, 1995), AGNPS (Agricultural None Point Source model) (Young et al., 1989), SWAT (Soil and Water Assessment Tool) (Arnold et al., 1998), HSPF (Hydrologic Simulation Program Fortran) (Bicknell et al., 2001), European Soil Erosion Model (EUROSEM) (Morgan et al., 1998), etc.

2.5 Soil Erosion and Agricultural Management Practices

Soil erosion is a process aggravated by improper land management practices. Some of the outcomes of erosion and sediment accumulation are deterioration of soil quality and productivity, loss of water quality, and vulnerability to droughts. The accumulation of sediment into waterbodies especially in dam reservoirs causes high sediment accumulation and costs high capital to withdraw sediments. Mainly in areas of intensive agricultural land uses, agricultural chemicals are added into soil particles and transported to water bodies which result in contamination (Hurni, 1989; Steegen et al., 2001).

Limited studies in Ethiopia assert the presence of significant soil erosion variability in the country. Mean soil loss varies remarkably from 0 t ha^{-1} yr^{-1} to 100 t ha^{-1} yr^{-1} in the Southeast and Northwest part of the country respectively (Haregeweyn et al., 2015; Dile et al., 2013; Melaku et al., 2018; Setegn et al., 2010; Sonneveld et al., 2011). Analysis of sediment discharge data from catchments in Gibe basin of Ethiopia revealed that sediment yield ranges from 5 to 66 t ha^{-1} yr^{-1} (Vanmaercke et al., 2010). On the other hand, reservoir sediment surveys conducted in North Ethiopia micro-dam watersheds revealed that there has been great spatial variation from 2 to 19 t ha^{-1} yr^{-1} (Haregeweyn et al., 2012). The high sediment deposition rates have a severe impact on the life span of a number of reservoirs (Haregeweyn et al., 2006). Studies show that there is a significant variation of erosion and sediment yield in different parts of the country which indicates the importance of further studies in watershed and sub-watershed scales to precisely predict soil erosion. In Ethiopia specifically in Northwest Highlands where the study watershed is situated, deterioration of soil quality because of erosion threatens agricultural productivity.

The best management practices (BMPs) are ways to reduce impacts of soil erosion including pesticides and nutrients. Agricultural management methods can be categorized into vegetative (eg. spacing between cropping, filter strips) and mechanical (eg. soil and stone bunds, terraces, check dams) (Troeh et al., 2004). Miller et al. (2012) on the other hand

classified management practices as avoiding, controlling, and trapping. Avoiding methods have the function in preventing the incoming of sediments or pollutants into an area and the controlling methods help to control the impact of pollution if not possible to avoid the pollution. The methods of trapping are aimed at capturing pollutants near the area of the source.

To reduce the impacts of runoff on soil erosion and sedimentation, the government of Ethiopian began soil conservation programs since the 1970s. Among the agricultural management practices that have been implemented were soil bunds, fanyajuus, bench terraces, waterways, afforestation, grass strips, agro-forestry system (El-Swaify and Hurni, 1996). Grass filter strips are areas of vegetation between waterbodies and other land uses like cultivation and grazing. The purpose of filter strips is to trap pollutants (sediment, organic material, nutrients, and chemicals) during runoff and slow the velocity of the runoff. Filter strips allow the infiltration of pollutants in areas where the overland flow is shallow and widely dispersed across the width of the strip. Soil bunds are physical measures with an embankment of either soil or stones or both soil and stones, which are built along the contour and could be strengthened with vegetative measures (Morgan, 1995). Stone bunds reduce the length of the slope, create retention basins for runoff and sediment, reduce the hillslope gradient, and mitigate the erosive power of overland flow (Bosshart, 1997). Bunds facilitate water infiltration by retaining water behind the bunds. Reports in Ethiopia showed that soil bunds reduce erosion by 39% (Gebreegziabher et al., 2008), 50% (Herweg and Ludi, 1999).

The limited performance of management practices has been reported due to the top-down government approach, limited participation of stakeholders including the farmers, and inappropriate implementation of the structures (Shiferaw and Holden, 1999; Herweg and Ludi, 1999; Hengsdijk et al., 2005). Involvement and investment of farmers on the management practices are limited by the efficiency of the practices on reducing erosion and runoff (Shiferaw and Holden, 2001; Raes et al., 2007). Even though reports have shown that management practices have the capability of reducing soil erosion and trapping sediments their effectiveness is area-specific and highly variable (Shiferaw and Holden, 2001; Raes et al., 2007).

In the process of reducing soil erosion problems, the first priority is tracing the areas of

significant soil erosion and sediment yield production, and where conservation practices need to be the focus on. The environmental effects of BMPs can be evaluated through field-level experiments and models simulation. In order to minimize the impacts of soil erosion, data-based information about erosion, sediments, and the location of hotspots need to be identified. Studies related to quantifying the degree and spatial distribution of soil erosion employing physical-based and distributed models play a paramount role in prioritizing basins and sub-basins that demand soil and water conservation measures (Haregeweyn et al., 2015; Dile et al., 2013). Distributed and physical-based watershed-scale models have been used to assess the effectiveness of management practices and among these models, the SWAT has gained recognition by different authors (Demissie et al., 2013; Nadew et al., 2018; Bracmort et al., 2006; Haregeweyn et al., 2012).

2.6 Impact of LULC and Climate Change on Hydrology and Erosion

Basically economic development is driving LULC and climate change which is affecting the availability of water at global and regional levels (Luck et al., 2015). The increasing demand for fuelwood and water due to the rapid population growth in combination with the increasing temperature and rainfall variability has been imposing pressures on the biophysical environment which has been altering the hydrology of basins. The increasing of cultivated lands and urbanization mainly driven by the increasing population impose strong pressure on water resources which in turn affects the hydrological cycle of regions (Tomer et al., 2009; Dibaba et al., 2020). The LULC changes are the main driving factors for the hydrologic cycle (Vlek et al., 2017). The frequent LULC changes combined with the changing climate have an impact on watershed hydrology by altering the hydrological process of watersheds (Shawul et al., 2019). The climate and physical conditions of basins determine their hydrological response to the LULC changes which indicate a site-specific investigation of the impact of LULC and climate changes on the basin's hydrology. Anthropogenic activities are causes for the prevalence of LULC and climate changes that affect the hydrological cycle (Mango et al., 2011). The IPCC (2007) report assured that global warming is occurring. Changes in the patterns of precipitation and distribution of temperatures that alter the hydrological cycle, changes in flow, sediments, and pollutants, is because of climate change (Tu, 2009). Various studies had been performed on the impact of climate change on hydrology (Boyer et al., 2010, Bauwens et al., 2011) and sediment yield (Li et al., 2011). Most of these studies indicated that alterations in hydrology and sediment load are closely associated with changes in temperature and precipitation. The alteration of the hydrological cycles because of climate

change impacts on the quantity and quality of water resource (Nyenje and Batelaan, 2009). For the management and planning of watershed-scale water resources, their hydrological response to the changing climate and LULC needs to be considered by managers of water resources (Mango et al., 2011).

Chapter 3 : Predict the LULC Change Scenario of Rib and Gumara Watersheds

3.1 Introduction

Knowledge of LULC dynamics is vital to estimate future changes and support current and future sustainable management practices planned to preserve essential landscape functions (Lin et al., 2007). Few land-use modelling studies (Braimoh and Vlek, 2005; Houessou et al., 2013) have been conducted in Africa, and there is a considerable gap in land use prediction incorporating their driving factors in Ethiopia. Many spatially explicit models have been employed with the aim of predicting the locations of LULC changes using empirical statistical models (Irwin and Geoghegan, 2001; Lambin et al., 2000). In this study Dyna-CLUE model (Verburg and Overmars, 2009) was chosen since it incorporated the non-spatial and spatial modules (Verburg et al., 2002) and it integrates statistical analyses and decision rules to define the LULC sequences (Schaldach and Priess, 2008).

3.1.1 Dynamic conversion of land use and its effects (Dyna-CLUE) model

The CLUE framework model was developed by Veldkamp and Fresco (1996). It predicts future land-use change using empirically calculated relations between driving factors and land use. In modeling of land-use change, the CLUE considers the internal competition among land-uses. The model was developed for the national and continental levels. The CLUE modelling approach was modified by (Verburg et al., 2002) with its name called CLUE-S (Conversion of Land-Use and its Effects at Small Regional Extent) at Wageningen University. The Dyna-CLUE versions were later developed in the same department by (Verburg and Overmars, 2009).

The Dyna-CLUE has four modules: (1) land-use requirements, which consists of the land available to change which could be estimated by considering the demographic and socioeconomic aspects of regions; (2) location characteristics, which represents the suitability of a locality to specific land use which is identified by analyzing the land use drivers; (3) spatial policies and restrictions, which represents the locations prohibited by law for specific land use (4) land-use type specific conversion settings, which could be determined using the behavior of each land-use (Verburg et al., 2002; Verburg and Veldkamp, 2004). The study watersheds are among the Ethiopian highland watersheds which have been under frequent LULC conversions that impact the watersheds hydrologic processes and soil erosion conditions. Understanding and predicting the trends of the LULC changes incorporating area

specific fundamental LULC drivers is an asset for hydrologic and soil erosion studies and designing and implementing suitable and sustainable watershed management schemes. Therefore, this study aims to predict the LULC of Rib and Gumara watersheds with the Dyna-CLUE land-use model using the local land-use driving factors and conversion sequences.

3.2 Materials and Methods

3.2.1 Description of the study area

3.2.1.1 The Nile River

The Nile River Basin covers an area of 3 million km^2 (Abtew and Melesse, 2014). Its basin includes eleven countries, Ethiopia, Eritrea, Kenya, Burundi, the Democratic Republic of Congo, Rwanda, South Sudan, Sudan, Tanzania, Uganda, and Egypt. The Nile has two major tributaries, the Blue Nile and the White Nile. Ethiopia with 12 % of the drainage basin generates 86 % of the river flow. The remaining 14 % comes from the White Nile which has a larger drainage basin (Abtew and Melesse, 2014). The Nile River, which has 6,650 km in length, is the longest river in the world. Its tributary White Nile rises in The Great Lakes region of Central Africa from Lake Victoria, Uganda, and flows to South Sudan and Sudan. The Blue Nile starts at Lake Tana in Ethiopia and flows into Sudan. The two rivers meet at The Sudanese capital, Khartoum, and flow north through Egypt to drain into the Mediterranean Sea (Abtew and Melesse, 2014).

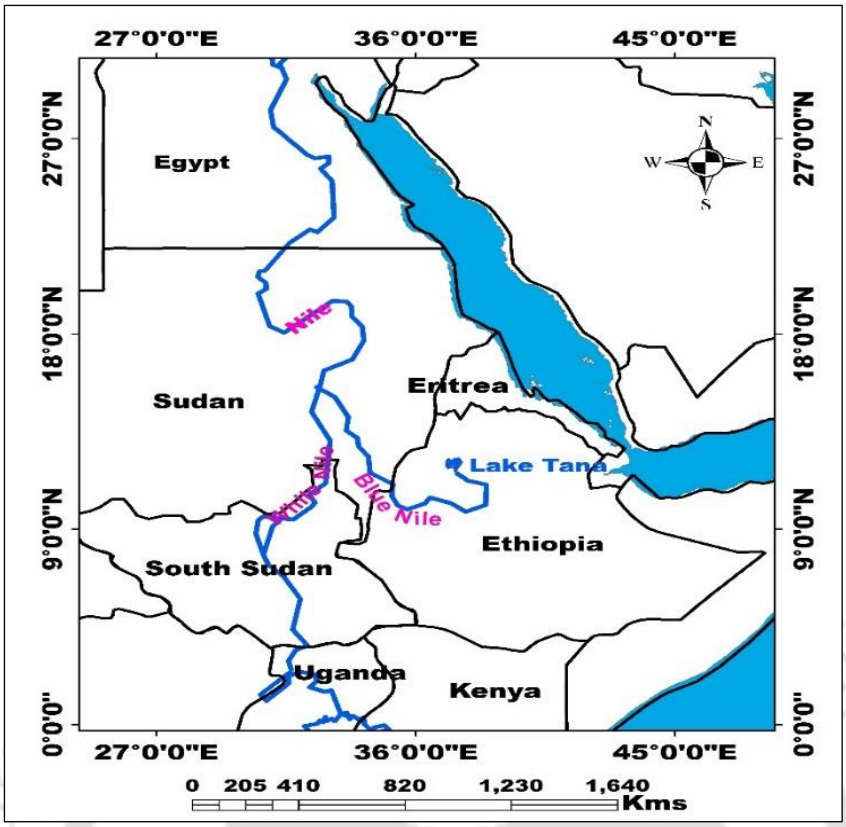

Figure 3-1 Drainage of the Nile River

3.2.1.2 Blue Nile River

The Blue Nile River (Abay River in local language) originates from Lake Tana in Ethiopia. The river has a drainage area of 199,812 km^2 and supplies nearly 86 % of the water of the Nile River during high flow season. The mean annual flow of the Blue Nile from Lake Tana at Bahir Dar city is $3.7x10^9 m^3 yr^{-1}$ with 70 % of the flow occurring from June to September. At Khartoum, the Blue Nile with a mean annual flow of $48.3 x10^9 m^3 yr^{-1}$ joins the White Nile to become the Nile (Abtew and Melesse, 2014).

The study watersheds are located in the Lake Tana Basin, the source of the Blue Nile River. The Lake Tana Basin, located in the Northwestern Ethiopian Highlands, with a catchment area of 15077 km^2 (including the lake area), consists of the Gilgel Abay, Gumara, Rib, and Megech rivers. About 93% of the annual inflow to Lake Tana is believed to come from these rivers (Kebede et al., 2006), and a better understanding of the hydrology of these rivers plays a crucial role in the efficient management of the lake and its basin ecosystems. The mean and maximum depth of the Lake is 7.2m and 14m respectively (Wale, 2009) with a total area of 3600 km^2 at an elevation of 1786 m amsl. It is the largest lake in Ethiopia and among the

largest in the Nile Basin.

3.2.1.3 Rib and Gumara watersheds

Rib watershed is located in Northwestern Ethiopia and stretches between 11°42'34"–12°13'45" N and 37°36'6"–38°14'20"E. It is situated in South Gonder Zone of Amhara National Regional State, Ethiopia. It has a total area of about 1578 km^2. Within the watershed, elevation ranges from 1786–4098m amsl. The river Rib originates from Mount Guna, one of the highest mountain ranges of Ethiopia, near to 4135m amsl and ends to Lak Tana. The river flows on the hilly areas at its upper part and to the flat plans around Lake Tana.

Gumara watershed, drained by Gumara River originated from Guna Mountain, is located in South Gonder Zone of the Amhara National Regional State, Ethiopia. Gumara watershed is situated between 11°34' 20"–11°54' 27"N and 37°31' 22"–38°11'1"E. The upper and middle parts of the watershed is characterized by mountainous, highly rugged and dissected topography with steep slopes and the lower part is characterized by valley floor with flat to gentle slopes. Elevation in the watershed varies between 1786–3704m amsl. The size of Gumara watersheds is 1415.9 km^2.

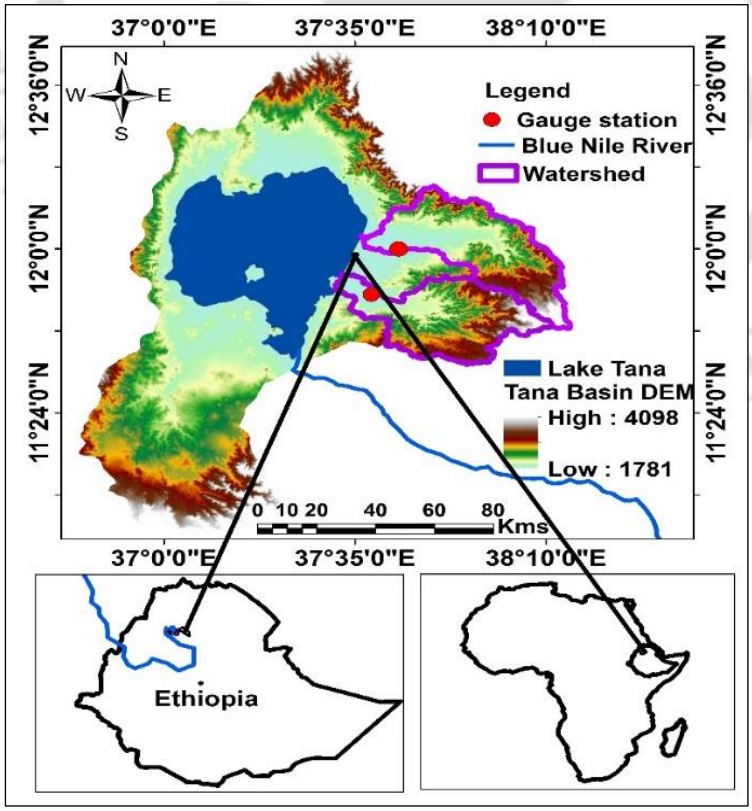

Figure 3-2 Location map of Rib and Gumara watersheds

3.2.1.4 Rainfall and temperature in the watersheds

Based on the rainfall pattern, the year is divided into two seasons: a rainy season mainly centered on the months of June to September, and a dry season from October to March. April and May are an intermediate season where minor rains often occur. The mean annual precipitation and temperature of Rib are about 1379 mm and 21.4^{0}C respectively. The mean annual rainfall of Gumara watershed is 1439mm though there is a slight spatial variation with in the area. The mean annual temperature of Gumara is 22.6^{0}C. The lower portions of the watersheds are located along the major flooding zones of Ethiopia. The lower courses of Gumara and Rib rivers are frequently affected by flooding which causes loss of life and destruction of properties.

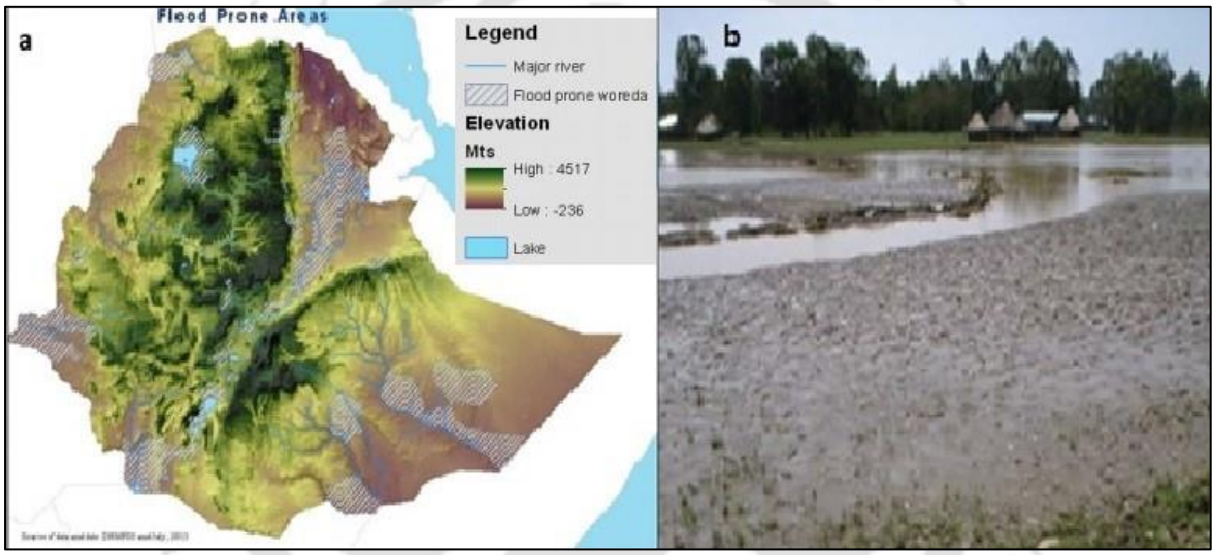

Figure 3-3 Flood prone areas in Ethiopia (a) and flooding of Gumara River (b) (Disaster and risk management bureau of Amhara Region, Ethiopia)

3.2.1.5 Demographic characteristics of the study watersheds

The total population of Ethiopia is 94,351,001 by 2017 (CSA, 2017). The rate of natural increase is approximately 2.38 percent per year. The population and demand for land for cultivation are increasing trough time which has a great impact on erosion and degradation. The population in the Amhara Region where the study area is found is about 21,134,988 in 2017 (CSA, 2017). The population of the study area districts increases from 1,665915 in 2007 to 1,995367 in 2017 with a density of 170 P/km^2 (Table 3.1).

Table 3-1 Population number of the study area (CSA)

District	Population number		Population density
	2007	2017	2017
Ebinat	220177	261329	104
Libo-Kemkem	198435	242188	170
Lay-gaint	206499	251926	170
Farta	232181	272177	200
Fogera	228449	278679	259
Dera	248464	296808	183
Este	331710	392260	175
Total	1665915	1995367	170

3.2.1.6 Geology, soil and LULC of the watersheds

Ribb and Gumara watersheds are dominated by a huge volcano system named as Guna mountain shield volcano. It corresponds to the eruptive events that occurred during the early Miocene to the Pliocene period and classified in the shield basalt group. The common rock type for this material is basalt with a large amount of interbedded lava, volcanic ash, and other acidic rocks such as rhyolite and trachyte with rare ignimbrites. At the river mouths (near Lake Tana), the area is overlain by recent flood materials, which are mainly covered by silt to clay deposits (MoWR, 1998). The soil type includes Fluvisols, Leptosols, Luvisols, Nitosils, and Vertisols. The major land-use types in the watersheds include cultivation, grazing, patches of bushes, forests, plantations, and settlement (BoEPLAU, 2015).

3.2.2 Historical land use data input, Dyna-CLUE model

The data required to the Dyna-CLUE model are land-use, drivers of change, the demand for land-use change, and land-use type specific conversion settings. Many land-use modelling researches use historical remotely sensed images to empirically derive transition parameters across landscapes (Theobald and Hobbs, 2002; Wear and Bolstad, 1998; Conway and Lathrop, 2005). The assumption of the trend based modelling methodology is that future land use trends will resemble recent historical trends (Theobald and Hobbs, 2002). For this study, historic LULC data of 1984, 2003, and 2016 were derived from LANDSAT satellite images. After processing and correction on the Landsat images, both unsupervised and supervised image classification methods were conducted to categorize pixels into LULC classes.

Table 3-2 Satellite images and their properties for LULC classification

Satellite	Sensor	Acquisation date	Spatial resolution	Path and row
LANDSAT 5	TM	1984-03-15	30m	169/52
LANDSAT 7	ETM	2003-03-08	30m	169/52
LANDSAT 8	OLI-TIRS	2016-03-04	30m	169/52

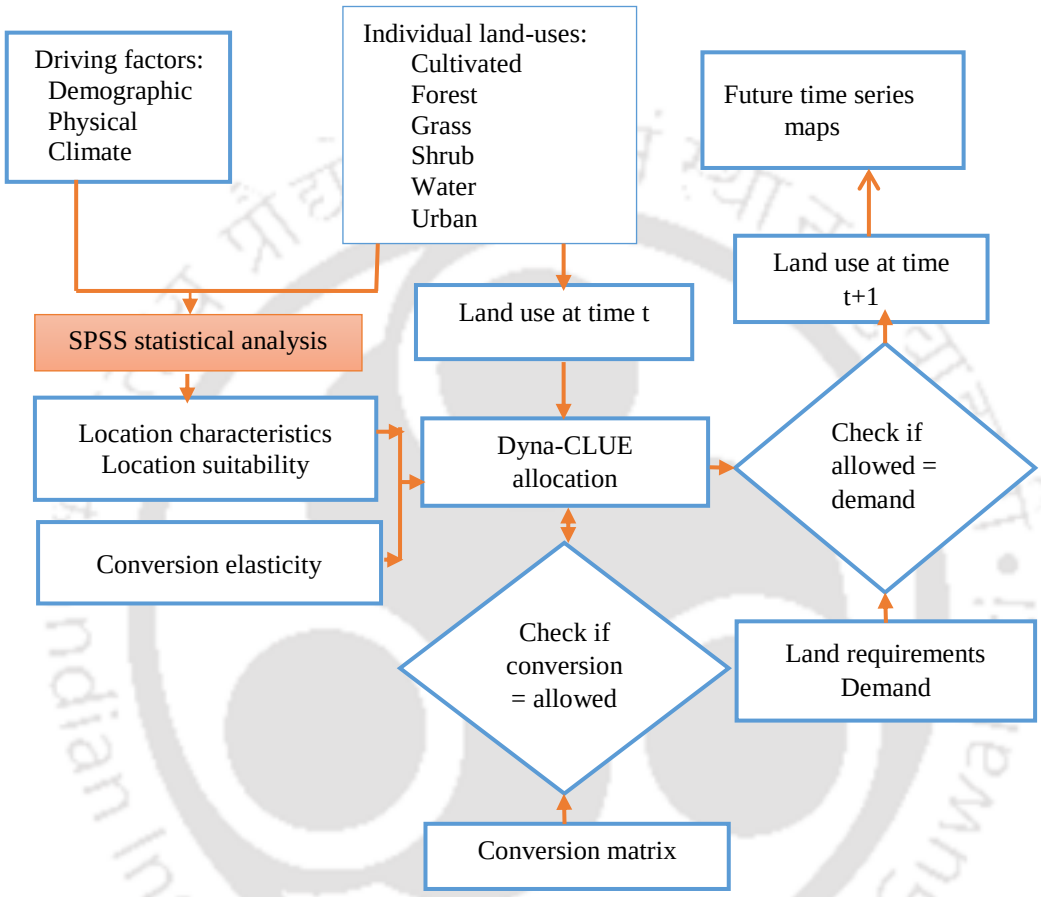

Figure 3-4 Diagrammatic presentation of flow of land use modeling

For the training of the image pixels for classification, Ground Control Points (GCPs) were collected directly from the field using GPS. Classification accuracy with confusion matrix using test pixels was undertaken. The 1984 LULC was used as a base map for LULC modelling. ASCII file for each land-use type and the whole land-use for the base map were prepared for both watersheds.

3.2.3 Land-use type specific conversion sequences

Not all land uses are possible to change, some land-use are very unlikely to change (e.g., arable land cannot be converted into primary rain forest) (Verburg and Overmars, 2009).

Land-use changes follow a certain pattern or sequence, for example, fallow land regularly follows shifting cultivation. In the Dyna-CLUE model, the land-use conversions that are possible and impossible are determined in a land-use conversion matrix. The conversion matrix is important to indicate to what land-use types a defined land-use is likely to convert.

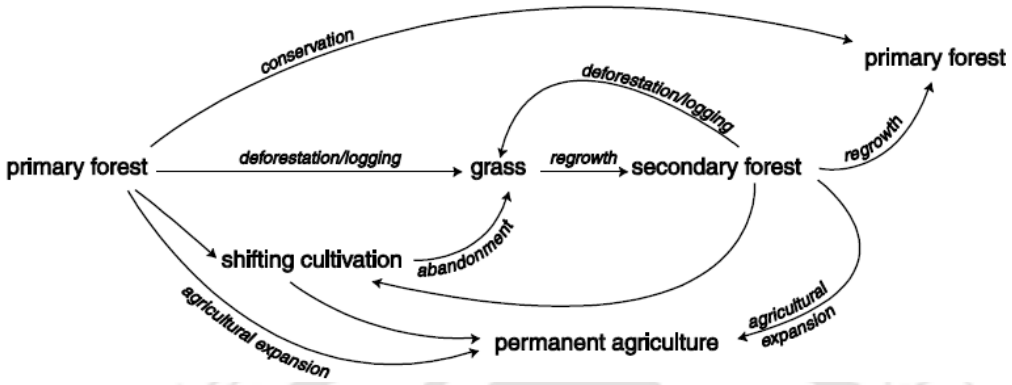

Figure 3-5 Land-use conversion sequence (Verburg, 2010)

The conversion matrix used in this study was determined using previous trends, i.e. analysis of changes between 1984 and 2016 (Tizora et al., 2018) and knowledge of experts and aged people in the locality. It specifies the temporal dynamics of predictions and designates the sequences of likely and unlikely conversions among land-use classes. In this study, there were eight land-use classes (intensively cultivated, shrubland, grassland, mixed forest, moderately cultivated, plantation, urban, and waterbody), which have a dimension of 8×8 matrix where rows and columns represent the present and possible future land use classes, respectively. If the conversion is allowed the value 1 is assigned to the cell, and if the conversion is not allowed the value 0 is used (Verburg, 2010).

Table 3-3 Land use conversion matrix of the watersheds

	Intensively cultivated	Shrub land	Grassland	Mixed forest	Moderately cultivated	Plantation	Urban	Water
Intensively cultivated	1	0	0	0	1	1	1	0
Shrub land	1	1	1	0	1	0	0	0
Grassland	1	0	1	0	1	1	1	0
Mixed forest	1	1	0	1	1	0	0	0
Moderately cultivated	1	0	1	0	1	1	1	0
Plantation	0	0	0	0	0	1	1	0
Urban	0	0	0	0	0	0	1	0
Water	0	0	0	0	0	0	0	1

3.2.4 Land use demand

Land-use demand is the planned land use size assigned to each land use category in each of the study years. The land-use demand for land-use modelling has to be computed using socio-economic models and trends extrapolation. To analyze land-use demand, trend extrapolation of the recent past into the near future is the most common procedure (Verburg, 2010). Future land-use patterns of the watersheds were predicted according to the current temporal trends of land-use transition from the past to the present.

Prior in determining the land use demand, land use maps of 1984, 2003 and 2016 were prepared from Landsat images considering required image processing and accuracy assessment on classified images.

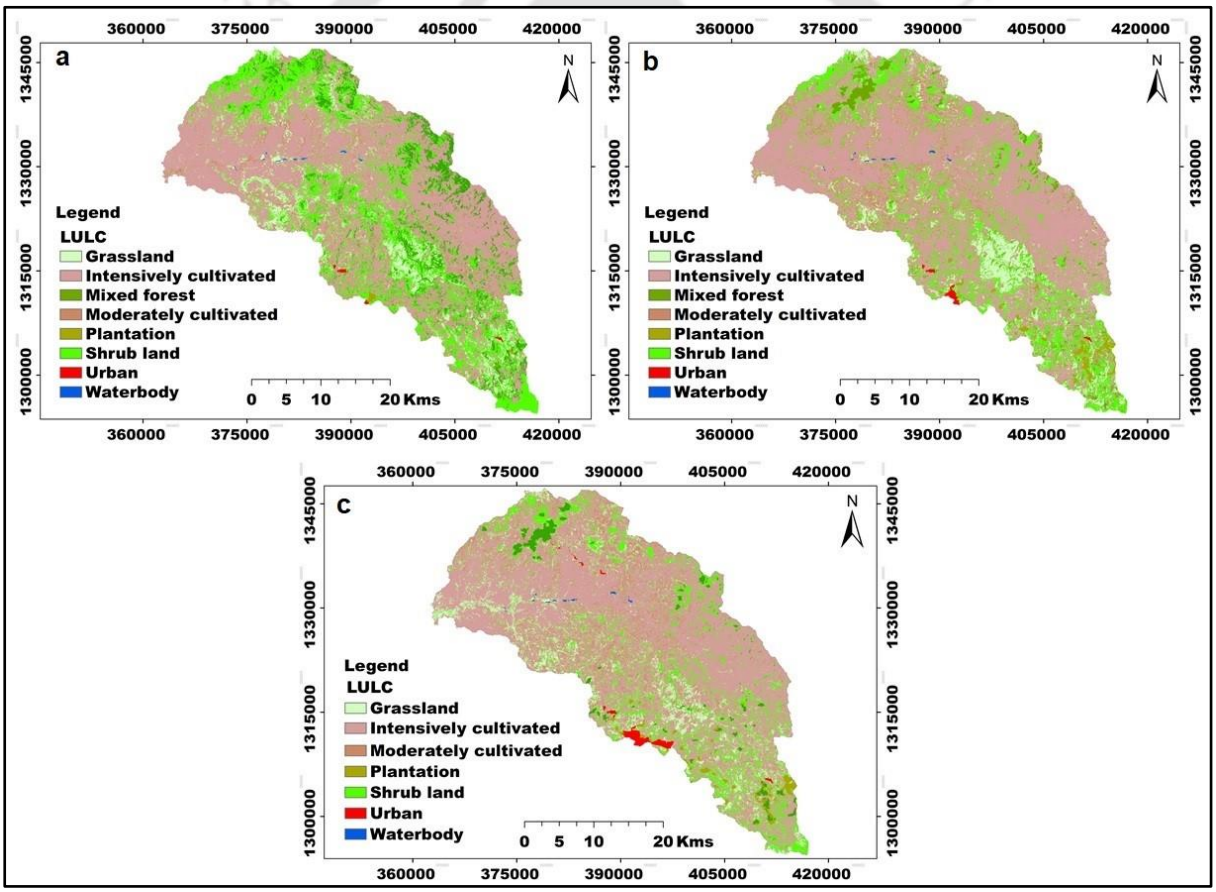

Figure 3-6 LULC maps of Rib in 1984 (a), 2003 (b) and 2016 (c)

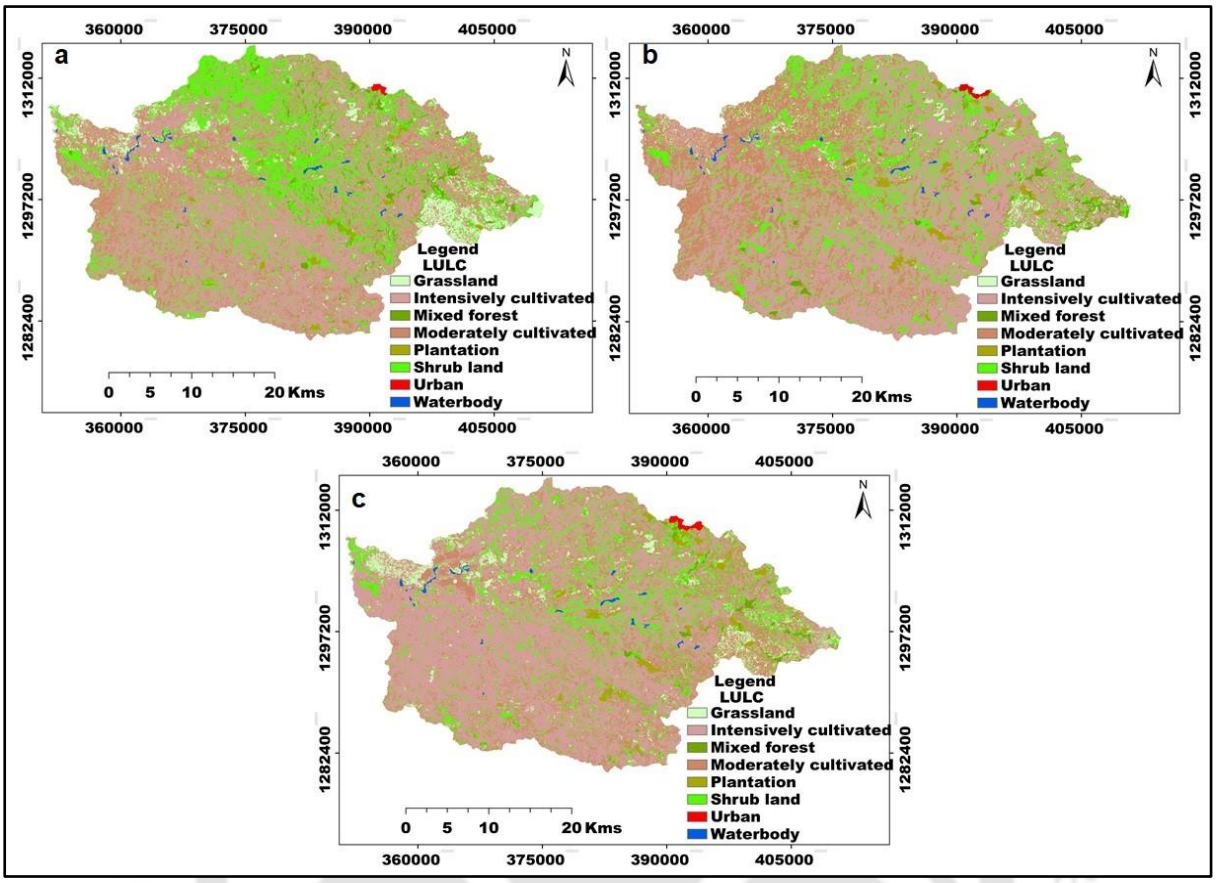

Figure 3-7 LULC maps of Gumara in 1984 (a), 2003 (b) and 2016 (c)

3.2.5 Classification accuracy assessment

Accuracy assessment or validation is important for data generated from remote sensing images. It determines the information value of the resulting data to a user. GCPs were collected from the field to identify the covers in the historical images discussing with aged people who are living in the area for a long time. The standard classification accuracy assessment methods are the kappa coefficient and error matrix (Lillesand and Kiefer, 2004). These methods resample ground truth points mainly acquired with GPS against the classified images.

The accuracies of classifications were obtained through GIS overlay of the thematic classified image and the ground truths. The kappa statistics (equation 3.2) measure the overall agreement between ground truth and image data. Its values range between 0 and 1, where 1 shows a complete agreement, and multiplied by 100 to obtain a percentage of accuracy.

According to (Landis and Koch, 1977; Congalton and Green, 1999), Kappa values have four categories: a strong agreement with values above 0.80 (80%), high agreement with values ranges between 0.60 and 0.80 (60% to 80%), moderate agreement with values ranges between 0.40 and 0.60 (40 to 60%), and a poor agreement with values below 0.40 (40%).

$$\text{Overall accuracy} = \frac{\text{Total correct}}{\text{Total tested}} * 100 \qquad (3.1)$$

Cohen's kappa coefficient (k):

$$k = \frac{N * d - q}{N^2 - q} \qquad (3.2)$$

Where, *N*, total samples number, *d*, sum of diagonal cells in the error matrix. $q = x_{+j} * x_{i+}$ where $x_{+j} = \sum_{i=1}^{n} x_{i,j}$ is the summation of rows for column j, $x_{i+} = \sum_{i=1}^{n} x_{j,i}$ is the summation of columns for row i.

3.2.6 Conversion elasticity

Conversion elasticity is a land-use type specific setting that indicates the temporal dynamics of the land-use predictions. It indicates the reversibility of land-use changes. High capital intensive land-uses that could result irreversible impact on an area could not be easily converted to others. These types of land uses have the tendency to stay a longer time with their present existence. Examples of such land uses are urban areas, fruit tree plantations. There are land-use types that could be easily converted when their location is found suitable for other land-use types. In such cases arable land may be converted to urban development and forest may give place for crop cultivation

A dimensionless factor from 0 (easily converted) to 1 (static to change) has been assigned to land-use types that indicates their relative elasticity to change. The user should specify this factor based on expert knowledge or observed behavior in the recent past (Verburg, 2010, Verburg and Overmars, 2009). Conversion elasticity for the Dyna-CLUE model in this study was assigned based on the analysis of previous land use data and expert knowledge in the locality. High elasticity were assigned to built-up and waterbodies, given their low probabilities of being converted to other land use types, whereas low elasticity values were allocated to shrub land, forests, and grass lands due to their higher likelihood of conversion to other land-use types because of agricultural land expansion.

Table 3-4 Conversion elasticity of the land use types

	Conversion elasticity	
Land use	Rib	Gumara
Intensively cultivated	0.7	0.7
Shrub land	0.1	0.2
Grassland	0.9	0.5
Mixed Forest	0.1	0.3
Moderately Cultivated	0.8	0.8
Plantation	0.7	0.8
Urban	1	1
Waterbody	1	1

3.2.7 Location characteristics or driving factors

Land-use changes are likely to occur at a grid cell that has higher preference or suitability. The land use preference is determined through the iteration procedure of the Dyna-CLUE that occurs between land-use classes and driving factors. The preference is a binomial "logit" model (Binary Logistic Regression) of probabilities that are computed from the interaction between each land use class (dependent variable), and driving factors (independent variables).

The stepwise logit regression method was used to select the relevant factors from the list of expected driving factors. The logit model determines the preference for a specific type of land-use based on the relation between the occurrence of a land-use type and the physical and socio-economic conditions of a specific location (location factors). The Dyna-CLUE model uses inputs of the local suitability of the locations derived from the logit model, the conversion elasticity, and the competitive strength of the land-use type to calculate the total probability of change of each grid cell of each land-use type (Verburg and Overmars, 2009). The Dyna-CLUE follows an iterative procedure until the allocated area of each land-use equals the land requirement in a scenario keeping the competitive strength of the different land-use types.

Land-use change derivers can be categorized into physical and socio-economic. Slope, elevation, aspect, and soil are among the physical drivers and population density and policies are the socio-economic drivers. Land use driving factors specified for this study were population density, topography (elevation and slope), soil depth, soil organic matter, distance to waterbody, roads, towns, and churches, rainfall and temperature (Millington et al., 2007),

which are the influential factors for land-use change in the study area.

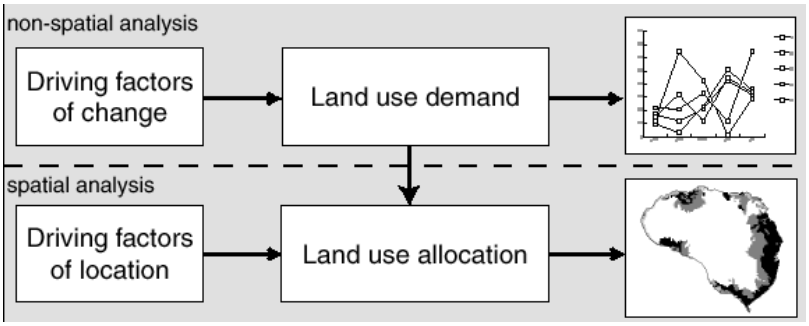

Figure 3-8 Structure of Dyna-CLUE model (Verburg and Overmars, 2009)

Probability maps for all land use types were established using binary logistic regression model using equation 3.3.

$$\log\left(\frac{p_i}{1-p_i}\right) = \beta_o + \beta_1 X_{1,i} + \beta_2 X_{2,i} \ldots, \beta_n X_{n,i} \qquad (3.3)$$

Where P_i is the probability of a grid cell for the occurrence of a land-use type on location i and the $X_{1,i}$----$X_{n\,i}$, are driving factors. β_0, β_1 ----β_n are coefficients of each driving factor in the binary logistic model. The coefficients (β) are determined in logistic regression using the land use pattern as dependent variable (Verburg, 2010).

3.2.8 Model validation

The model validation was conducted employing two metrics; namely the receiver operating characteristics (ROC) statistics (Verburg and Veldkamp, 2004) of the logistic regression to test the validity of the relationship between the land use-types and the drivers of change and the Kappa statistic (Arsanjani et al., 2013).

3.2.8.1 The ROC evaluation

The fitness of the model was evaluated with the ROC method, which determines predicted probabilities by comparing them with observed values over the entire domain of the probabilities. If the ROC value approaches one, the model prediction is considered perfect and if it approaches 0.5 it is considered completely random (Pontius and Schneider, 2001). Binary logistic regression analyses were performed with the statistical software SPSS using the stepwise regression method. The purpose of these analyses is to identify the effective driving factors behind land-use changes. The regression confidence degree in the analyses was set to 95% ($\alpha = 0.05$), and the beta coefficients which did not satisfy this condition were excluded.

3.2.8.2Validation with map comparison

Validation of the model was performed by comparing the maps of predicted land-use with the classified one, in the same period, 2016 for the present study (Verburg et al., 2002). The classified or observed land-use maps were validated against the Dyna-CLUE model simulated maps to find out how the model performed. The purpose of statistical validation was to find out how well the 2016 reference map agreed with the 2016 simulated map in terms of both the quantity and location of cells in each category of land uses. The location and quantity agreement in the statistical validation of the Dyna-CLUE model were addressed through the use of Map Comparison Kit (MCK 3 software) (Hewitt and Escobar, 2011; Visser and De Nijs, 2006) using the Kappa simulation algorithm. The algorithm expresses the degree of agreement in relation to the amount of change within the individual classes basing on the value of a coefficient. The Kapa statistics measure the similarity between two maps based on a contingency table. In this study, the location similarities between the simulated and the observed maps were measured using Kappa location or 'KLoc (Pontius, 2000) whereas the number of cells per category of land-uses was determined using the Kappa histo or 'KHisto' (Hagen, 2003). The kappa coefficient was used to measure the agreement between the simulated and the reality maps.

3.3 Result and Discussion

3.3.1 Classification accuracy assessment

The overall accuracy and kappa statistics of the 1984, 2003 and 2016 of Rib classified images were 85.6, 86.0, 89.8; and 82.9, 83.0, 87.4 respectively. The overall accuracy and kappa statistics of Gumara classified images were 84.0, 83.7, 89.3 and 81.0, 80.0, 86.0 respectively. The overall accuracy and the kappa values were above the minimum level of accuracy for the identification of land cover categories from remote sensor data and indicated the presence of strong agreement between classified and reference data.

3.3.2 Location characteristics or driving factors and the ROC evaluation

The ROC value of the land-use driving factors specified for this study (population density, elevation, slope, soil depth, soil organic matter, distance to waterbody, roads, towns and churches, rainfall and temperature) (Millington et al., 2007), were presented in Table 3.5 for Rib and Table 3.6 for Gumara.

Table 3-5 Beta coefficients and ROC values of the logistic regression results of Rib

	Intensively cultivated	Shrub land	Grass land	Mixed forest	Moderately cultivated	Plantation	Urban
Population density	-0.00326	0.00128	0.00687	0.00711	-0.00072	0.03187	0.00175
Distance to roads	0.00000	-0.00001	0.00008	-0.00036	-0.00007	-0.00048	-0.00473
Distance to towns	0.00010	-0.00006	-0.00011	-0.00004	-0.00002	-0.00024	---
Distance to church	0.00007	-0.00011	-0.00001	-0.00060	-0.00008	-0.00016	-0.00038
Distance waterbody	-0.00004	---	0.00002	0.00011	0.00008	0.00028	0.00032
Elevation	-0.00071	0.00094	-0.00011	0.00207	-0.00009	0.00296	0.00169
Slope	-0.02219	0.05534	-0.03606	0.07737	-0.01575	0.05692	-0.08078
Aspect	0.00131	0.00017	-0.00150	0.00132	-0.00192	0.00083	---
Soil depth	0.00014	-0.00003	-0.00019	-0.00065	-0.00008	-0.00029	---
Soil organic matter	0.65149	---	---	---	---	---	---
Soil texture	0.43282	---	0.02185	---	---	---	---
Rain fall	0.00133	---	-0.00279	-0.00149	-0.00138	-0.01732	---
Temperature	-0.14509	0.01043	0.04676	0.52327	0.15055	-1.26177	---
Constant	-0.11747	-4.52056	0.41807	-17.7112	-1.66313	3.93219	-6.95837
ROC value	0.75	0.73	0.71	0.89	0.706	0.94	0.95

.

The ROC statistics in this study ranges from 0.706 for the moderately cultivated to 0.95 for the urban areas for Rib and 0.701 for the moderately cultivated to 0.99 for urban areas for Gumara. Waterbody has not shown changes in size between periods, which means it has not converted to other land-uses and other land-uses have not converted to a waterbody. Hence it has not calculated ROC value. The regression coefficients, as well as the constants, were significant at the 95% confidence level, indicating that the logistic regression model is capable of predicting the probability of occurrence of the land covers in the watersheds.

Table 3-6 Beta coefficients and ROC values of the logistic regression results of Gumara

	Intensively cultivated	Shrub land	Grassland	Mixed forest	Moderately cultivated	Plantation	Urban
Population density	-0.00622	0.00454	0.00829	0.00306	0.00016	-0.00141	0.30647
Distance to roads	0.00009	---	-0.00020	-0.00005	-0.00005	-0.00006	-0.00290
Distance to towns	-0.00001	0.00001	-0.00002	0.00004	0.00002	0.00025	---
Distance to churches	0.00008	---	-0.00021	-0.00026	---	-0.00042	---
Distance waterbody	0.00006	---	-0.00014	-0.00009	-0.00004	-0.00036	---
Elevation	-0.00073	-0.00051	0.00038	0.00309	0.00070	0.00339	0.00070
Slope	0.00330	0.01774	-0.02941	0.06028	-0.02411	0.05347	-0.04260
Aspect	---	0.00051	-0.00025	-0.00036	-0.00073	-0.00147	---
Soil depth	-0.00015	---	0.00015	0.00009	0.00041	---	---
Soil organic matter	0.61772	---	-0.36664	---	---	---	---
Soil texture	0.13164	-0.13721	0.47949	---	0.35733	---	---
Rain fall	---	0.00756	0.00478	0.03931	0.01441	0.13022	---
Temperature	0.09307	-0.12415	0.23025	---	-0.01775	0.61688	---
Constant	-0.33072	-10.50956	-16.94645	-70.0880	-24.76842	-213.715	-90.99380
ROC value	0.73	0.72	0.76	0.86	0.701	0.83	0.99

Value not significant at the 0.05 significance level is excluded from the model. ROC value ≥ 0.700 shows regression results can be acceptable (Mandrekar, 2010; Erdoğan et al., 2011)

3.3.3 Predicted LULC of the watersheds

A total of fourteen driving factors and eight LULCs were identified and prepared in an ASCII file format for the identification of the best predictive parameter for each LULC class in the study area using the binary logit regression as is indicated in Table 3.5 for Rib and Table 3.6 for Gumara. Combining the driving factors, land use demand, conversion elasticity, change matrix, and the base map of 1984 for both watersheds, the predicted 2016 and 2049 LULC maps were prepared (Figure 3-9 and 3-10).

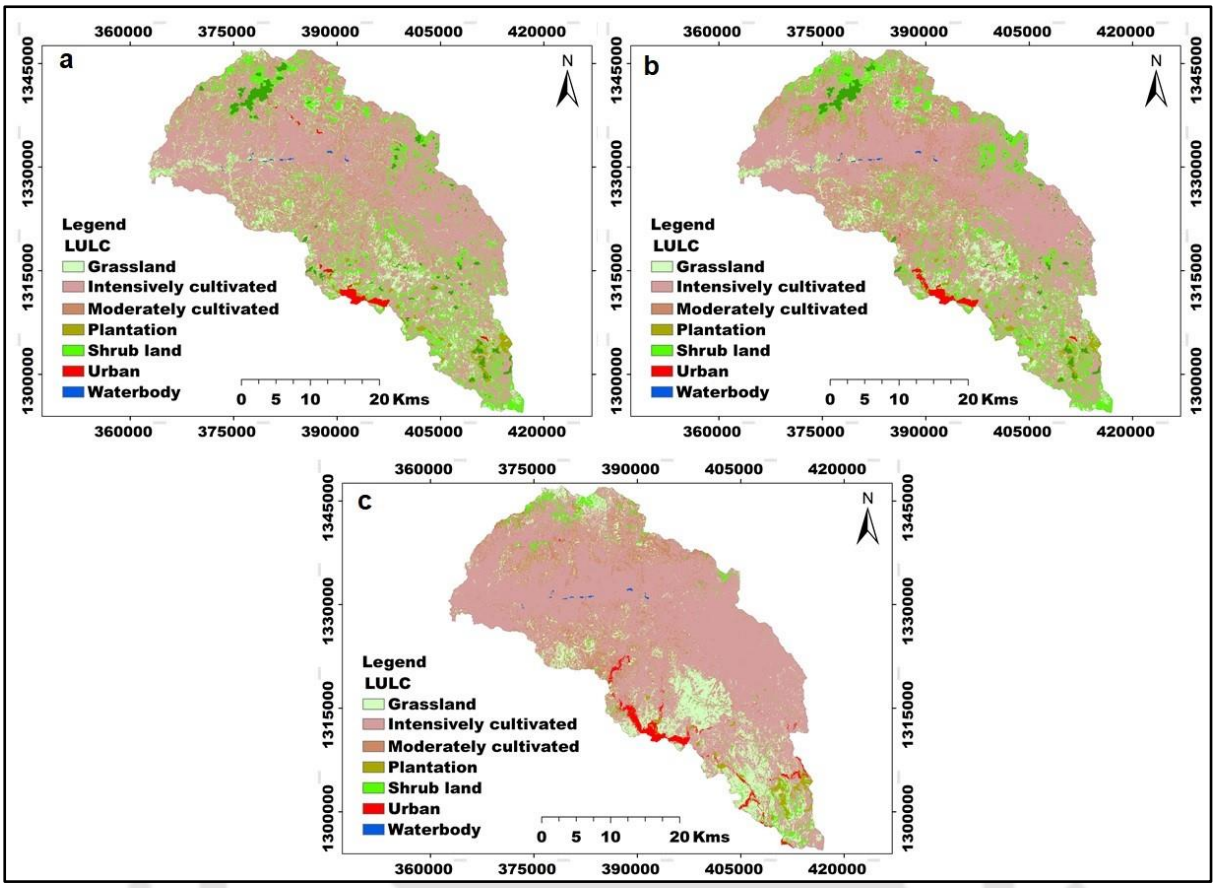

Figure 3-9 LULC map of Rib 2016 reality (a), 2016 simulated (b) and 2049 (c)

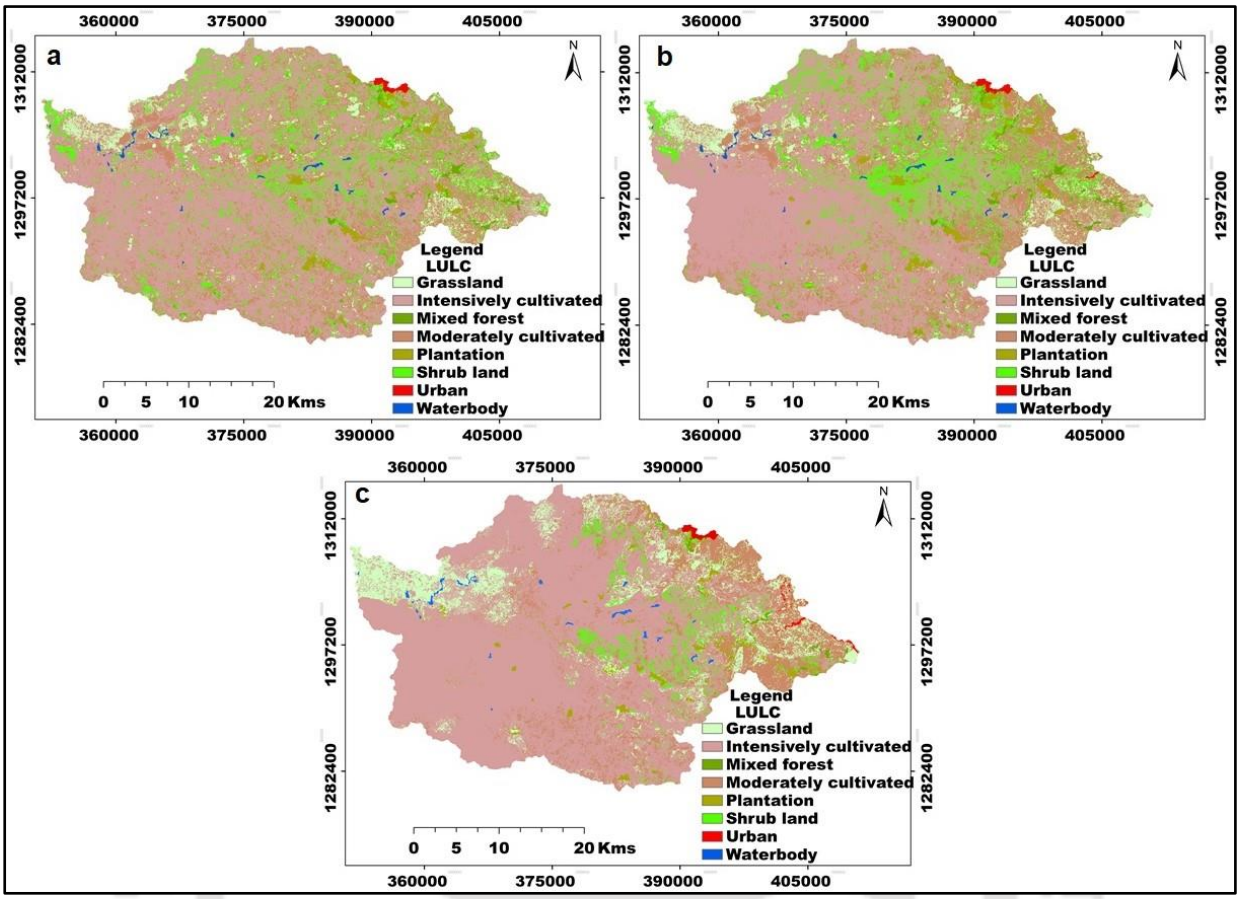

Figure 3-10 LULC map of Gumara 2016 reality (a), 2016 simulated (b) and 2049 (c)

From the land-use trends of 1984, 2003, and 2016 and the prediction maps of 2049 it could be understood that there were a large increasing trend in cultivation land and a small increase in urban and plantation on both watersheds. The increase in intensively cultivated land was 16.7, 5.4, and 11.0% and 9.4, 9.3, and 20.9% between the three-time periods of 1984-2003, 2003-2016, and 2016-2049 in Rib and Gumara respectively (Table 3-7 for Rib & Table 3-8 for Gumara).

On the other hand, there has been a large scale decrease in shrubland and mixed forests on both watersheds and all time periods. There was 23.1%, 25.4%, 82.5% and 19.1%, 23.6%, 74.1% reduction in shrubland between 1984-2003, 2003-2016 and 2016-2049 in Rib and Gumara respectively. There has been reduction of mixed forest by 63.4%, 40.7% and 100 % in Rib and 55.1%, 18.7%, and 63.1% in Gumara watersheds in the periods between 1984-2003, 2003-2016 and 2016-2049 respectively. Moderately cultivated land has shown an increase in Rib and a slight decreasing trend in Gumara. The magnitude of LULC change is presented in Figure 3-11 for Rib and Figure 3-12 for Gumara.

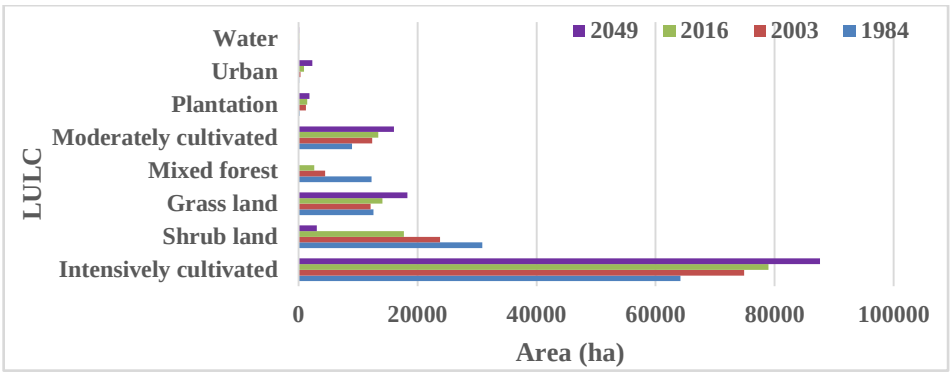

Figure 3-11 Trend of LULC change in Rib

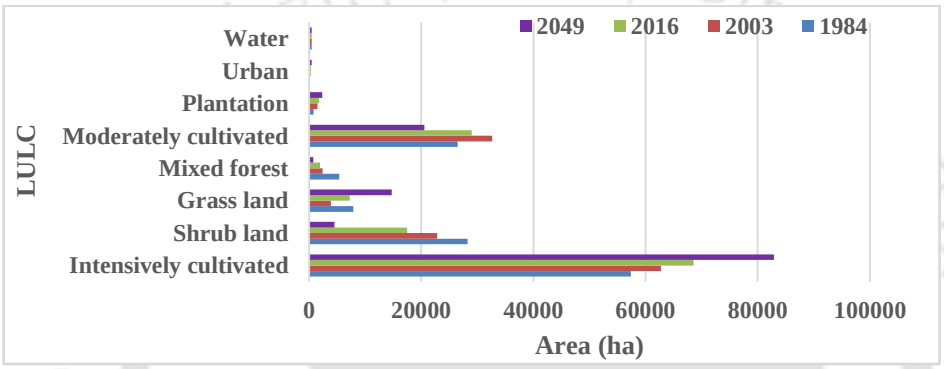

Figure 3-12 Trend of LULC change in of Gumara

Table 3-7 Change between land use and land covers in Rib

Year	Intensively cultivated	Shrub land	Grassland	Mixed forest	Moderately cultivated	Plantation	Urban	Water
1984	64153.17	30888.99	12611.34	12277.26	8974.98	183.69	130.86	103.32
2003	74893.82	23762.7	12100.32	4498.38	12403.62	1233.27	328.14	103.32
2016	78946.56	17728.29	14102.19	2666.88	13425.48	1454.31	896.58	103.32
2049	87622.47	3095.73	18285.93	0.00000	16057.89	1831.95	2326.23	103.32
			Change (ha)					
1984-2003	10740.6	-7126.3	-511.0	-7778.9	3428.6	1049.6	197.3	0.0
2003-2016	4052.7	-6034.4	2001.9	-1831.5	1021.9	221.0	568.4	0.0
2016-2049	8675.9	-14632.6	4183.7	-2666.9	2632.4	377.6	1429.7	0.0
			Change (%)					
1984-2003	16.7	-23.1	-4.1	-63.4	38.2	571.4	150.8	0.000
2003-2016	5.4	-25.4	16.5	-40.7	8.2	17.9	173.2	0.000
2016-2049	11.0	-82.5	29.7	-100.0	19.6	26.0	159.5	0.000

There has been a slight expansion of plantation and urban land-uses on both watersheds with a little higher scale in in Rib than in Gumara. Grassland has shown an increasing trend between all time periods in Rib and between 1984 and 2003 in Gumara, but it has shown a decreasing experience after 2003 in Gumara. The change in grassland on both watersheds is significant with values of -4.1%, 16.5%, 29.7% in the Rib and 50.8%, 86.3%, and 103.9% in Gumara in the three periods. Generally, it can be concluded that there has been a great reduction in vegetation and expansion of cultivation lands in both watersheds in all-time slices.

Table 3-8 Change between land use and land covers in Gumara

Year	Intensively cultivated	Shrub land	Grass land	Mixed forest	Moderately cultivated	Plantation	Urban	Water
1984	57358.71	28245.42	7885.71	5340.87	26466.21	824.76	141.84	435.78
2003	62729.19	22847.31	3880.17	2396.79	32667.3	1509.66	233.28	435.78
2016	68549.31	17463.33	7228.08	1949.58	29008.62	1761.3	303.3	435.78
2049	82890.81	4530.96	14739.12	720.09	20580.03	2367.9	434.61	435.78
Change (ha)								
1984-2003	5370.5	-5398.1	-4005.5	-2944.1	6201.1	684.9	91.4	0.0
2003-2016	5820.1	-5384.0	3347.9	-447.2	-3658.7	251.6	70.0	0.0
2016-2049	14341.5	-12932.4	7511.0	-1229.5	-8428.6	606.6	131.3	0.0
Change (%)								
1984-2003	9.4	-19.1	-50.8	-55.1	23.4	83.0	64.5	0.0
2003-2016	9.3	-23.6	86.3	-18.7	-11.2	16.7	30.0	0.0
2016-2049	20.9	-74.1	103.9	-63.1	-29.1	34.4	43.3	0.0

3.3.4 Model statistical validation

Validation of the model was performed with the comparison between predicted land use map and the classified map, in the same period, 2016 for the present study (Rykiel, 1996; Verburg et al., 2002). The comparison has been performed through the use of Map Comparison Kit (MCK software). The Kappa, KLocation, and KHisto values of Rib and Gumara respectively were (0.734, 0.762, and 0.963) and (0.730, 0.751, and 0.971). The Kappa statistics result of Rib and Gumara were presented in Table 3-9.

Table 3-9 The per category kappa statistics of Rib and Gumara classification

	Intensively cultivated	Shrub land	Grassland	Mixed forest	Moderately cultivated	Plantation	Urban	Water
Rib								
Kappa	0.750	0.748	0.709	0.763	0.703	0.815	0.857	1.000
KLoc	0.764	0.755	0.741	0.812	0.754	0.845	0.901	1.000
KHisto	0.982	0.991	0.957	0.941	0.897	0.964	0.951	1.000
Gumara								
Kappa	0.726	0.710	0.761	0.827	0710	0.825	0.920	1.000
KLoc	0.754	0.714	0.783	0.955	0.720	0.951	0.979	1.000
KHisto	0.963	0.993	0.972	0.866	0.987	0.867	0.939	1.000

Kappa value and over all accuracy of Rib and Gumara respectively were 0.734, 0.843 and 0.730, 0.831. The result of the kappa statistics of Rib and Gumara indicated that the reality and simulated maps have high agreement (Landis and Koch, 1977; Congalton and Green 1999); hence the model is capable in predicting the LULC of the watersheds.

3.4 Conclusion

The capability of the Dyna-CLUE model in predicting LULC in Rib and Gumara watersheds were tested from 2016 to 2049 using land-use data from 1984 to 2016 and the driving forces in the area. The result showed that the model was feasible to predict the future LULC scenario of the watersheds. Large scale conversion of LULC had occurred from 1984 to 2016 and from 2016 to 2049 in both watersheds. A large increase has been observed in cultivated land and a low and gradual increase has occurred in plantation and urban LULCs. On the other hand, there has been a reduction in vegetation cover (shrubland and mixed forests) in all time periods. Generally, grassland has shown an increasing trend even though there were fluctuations in between periods. Growth of population and a decrease in the productivity of land are the main causes of LULC change in the area. This accelerated increase in land use conversion mainly in cultivated lands and a decrease in vegetation might have an impact on the increase in sediment yield in the Lake Tana reservoir and the channels of rivers.

Chapter 4 : Examine the Climate Change of Rib and Gumara Watersheds under SRES and RCP scenarios

4.1 Introduction

In many parts of the developing world especially in arid and semi-arid regions, changes in rainfall and temperature patterns are widely observed (Collier et al., 2008). Recent studies and modeling reports indicated that there have been warm temperature extremes, mainly in minimum temperatures. The temperature has shown a significant increase over the 20th century and will continue to increase throughout the 21st century. According to evidence, worldwide there have been more drought and flood events, with increasing intensity and frequency in the future (Tebaldi et al., 2006). Africa's average temperature increase is faster than the world average and has the tendency to continue in the future. The IPCC third assessment report (IPCC, 2007) indicated that the developing world is expected to suffer most from the negative impacts of climate change and climate variability. Africa is among the vulnerable continents to climate change (IPCC, 2007).

Studies showed that Ethiopia is susceptible to climate change (Conway and Schipper, 2011). In Ethiopia, droughts and floods are the main climate-driven hazards. A study by (Funk et al., 2005) showed that in Ethiopia rainfall is expected to decline in the future. As global studies have shown, there is substantial variability in precipitation (increase and decrease by about 20%) (Bates et al., 2008). Grate spatial variation in precipitation (rise and drop between 25–50%) has been reported in East Africa (Faramarzi et al., 2013). Rainfall variability is more evident in African which resulted in variation in water availability. Different studies were conducted in Ethiopia presenting the changing climate. Shawul et al. (2016) reported that the projected mean annual maximum and minimum temperature shows a rising trend in the South-eastern part of Ethiopia. As explained in (ENMA, 2007), the future mean annual temperature will vary within the ranges 0.9°C–1.1°C, 1.7°C–2.1°C, and 2.7°C–3.4°C by 2030, 2060, and 2090 time slices respectively in Ethiopia.

It is important to understand the effects of climate change on water resources to implement appropriate climate change adaptation and mitigation strategies. Implementation of appropriate strategies to mitigate the impact of climate on water resources, land and soils require an assessment of the impact of climate change on hydrology and sediments (IPCC, 2014). Climate change scenarios from GCMs are frequently used to assess the hydrological

impacts of climate change (Fowler et al., 2007; Abdo et al., 2009). Since the impact of climate change could be significantly variable in different regions, it is important to conduct such a study at agro-ecological regions to develop and implement adaptation and mitigation strategies.

4.2 Materials and Methods

4.2.1 Data used

Large scale or global climate models are currently used to advance the scientific knowledge and understanding about the variabilities and changes of climate variables. The large scale GCMs provide understanding about the changing global climate condition. The coarse (>100 km) resolution GCM outputs are unable to be used for impact assessment studies and decision-making process either at local or regional levels. In addition, the characteristics of biases and uncertainties associated with GCMs are higher in local scales, which hinder their applicability in local-scale studies. In this study, the future climate prediction was assessed based on the IPCC Fourth Assessment Report (IPCC-AR4) (2007) and Fifth Assessment Report (IPCC-AR5) (2014) emission scenario. Future climate change scenarios from the REMO regional climate model were obtained from the International Water Management Institute (IWMI). Dynamically downscaled temperature and rainfall time series of REMO-ECHAM5 outputs based on the AR4 IPCC SRES A1B climate change scenario on a daily time scale were used for the study as recommended by Hattermann (2011) for hydrological impact assessments. The ECHAM5 is the fifth generation of the ECHAM general circulation model developed at the Max Planck Institute for Meteorology in Hamburg. The REMO is originally developed at the Max-Planck-Institute for Meteorology and its physical core is based on the physical package of ECHAM GCM (Roeckner et al., 1996). Nowadays REMO has been maintained by the Climate Service Center Germany (GERICS) in Hamburg with further developments or updates (Preuschmann, 2012). Climate projections from REMO RCM models were obtained in grids of 0.5° x 0.5°.

The applicability of CORDEX-Africa GCM/RCM in climate researches has been increasing from time to time. Coordinated Regional Climate Downscaling Experiment (CORDEX) is supported by the World Climate Research Programme (WCRP) to foster global partnerships to generate high resolution historical and future climate projections at the regional scale (Endris et al., 2016). The RCM has been integrated into the CORDEX-Africa domain since

Africa is one of the vulnerable regions to climate variability. CORDEX-Africa is one of the special concerns of the CORDEX program (Solomon et al. 2007). CORDEX-Africa provides projected climate outputs at a relatively higher resolution of 0.44^0 x 0.44^0 (Endris eta al., 2016). This study used the RACMO22T RCM model from the driving model of Hadley Global Environment Model 2-Earth System (HadGEM2-ES) in CORDEX-Africa for the Representative Concentration Pathways (RCPs).

Nowadays, there is the availability of recent RCPs scenarios of the CMIP5 project developed during the fifth IPCC assessment report AR5 (Taylor et al., 2012). CMIP5 has finer resolution and well-integrated earth system components than the previous climate data projects. The CORDEX project, after processing on GCM/RCMs have been producing dynamical downscaled high resolution historical and future climate data based on CMIP5 simulations which could be used for impact and adaptation studies (Gbobaniyi, 2014; Panitz et al., 2014; Nikulin, 2012; Brands et al., 2013). Precipitation and temperature data from the RCP scenarios (RCP2.6, 4.5 and 8.5) are available from the CORDEX-Africa regional climate model for historical periods from 1951 to 2005 for calibration and from 2006 to 2100 for future periods for validation with observed data.

For this study, the future scenario period (2025–2099) and historical/baseline period (1981–2005) were considered to evaluate patterns of climate change. The RCPs scenarios; RCP2.6, RCP4.5, and RCP8.5 were considered for the study since CORDEX-Africa prioritizes these scenarios which could have greater performance in climate studies in the region (Alemseged, 2015). The RCP (2014) scenarios for future climate analysis with time periods of the 2030s, 2060s, and 2090s were used. This was intended to analyze climate change projections under low (RCP2.6), low-medium (RCP4.5), and high (RCP8.5) emission scenarios.

4.2.2 Bias correction on climate data

The RCM climate data outputs with the A1B emission scenario and RCM CORDEX-Africa under emission scenarios of RCP2.6, RCP4.5, and RCP8.5 were bias-corrected for climate change impact studies. Bias correction was performed on daily precipitation, minimum, and maximum temperatures using delta change method to minimize the systematic statistical deviation of climate model data from the observed data before using for future climate change projections. The underlying idea of the widely used delta-change method (Andréasson et al., 2004; Bosshard et al., 2011; Graham et al., 2007, Middelkoop et al., 2001; Moore et al.,

2007; Shabalova et al., 2003) is to use the RCM-simulated future change (anomalies) for a perturbation of observed data rather than to use the RCM simulations for future conditions directly. To predict the future climate, the RCM-simulated anomalies between the historical and future scenario runs are superimposed upon the observational time series. This is usually done on a monthly basis. A multiplicative and additive correction was used for precipitation and temperature respectively. Bias correction on daily maximum and minimum temperature and rainfall is represented in equations 4-1 and 4-2 respectively.

$$T_{fut,corr,d} = T_{\text{obs},d} + (\overline{T}_{\text{fut},m} - \overline{T}_{ref,m}) \quad (4.1)$$

$$P_{fut,corr,d} = P_{\text{obs},d} * \left(\frac{\overline{P}_{\text{fut},m}}{\overline{P}_{ref,m}} \right) \quad (4.2)$$

Where $T_{fut,corr,d}$ is the future corrected daily temperature (temperature max. and min.), $T_{obs,d}$ is the observed daily temperature for the base years, $\overline{T}_{fut,m}$ is the monthly mean GCM/RCM temperature for the future years and $\overline{T}_{ref,m}$ is the monthly mean GCM/RCM temperature of base years. $\overline{P}_{fut,corr,d}$ is the future corrected daily rainfall, $\overline{P}_{obs,d}$ is the observed daily rainfall, $\overline{P}_{fut,m}$ is the monthly mean GCM/RCM rainfall for future years, and $\overline{P}_{ref,m}$ is the monthly mean GCM/RCM rainfall for the base years.

4.3 Results and Discussion

4.3.1 Prediction of precipitation in the A1B scenario, Rib

The rainy season is divided into a minor rainy season from March to May which is also known as 'Belg' and a major rainy season from June to September known as 'Kiremit'. The dry season or locally called 'Bega', occurs between October and February. The climate analysis results showed that there will be a general decrease in mean annual precipitation in all scenarios and time slices (2030s, 2060s, and 2090s) in both watersheds. In the 2030s there will be a decrease in monthly mean daily precipitation except in the months of December, August, September, November, and January in Rib watershed. During these months there will be an increase of precipitation by 13.45%, 17.8%, 7.3%, 5.2%, and 3.2 % respectively from the base period. There is variation in the increase of precipitation from 3.2% in January to 17.8% in August in the 2030s scenario. During the 2030s, high decrease in precipitation will be observed in February, March, and May with values of 55.67%, 52.7% and 41%

respectively. In most months of the 2060s, there will be a decrease in precipitation. October, September, December, and August will show an increase of 40.7%, 17.1%, 16.9%, and 7.8% respectively in the 2060s, whereas other months will experience a decrease. The highest decrease will be shown in February (54.5%), followed by March (50.2%). Only the months of December, November, and January will show an increase with 44.9%, 32.3%, and 29.0% respectively in the 2090s. In all other months, there will be a reduction within a range between 2.5% to 62.6% in September and April. April, June, May, March and July shows the highest reduction with values of 62.8%, 61.8%, 58.2%, 50.5% and 41.1 respectively.

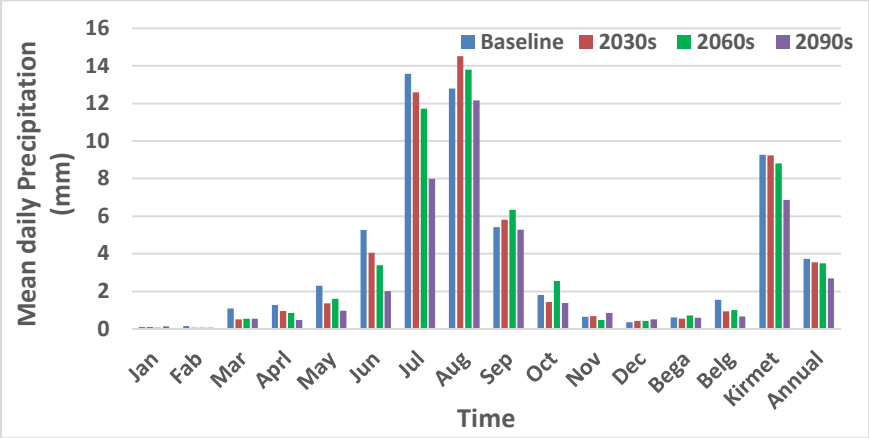

Figure 4-1 Monthly, seasonal and annual mean daily precipitation of the base period and the A1B scenario of Rib

There will be a consistent decrease in seasonal and annual precipitation in all scenarios except the Bega season. During Bega, there will be 12.7% decrease in 2030s, 16% increase in 2060s, and 4.48% decrease in 2090s. Consistent and highest decrease will be shown in Belg season, with 39.3%, 35.7% and 57.7% in 2030s, 2060s and 2090s respectively. Kiremt will show low reduction with 0.2%, 4.9% and 25.9% during 2030s, 2060s and 2090s. Generally, the projected precipitation in Rib watershed has decreasing trend in all scenarios. The average annual precipitation will be decrease by 5.1%, 6.6 %, and 27.7% in the 2030s, 2060s, and 2090s respectively.

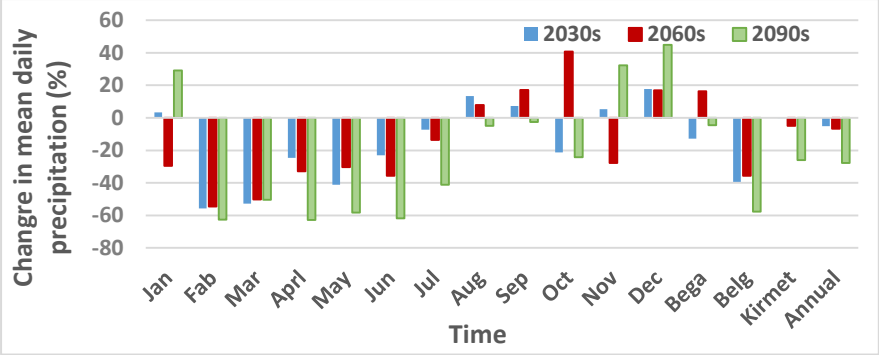

Figure 4-2 Percentage change in monthly, seasonal, and annual mean daily precipitation between 2025-2099 of the A1B scenario compared to the base period (1981-2005) in Rib

4.3.2 Prediction of precipitation in RCP Scenario, Rib

RCP2.6, low range, RCP4.5 mid-range and RCP8.5 high-range climate scenarios with radiative forcing of 2.6, 4.5 and 8.5 W/m^2 by 2100 respectively (Riahi et al., 2011; Thomson et al., 2011) were expected to capture a reasonable range in climatic and hydrological projections.

4.3.2.1 RCP 2.6 scenario

The result of the study showed that the future mean annual precipitation generally shows a slight decrease over the watershed. In scenario RCP2.6, the change in monthly mean daily precipitation varies between -61.5% in March to 68.7% in November of the 2030s, -82.7% in February to 67.4% in October of the 2060s, and -57.3% in March to 60.9% in February in the 2090s. High decrease will be observed in March, December, and May with decreasing values of 61.5%, 34.7%, 24.5%, and a minimum decrease will be on September, July, and June with 10.1%, 18.7%, and 14.4% respectively in the 2030s. Months that will show an increase in the 2030s of the RCP2.6 scenario are August, November, October, April, February, and January with values of 10.64%, 68.7%, 64.0%, 42.4%, 26.9%, and 26.7% respectively. There will be a significant seasonal variation in the RCP2.6 predicted precipitations. There will be an increase during the Bega season by 48.1% and a decrease in Belg and Kiremt seasons by 14.8%, 6.7% respectively in 2030s scenario. The mean annual decrease will be 3.8% compared with the baseline period in the 2030s (Figure 4.4).

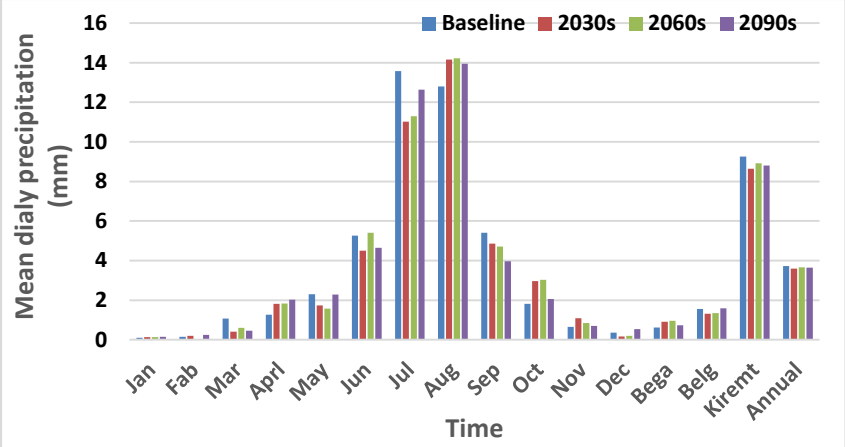

Figure 4-3 Monthly, seasonal and annual mean daily precipitation of the base period (1981-2005) and RCP26 scenario (2025-2099) of Rib

As is observed from Figure 4.4, in the RCP2.6 2060s scenario, a high reduction of precipitation will be observed in February, March, and December (82.7%, 43.9%, and 41.5%) and a minimum reduction will be in September and July (12.9%, 16.7%) respectively. October and April will show an increase by 67.4% and 44.0% respectively. The highest increase will be in Bega by 55.3%, and a slight decrease in Krimt by 3.78% compared to the base period in the 2060s. The smaller annual reduction will be in the 2060s with a value of 1.9%. In the 2090s, March and September will show a decrease by 57.3% and 26.6%, whereas February, April, December, and January will show an increase by 60.9%, 59.3%, 53.1%, and 48.7 % respectively. Generally, the 2090s of the RCP2.6 scenario will show a slight increase in precipitation than the other two scenarios (2030s and 2060s). With regard to seasonal change, Bega and Belg will show an increase by 20.6% and 2.6% respectively and kiremt will show a decrease by 5.0%. The mean annual decrease is about 2.4%.

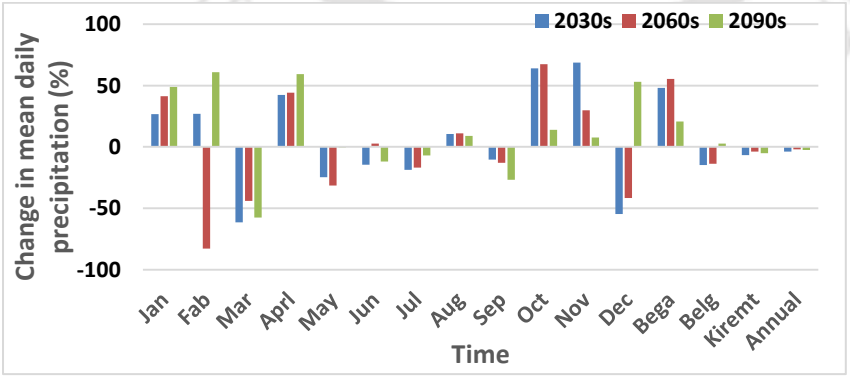

Figure 4-4 Percentage change in monthly, seasonal, and annual mean daily precipitation in RCP2.6 scenarios from 2025-2099 and baseline period (1981-2005) of Rib

4.3.2.2 Precipitation in RCP4.5 scenario

Bega precipitation will show an increasing trend whereas Belg, Kiremt, and Annual precipitation will have a decreasing trend in all scenarios. The change in the 2030s varies between -44.9% in October to 63.8% in January. The Bega months of December, January, and February will show an increase in the 2030s by 23.3%, 63.6%, and 58.9% respectively. In the 2060s the range of variation is between -57.9% in May to 66.2% in November. March and January shows the highest decrease and increase with 64.3% and 69.6% respectively in the 2090s. There is a consistent decrease in precipitation in Belg and Kiremt seasons by 19.0%, 40.9%, and 37.8%, and 2.2%, 8.5%, and 4.7% in the 2030s, 2060s and 2090s respectively.

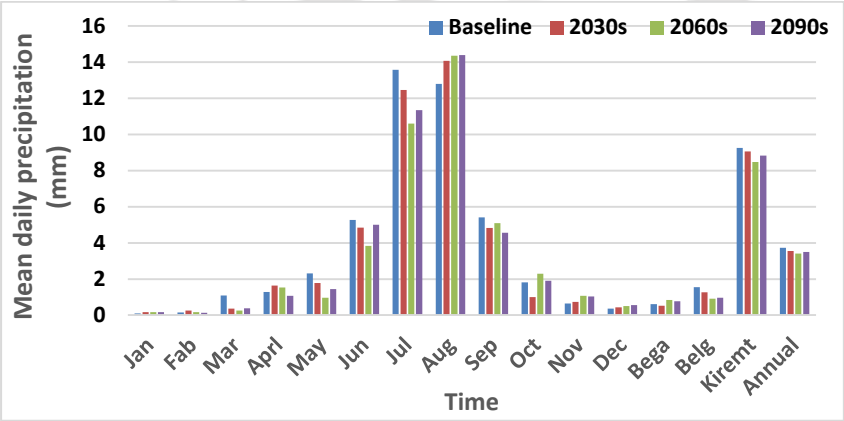

Figure 4-5 Monthly, seasonal and annual mean daily precipitation of the base period and the RCP4.5 scenarios (2025-2099) of Rib

The annual precipitation shows a decrease in all RCP4.5 scenarios, as seen in (Figure 4.6) with percentage values of 4.9%, 8.78%, and 6.2% in the 2030s, 2060s, and 2090s respectively. In general, except in the Bega season, all other seasons and the mean annual precipitation shows a reduction in the RCP4.5.

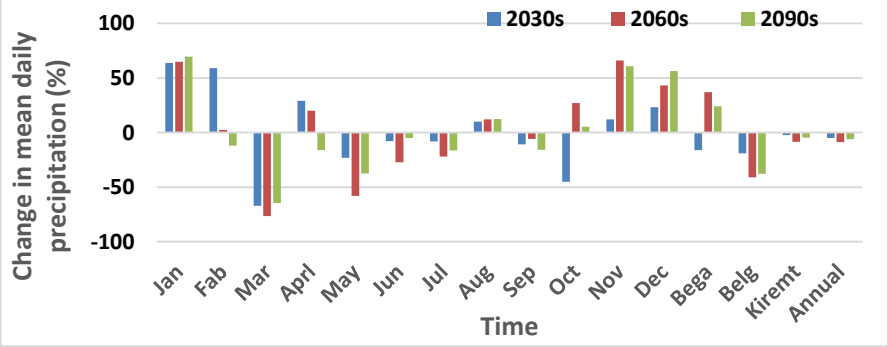

Figure 4-6 Change in monthly, seasonal, and annual mean daily precipitation in RCP4.5 (2025-2099) from the base period (1981-2005) Rib

4.3.2.3 Precipitation in RCP8.5 scenario

The months of January, August, September, October, and November will show an increase in all scenarios of RCP8.5, whereas March, April, June, and July shows a decreasing trend. The change in December and February is not consistent, and varies between (+9.1%, -33.1%, +37.2%) and (-10.6%, +17.7% and +36.6%) in 2030s, 2060s and 2090s respectively. In the 2030s precipitation varies between +62.9% in January to -54.7% in May and in the 2060s it varies between +77.6% in January to -69.7% in March. The highest increase in the 2090s will be in January by +79.26% and the highest decrease in May by 77.0%. A higher increase will be observed in January and November by 62.9%, 77.6%, and 79.3%, and 68.6%, 58.9%, and 33.6% in the 2030s, 2060s, and 2090s respectively. A high decrease will be in March by 63.6%, 69.7% 77.0% in the 2030s, 2060s, and 2090s respectively. There will be a continuous increase in Bega by 37.5%, 18.9%, and 23.6% and decrease in Belg by 44.0%, 34.7%, and 65.4% in the 2030s, 2060s, and 2090s respectively. The Kiremt and the mean annual precipitation will show an increase of 3.4% and 0.8% in the 2030s and a decrease of 3.7% and 5.4% in 2060s and 13.9%, 16.7% in the 2090s respectively.

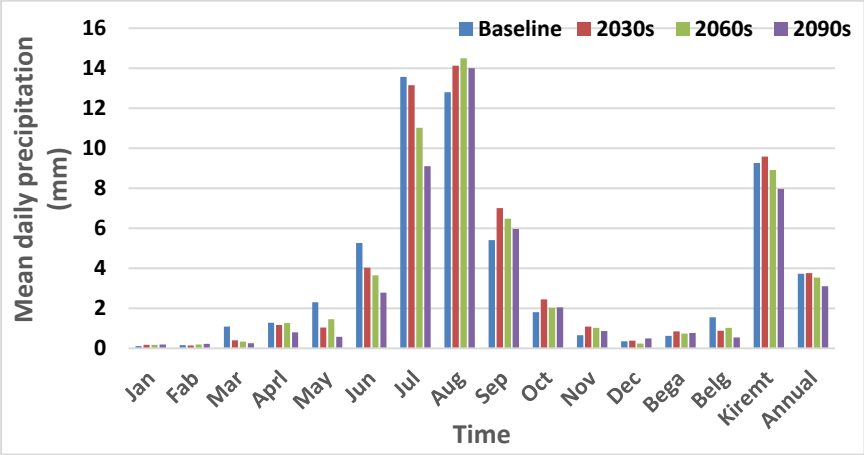

Figure 4-7 Monthly, seasonal and annual mean daily precipitation in the RCP8.5 (2025-2099) and the base period (1981-2005) in Rib

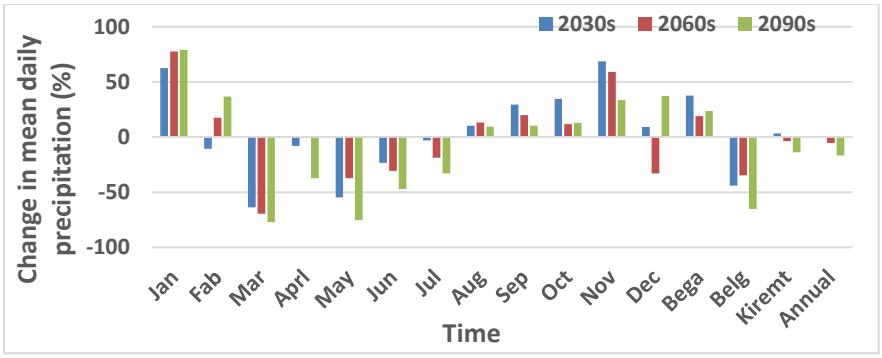

Figure 4-8 Change in monthly, seasonal, and annual mean daily precipitation in RCP8.5 scenarios (2025-209) from the base period (1981-2005) in Rib

In general the precipitation of the watershed shows a decreasing trend in all scenario periods (Figure 4-10). A brief illustration about the change compared to the baseline period and the trend in precipitation in all scenario periods (A1B and RCPs) in Rib is presented in Figure 4-9 and 4-10 respectively.

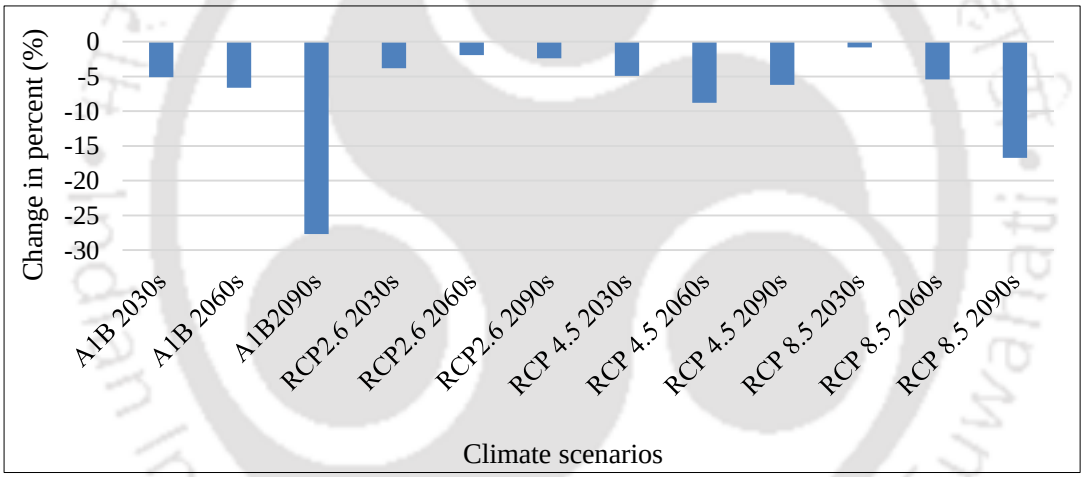

Figure 4-9 The percentage change in precipitation in all scenario periods in Rib

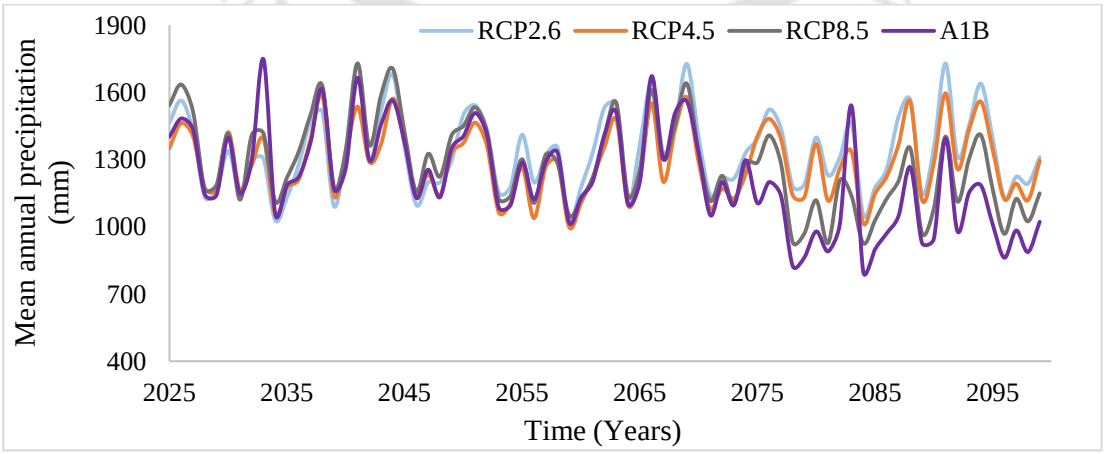

Figure 4-10 Future trend of mean annual precipitation of Rib in A1B and RCP scenarios

4.3.2.4 Projected temperature in the A1B scenario, Rib

The projected maximum temperature shows an increasing trend in all A1B scenarios (Figure 4-11). Mean monthly maximum temperature varies from +0.9°C to +1.87°C in 2030s, +2.1°C to +2.9°C in 2060s and +3.4°C to +4.65°C in 2090s. A high increase by 1.87°C, 2.94°C, and 4.65°C will be observed in May in the 2030s, 2060s, and 2090s respectively. The seasonal and annual average increase in maximum temperature will be observed in the projected scenarios. The Belg shows the highest increase by +1.58°C in 2030s, 2.8°C in 2060s, and 4.5°C in the 2090s. The increase of the Bega temperature will be +1.17°C in the 2030s, +2.55°C in the 2060s, and 4.1°C in the 2090s. There will be an increase in Kirmet season in all the scenarios by 1.3°C, 2.47°C, and 4.1°C in the 2030s, 2060s, and 2090s respectively. The annual average increasing trend varies between 1.3°C in the 2030s to 4.16°C in 2090s (Figure 4-11)

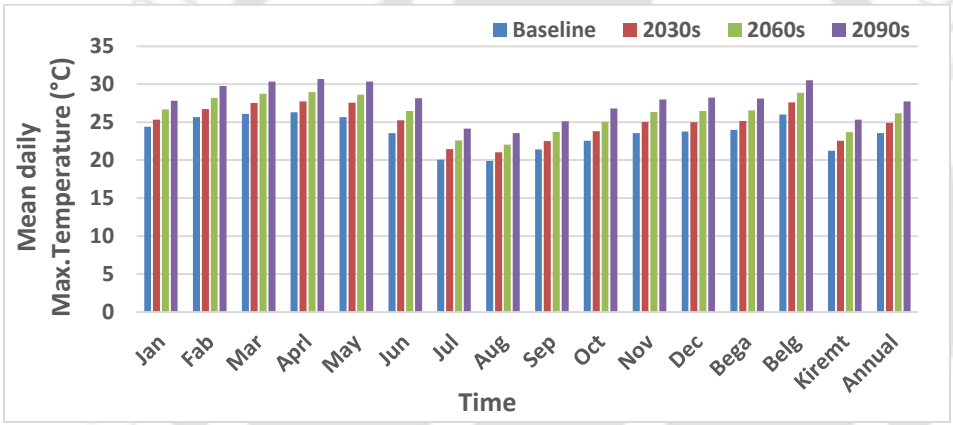

Figure 4-11 Observed (1981-2005) and A1B scenario projected (2025-2099) monthly, seasonal and annual mean daily maximum temperature of Rib

The projected seasonal maximum temperature indicated a consistent increase in Bega, Kiremt and annual basis, in both scenarios for all time periods in the watershed (Figure 4-12)

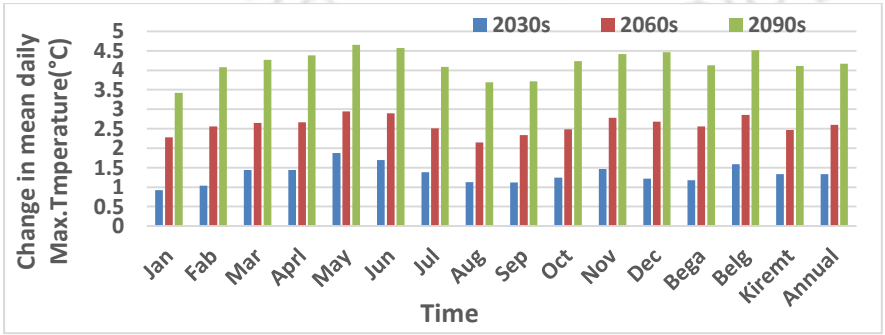

Figure 4-12 Change in monthly, seasonal and annual mean daily maximum temperature in the A1B scenario (2025-2099) compared to the baseline (1981-2005) in Rib

There will be a consistent increase in the minimum temperature in all scenario periods and months except in August in the 2030s. August will show a minor decrease in the 2030s (Figure 4.13 and 4.14). Mean monthly minimum temperature varies between -0.01°C in August to +2.67°C in June during the 2030s, +1.1°C in August to +4.0°C in May during the 2060s, and +2.95°C in August to +4.65°C in June during the 2090s.

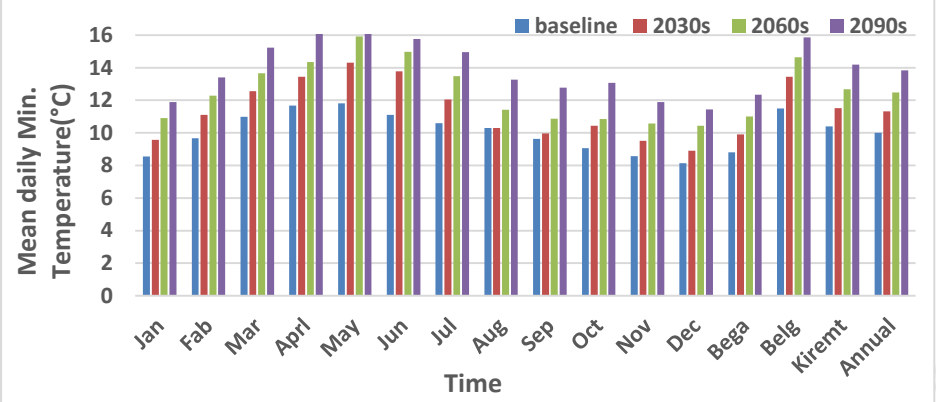

Figure 4-13 Observed (1981-2005) and A1B scenario projected (2025-2099) monthly, seasonal and annual mean daily minimum temperature in rib

On the other hand, June shows a higher increase almost in all scenarios. It is clearly seen that June and July of the Kiremt season show a higher increase than August and September of the same season (Figure 4.13 and 4.14).

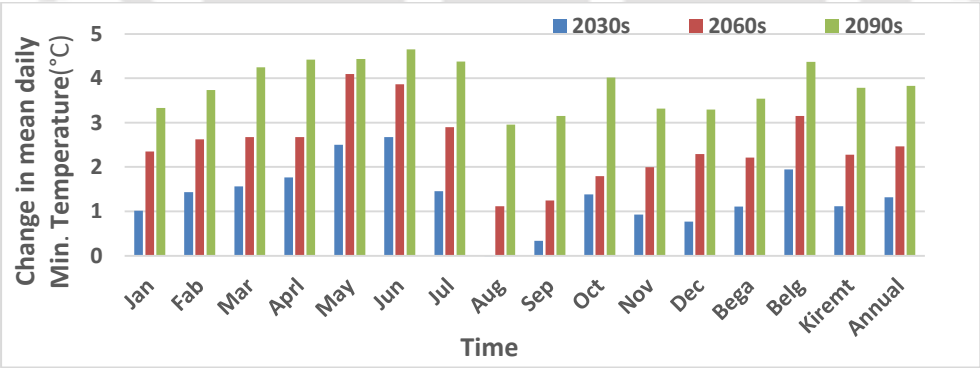

Figure 4-14 Change in monthly, seasonal and annual mean daily minimum temperature in A1B scenario (2025-2099) compared to the baseline (1981-2005) in Rib

In terms of seasons, Belg shows a higher minimum temperature increase by +1.94°C, +3.14°C, and +4.36°C during 2030s, 2060s, and 2090s. Bega shows the lowest increase by +1.1°C in the 2030s, +2.2°C in the 2060s, and +3.5°C in the 2090s. There will be a consistent increase in Kirmet in all time slices of the A1B scenario by +1.1°C, +2.27°C, and +3.78°C in

the 2030s, 2060s, and 2090s respectively. The average annual increase will be +1.3°C in the 2030s, +2.5°C in 2060s, and +3.8°C in the 2090s (Figure 4.14).

4.3.2.5 Temperature of Rib in the RCP2.6 scenario

Overall the maximum and minimum temperature in all RCP scenarios show an increasing trend. The maximum increase in temperature is observed in the 2090s scenario. Maximum temperature varies between +0.7°C in March to +2.0°C in June in the 2030s, +1.0°C in March to +1.87°C in May in 2060s and +0.75°C in March to +1.8°C in November 2090s. The Lowest increase will be observed in March in all scenarios (Figure 4.15 & 4-16).

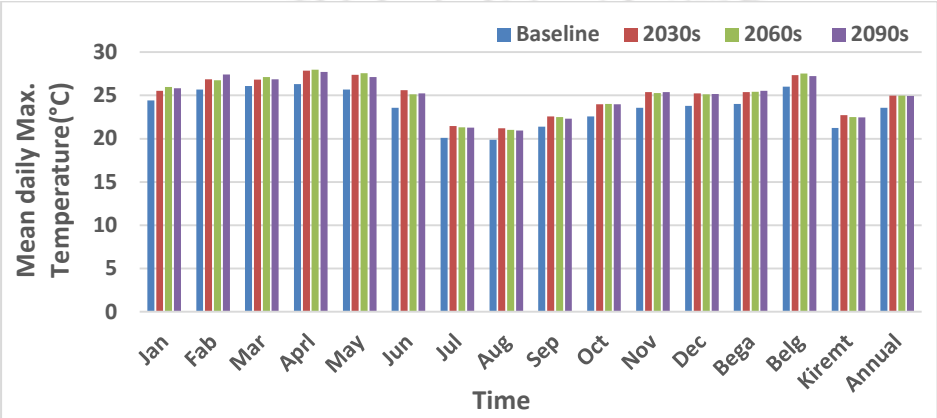

Figure 4-15 Observed (1981-2005) and RCP2.6 scenario projected (2025-2099) mean daily maximum temperature of Rib

The projected scenario indicated that there will be a variation between the seasonal and annual increase in maximum temperature (Figure 4.15). High increase in Bega and Belg seasons will be observed in the 2090s and 2060s respectively. The highest increase in Kiremt season will be observed in the 2030s. The Belg temperature increase varies between +1.3°C in 2030s, +1.5°C in 2060s, and 1.2°C in 2090s. The increase in Bega temperature varies between +1.39°C in the 2030s, +1.4°C in 2060s, and 1.55°C in the 2090s. The increase in maximum temperature in Kirmet will be 1.47°C, 1.26°C, and 1.2°C in the 2030s, 2060s, and 2090s respectively. The annual average increasing trend varies between 1.4°C in the 2030s to 1.35°C in the 2090s.

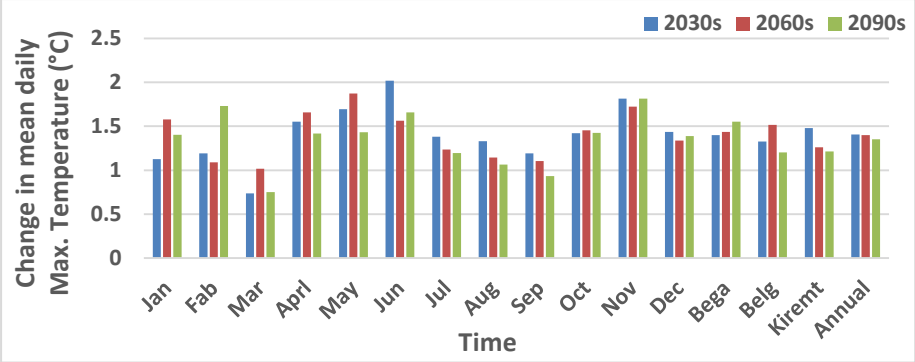

Figure 4-16 Change in monthly, seasonal and annual mean daily maximum temperature in the RCP2.6 (2025-2099) compared to the baseline period (1981-2005) in Rib

The lowest increase in minimum temperature will be observed in August by +0.5°C, +0.7°C, and +0.6°C in the 2030s, 2060s, and 2090 respectively. The month of May shows a higher increase in minimum temperature in the 2030s and 2060s by + 2.43°C and +2.47°C respectively. The highest increase will be in March with a value of +2.0°C in the 2090s.

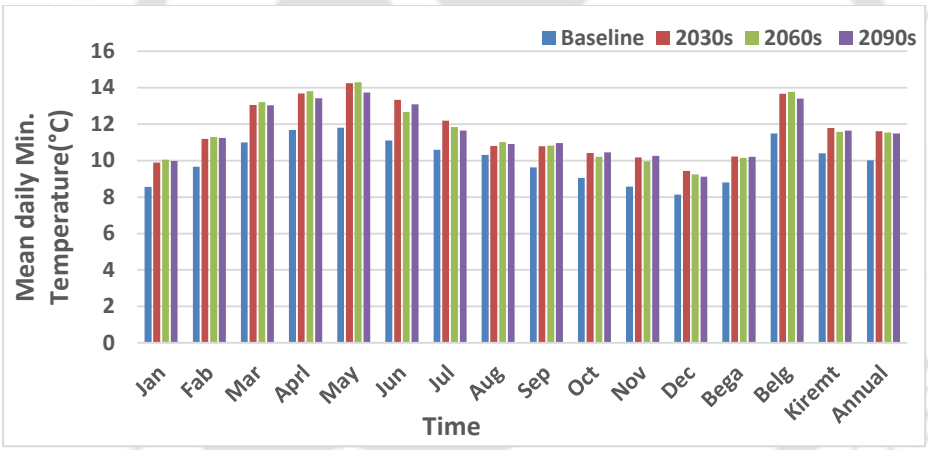

Figure 4-17 Observed (1981-2005) and RCP2.6 scenario projected (2025-2099) monthly seasonal, and annual minimum temperature of Rib

The Bega maximum temperature is increase by 1.4°C, 1.35°C, and 1.4°C in the 2030s, 2060s, and 2090s respectively. With respect to seasons, Belg shows a higher minimum temperature increase by +2.16°C, +2.27°C, and +1.9°C during the 2030s, 2060s, and 2090s (Figure 4.18). Kiremt will experience a lower increase with values of +1.37°C, +1.17°C, and +1.24°C in the 2030s, 2060s, and 2090s. The highest annual increase in the RCP2.6 scenarios will be in the 2030s by +1.59°C and the lowest increase in the 2090s by +1.47°C.

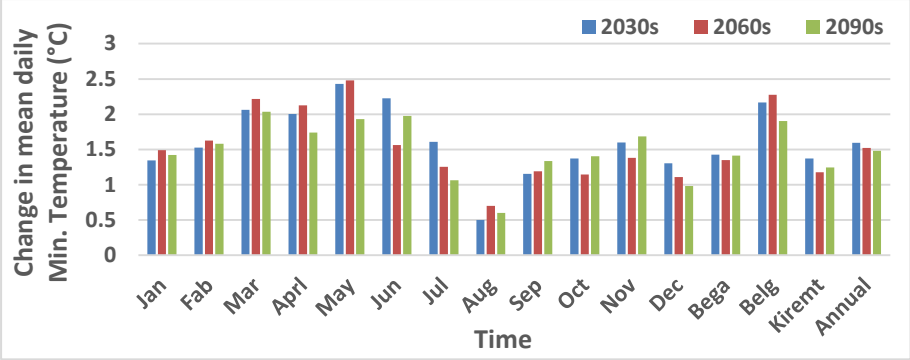

Figure 4-18 Change in monthly, seasonal and annual mean daily minimum temperature in the RCP2.6 scenario compared to the baseline period in Rib

4.3.2.6 Temperature of Rib in the RCP4.5 scenario

Temperature shows an increase in all of the RCP4.5 scenarios. The increase in maximum temperature in the 2030s varies between +1.30°C in December to +1.99°C in November. March shows the lowest increase by +1.63°C and +1.93°C, and June shows the highest increase by +2.87°C and +2.98°C in the 2060s and 2090s respectively.

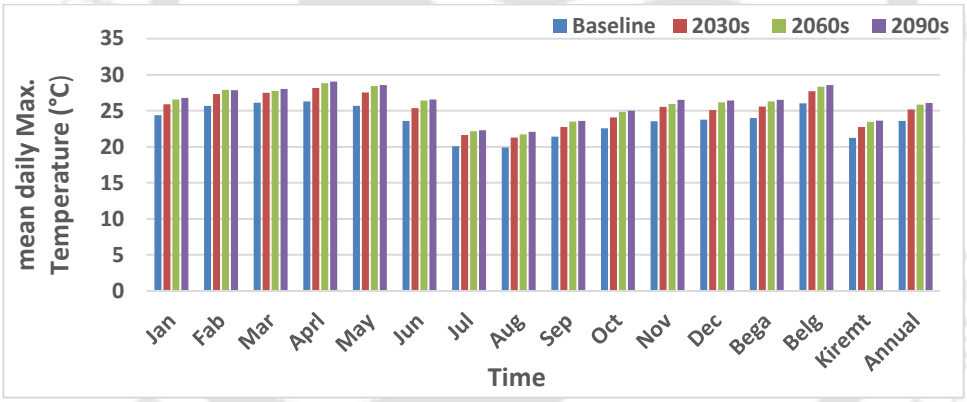

Figure 4-19 Observed (1981-2005) and RCP4.5 scenario projected (2025-2099) monthly seasonal, and annual maximum temperature of Rib

In the RCP4.5 scenario, all seasons (Bega, Belg, and Kiremt) shows an increase of temperatures. The Bega, Belg and Kiremt maximum temperature increase in the 2030s, 2060s, and 2090s respectively were +1.59°C, 2.29°C, 2.53°C; +1.7°C, + 2.3°C, +2.52°C, and +1.52°C, + 2.22°C, +2.39°C. The annual increase will vary between +1.59°C in the 2030s to +2.49°C in the 2090s.

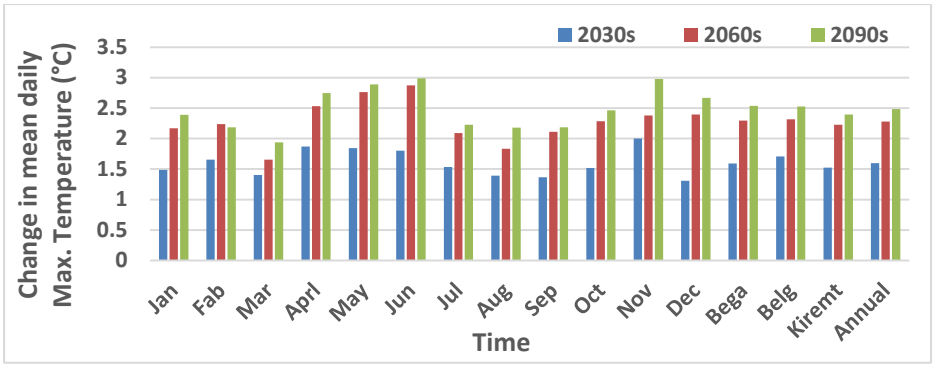

Figure 4-20 Change in monthly, seasonal and annual mean daily maximum temperature in the RCP4.5 compared to the base period in Rib

The high minimum temperature increase will be observed in July in RCP4.5 with values of +2.16°C, 3.2°C, and +3.0°C in the 2030s, 2060s, and 2090s respectively, and the low increase will be observed in December with values of +1.17°C, +1.9°C in 2030s and 2090s. The lowest increase with 1.57°C will be in November in the 2060s. The variation in minimum temperature increase in the 2060s is between +1.57°C to +3.21°C in November and July and in 2090s is between +1.9°C, to +3.0°C in December and July respectively.

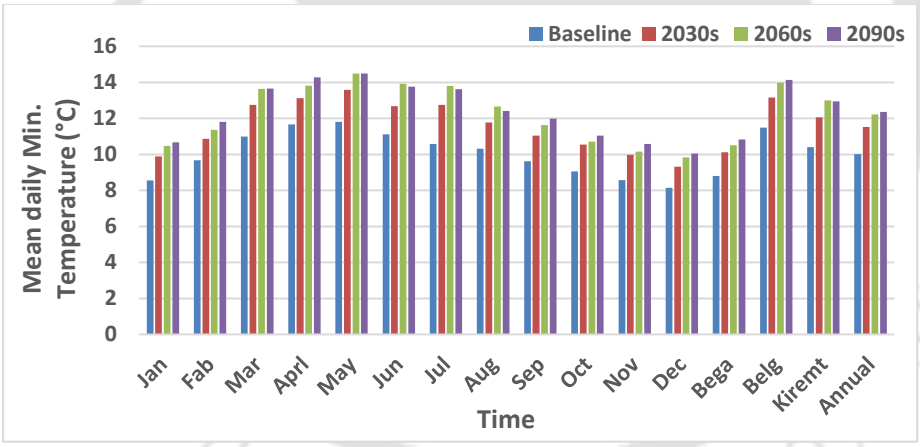

Figure 4-21 Observed (1981-2005) and RCP4.5 scenario projected (2025-2099) monthly, seasonal and annual mean daily minimum temperature of Rib

There will be a continuous increase in Bega, Belg, and annual minimum temperatures. The Bega and Belg minimum temperature increase in the 2030s, 2060s, and 2090s respectively will be +1.3°C, +1.7°C, +2.0°C and +1.66°C, + 2.49°C, +2.64°C. The highest increase in Kiremt will be +2.59°C in the 2060s and the lowest increase is +1.6°C in the 2030s. The annual minimum temperature increase ranges between +1.5°C to +2.35 °C in the 2030s and 2090s respectively.

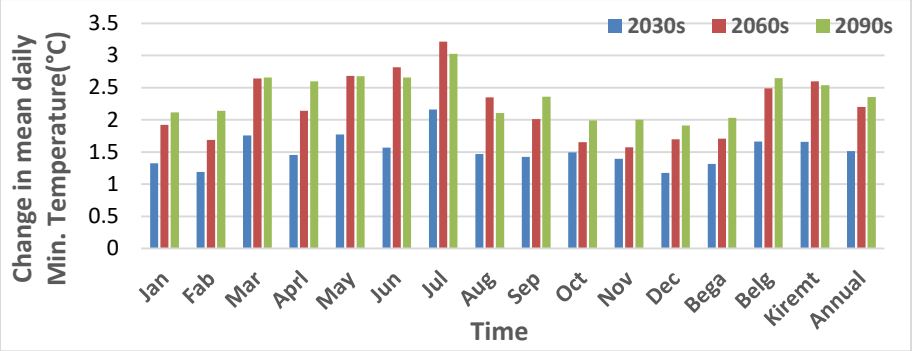

Figure 4-22 Change in monthly, seasonal and annual mean daily minimum temperature in the RCP4.5 compared to the base period in Rib

4.3.2.7 Temperature of Rib in the RCP8.5 scenario

In the RCP8.5 scenario, higher maximum and minimum temperature increase will occur in the 2060s and 2090s, with the highest in the 2090s. The monthly and annual increases will be continuous and consistent in all RCP8.5 time slices. The maximum temperature increase ranges between +1.25°C to +2.54°C in March and May in the 2030s; 2.96°C to +4.29°C in August and May in 2060s, and +4.5°C to +4.98°C in August and June in 2090s. May and June will experience a higher increase in the RCP8.5.

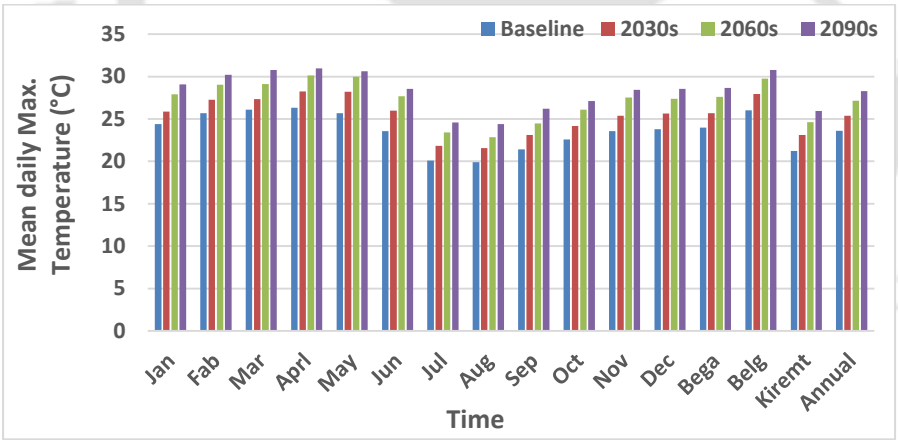

Figure 4-23 Observed (1981-2005) and RCP8.5 scenario projected (2025-2099) monthly, seasonal and annual mean daily maximum temperature of Rib

Belg will show the highest increase by +1.9°C, +3.7°C, and +4.75°C in the 2030s, 2060s, and 2090s respectively. The Bega and Kiremt increase in maximum temperature in the 2030s, 2060s and 2090s respectively were +1.66°C, +3.58°C, +4.67°C and +1.87°C, 3.37°C, +4.69°C. The annual increase in maximum temperature will be +1.79°C, +3.55°C, and +4.7°C in the 2030s, 20605, and 2090s respectively.

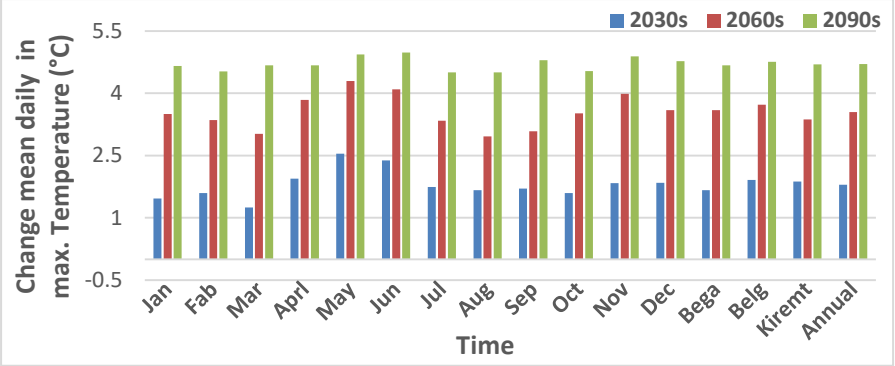

Figure 4-24 Change in monthly, seasonal and annual mean daily maximum temperature of the RCP8.5 scenarios compared to the base period in Rib

Minimum temperature varies between +0.9°C to +2.36°C in September and June in the 2030s, +2.6°C to +4.79°C in September and July in the 2060s and +4.1°C, to 4.99°C in December and July in the 2090s. September will experience a lower minimum temperature increase in 2030s and 2060s. The highest temperature increase will be in minimum temperature than the maximum temperature in all months of the 2090s with an increase of greater than +4.5°C.

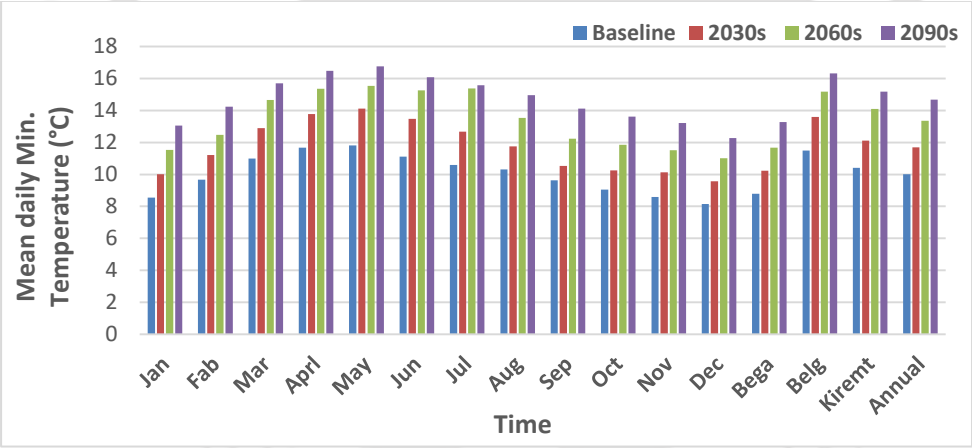

Figure 4-25 Observed (1981-2005) and RCP8.5 scenario projected (2025-2099) monthly, seasonal and annual mean daily minimum temperature of Rib

The Bega, Belg, Kiremt and annual minimum temperature increase in the 2030s, 2060s, and 2090s respectively were +1.43°C, +2.88°C, +4.48°C; +2.1°C, +3.69°C, +4.82°C; +1.7°C, +3.69°C, +4.78°C and +1.69°C, +3.38°C, +4.67°C (Figure 4.26).

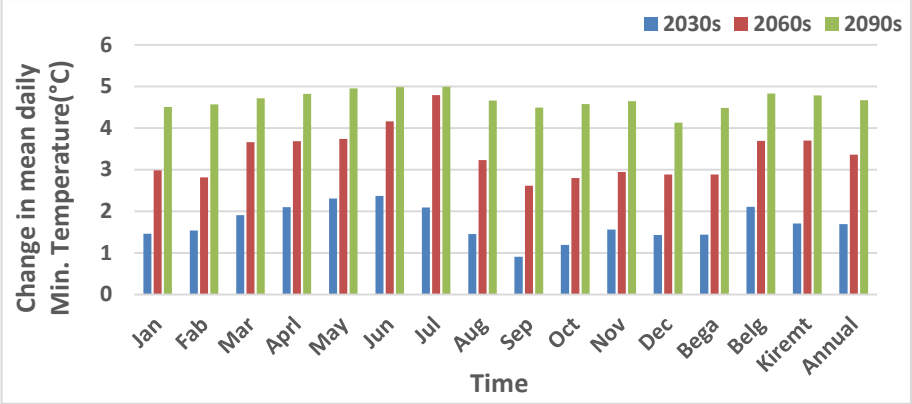

Figure 4-26 Change in monthly, seasonal and annual mean daily minimum temperature in the RCP8.5 scenarios and the base period in Rib

The percentage of variation of maximum and minimum temperatures between scenario periods and the trend of increase in all scenarios (A1B and RCPs) in Rib is illustrated in Figure 4-27 and 4-28 respectively as follows.

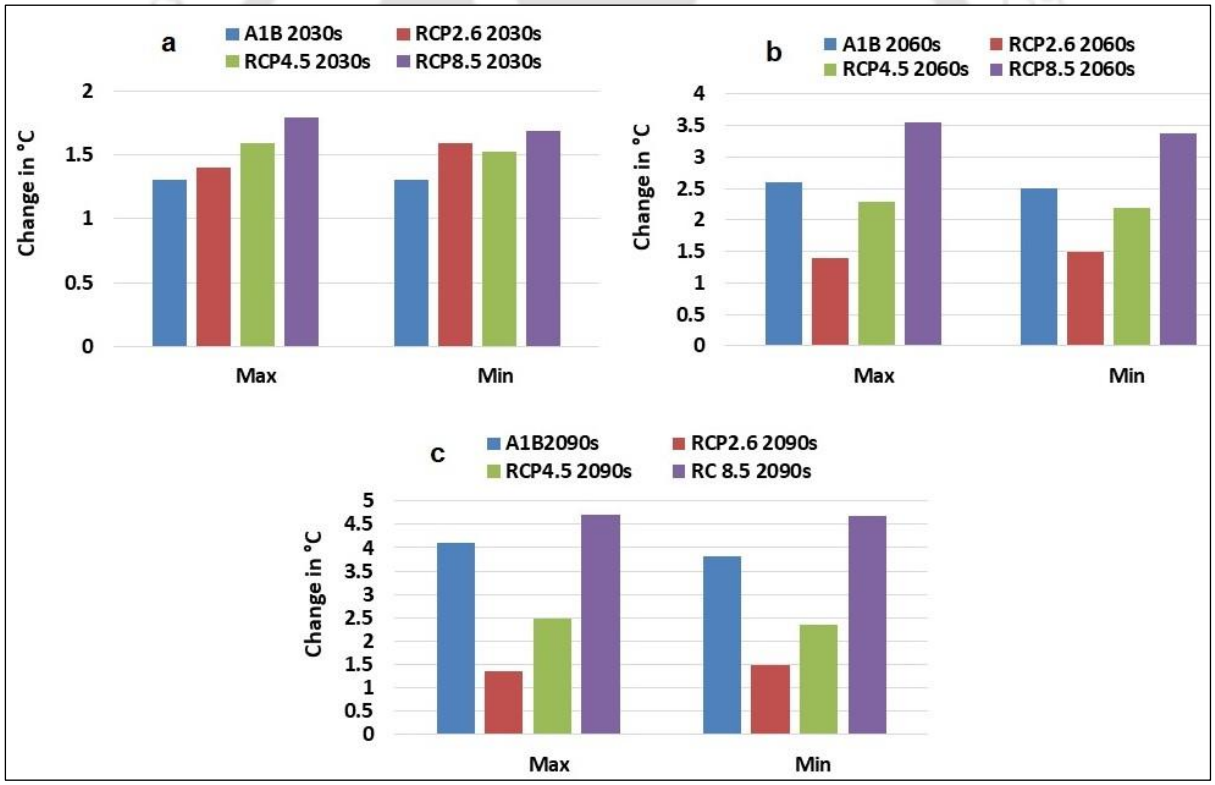

Figure 4-27 Change in maximum and minimum temperatures in all scenarios (A1B and RCPs) from the base period in the 2030s (a), 2060s (b) and 2090s (c), Rib

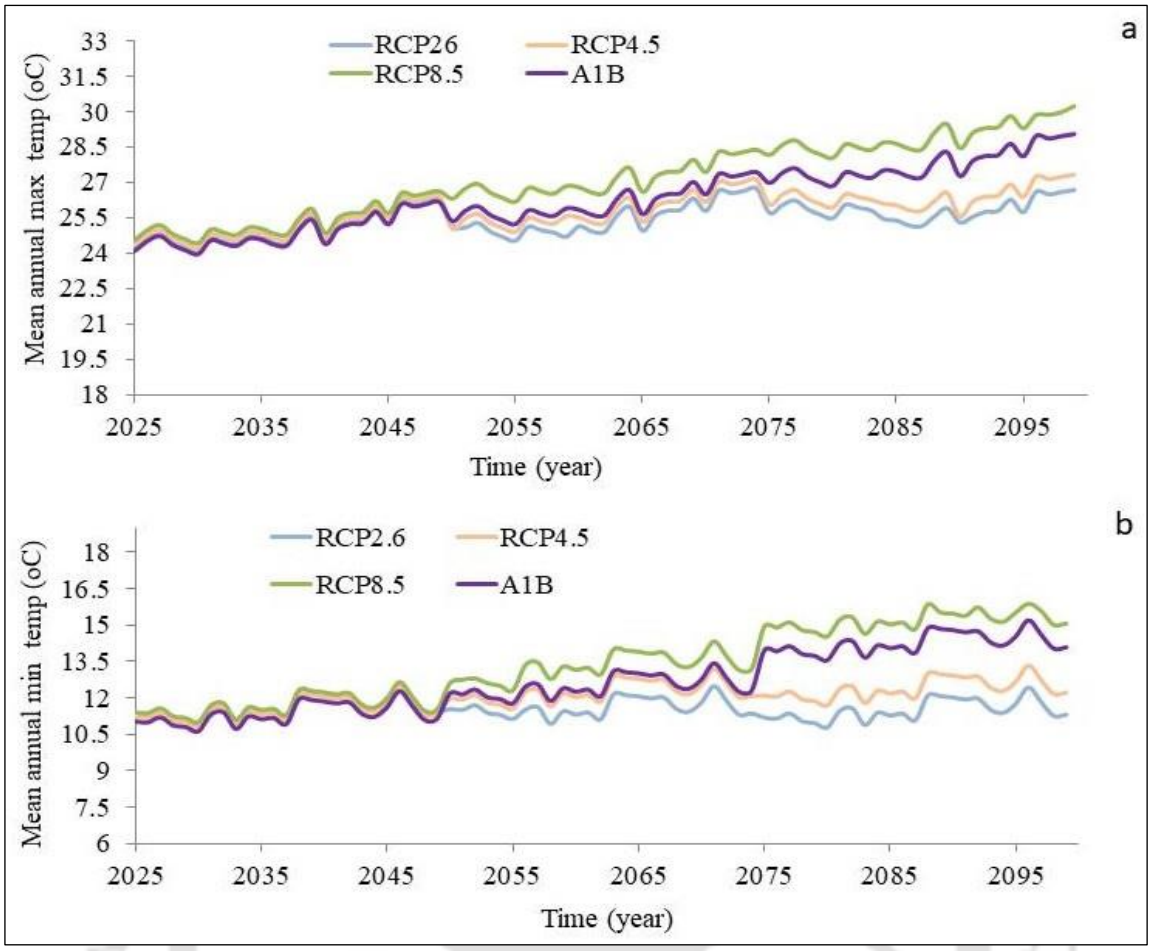

Figure 4-28 Future trend of mean annual max (a) and min (b) temperature of Rib in A1B, RCP2.6, RCP4.5 and RCP8.5 scenarios

4.3.3 Precipitation projection in Gumara

4.3.3.1 Precipitation in the A1B scenario

The climate analysis results (Figure 4.29 and 4.30) showed a general decrease in mean annual precipitation in the A1B scenario. In the 2030s December, January August, and November show an increase of precipitation by 73.6%, 34.7%, 11.5%, % 5.2%, and 67.5 % respectively from the baseline period. In the 2030s high precipitation decrease will occur in February, May, and March by 43%.7, 40.9%, and 35.3% reactively. A low reduction in precipitation will be observed in September by 1.1% in the 2030s from the baseline period. The change in precipitation varies between -43.3% in February to 73.6% in December in the 2030s, -39.1% in March to 48.3% in December in the 2060s, and -63.3% in June to 64.9% in November in the 2090s respectively.

December, October, November, September, February, and August will show an increase of precipitation in the 2060s by 48.3%, 40.9%, 25.9%, 13.2%, 4.9%, and 3.6% respectively. The highest decrease in precipitation will be shown in March by 39.1%, followed by May by 31.1%. In the 2090s, December, November, January, and September will show an increase by of 77.1%, 64.9%, 67.3, 0.4% respectively. Other months will show a reduction within a range between -4.6 % to -63.3% in August and June of the 2090s. The highest reduction will be shown in June, April, May, March, and July by 63.3%, 61.1%, 57.1%, 40.7%, and 38.7 respectively.

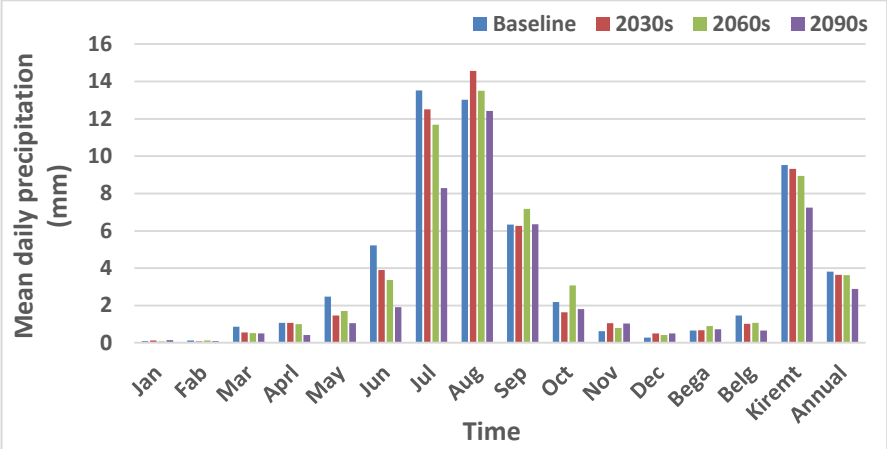

Figure 4-29 Monthly, seasonal and annual mean daily precipitation in the A1B scenario and base period of Rib

There will be a decrease in seasonal and annual precipitation in all time slices except Bega. In Bega, there will be an increase by 2.1%, 35.7%, and 8.5% in the 2030s, 2060s, and 2090s. The highest reduction will be shown in Belg by 30.1%, 26.7%, and 54.9% in the 2030s, 2060s, and 2090s respectively. Kiremt will show decrease by 2.2% & 23.9% in the 2030s and 2090s and increase by 6.2% in 2060s. Generally, the projected precipitation in Gumara watershed shows a decreasing trend in A1B scenario.

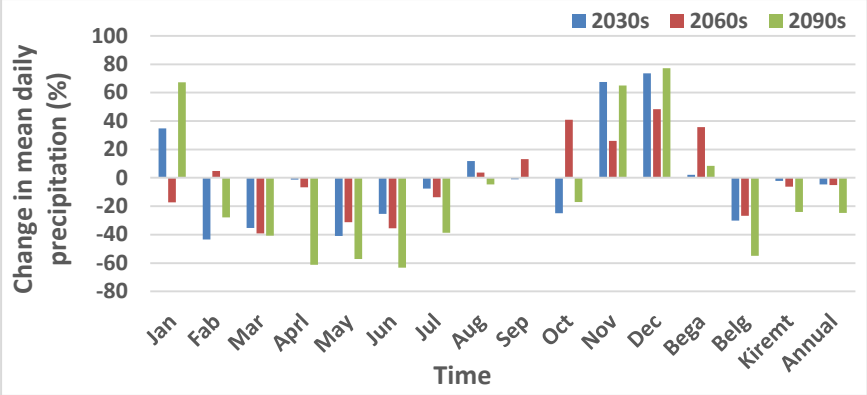

Figure 4-30 Percentage change in monthly, seasonal, and annual mean daily precipitation between 2025-2099 of the A1B scenario compared to the base period (1981-2005) in Gumara

4.3.3.2 Precipitation in RCP2.6 scenario

The mean annual precipitation will show a slight decrease over the watershed (Figure 4-31 & 4-32). In the RCP2.6, the change in mean monthly precipitation varies between -62.6% in March to 74.7% in January in the 2030s, -52.0% in February to 76.4% in October in the 2060s, and -57.6% % in March to 65.8% in April in the 2090s. High decrease will be observed in March, December, and May by 62.57%, 54.59%, and 25.29%, and a minimum decrease will be observed in September, June, and July by 9.7%, 16.1%, and 21.3% respectively in the 2030s. There will be an increase in January, October, February, November, April, and August by 74.7%, 71.9, 66.1%, 60.9%, 50.1%, and 11.4% respectively in the 2030s. There is significant seasonal variation in predicted precipitation. Bega will show an increase between 20.6% in the 2090s to 58.7% in the 2030s. Belg will show a decrease of 13.6% in the 2060s and 14.7% in the 2030s.

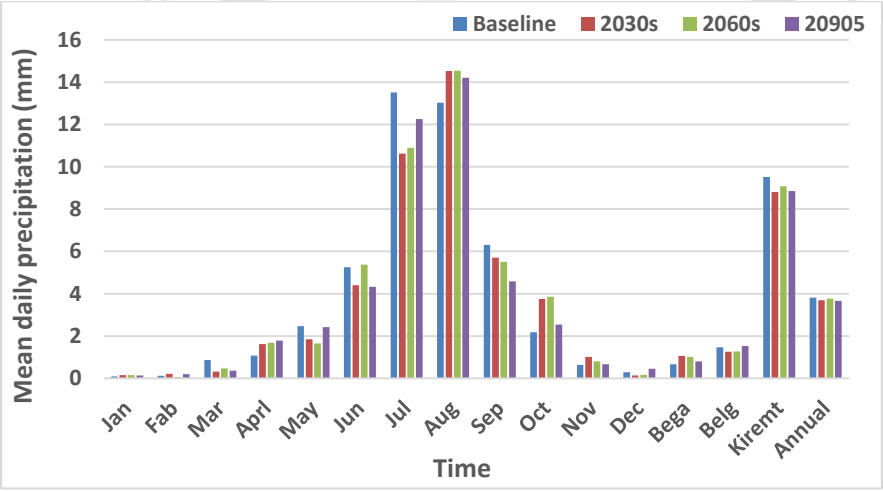

Figure 4-31 Monthly, seasonal and annual mean daily precipitation of the base period (1981-2005) and RCP26 scenario (2025-2099) of Gumara

There will be a decrease in Kiremt by 7.4% and 7.0% in 2030s and 2090s. The average annual decrease varies between -3.3% to -4.0% in 2030s and 2090s (Figure 4-32).

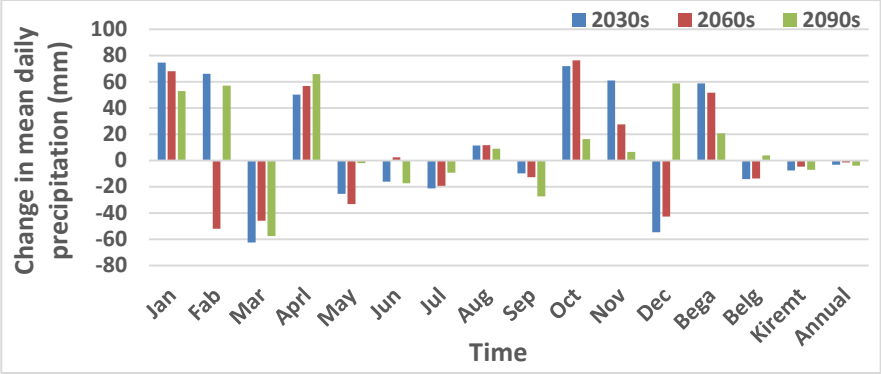

Figure 4-32 Percentage change in monthly, seasonal, and annual mean daily precipitation in the RCP2.6 scenario (2025-2099) compared to the base period (1981-2005) in Gumara

4.3.3.3 Precipitation in RCP4.5 scenario

In the 2030s the highest decrease and increase will be observed in March and January by 69.0% and 80.7% respectively (Figure 4-33). The high reduction will be observed in March, May, and June by 77.3%, 58.6%, and 32.4% respectively, and a low reduction will be observed in February and September by of 3.7%, 6.3% respectively in the 2060s. November, January, and December will show a high increase by 79.1%, 72.3%, 69.9% respectively in the 2060s.

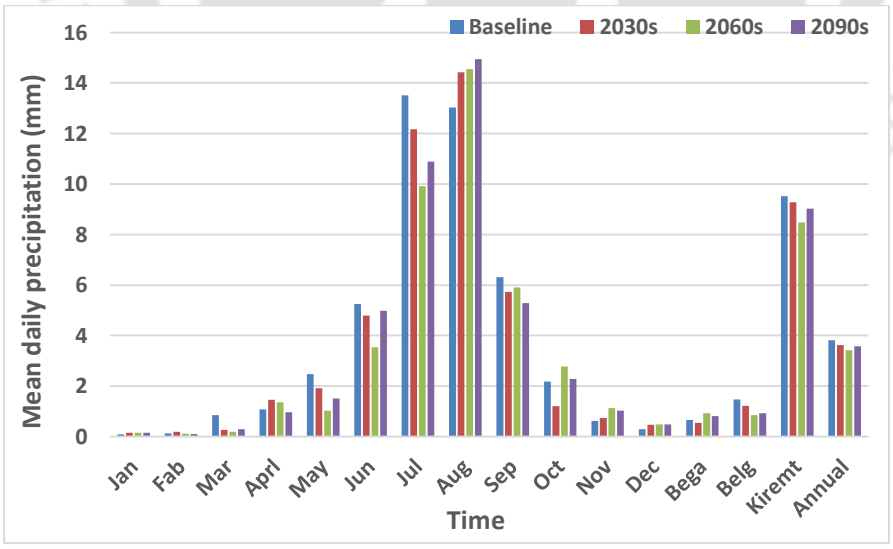

Figure 4-33 Monthly, seasonal and annual mean daily precipitation in RCP4.5 scenario ((2025-2099) and the base period (1981-2005) in Gumara

In the 2090s, the change in precipitation varies between -65.1% in March to 76.2% in January. March shows the highest decrease by 69.0%, 77.3%, and 65.1% and January shows the highest increase by 80.7%, 72.3%, and 76.2% in the 2030s, 2060, and 2090s respectively.

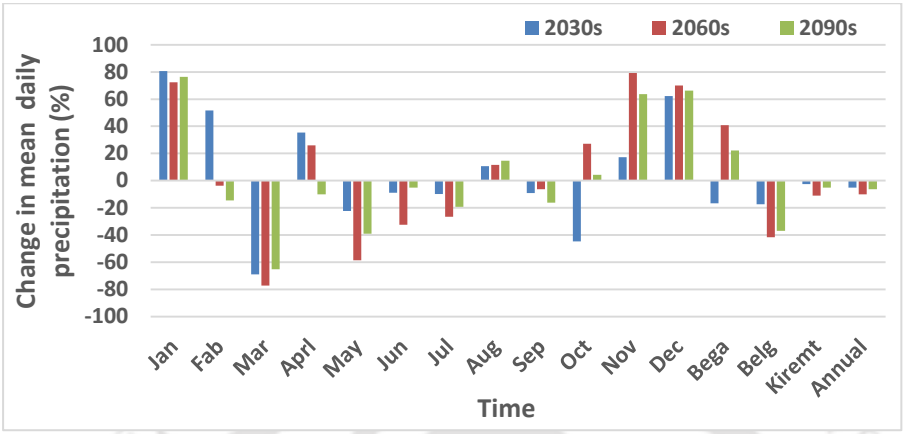

Figure 4-34 Change in monthly, seasonal, and annual mean daily precipitation in RCP4.5 scenario (2025-2099) compared to the base period (1981-2005) in Gumara

The Bega will show an increasing by 40.8% and 22.1% in the 2060s and 2090s whereas Belg, Kiremt, and Annual precipitation will show a decreasing trend in all time slices. There will be a consistent decrease in Belg by 17.2%, 41.6%, and 37.0% in the 2030s, 2060s, and 2090s respectively. There will be a highest decrease in Kiremt by 10.9% in the 2060s followed by 5.2% and 2.5% in the 2090s and 2030s respectively. The average annual precipitation will show a reduction in the RCP4.5 as presented in Figure 4-34 by values of 5.0%, 10.2%, and 6.3% in the 2030s, 2060s, and 2090s respectively. Except Bega all other seasons and the annual precipitation will show a reduction in the RCP4.5.

4.3.3.4 Precipitation in RCP8.5 scenario

January, August, September, October, and November will show an increase in all time slices of the RCP8.5, whereas March, May, June, and July will show a decreasing trend. In the 2030s the variation will be between -65.3% in March to 83.4 % in January and in 2060s it will be -70.4% in March to 84.8% in November.

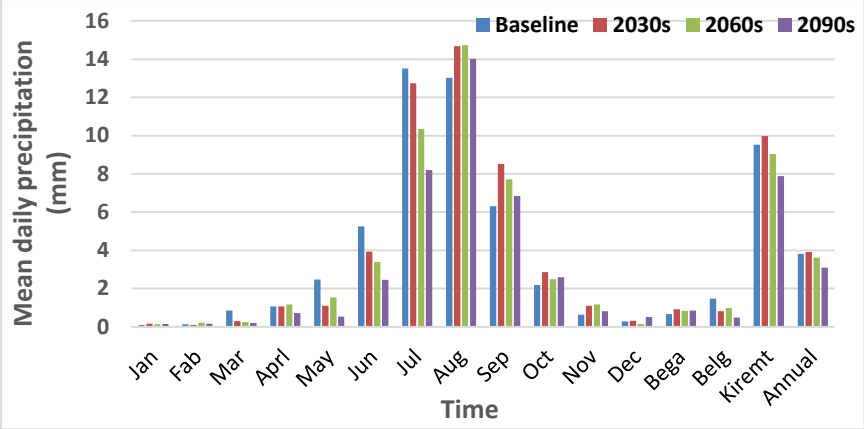

Figure 4-35 Monthly, seasonal and annual mean daily precipitation in the RCP8.5 scenario (2025-2099) and the base period (1981-2005) in Gumara

In the 2090s change in precipitation varies between -78.7% in May to 81.3% in December. There will be an increase in the Bega by 37.0%, 25.4%, and 28.4 in the 2030s, 2060s, and 2090s respectively. The Belg and Kiremt will show a decrease by 43.9%, 32.8%, 67.6% and 4.6%, 5.0%, 17.2% in 2030s, 2060s and 2090s respectively. There will be an annual increase by 2.3% in the 2030s and a decrease by 5.4% in the 2060s and 18.7% in the 2090s.

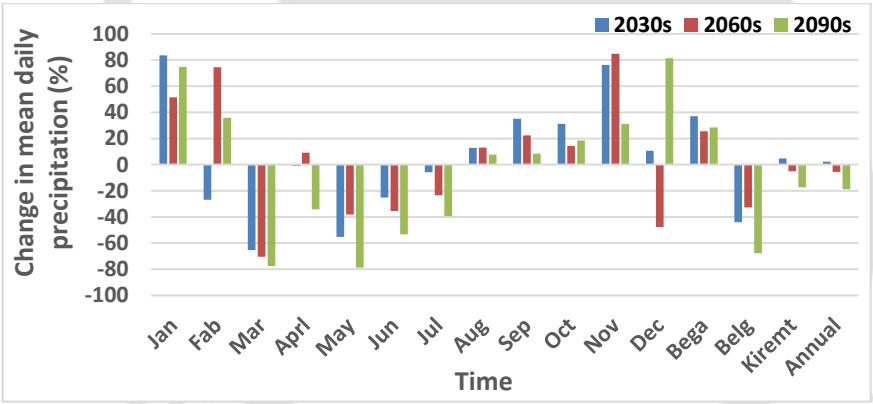

Figure 4-36 Change in monthly, seasonal, and annual mean daily precipitation in the RCP8.5 scenario (2025-2099) compared to the base period (1981-2005) in Gumara

The percentage of change compared to the baseline period, variation between scenario periods, and the trend of precipitation in all scenarios (A1B and RCPs) in Gumara is illustrated in Figure 4-37 and 4-38 as follows.

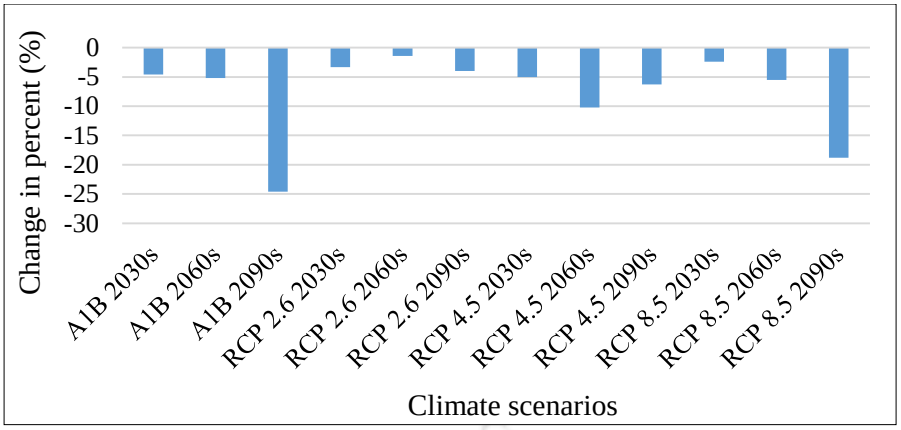

Figure 4-37 The percentage change in precipitation in all scenario periods in Gumara

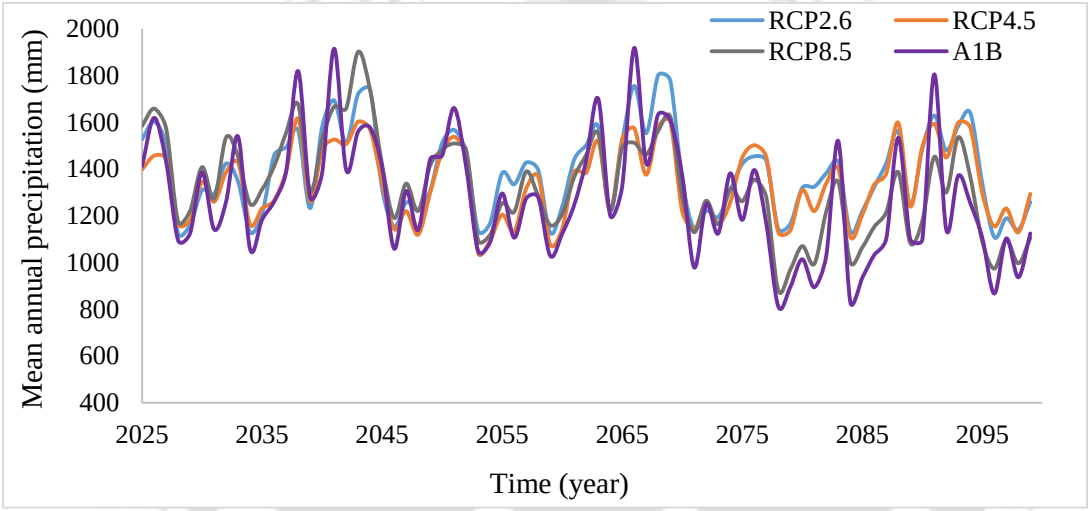

Figure 4-38 Future trend of mean annual precipitation of Gumara in A1B, RCP2.6, RCP4.5, and RCP8.5 scenarios

4.3.4 Projected temperature of Gumara

4.3.4.1 Projected temperature in the A1B scenario

Increasing maximum temperature will be shown in A1B scenarios (Figure 4-39 and 4-30). Monthly maximum temperature varies between + 0.92°C to +1.93°C in 2030s, + 2.06°C to +3.3°C in 2060s and + 3.39°C to +4.96°C in 2090s. A high increase will be observed in May by 1.93°C, 3.3°C, and 4.96°C in the 2030s, 2060s, and 2090s and a low increase in January by 0.92°C and 3.39°C in the 2030s and 2090s and in August by 2.0°C in the 2060s.

The seasonal and annual average increase in maximum temperature will be observed in the projected scenario. There will be Belg increase by +1.6, +2.8, and +4.5 in the 2030s, 2060s,

and 2090s respectively. The Bega temperature will increase by +1.2°C in the 2030s, +2.57°C in the 2060s, and 4.1°C in the 2090s. The Kirmet temperature will increase in A1B scenario by 1.29°C, 2.4°C, and 4.0°C in the 2030s, 2060s, and 2090s respectively. The annual average increasing trend varies between 1.3°C in the 2030s to 4.18°C in the 2090s.

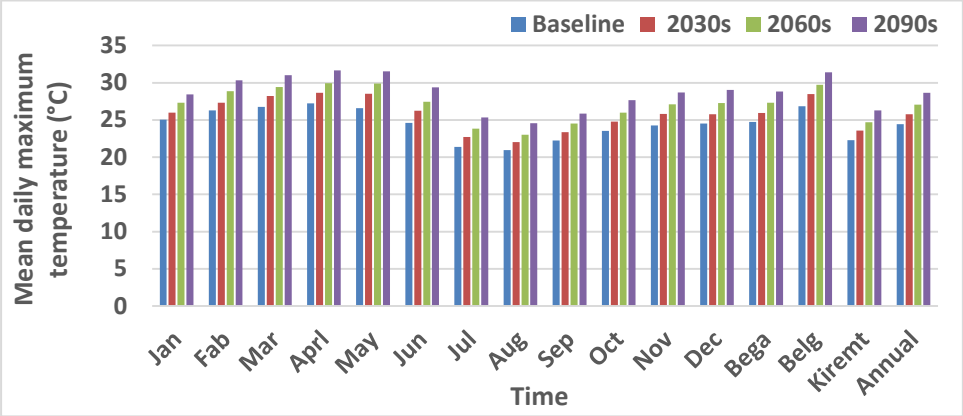

Figure 4-39 Observed (1981-2005) and A1B scenario projected (2025-2099) monthly, seasonal and annual mean daily maximum temperature of Gumara

The projected seasonal maximum temperature (Figure 4-40) indicated that there will be a consistent increase in the Bega (1.19°C, 2.57°C, and 4.1°C), Kiremt (1.6°C, 2.88°C, and 4.55°C), and annual (1.33°C, 2.59°C, and 4.18°C) in the 2030s, 2060s, and 2090s respectively.

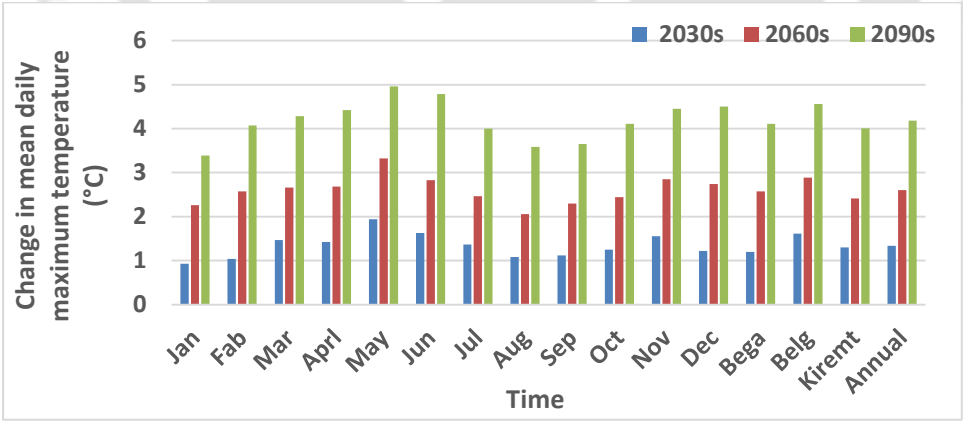

Figure 4-40 Change in monthly, seasonal and annual mean daily maximum temperature in the A1B scenario (2025-2099) compared to the baseline (1981-2005) in Gumara

There will be a consistent increase in the minimum temperature in all time slices and months except in August in the 2030s. August shows a minor decrease (0.05%) in the 2030s of the A1B scenario (Figure 4-42).

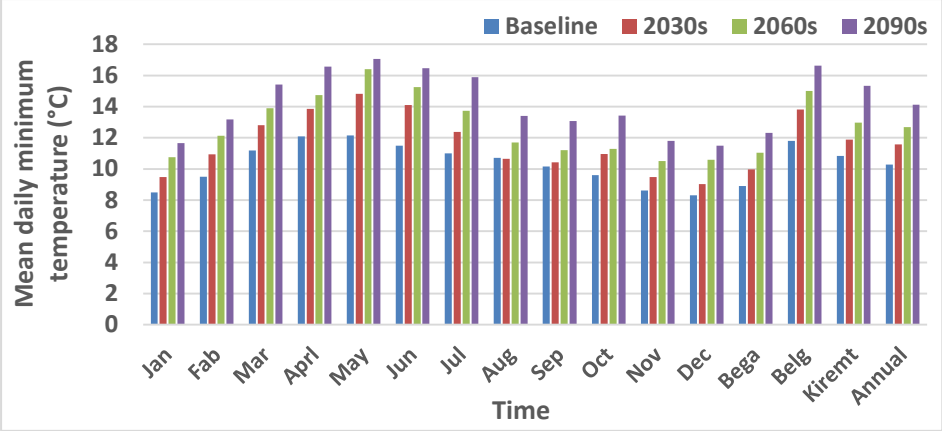

Figure 4-41 Observed (1981-2005) and A1B scenario projected (2025-2099) monthly, seasonal and annual mean daily minimum temperature of Gumara

The minimum temperature decrease by 0.05% in August and increase by +2.66°C in May in the 2030s. The increase in in minimum temperature varies between +0.98°C in August to +4.24°C in May in the 2060s and +2.68°C in August to +4.98°C in June in the 2090s. In the 2030s, August shows a slight decrease by 0.05%, and it shows a lower increase than other months in the 2060s and 2090s. The month of May will show the highest increase by 2.66°C and 4.24°C in the 2030s and 2060s. In the 2090s June will show the highest increase by 4.98°C (Figure 4-42).

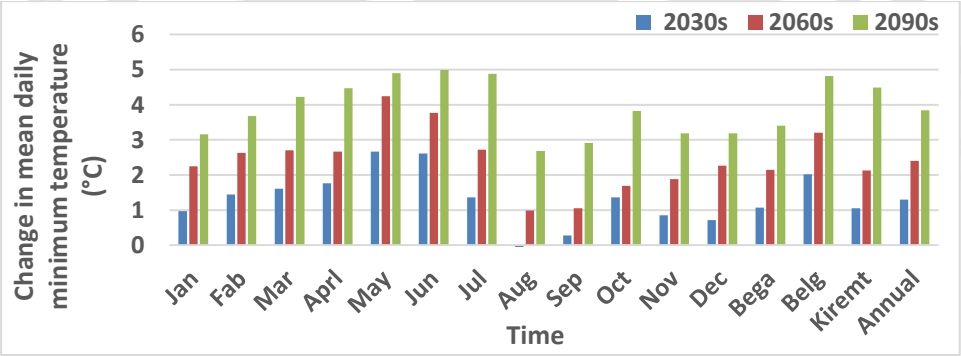

Figure 4-42 Change in monthly, seasonal and annual mean daily minimum temperature in the A1B scenario (2025-2099) compared to the baseline (1981-2005) in Gumara

The Belg season will show a higher minimum temperature increase by +2.0°C, +3.2°C, and +4.8°C in the 2030s, 2060s, and 2090s respectively. The increase of Bega temperature will be +1.0, +2.1, and +3.4 in The 2030s, 2060s, and 2090s. Kiremt will show a low minimum temperature increase by +1.0°C in the 2030s and +2.1°C in 2060s. In the 2090s the lowest increase will be in the Bega by +3.4°C. The average annual increase will be +1.29°C in the 2030s, +2.4°C in the 2060s, and +3.84°C in the 2090s (Figure 4-42).

4.3.4.2 Temperature in the RCP2.6 scenarios

The monthly maximum temperature increase varies between +0.94°C in March to +2.1°C in June in the 2030s, +1.12°C in September to +2.0°C in May in the 2060s and +0.92°C in September to +1.92°C in November in the 2090s. The lowest increase will be observed in March by 0.94°C in the 2030s, in September by 1.1°C in the 2060s, and in September by 0.92°C in 2090s (Figure 4-44)

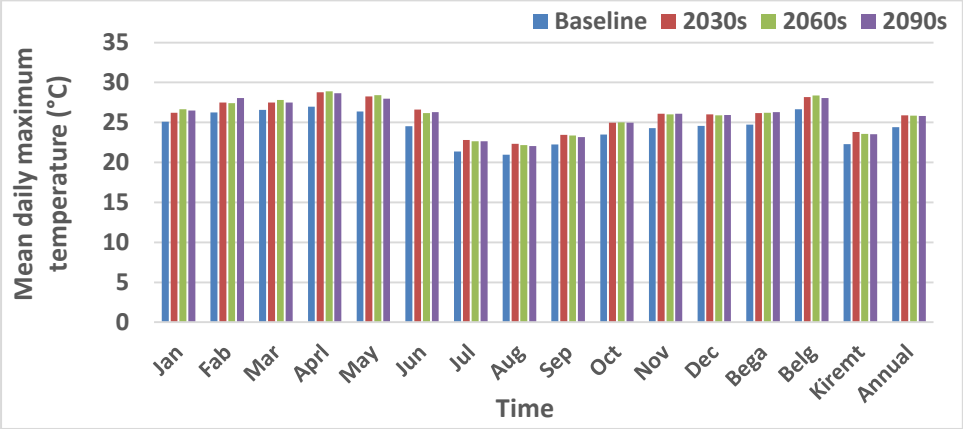

Figure 4-43 Observed (1981-2005) and RCP2.6 scenario projected (2025-2099) monthly, seasonal and annual mean daily maximum temperature of Gumara

Bega will show a high increase in the 2090s by 1.57°C and Belg by 1.73°C in the 2060s. Kiremt shows the highest increase in the 2030s by 1.5°C. The Bega temperature increase will be +1.4°C in the 2030s, +1.46°C in the 2060s, and 1.57°C in the 2090s. The increase in Kirmet will be +1.5°C, +1.3°C, and +1.25°C in the 2030s, 2060s, and 2090s respectively. The annual average increase will be 1.48°C in the 2030s and 2060s and 1.42°C in 2090s (Figure 4-44)

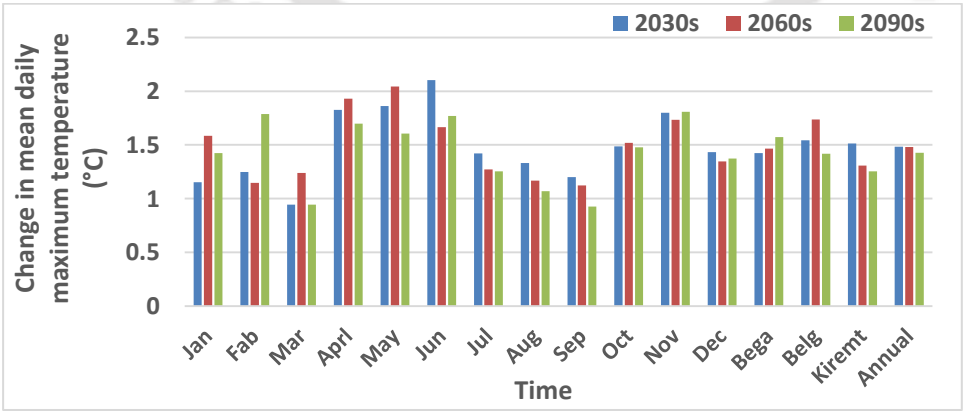

Figure 4-44 Change in monthly, seasonal and annual mean daily maximum temperature of the RCP2.6 scenario (2025-2099) compared to the baseline (1981-2005) in Gumara

The lowest minimum temperature increase will be observed in August by +0.55°C, +0.74°C, and +0.63°C in the 2030s, 2060s, 2090 respectively. The month of May will show a high increase by + 2.42°C and +2.48°C in the 2030s and 2060s respectively, and in the 2090s the highest increase will be in June by +2.0°C.

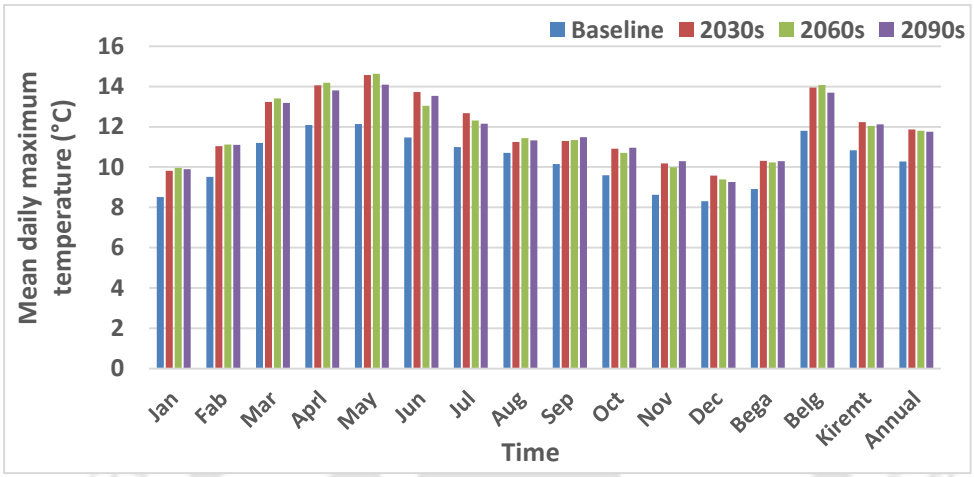

Figure 4-45 Observed (1981-2005) and RCP2.6 scenario projected (2025-2099) monthly, seasonal and annual mean daily minimum temperature of Gumara

Belg will show the highest minimum temperature increase by +2.14°C, +2.26°C, and +1.88°C in the 2030s, 2060s, and 2090s respectively. The lower seasonal increase was observed in Kiremt by +1.4°C, +1.2°C, and +1.29°C in the 2030s, 2060s, and 2090s time slices. The highest annual increase in the RCP2.6 will be observed in the 2030s by 1.58°C and the lowest increase by 1.48°C in the 2090s.

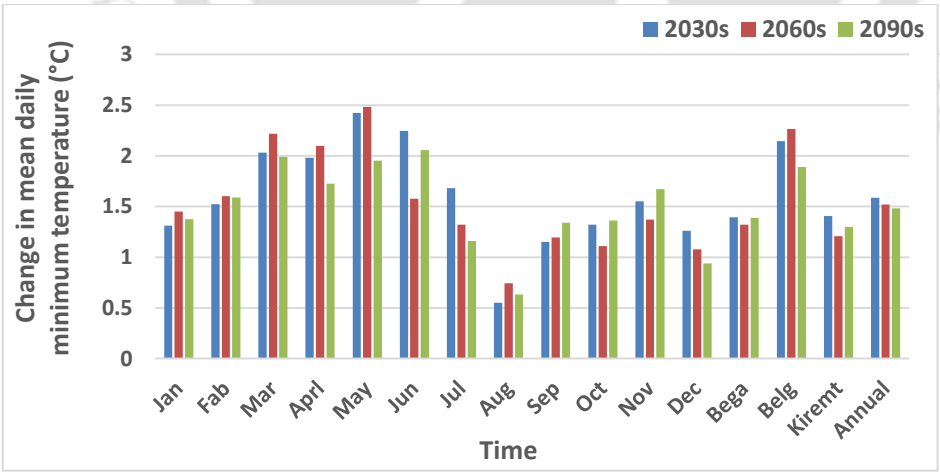

Figure 4-46 Change in monthly, seasonal and annual mean daily minimum temperature in the RCP2.6 scenario (2025-2099) compared to the baseline (1981-2005) in Gumara

4.3.4.3 Temperature in the RCP4.5 scenario

The increase in maximum temperature in the 2030s varies between +1.3°C in December to +2.13°C in April. In 2060s August and June show the lowest and highest increase by +1.86°C, and +3.0°C respectively. March shows the lowest increase by +2.14°C and November shows the highest increase by +3.0°C in the 2090s (Figure 4-48).

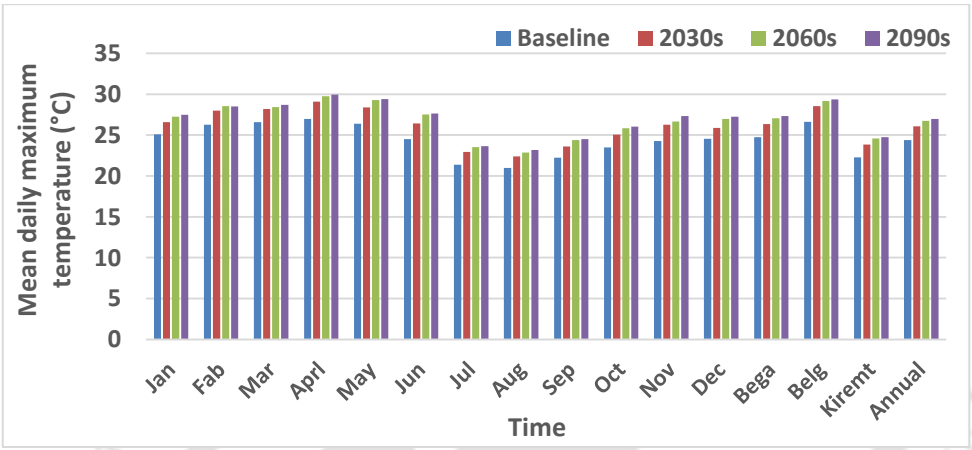

Figure 4-47 Observed (1981-2005) and RCP4.5 scenario projected (2025-2099) monthly, seasonal and annual mean daily maximum temperature of Gumara

The Bega, Belg and Kiremt maximum temperature in the 2030s, 2060s, and 2090s will increase by +1.61°C, 2.31°C, and 2.57°C; +1.91°C, + 2.52°C, and +2.72°C, and +1.56°C, + 2.29°C and +2.45°C respectively. There will be a continuous annual increase by +1.67°C and +2.57°C in the 2030s and 2090s respectively.

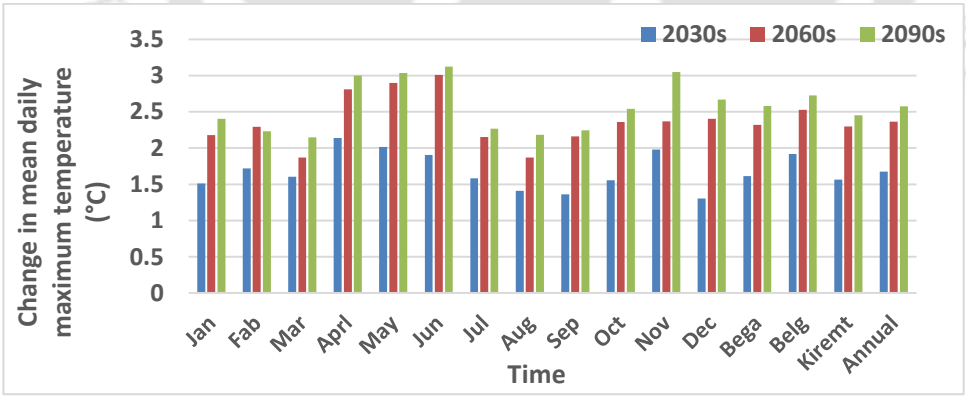

Figure 4-48 Change in monthly, seasonal and annual mean daily maximum temperature in the RCP4.5 scenario (2025-2099) compared to baseline (1981-2005) in Gumara

A high minimum temperature increase will be shown in July in all time slices of the RCP4.5 scenario with values of +2.2°C, 3.77°C, +3.37°C in the 2030s, 2060s, and 2090s respectively. A low increase will be in December in the 2030s and 2090s by +1.16°C, +1.91°C. The

increase in the 2030s varies between +1.16°C in December to +2.21°C in July. The increasing variation in the 2060s will be between +1.57°C in November to +3.77°C in July and in the 2090s between +1.91°C, in December to +3.37°C in July.

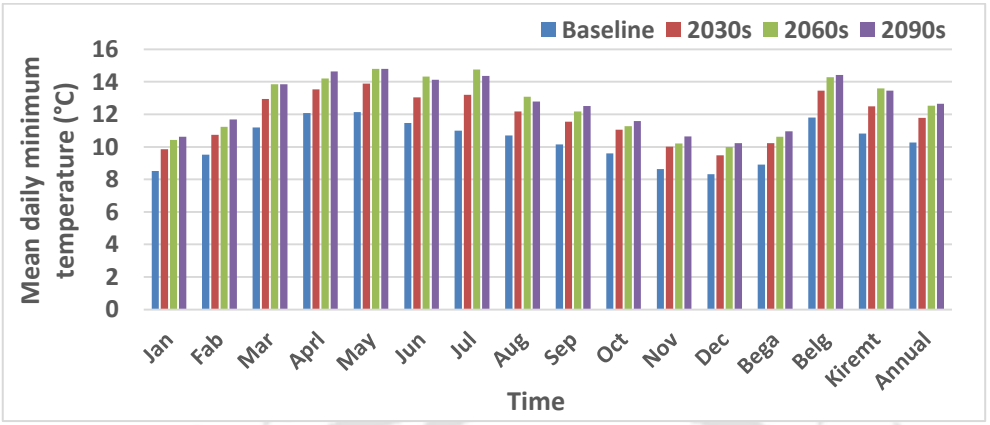

Figure 4-49 Observed (1981-2005) and RCP4.5 scenario projected (2025-2099) monthly, seasonal and annual mean daily minimum temperature of Gumara

The Bega and Belg increase in minimum temperature in the 2030s, 2060s and 2090s respectively will be +1.3°C, +1.7°C, and +2.0°C and +1.64°C, + 2.47°C, and +2.61°C. There will be a continuous annual increase by +1.51°C and +2.37°C in the 2030s and 2090s respectively. The highest increase in Kiremt will be +2.75°C in the 2060s. The annual increase in minimum temperature will be +1.51°C in the 2030s and +2.37°C in the 2090s.

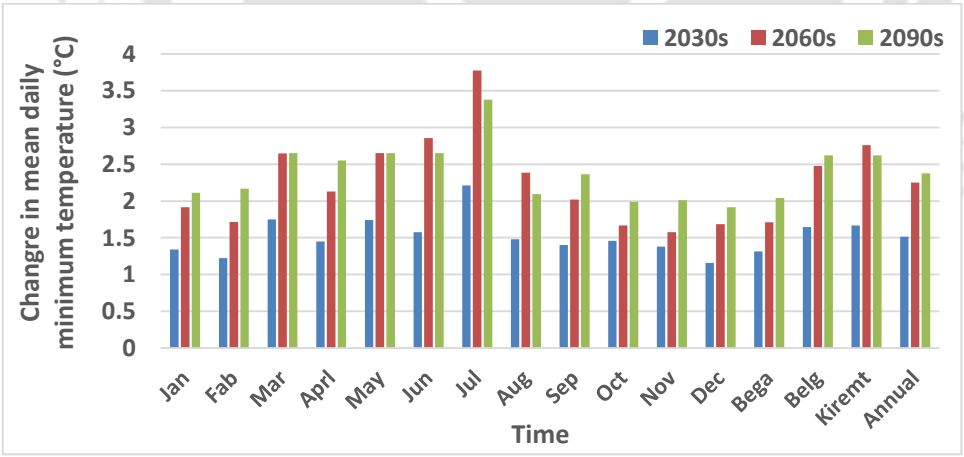

Figure 4-50 Change in monthly, seasonal and annual mean daily minimum temperature in the RCP4.5 scenario (2025-2099) compared to the baseline (1981-2005) in Gumara

4.3.4.4 Temperature in the RCP8.5 scenario

High maximum and minimum temperature increase will be observed in the 2060s and 2090s, with the highest in 2090s in RCP8.5 scenario. The maximum temperature increase varies between +1.46 °C to +2.68°C in March and May in the 2030s; +2.96°C to +4.45°C in August

and May in 2060s, and +4.5°C to +4.99°C in August and May in 2090s. August, May, and June will experience a higher temperature increase in the RCP8.5 scenario.

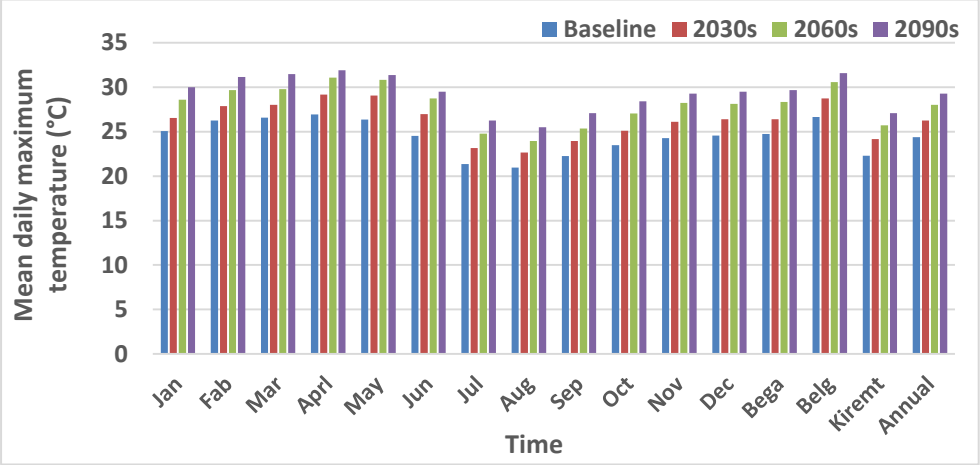

Figure 4-51 Observed (1981-2005) and RCP8.5 scenario projected (2005-2099) monthly, seasonal and annual mean daily maximum temperature of Gumara

When seasonal temperature changes are compared, Belg shows the highest increase by +2.1°C, +3.93°C, and +4.94°C in the 2030s, 2060s, and 2090s respectively. The Bega and Kiremt maximum temperature will increase in the 2030s, 20605 and 2090s by +1.67°C, +3.6°C, and +4.93°C and +1.9°C, 3.42°C, and +4.8°C respectively. The annual increase will be +1.86°C, +3.62°C, and +4.89°C in the 2030s, 20605, and 2090s.

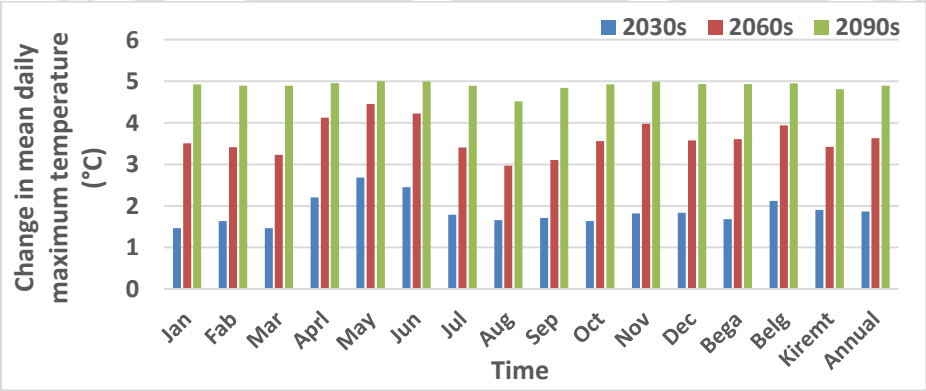

Figure 4-52 Change in monthly, seasonal and annual mean daily maximum temperature in the RCP8.5 scenario (2025-2099) compared to the baseline (1981-2005) in Gumara

The increase in minimum temperature varies between +0.86°C and +2.37°C in September and June in the 2030s, +2.59°C and +4.9°C in September and July in the 2060s and +4.1°C and 5.0°C in December and July in the 2090s respectively. The highest temperature increase will be in the minimum than the maximum temperature in the 2090s, and all months willhave shown an increase by greater than +4.1°C (Figure 4-54).

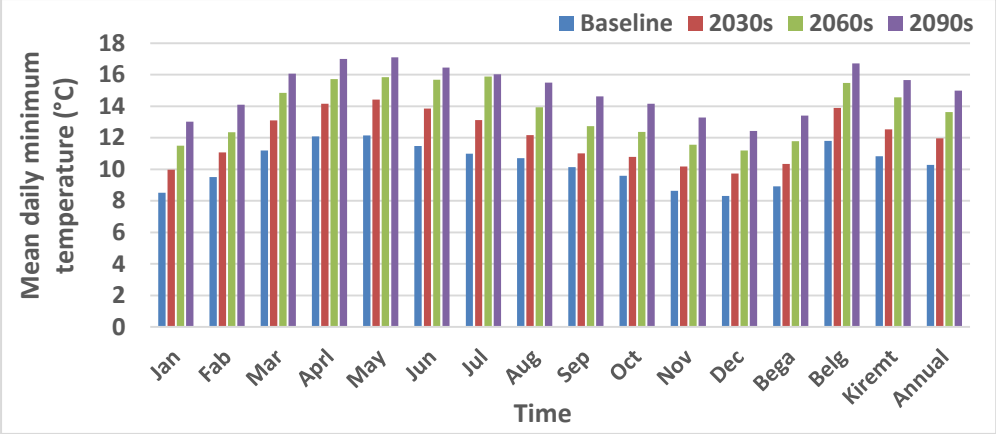

Figure 4-53 Observed (1981-2005) and RCP8.5 scenario projected (2025-2099) monthly, seasonal and annual mean daily minimum temperature of Gumara

The Bega, Belg, Kiremt and annual minimum temperature will increase in the 2030s, 2060s, and 2090s respectively by +1.43°C, +2.87°C and +4.48°C; +2.0°C, +3.66°C, and +4.9°C; +1.7°C, +3.73°C, and +4.82°C, and +1.68°C, +3.36°C, and +4.7°C.

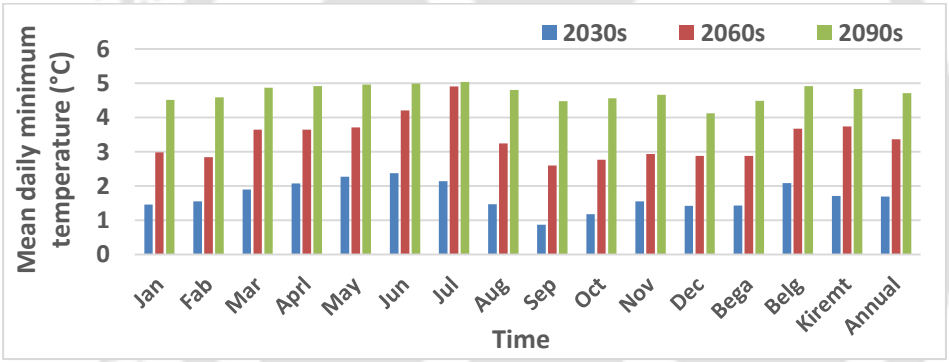

Figure 4-54 Change in monthly, seasonal and annual mean daily minimum temperature in the RCP8.5 scenario (2025-2099) compared to the baseline (1981-2005) in Gumara

The percentage of variation in maximum and minimum temperatures between scenario periods and the trend of increase in all scenarios (A1B and RCPs) in Gumara is illustrated in Figure 4-55 and 4-56 respectively as follows. As it is shown in Figure 4-56, both maximum and minimum temperatures show an increasing trend in all climate scenario periods.

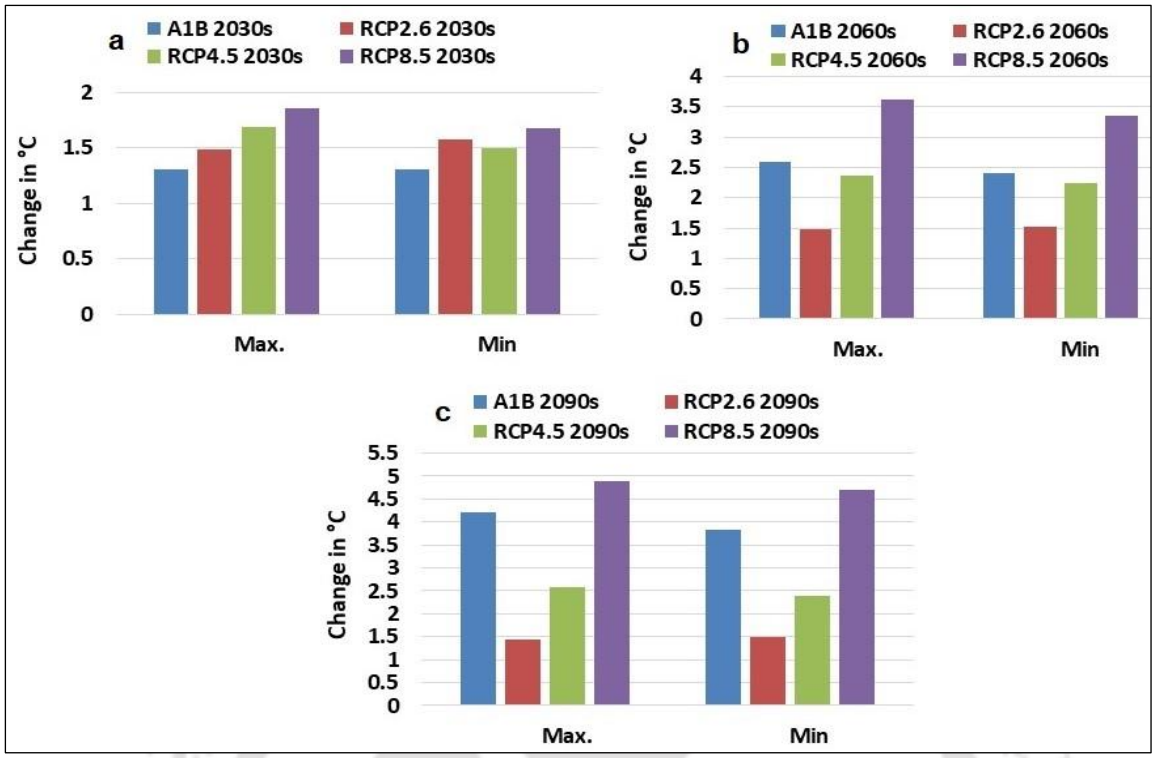

Figure 4-55 Change in maximum and minimum temperatures in all scenarios (A1B and RCPs) from the base period in the 2030s (a), 2060s (b) and 2090s (c), Gumara

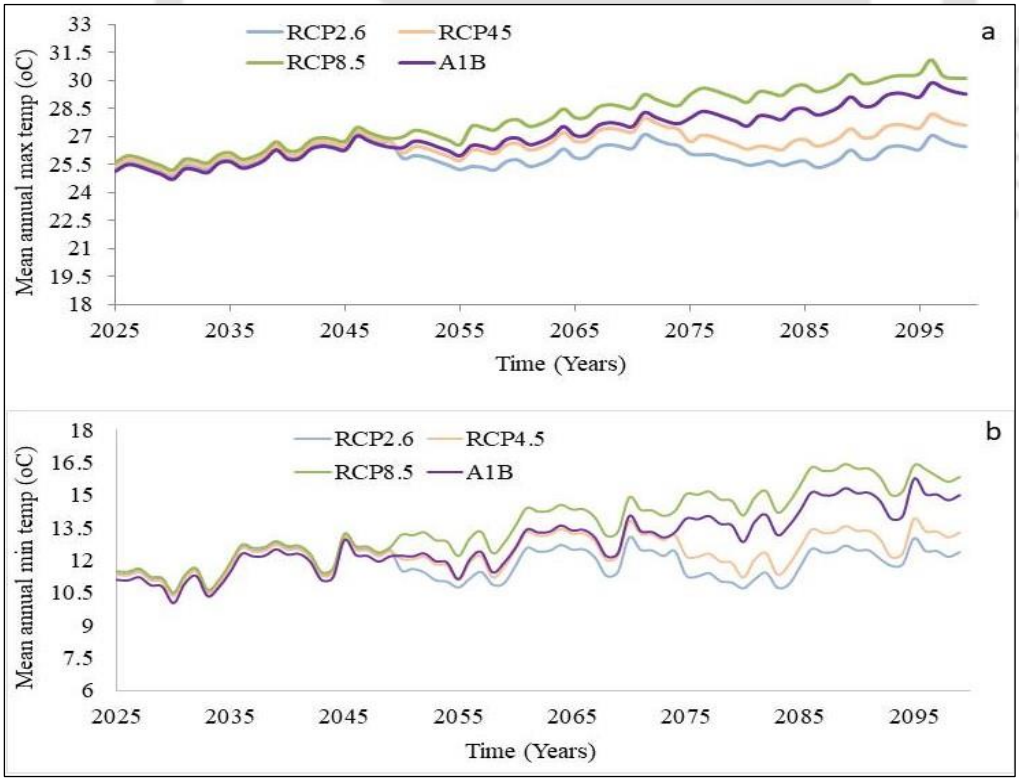

Figure 4-56 Future trend of mean annual max (a) and min (b) temperature of Gumara in A1B, RCP2.6, RCP4.5 and RCP8.5 scenarios

Mean annual precipitation will decreases by 5.1%, 6.6% and 27.7% in Rib and 4.6%, 5.2%, and 24.6% in Gumara in the 2030s, 2060s, and 2090s of the A1B scenarios respectively as it is compared with the base scenario. In Rib, in the 2030s the average precipitation will decrease by 3.8% in RCP2.6, 4.9% in RCP4.5, and 0.8 in RCP8.5. In the 2060s (mid-century) precipitation will decrease by 1.9% in RCP2.6, 8.8% in RCP4.5 and 5.4% in RCP8.5, and in the 2090s (end-of-century) by 2.4% in RCP2.6, 6.2% in RCP4.5 and 16.7% in RCP8.5 in Rib watershed. In Gumara, in the 2030s the average precipitation will decrease by 3.3% in RCP2.6, 5.0% in RCP 4.5 and 2.4% in RCP8.5. The 2060s (mid-century) precipitation will decrease by 1.4% in RCP2.6, 10.2% in RCP4.5 and 5.5% in RCP8.5, and in the 2090s (end-of-century) by 4.0% in RCP2.6, 6.3% RCP4.5 and 18.8% in RCP8.5 (Table 4-1).

There will be an average maximum and minimum temperature increase by 1.3°C and 1.3°C in the 2030s, 2.6°C and 2.5°C in the 2060s and 4.1°C and 3.82°C in the 2090s respectively in Rib, and by 1.3°C and 1.3°C in the 2030s, 2.6°C and 2.4°C in the 2060s and 4.2°C and 3.84°C in the 2090s respectively in Gumara in the A1B scenario (Table 4-1).

The average increase of maximum and minimum temperatures respectively in the 2030s will be 1.4°C and 1.59°C in RCP 2.6, 1.59°C and 1.52°C in the RCP 4.5 and 1.79°C and 1.69°C in the RCP 8.5. In the 2060s, the maximum and minimum temperature increase will be 1.39°C and 1.5°C in RCP 2.6, 2.28°C and 2.2°C in the RCP 4.5 and 3.55°C and 3.38°C in the RCP 8.5, and in the 2090s will be 1.35°C and 1.48°C in RCP 2.6, 2.49°C and 2.35°C in the RCP 4.5 and 4.7°C and 4.67°C in the RCP 8.5 in Rib watershed. In Gumara the average increase in maximum and minimum temperature respectively in the 2030s will be 1.48°C and 1.58°C in RCP 2.6, 1.67°C and 1.5°C in the RCP 4.5 and 1.86°C and 1.68°C in the RCP 8.5. In the 2060s the maximum and minimum temperature increase will be 1.48°C and 1.52°C in RCP 2.6, 2.36°C and 2.25°C in the RCP 4.5, 3.62°C and 3.36°C in the RCP 8.5, and in the 2090s the increase will be 1.43°C and 1.48°C in RCP 2.6, 2.57°C and 2.38°C in the RCP 4.5, 4.89°C and 4.7°C in the RCP 8.5. The result showed that in the RCP2.6 scenario, the increase in minimum temperature exceeds the maximum temperature and in RCP4.5 and 8.5 the increase in maximum temperature is higher than the minimum temperature. The lowest and highest increase in both maximum and minimum temperatures respectively will be in the RCP2.6 and 8.5 of the 2030s, 2060s, and 2090s (Table 4-1).

Table 4-1 Projected mean annual precipitation and temperature variation of Rib and Gumara

Scenarios		Precipitation %		Max. Temperature °C		Min. Temperature °C	
		Rib	Gumara	Rib	Gumara	Rib	Gumara
SRES A1B	2030s	-5.10	-4.60	1.30	1.30	1.30	1.30
	2060s	-6.60	-5.20	2.60	2.60	2.50	2.40
	2090s	-27.70	-24.60	4.10	4.20	3.82	3.84
RCP 2.6	2030s	-3.80	-3.30	1.40	1.48	1.59	1.58
	2060s	-1.90	-1.40	1.39	1.48	1.5	1.52
	2090s	-2.40	-4.00	1.35	1.43	1.48	1.48
RCP 4.5	2030s	-4.90	-5.00	1.59	1.69	1.52	1.50
	2060s	-8.80	-10.20	2.28	2.36	2.20	2.25
	2090s	-6.20	-6.30	2.49	2.57	2.35	2.38
RCP 8.5	2030s	-0.82	-2.40	1.79	1.86	1.69	1.68
	2060s	-5.40	-5.50	3.55	3.62	3.38	3.36
	2090s	-16.7	-18.80	4.70	4.89	4.67	4.70

Through all the climate predictions there are concerns of uncertainties/bias related to climate models. The climate models which are an important means in climate predictions are influenced by greenhouse gases emissions; processes controlling the atmosphere composition (terrestrial and marine components of carbon and nitrogen cycles), and the interaction between ocean, land, and cryosphere systems. These processes introduce uncertainty on climate models and affect climate prediction and modelling (Schwierz et al., 2006). The uncertainty associated with emissions is basically because of unknowable knowledge and is inherently irreducible (Schwierz et al., 2006; Hulme and Carter, 1999). Uncertainty may also arise due to the resolution of simulations, either a coarse or relatively finer resolution of global climate models. The GCMs have lower resolution than the RCMs which experiences a higher probability of uncertainty in the outputs. GCMs and RCMs are affected to some extent by all types of uncertainty.

Climate model biases are long-term average deviations between simulations and observations (Wilcke et al., 2013). Bias-corrected climate model output may assist in real-world adaptation decisions (Hewitson et al., 2014). RCMs have enhanced performance over GCMs due to their better representation of geographical features because of higher spatial resolutions (12.5–50 km) and better depiction of physical processes by means of sub-grid scale parameterization (Yang et al., 2010; Thoeun, 2015). Though these advantages, RCMs model outputs may still produce substantial systematic biases which might lead to inaccuracies if used uncorrected for impact studies (Luo et al., 2018; Switanek et al., 2017). RCMs biases depend on GCMs simulated variables, which could be significant for precipitation due to its

highly nonlinear nature and large spatial variability (Kotlarski et al., 2014). RCMs substantially increase the spatial and temporal resolutions of GCMs outputs, but not absolutely resolve the scale gap between the simulated grid cell values and point-scale data of precipitation (Volosciuk et al., 2017). To resolve the uncertainty related to model outputs, it is desirable to consider several GCM-RCMs and various emission scenarios (Shrestha and Htut, 2016). In addition, post-processing of RCMs outputs through bias correction methods removes systematic biases of simulated data for climate change impact studies (Hansen et al., 2010). In this study, two GCM-RCMs outputs and four scenarios were processed for comparison and a delta-change method of bias correction is used to minimize the uncertainties associated with the RCMs. In the delta-change method, observational time series is used as a baseline which makes it a robust method capable of correcting the mean values even though it has limitations in correcting standard deviation (variance).

4.4 Conclusion

Prediction of precipitation is highly liable to uncertainty than temperature because of its high variability in space and the coarse GCM models. Even though there are increasing and decreasing fluctuations in both watersheds, the general trend showed that precipitation is decreasing in all A1B and RCP scenarios. In general, January will show high precipitation increase in most of the scenarios, and March and May will show a higher decrease. August will show the least reduction in precipitation in all scenarios. In seasonal precipitation anomalies, the highest decrease will be shown in Belg season (March, April, and May) and the highest increase in Bega especially in the months of January and February. From the Kiremt (summer) months, July will show a relatively higher decrease. A high decrease of precipitation will occur in the 2090s in both watersheds and all scenarios (A1B and RCP) except the 2060s of the RCP4.5. The highest reduction will be in the 2090s of the A1B scenario than the RCPs. The result revealed that in the historical periods or existing condition highest rainfall has been occurred in July but in the future predictions, it will shift to August.

Temperature trends (minimum and maximum) show increasing in both watersheds. July from the Kiremt season and May from the Belg will have a relatively higher increasing trend in both temperatures. The highest increasing trend will be observed in the Belg season. A higher temperature increase (minimum and maximum) will occur in the 2090s of all scenarios except in the RCP2.6. In the RCP2.6, a higher increase in temperature will be in the 2030s in both watersheds. A decrease in precipitation and an increase in temperatures in almost all

scenarios will have implications on the hydrologic components such as surface runoff, groundwater flow, evaporation, and soil erosion in the watersheds. The precipitation and temperature scenarios together with the future LULC could be used as an input to predict the future hydrologic and sediment yield conditions of the watersheds.

Chapter 5 : Evaluation of the ArcSWAT Model in Simulating Watershed Hydrology and Sediment Yield in Rib and Gumara Watersheds

5.1 Introduction

5.1.1 The SWAT modelling approach

The Soil and Water Assessment Tool (SWAT) model was developed by Dr. Jeff Arnold US Department of Agriculture, Agriculture Research Service (USDA-ARS) in the mid of the 1990s. The SWAT is physically-based, semi-distributed and basin scale model which is aimed to predict the effect of management practices on sediment, water, and agro-chemical yields in basins (Neitsch et al., 2011; Arnold et al., 2012). It can integrate various environmental processes and efficient in performing in large watersheds and basin-scales at a reasonable time (Neitsch et al., 2011). As it is physically-based and basin-scale, its capacity of spatial detail is described by dividing basins to sub-basins and HRUs which has a distinct slope, soil, and land-use (Neitsch et al., 2011; Arnold et al., 2012). The sediment yield and river discharge predicting capability of SWAT has been verified by different authors (Setegn et al., 2010; Neitsch et al., 2011, Arnold et al., 2012, Dessu and Melesse, 2012) The model has an advantage since it incorporated several environmental processes, uses readily available inputs, user friendly, physically based and distributed, and computationally efficient to operate in large basins at a reasonable time (Neitsch et al., 2011). The model allows the simulation of a high level of spatial detail by dividing the watershed into a large number of sub-watersheds and HRUs.

Watershed and sub-watershed could be delineated using the Digital Elevation Model (DEM) in ArcSWAT. Flow direction and accumulation are important concepts to define the stream networks from the DEM to specially delineate the HRUs in SWAT. The HRUs are defined as homogeneous spatial units of land characterized by similar geomorphologic and hydrological properties. In SWAT Flow, sediment yield, and nutrient loading obtained from each sub-watershed are routed through the river system. The calculations are performed on HRU basis and flow and water quality variables are routed from HRU to the sub-watersheds and subsequently to the watershed outlet.

5.1.1.1 Hydrologic component of in the SWAT model

The simulation of the hydrology of a watershed is processed with two separate divisions. One

is the land phase of the hydrological cycle that controls the amount of water, sediment, nutrient, and pesticide loadings to the main channel in each sub-watershed or sub-basin. The second division is the routing phase of the hydrologic cycle that can be defined as the movement of water, sediments, nutrients, and organic chemicals through the channel network of the watershed to the outlet (Neitsch et al., 2011). In the land phase, the hydrological cycle in SWAT is simulated based on the water balance equation using equation 5.1

$$SW_t = SW_o + \sum\left(R_{day} - Q_{surf} - E_a - W_{seep} - Q_{gw}\right) \qquad (5.1)$$

Where SW_t is the final soil water content at time t (mm), SW_o is the initial soil water content on day i (mm), t is the time (days), R_{day} is the amount of precipitation on day i (mm), Q_{surf} is the amount of surface runoff on day i (mm), E_a is the amount of evapotranspiration on day i (mm), W_{seep} is the amount of water entering the vadose zone from the soil profile on day i (mm) and Q_{gw} is the amount of water return to the ground (base flow) on day i (mm).

Surface runoff in SWAT could be estimated with the SCS curve number procedure (SCS, 1972) and the Green & Ampt infiltration method (Green and Ampt, 1911). Surface runoff from daily rainfall is estimated by a modified soil conservation service (SCS) curve number method by using local land use, soil type, and antecedent moisture condition. By using daily or sub-daily rainfall as an input, SWAT simulates surface runoff volumes and peak runoff rates for each HRU. For its simulation SWAT uses Natural Resource Conservation Service (NRCS) soil classification based on the infiltration properties of the soil (Neitsch et al., 2011) having four groups (A, B, C, and D) with high, moderate, low, and very low infiltration rates respectively. SCS curve number method for calculating surface runoff is based on equation 5.2.

$$Q_{surf} = \frac{(R_{day} - 0.2S)^2}{(R_{day} + 0.8S)} \qquad (5.2)$$

Where, Q_{surf} is the accumulated runoff or rainfall excess (mm), R_{day} is the rainfall depth for the day (mm), S is the retention parameter (mm). The retention parameter will be determined using equation 5.3.

$$S = 25.4\left(\frac{1000}{CN} - 10\right) \qquad (5.3)$$

Where CN = curve number ranging between $0 \leq CN \leq 100$.

In the routing phase of hydrological cycle, SWAT uses variable storage routing (Williams, 1995) or the Muskingum routing method to rout flow in channels. In the variable storage routing method, flow routed through the stream network of the watershed from upland areas to the main channel using the concept of continuity equation represented as equation 5.4.

$$\Delta V_{stored} = V_{in} - V_{out} \qquad (5.4)$$

Where $\Delta V_{stored,}$ is change of volume stored (m^3), $V_{in,}$ is volume of inflow (m^3) and $V_{out,}$ is volume of outflow.

5.1.1.2 Erosion and sediment yield component in the SWAT model

Movement of sediment at the HRU level in SWAT is routed through the stream network to basin outlet (Neitsch et al., 2011) using MUSLE Equation (Williams and Berndt, 1977), as described in equation 5.5.

$$SY = 11.8\left(Q_{surf} q_p A\right)^{0.56} K_{USLE} C_{USLE} P_{USLE} LS_{USLE} R \qquad (5.5)$$

where SY is the sediment yield (metric tons), Q_{surf} is the surface runoff volume (mm H_2O /ha), q_p is peak runoff rate (m^3/s), A is an area in HRU basis (ha), K, P, C, LS are the USLE soil erodibility, support practice, cover management and topographic factors respectively. R represents the percent of the stoniness of the land. The conveyance of sediment in channels in SWAT is controlled by the processes of degradation and deposition that are predicted with stream power equation (Neitsch et al., 2011; Williams, 1980). Deposition of sediment, $sed_{dep,}$ is estimated with equation 5.6:

$$sed_{dep} = \left(sed_{ch,i} - sed_{ch,\mathrm{mx}}\right).V_{ch} \qquad (5.6)$$

Where $sed_{ch,i}$ suspended sediment in the channel in the initial period (ton/m^3 or kg/L), $sed_{ch,mx}$ is the maximum accumulated sediment conveyed by the water (ton/m^3) and V_{ch} is the water volume in the channel (m^3). Re-entrained sediment has been predicted using equation 5.7.

$$sed_{\deg} = \left(sed_{ch,\mathrm{mx}} - sed_{ch,i}\right).V_{ch}.K_{ch}.C_{ch} \qquad (5.7)$$

Where sed_{deg} is sediment re-entrained in the channel segment, K_{ch} and C_{ch} are the USLE channel erodibility and channel cover factors respectively. The q_{peak} is peak runoff rate, which indicate the erosive power of the storm and used to predict sediment yield. SWAT calculates peak runoff rate using the modified rational method as described as in equation 5.8.

$$q_{peak} = \frac{\alpha_{tc} . Q_{surf} . Area}{3.6 t_{conc}} \qquad (5.8)$$

Where, α_{tc} is the fraction of daily rainfall that occurs during the time of concentration, Q_{surf} is the surface runoff (mm H2O), *Area* is the sub-basin area (km²), t_{conc} is the time of concentration (hr), and 3.6 is a conversion factor.

5.2 Martials and Methods

5.2.1 Methodological structure

The main data sets for hydrology and sediment studies include soil, topography, flow, sediment, land-use, and weather elements among others. The methodological procedure for the study is presented in the Figure 5-1.

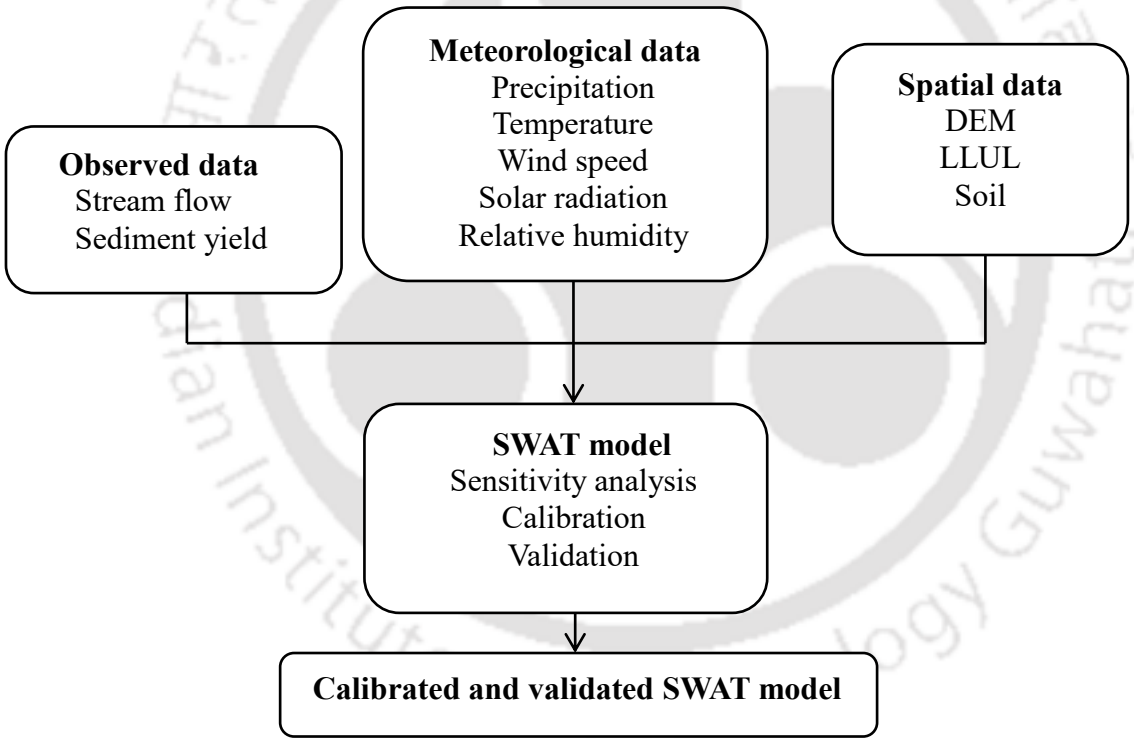

Figure 5-1.Schematic representation of methodology

5.2.2 Data sets

Important data sets for the watershed hydrology and sediment modeling were acquired from different sources and the necessary data processing procedures were undertaken. The description of data sets and their source for this study are presented in Table 5.1.

Table 5-1 Data and data sources of the study

Data	Source
Topography	USGS data base (https://earthexplorer.usgs.gov/)
	Amhara Regional State Water and Energy Bureau, Ethiopia
Weather/meteorological	Ethiopian Meteorological Agency (EMA)
RCM/GCM	CORDEX-Africa and International Water Management Institute (IWMI)
Sediment	Ministry of Water Resource of Ethiopia (MoWR)
LULC	Landsat Image (UEGS database (https://earthexplorer.usgs.gov/)
Soil	Amhara National Regional State Bureau of Environmental Protection, Land Administration and Use (BoEPLAU)
	Abay Basin Master plan project, Ethiopia (MoWR)
Hydrologic data	Ministry of Water Resource of Ethiopia (MoWR)

5.2.2.1 Meteorological data

Meteorological variables are required as input for the ArcSWAT model to predict streamflow and sediment yield in watersheds. Meteorological variables required for the study; temperature, rainfall, relative humidity, wind speed, and sunshine hours were acquired from Ethiopian Meteorological Agency (EMA). Weather data from the stations of Debre Tabor, Woreta, Wanzaye, Addis Zemen, Bahir Dar, Nefas Mewucha were collected and the weather generator for the SWAT weather database was prepared. Weather generator (wgn) data is used to generate meteorological data for stations that have missing weather elements. The geographic distributions of weather stations in the watersheds are presented in Figure 5.2.

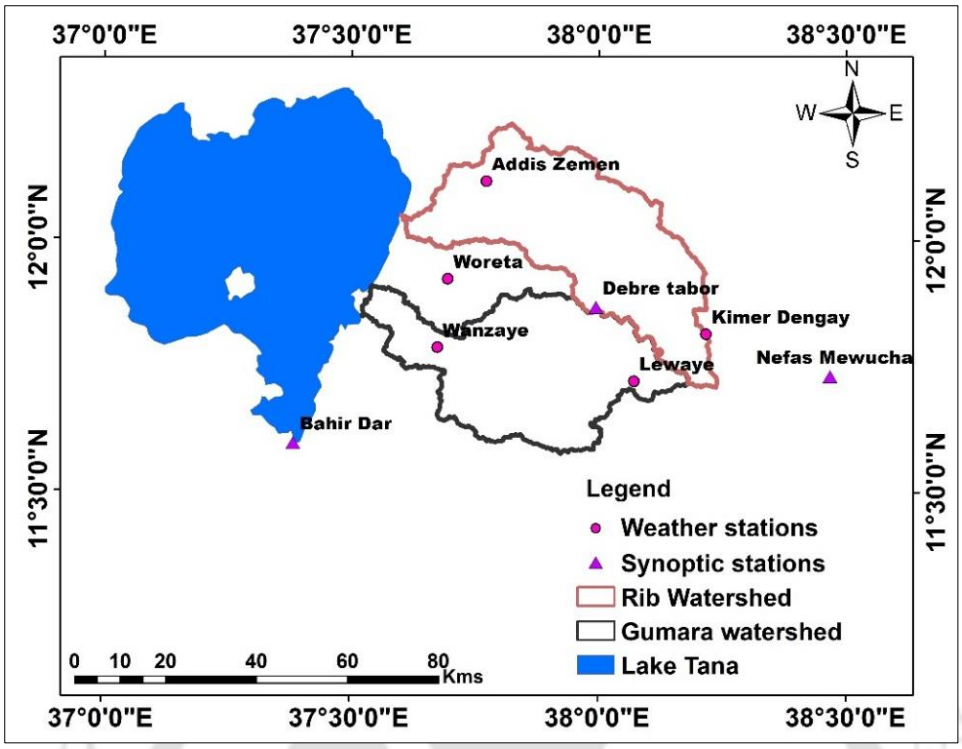

Figure 5-2 Spatial distributions of meteorological stations

Debre Tabore station receives the highest amount of rainfall followed by Wanzaye with 1451mm and 1439mm respectively. The average annual rainfall of stations located in the watersheds ranges between 1312–1451 mm (Table 5.2).

Table 5-2 Average annual rainfall of stations

Station	Debre Tabore	Wanzaye	Woreta	Addis Zemen
Average annual rainfall	1451	1439	1312	1313

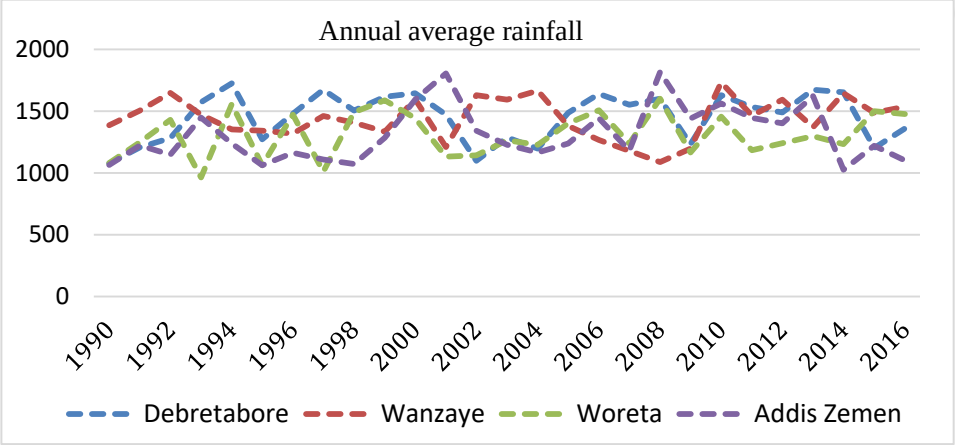

Figure 5-3 The annual rainfall of stations

As is indicated in Figure 5-4 all stations receives higher temperatures in the months of February, March April, and May and low temperatures during Jun, July, August, and

September. Wanzaye and Debre Tabore have the highest and lowest maximum temperature respectively than other stations (Figure 5.4a). Debe Tabore station has a lower minimum temperature whereas Woreta has a higher minimum temperature. Almost in all stations, the lowest minimum temperature is recorded in January and December (winter months). But the highest minimum temperature is recorded in April and May (Figure 5.4b).

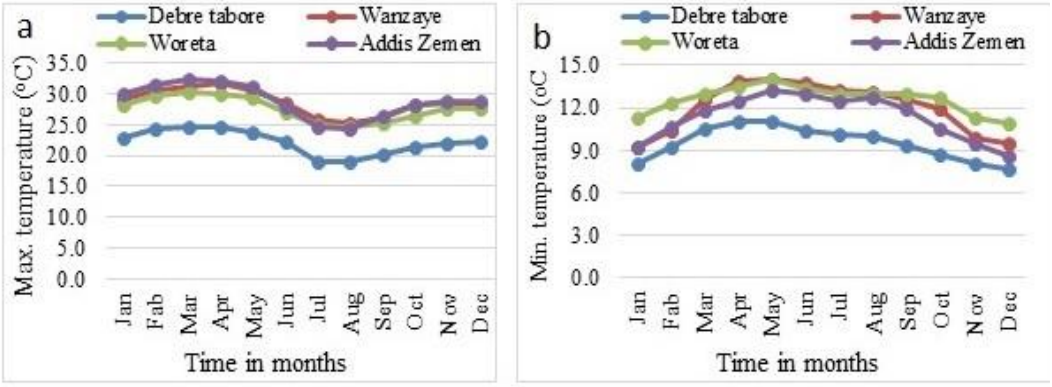

Figure 5-4 Monthly maximum (a) and minimum (b) temperature of stations

The meteorological variables are prepared in a format suitable for ArcSWAT and the weather generator (wgn) data which is used to fill the missing data of stations is prepared.

5.2.2.2 Hydrology and sediment data

Observed streamflow and sediment data of the gauge stations were obtained from the Ministry of Water and Energy of Ethiopia (MoWR) and organized for calibration and validation of the SWAT model. Twenty-seven years of flow data were collected from the rivers gauge stations. Three years' data from 1990-1992 was used for the warm-up period and data from 1993-2007 was used for SWAT calibration and from 2008-2016 was for validation.

When there is a lack of a long time and continuous data of sediment measurement it is widely applicable to use sediment rating curves to fill the gaps and generate sediment yield data. Sediment Rating Curve (SRC) is widely employed as an empirical technique for relating suspended sediment concentrations and stream discharge. The SRC introduces a causative linkage between two variables, discharge (Q) treated as an independent predictor variable and suspended sediment as a dependent variable (Glysson, 1987). The power function SRC was used for this study as it is presented in equation 5.9.

$$C = aQ^b \qquad (5.9)$$

Where *a* and *b* are the rating coefficient and exponent respectively (Syvitski et al., 2000). SRC equations are used widely in producing suspended load estimates for periods when

there is a shortage of available sediment data. The graph of sediment rating curve is presented in Figure 5-5 for Rib and 5.6 for Gumara.

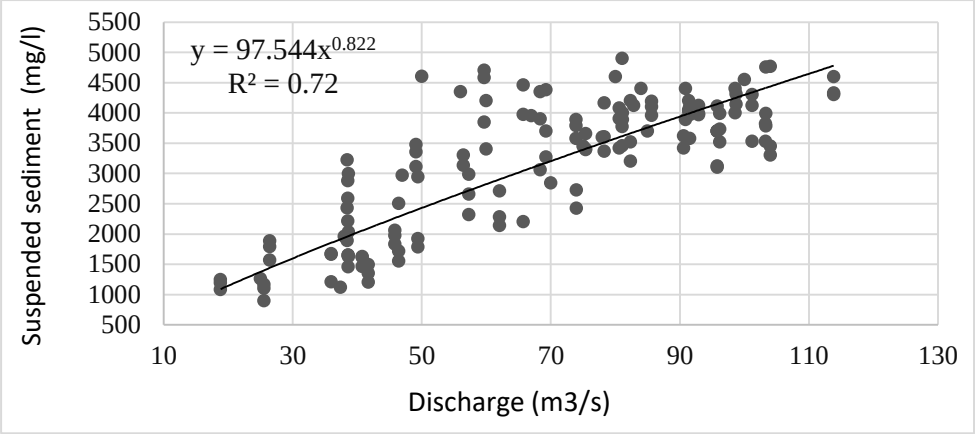

Figure 5-5 Sediment rating curve of Rib

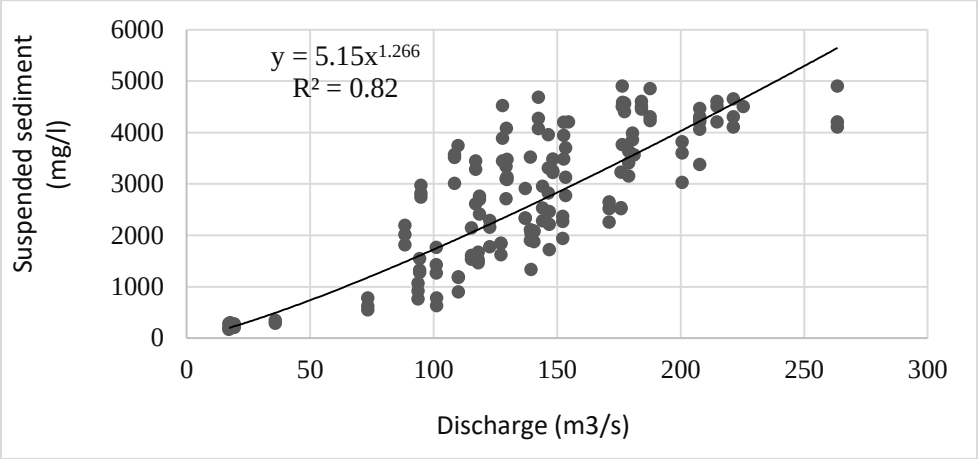

Figure 5-6 Sediment rating curve of Gumara

5.2.2.3 Digital elevation model (DEM)

Shuttle Radar Topographic Mission Digital Elevation Model (SRTM- DEM) data of 30m spatial resolution were used to process watershed topographic characteristics (slope, stream length, sub-watersheds, HRUs) of the watersheds. The elevation of Rib and Gumara from the source to the gauge stations range between 1794–3687m and 1797–4087 m amsl respectively (Figure 5.7).

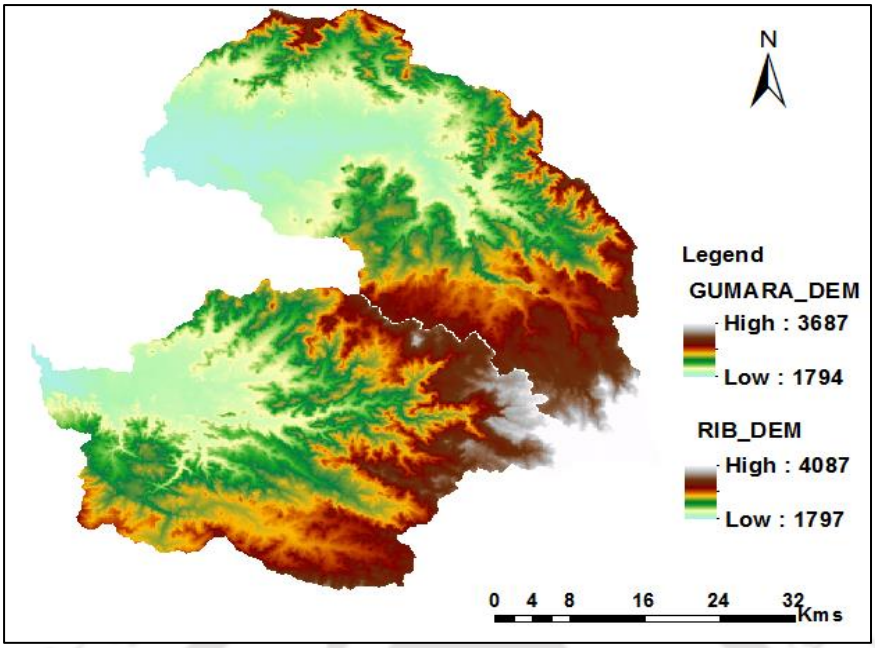

Figure 5-7 DEM of Rib (top) and Gumara (bottom)

5.2.2.4 Soil types of the watersheds

The spatial soil layer was acquired from MoWR (1998) Abay Basin Master Plan Project. Soil chemical and physical properties were prepared using MoWR (1999) Abay basin master plan project, Bureau of Environmental Protection, Land Administration and Use of Amhara National Regional State of Ethiopia (BoEPLAU, 2015), and FAO (1998).

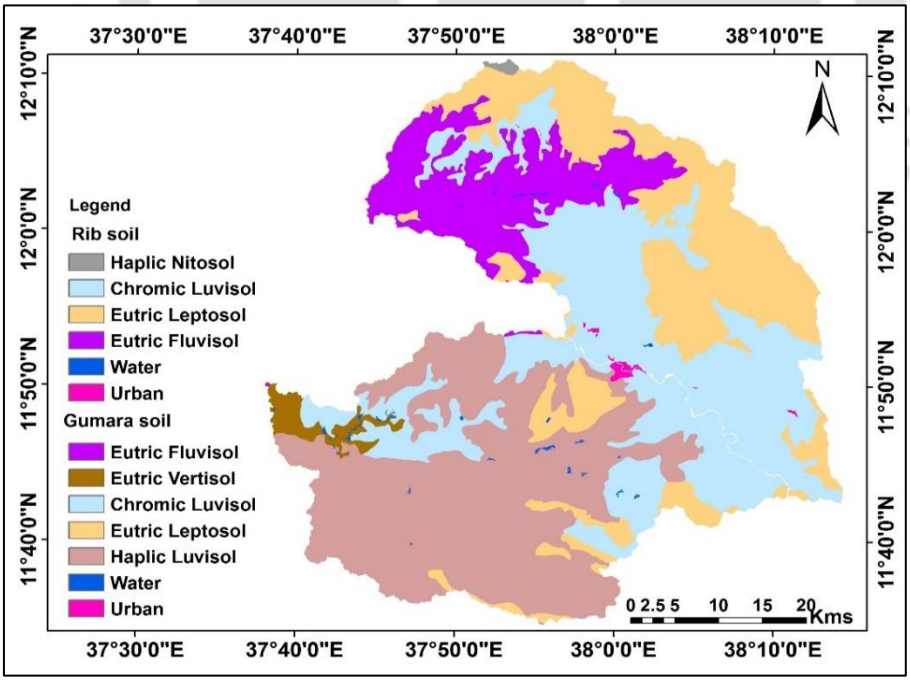

Figure 5-8 Soil type map of Rib (top) and Gumara (bottom)

The dominant soil types of Rib are Chromoc Luvisol and Eutric Fluvisol which covers 38.9% and 23.2 % of the watershed respectively. The dominant soils of Gumara are Haplic Luvisol and Chromoc Luvisol which covers 63.4% and 24.1% of the watershed respectively (Figure 5.8 and Table 5.3).

Table 5-3 Soil types of Rib and Gumara watersheds

Rib			Gumara		
Soil type	Area (ha)	% cover	Soil type	Area (ha)	% cover
Eutric Fluvisol	30062.9	23.2	Eutric Fluvisol	167.8	0.1
Chromic Luvisol	50255.6	38.9	Chromic Luvisol	30555	24.1
Eutric Leptosol	48147.8	37.2	Eutric Leptosol	11201.0	8.8
Water	132.9	0.1	Water	437.3	0.3
Urban	324.2	0.3	Urban	332.6	0.26
Haplic Nitosol	411.5	0.3	Eutric Vertisol	3766.9	3.0
-----	-----	----	Haplic Luvisol	80464.1	63.4
	129334.9	100		126924.6	100

5.2.2.5 Land use and land cover

LULC layers were prepared through the classification of Landsat satellite images. The LULC types of Rib and Gumara watersheds are intensively cultivated, moderately cultivated, mixed forest, plantation, shrublands, grasslands, waterbody, and urban areas. SWAT requires the LULC data to define the Hydrological Responses Units (HRU).

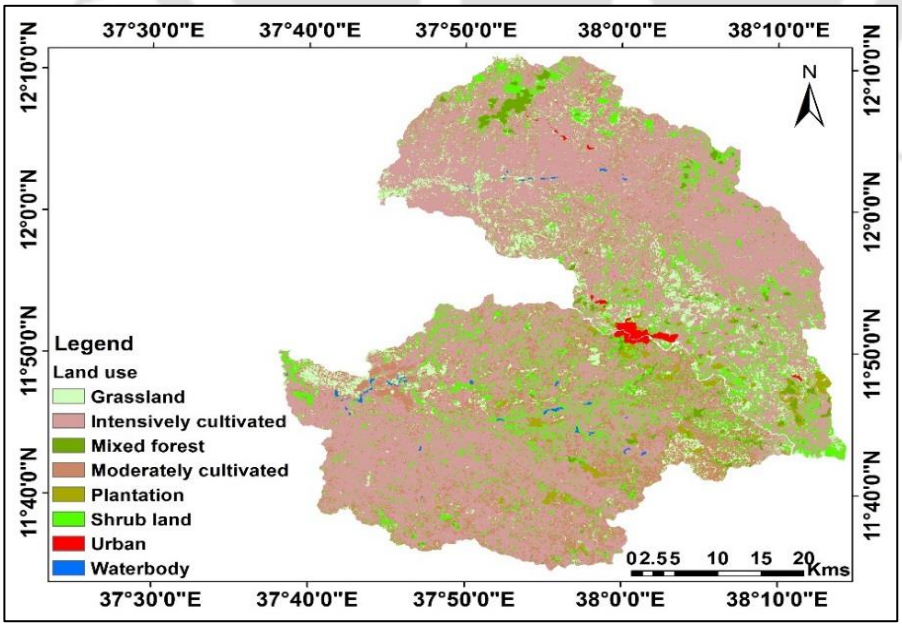

Figure 5-9 LULC map of Rib (top) and Gumara (bottom)

Table 5-4 Description of land use and land covers

LULC types	Description
Intensively cultivated	Areas used for crop cultivation, both annuals and perennials. It includes areas currently under crop and land under preparation.
Mixed forest	Land covered with different natural tree species, dense trees and undergrowth that formed nearly closed canopies
Shrubland	Areas with scattered trees mixed with short bushes, grasses and open areas
Moderately cultivated	Areas used for crop cultivation, both annuals and perennials, and the scattered rural settlements. Trees scattered in cultivated fields, patches of grasses in between crop fields, and field boundaries are part of this land-use type.
Plantation	Areas covered by eucalyptus plantations
Grassland	Grassy areas used for communal grazing, lands that includes very little or dense grass. It also includes other small seized plant species used for grazing.
Town	Areas of manmade constructions including buildings, houses and roads
Water	Areas with surface water in the form of ponds and rivers

Rib and Gumara are dominantly covered by intensively cultivated land with area coverage of 65.1% and 55.6 % of the watersheds respectively. Moderately cultivated lands and shrublands constitute 22.6% and 13.0% of rib and shrublands and grasslands account 12.6% and 10.4 % of Gumara watershed.

Table 5-5 LULC classes of Rib and Gumara watersheds

LULC class	SWAT code	Rib		Gumara	
		Area	% cover	Area	% cover
Intensively cultivated	DWHT	84261.0	65.1	70574.6	55.6
Shrubland	RNGB	16347.9	12.6	16462.2	13.0
Grassland	PAST	13414.5	10.4	6787.9	5.4
Mixed forest	FRST	2663.2	2.1	1830.1	1.4
Moderately cultivated	AGRL	10183.6	7.9	28765.9	22.6
Plantation	FRSD	1466.5	1.1	1767.0	1.4
Urban	URBN	896.0	0.7	303.5	0.2
Waterbody	WATR	102.3	0.1	433.4	0.3
		129334.9	100	126924.6	100

5.2.2.6 Slope classes of watersheds

As is presented in Table 5.6, much of the watersheds are within the slope class of 0–8, 8–15, and 15–30%. Slopes between 0–8, 8–15, and 15–30% cover 32.6%, 22.4%, and 25.7% of the

area of Rib watershed respectively. Slopes between 0–8, 8–15, and 15–30% cover 26%, 26.9%, and 35.3% respectively of Gumara.

Table 5-6 Slope classes of Rib and Gumara

		Rib		Gumara	
Slope	Description	Area in ha	% area	Area(ha)	% Area
0-8	Flat	42182.6	32.6	32950.7	26.0
8-15	Gently sloping	28912.9	22.4	34137.1	26.9
15-30	Sloping	33268.0	25.7	44755.6	35.3
30-50	Steep	17372.6	13.4	14784.3	11.7
>50	Very steep	7598.8	5.9	296.9	0.23
		129334.9	100	126924.6	100

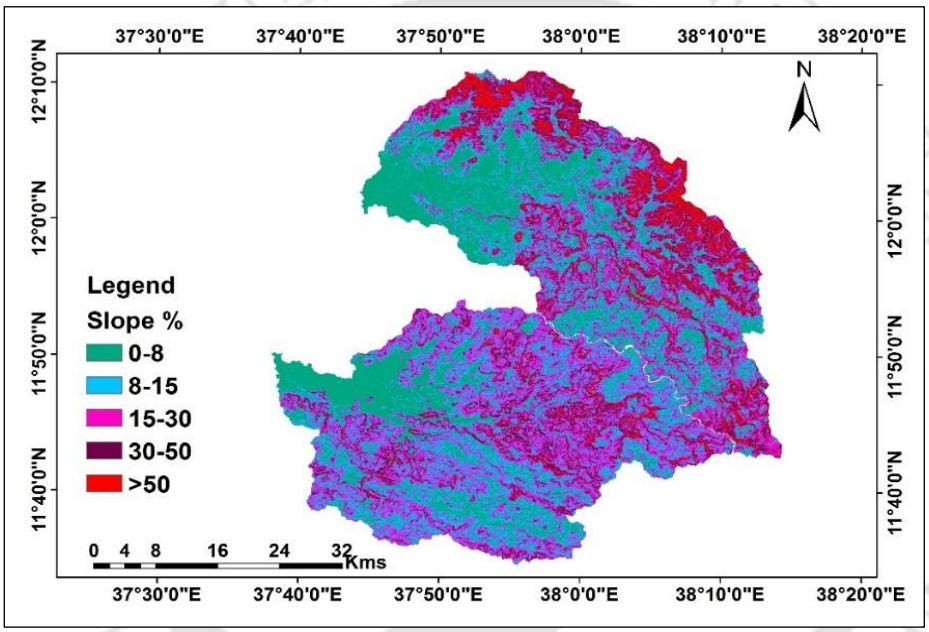

Figure 5-10 Slope map of Rib (top) and Gumara (bottom)

As indicated in Figure 5-10, slopes between 0–8% dominate the lower parts of both watersheds. Slopes between 8–15% and 15–30% mainly cover the middle and upper parts of both watersheds and slope >50% covers a significant portion of the upper part of both watersheds (Figure 5-10).

5.3 Results and Discussion

5.3.1 Watershed and sub-watershed delineation

The model setup involved the steps of data preparation, sub-watershed delineation, HRU definition, sensitivity analysis of parameters, calibration and validation, and uncertainty analysis. Spatial data sets were made to have a common projection system, WGS84 UTM

Zone 37 N. The DEM was used to delineate the watershed and sub-watersheds to analyses the drainage patterns of the land surface terrain. Flow direction and accumulation are the concepts behind to define the stream networks using DEM in the SWAT model. To delineate watersheds and sub-watersheds procedures of DEM setup, stream definition, watershed outlets selection, and definition and calculation of sub-watershed parameters were performed.

In the stream definition, the threshold value that defines the minimum drainage area required to form the origin of a stream was set. A threshold area of 2150 and 1500 ha for Rib and Gumara respectively were set to increase the number of stream networks that enable the exploration of the accurate amount of flow and sediment generated from the stream networks. So that 37 and 35 sub-watersheds for Rib and Gumara respectively were obtained using the defined threshold area values (Figure 5.11). The LULC and soil data were prepared in accordance with SWAT database format and their look up table which is an input for HRU definition is prepared.

5.3.2 Hydrological response units (HRUs)

Soil and LULC map of the watersheds were prepared and overlaid in ArcSWAT to define HRUs. The land use, soil, and slope datasets were imported, overlaid, and linked with the SWAT databases. Areas with the same soil type, land use, and range of slope classes form a unique hydrological response unit (HRU). Subdividing the sub-watershed into areas having unique land use, soil, and slope combinations make it possible to study the differences in hydrologic conditions for different spatial units. From 37 and 35 sub-watersheds of Rib and Gumara a total of 420 and 490 HRUs respectively were defined. As the number of the HRUs increases, it is possible to create more homogeneous soil, land use, and slope units for precise estimation hydrologic and sediment outputs

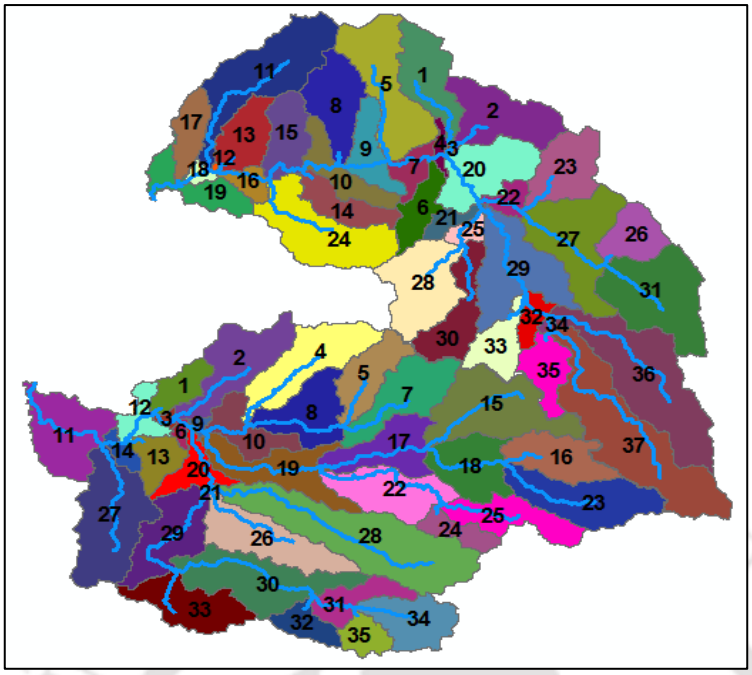

.

Figure 5-11 Streams and sub-watersheds of Rib (top) and Gumara (bottom)

The total areas of the watersheds of Rib and Gumara up to the outlet where flow and sediment data were collected are 1294.4 km^2 and 1269 km^2 respectively. The distributions of HRUs in sub-watershed levels for Rib and Gumara are presented in Figure 5-12 and 5-13 respectively. The minimum number of HRUs per sub-watershed level in both watersheds is 2. The maximum number of HRUs in a sub-watershed in Gumara is 26 and in Rib is 23.

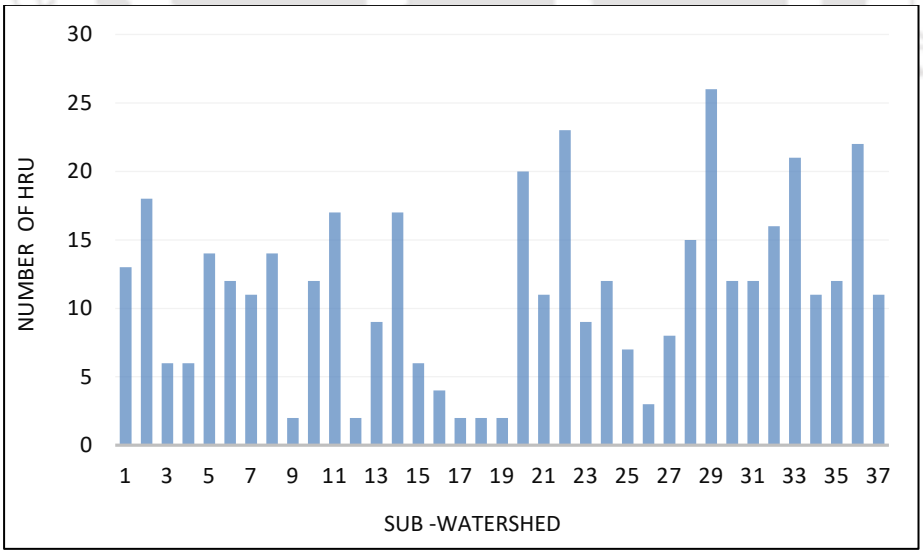

Figure 5-12 HRU distribution in sub-watersheds, Rib

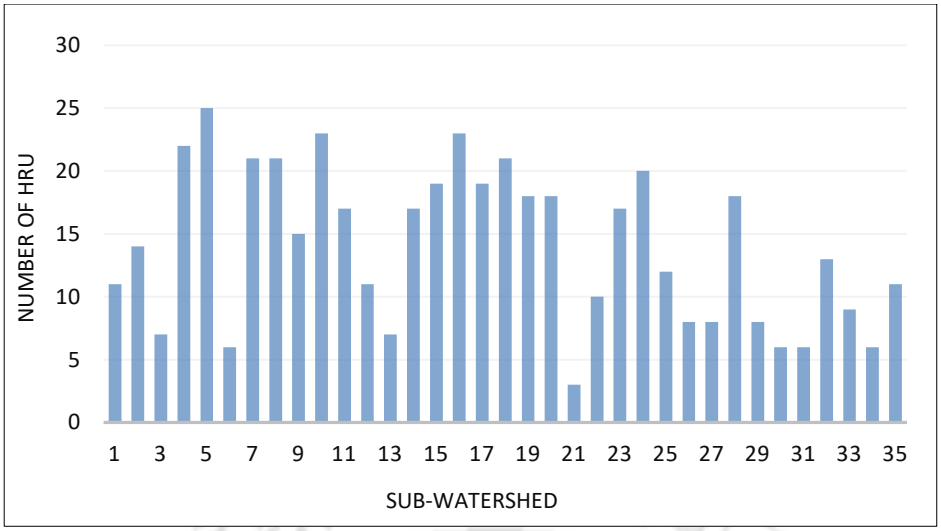

Figure 5-13 HRU distribution in sub-watersheds, Gumara

5.3.3 Sensitivity analysis

Sensitivity analysis was done using SWAT Calibration and Uncertainty Procedures (SWAT-CUP) (Abbaspour et al., 2007). The SWAT-CUP is a program that integrated with ArcSWAT to perform calibration, validation, and sensitivity analysis. After the pre-processing of the data and SWAT model setup, ArcSWAT simulation was done from 1990 to 2016 by considering 1990-1992 as warm-up periods. Sensitivity analysis was conducted to select the most sensitive parameters. Twenty-six parameters were taken into consideration and the most sensitive parameters, fourteen for Rib and thirteen for Gumara, were found which affect the streamflow.

Parameter sensitivities are determined with multiple regression system, which regress the Latin Hypercube One-factor-At-a-Time (LH-OAT) generated parameters against the objective function values in SUFI-2. The SUFI-2 parameter estimation procedure (Abbaspour et al., 2007) calculates the measurement of sensitivity and uncertainty for each of the calibration parameters during the optimization process. The SWAT-CUP measures of relative sensitivity and significance of sensitivity are expressed using t-statistics and the corresponding p-values respectively.

Model calibration involves modification of input parameters and comparison of predicted output with observed values until a defined objective function is achieved (James and Burges, 1982). Validation provides information on the performance of the model. Parameters

identified in sensitivity analysis have been used to calibrate the model using measured streamflow of both watersheds. Flow validation was performed with an independent measured data with the aim to guarantee the model whether it has the capability to predict a hydrological response variable for future time periods or conditions. SWAT-CUP Sequential Uncertainty Fitting Version-2 (SUFI-2) algorithm (Abbaspour et al., 2015) was used to calibrate and validate the model. Five different algorithms procedures are associated to SWAT-CUP such as Generalized Likelihood Uncertainty Estimation (GLUE) (Beven and Binley, 1992), Particle Swarm Optimization (PSO) (Kennedy and Eberhart, 1995), Parameter Solution (ParaSol) (Van Griensven and Meixner, 2006), Mark chain Monte Carlo (MCMC) (Kassa and Foerch, 2007), and Sequential Uncertainty Fitting (SUFI-2) (Abbaspour et al., 2015). The SUFI-2 is applied in this research since it can supply the widest marginal parameter uncertainty intervals of model parameters among the other approaches.

Table 5-7 Sensitive parameters for flow calibration, Rib

Parameter	Description	Range	Fitted value	Rank
CN2	Initial SCS CNII	±0.2	-0.11	1
SOL_AWC	Soil available water capacity	0-1	0.77	2
CANMX	Maximum Canopy storage	0-100	94.4	3
OV_N	Manning's "n" value for overland flow	0.01-30	22.6	5
SURLAG	Surface runoff lag time	0.05-24	23.7	7
RCHRG_DP	Deep aquifer percolation fraction	0-1	0.42	4
GWQMN	Threshold water depth in shallow aquifer for flow (mm)	0-5000	4922	8
ESCO	Soil evaporation compensation factor	0-1	0.02	9
SOL_K	Saturated hydraulic conductivity	0-2000	17.6	6
HRU_SLP	Average slope Steepness	0-1	0.76	10
GW_DELAY	Groundwater delay (days)	0-500	337	11
ALPHA_BF	Base flow alpha factor or base flow recession constant (days)	0-1	0.12	12
REVAPMN	Threshold depth of water in shallow aquifer for ‘revap’ (mm)	0-500	49.2	13
SLSUBBSN	Average slope length	10-150	31	14

After identifying the sensitive parameters observed flow data were used to calibrate and validate the model. As shown in Table 5.7, the top main sensitive streamflow parameters for Rib were initial SCS CN II (CN2), the soil layer available water capacity (SOL_AWC) and maximum canopy storage (CANMX). The most sensitive parameters considered for Gumara calibration were, base flow alpha factor (ALFA_BF), groundwater delay (GW_DELAY), soil bulk density (SOL_BD), deep aquifer percolation fraction (RCHRG_DP). As indicated in Table 5-7 and 5-8, the parameters of soil saturated hydraulic conductivity (SOL_K) and soil bulk density (SOL_BD) control the surface runoff formation whereas groundwater "revap"

coefficient (GW_REVAP) and groundwater delay (GW_DELAY) control the groundwater generation. The GW_REVAP is a dimensionless coefficient controlling the rate of water movement between the root zone and the shallow aquifer. Groundwater delay is the time required for the water leaving the bottom of the root zone to reach the shallow aquifer.

Table 5-8 Sensitive parameters for flow calibration, Gumara

Parameter	Description	Range	Fitted value	Rank
ALFA_BF	Base flow alpha factor/base flow recession constant (days)	0 - 1	0.297	1
GW_DELAY	Groundwater delay (days)	0-500	12.34	2
GW_REVAP	Groundwater ‘’revap’’ coefficient	0.02-0.2	0.0538	3
SOL_BD	Soil bulk density	0.9 -2.5	2.074	4
RCHRG_DP	Deep aquifer percolation fraction	0-1	0.029	5
CH_K2	Main channel effective hydraulic conductivity (mm/hr)	-0.01-500	106.8	6
SOL_AWC	Soil available water capacity (mm)	0-1	0.83	7
GWQMN	Threshold water depth in shallow aquifer required for flow	0-5000	1030.7	8
CN2	Initial SCS CNII	±0.2	-0.13	9
SLSUBBSN	Channel slope	10-150	19.28	10
SOL_K	Saturated hydraulic conductivity (mm/hr)	0- 2000	18.51	11
ESCO	Soil evaporation compensation factor	0-1	0.357	12
EPCO	Plant evaporation compensation factor	0-1	0.3162	13

Regarding sediment calibration and validation, a total of sixteen sediment parameters were undergone for the absolute sensitivity analysis, and eight sensitive parameters were selected for calibration and validation for both watersheds. The name of parameters, parameter ranges, and rankings was listed in Table 5.9 for Rib and Table 5.10 for Gumara. Channel erodebility factor (CH_ERODMO) has found to be the highest sensitive channel soil erosion variable followed by the exponent of re-entrainment parameter for channel sediment routing (SPEXP) in Rib (Table 5.9) and channel cover factor (CH_COV2) and USLE equation support practice factor (USLE_P) were the most sensitive parameters for Gumara (Table 5.10). Among the eight sensitive sediment parameters, channel erosion parameters were the highest-ranked.

Table 5-9 Parameters, optimized values and ranges of sediment yield calibration for Rib

Parameter	Description	Range	Optimized value	t-Stat	P-Value	Rank
CH_ERODMO	Channel erodebility factor	0-1	0.95	25.49	0.00	1
SPEXP	Exponent of re- entrainment parameter for channel sediment routing	1-1.5	1.48	13.30	0.02	2
SPCON	Linear re-entrained factor parameter for channel sediment routing	0.0001-0.01	0.0038	-3.75	0.09	4
CH_COV2	Channel cover factor	-0.001 - 1	1.0	-1.04	0.65	8
USLE_C	Min value of USLE C factor applicable to the land cover	0.001-0.5	0.47	-5.66	0.08	3
USLE_P	USLE support parameter	0-1	0.42	2.34	0.18	5
HRU_SLP	Average slope steepness	0-1	0.48	1.53	0.49	6
SOL_AWC	Available water capacity of the soil layer	0-1	0.36	-1.11	0.60	7

Table 5-10 Parameters, optimized values and ranges of sediment yield calibration for Gumara

Parameter	Description	Range	Optimized value	t-Stat	P-Value	Rank
CH_ERODMO	Channel erodebility factor	0-1	0.91	5.22	0.21	5
SPEXP	Exponent of re- entrainment parameter for channel sediment routing	1-1.5	1.32	7.4	0.05	3
SPCON	Linear re-entrained factor parameter for channel sediment routing	0.0001-0.01	0.0036	6.39	0.13	4
CH_COV2	Channel cover factor	-0.001 - 1	0.94	17.2	0.00	1
USLE_C	Min value of USLE C factor applicable to the land cover	0.001-0.5	0.43	-3.6	0.35	6
USLE_P	USLE support parameter	0-1	0.58	12.3	0.01	2
HRU_SLP	Average slope steepness	0-1	0.20	2.23	0.43	7
SOL_AWC	Available water capacity of the soil layer	0-1	0.18	-1.33	0.50	8

5.3.4 The performance evaluation statistics for flow calibration and validation

The model performance was evaluated using quantitative statistics recommended and used by (Duan et al., 2009). The goodness of the model fit related to streamflow and sediment yield was assessed using Nash-Sutcliffe efficiency (NSE), percent bias (PBIAS), coefficient of determination (R2), and Ratio of the RMSE to the standard deviation of measured data RSR.

$$NSE = 1 - \frac{\sum_{i=1}^{N}\left(S_i - O_i\right)^2}{\sum_{i=1}^{N}\left(O_i - \overline{O}\right)^2} \qquad (5.10)$$

The NSE is calculated using equation 5.10 and it indicates how well the plot of observed versus simulated values fits the 1:1 line. NSE ranges b/n $-\infty$ and 1, with 1 being the exact value. A model is accepted, if performance statistics of NSE > 0.5, R^2 > 0.6, and RSR<0.6 for the model simulation. The largest disadvantage of Nash-Sutcliffe efficiency is that the differences in observed versus simulated values are calculated as squared values. As a result, larger values in a time series are strongly overestimated whereas lower values are neglected (Legates and McCabe, 1999).

PBIAS measures the average tendency of the simulated data to be larger or smaller than their observed counterparts. The optimal value of PBIAS is 0 with low-magnitude values indicating accurate model simulation. Positive values indicate model underestimation bias, and negative values indicate model overestimation bias (Gupta et al, 1999). The PBIAS is calculated using equation 5.11.

$$PBIAS = 100\frac{\sum_{i=1}^{N}\left(S_i - O_i\right)}{\sum_{i=1}^{N} O_i} \qquad (5.11)$$

R^2 is an indicator of relationship strength between the observed and simulated values and it is calculated using equation 5.12.

$$R^2 = \left[\frac{\sum_{i=1}^{N}\left(O_i - \overline{O}\right)\left(E_i - \overline{E}\right)}{\sqrt{\sum_{i=1}^{N}\left(O_i - \overline{O}\right)^2}\sqrt{\sum_{i=1}^{N}\left(O_i - \overline{E}\right)^2}}\right]^2 \qquad (5.12)$$

RSR varies from the optimal value of 0 perfect model simulations, to a large positive value (Moriasi et. al, 2007). The lower the RMSE provides the lower RSR and results for the better the model simulation performance. RSR is computed using equation 5.13.

$$RSR = \frac{RMSE}{STDE_{obs}} = \frac{\left[\sqrt{\frac{\sum_{i=1}^{n}\left(O_i - E_i\right)^2}{n}}\right]}{\left[\sqrt{\sum_{i=1}^{n}\left(O_i - \overline{O}_i\right)^2}\right]} \qquad (5.13)$$

The daily and monthly calibration and validation statistics of Rib flow respectively were R^2 (0.64, 0.63; 0.84, 0.75), NSE (0.62 0.60; 0.83, 0.74), PBIAS (10.7%, 7.4 %; 0.9%, 8.5%), and RSR (0.63 0.61; 0.41, 0.51). The daily and monthly calibration and validation values of Gumara respectively were found as R^2 (0.68, 0.67; 0.83; 0.80), NSE (0.66, 0.67; 0.82; 0.79), PBIAS (-14.4 %, 13.5 %; 5.1%, 12.1 %), and RSR (0.58, 0.58; 0.43 0.46). Model performance of streamflow could be evaluated "Good" if $0.6 < R^2 < 0.7$, $0.50 < RSR \leq 0.60$, $\pm 14 \leq PBIAS < \pm 30$ (Moriasi, 2007), and "Satisfactory" if, $0.50 < ENS \leq 0.65$ (Moriasi et al., 2007; Boskidis et al., 2012) (Table 5.11).

Table 5-11 Objective functions and model performance ratings of flow and sediment yield

Objective Function	Value range	Performance Classification	References
R^2	0.7 < R2 < 1	Very good	Moriasi et al., 2007
	0.6 < R2 < 0.7	Good	
	0.5 < R2 < 0.6	Satisfactory	
	R2 < 0.5	Unsatisfactory	
ENS	0.75 < ENS ≤ 1.00	Very good	Moriasi et al., 2007 Boskidis et al., 2012
	0.65 < ENS ≤0.75	Good	
	0.50 < ENS ≤ 0.65	Satisfactory	
	0.4 < ENS _≤ 0.50	Acceptable	
	ENS ≤ 0.4	Unsatisfactory	
RSR	0.00 ≤ RSR ≤ 0.50	Very good	Moriasi et al., 2007
	0.50 < RSR ≤ 0.60	Good	
	0.60 < RSR ≤ 0.70	Satisfactory	
	RSR > 0.70	Unsatisfactory	
PBIAS	PBIAS < ±15	Very good	Legates & McCabe, 1999
	±15 ≤ PBIAS < ±30	Good	
	±30 ≤ PBIAS < ±55	Satisfactory	
	PBIAS ≥±55	Unsatisfactory	

The daily flow calibration and validation value of R^2 for both watersheds were within the 'Good' performance ranges. The monthly flow calibration and validation value of R^2 for both watersheds were with in the 'Very Good' performance ranges. The daily flow calibration and validation statistics of NSE for Rib were 'Satisfactory' and Gumara were 'Good'. The monthly

NES value of flow calibration of Rib and calibration and validation values of Gumara were within the 'Very Good' performance ratings. The monthly NES flow validation performance value of Rib was within the 'Good' performance ranges. The daily calibration and validation of RSR statistics of Rib (0.63 0.61) and Gumara (0.58, 0.58) were within the 'Satisfactory' and 'Good' performance range of values respectively. The monthly RSR statistics of Rib calibration (0.4) and validation (0.51) were within the 'Very Good' and 'Good' rating scales, and Gumara calibration (0.43) and validation (0.46) were within the 'Very Good' performance range of values (Table 5.11). The daily and monthly calibration and validation values of PBIAS for both watersheds were within the ‘Very good’ performance evaluation statistics (Moriasi, 2007) (Table 5.11).

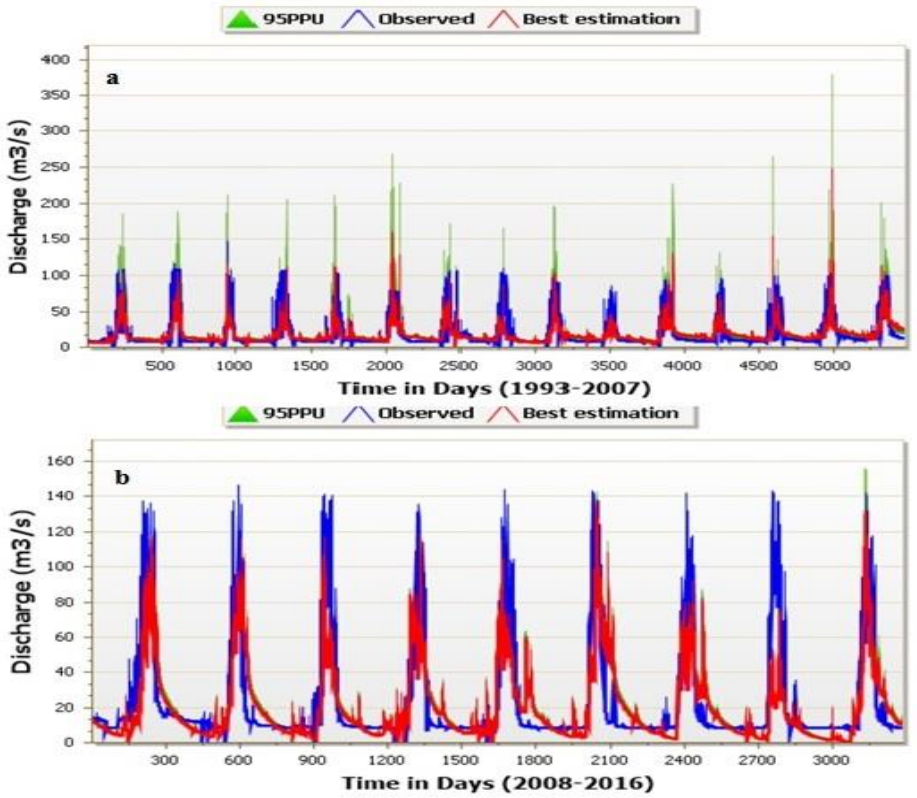

Figure 5-14 Hydrograph of measured versus simulated and 95PPU of daily flow calibration (a) and validation (b) of Rib

The P-factor value of streamflow for daily and monthly calibration and validation of Rib were (0.57, 0.17) and (0.81%, 0.69%) respectively. The R-factor values of flow in the order above were (0.33 0.07), and (0.64, 0.52). For Gumara the daily and monthly calibration and validation P-factor value of flow respectively were found as (0.93, 0.85) and (0.87%, 0.79%). The R-factor values of Gumara flow in the order above were (1.32, 1.06), and (0.73, 0.79).

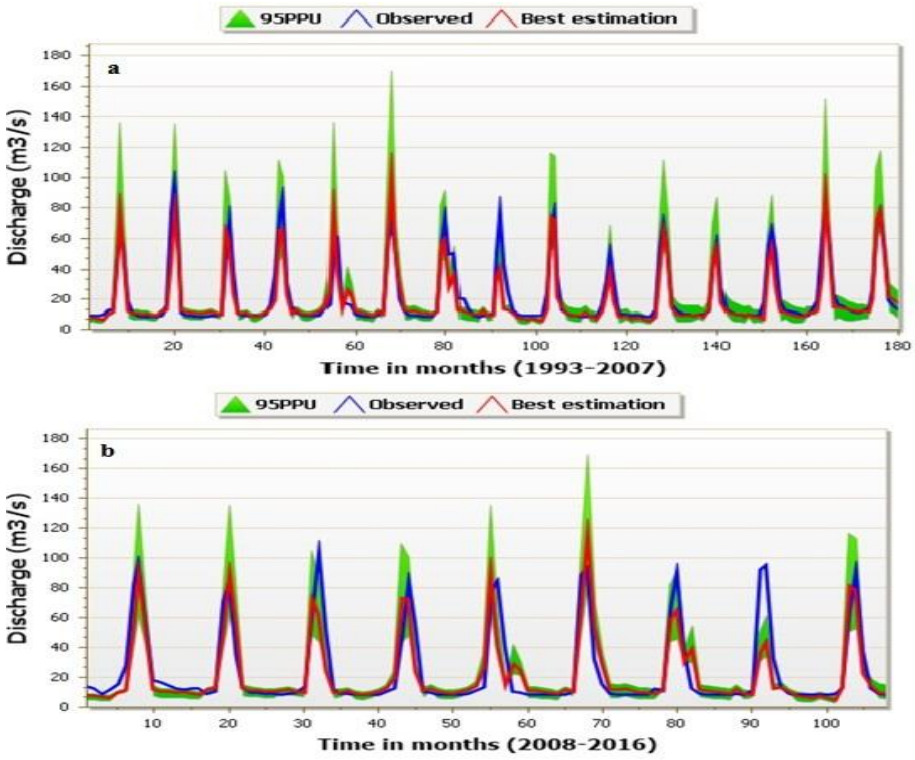

Figure 5-15 Hydrograph of measured versus simulated and 95PPU of monthly flow calibration (a) and validation (b) of Rib

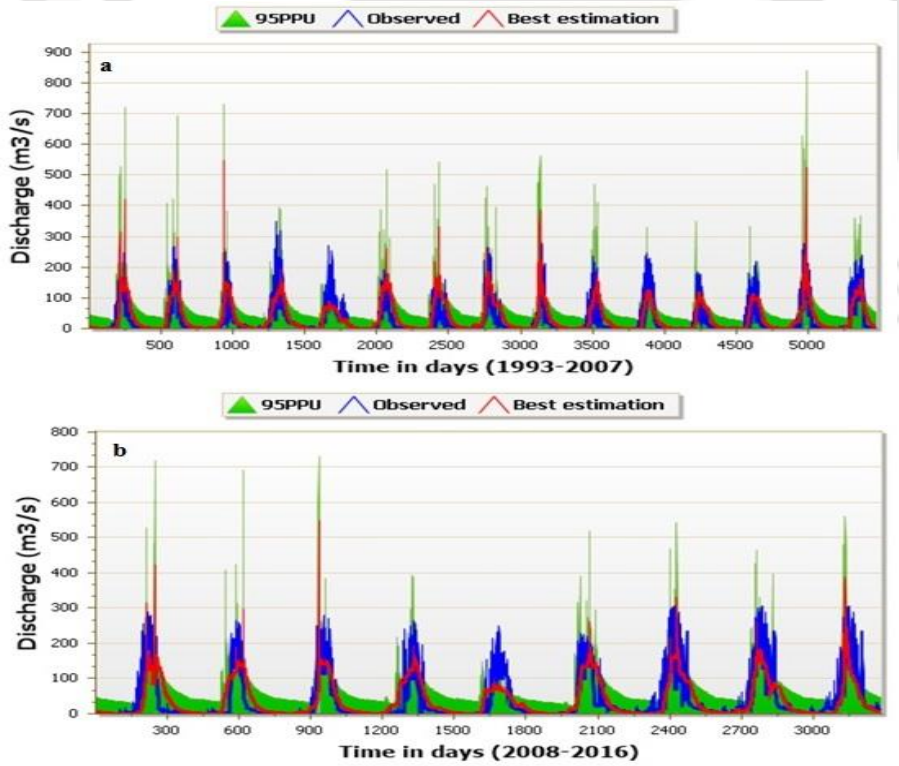

Figure 5-16 Hydrograph of measured versus simulated and 95PPU of daily flow calibration (a) and validation (b), Gumara

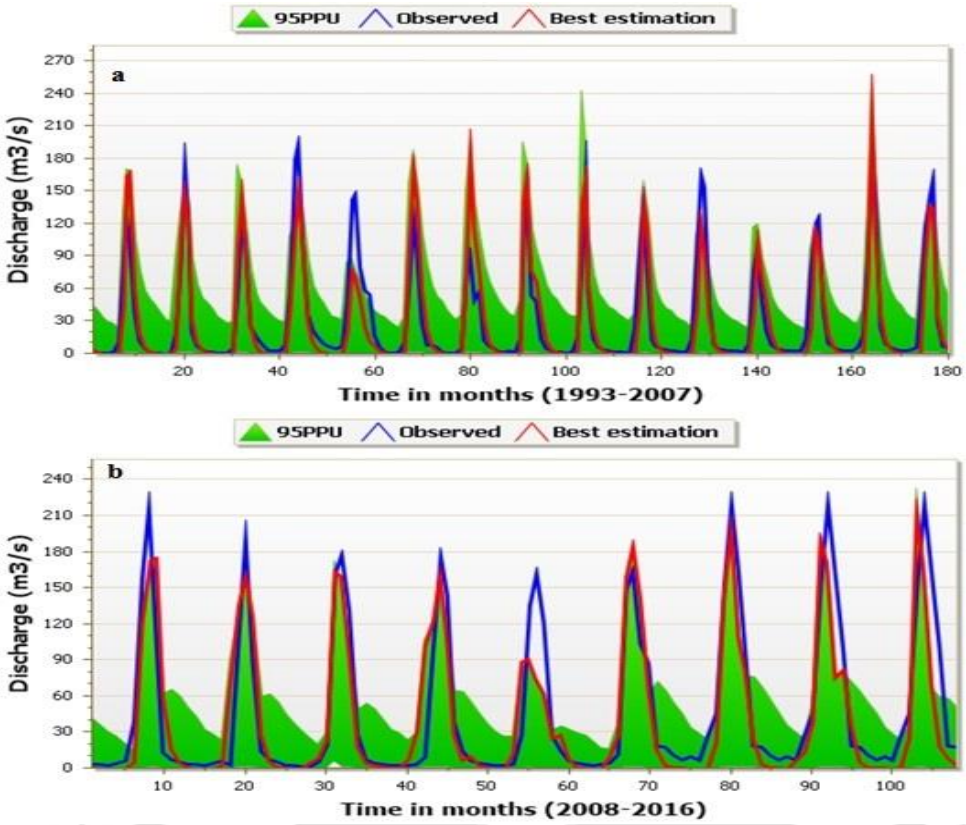

Figure 5-17 Hydrograph of measured versus simulated and 95PPU of monthly flow calibration (a) and validation (b), Gumara

Both watersheds had good R-factor and P-factor flow evaluation statistics except Rib daily validation which had a bit lower statistics (R-factor = 0.07 and P-factor = 0.17). The results showed that SUFI-2 had better goodness of fit of R-factor (thickness of the 95PPU) for streamflow (Table 5-12).

Table 5-12 Summary statistics of calibration and validation of flow, Rib and Gumara

	Components	p-factor	r-factor	R^2	NSE	PBIAS	RSR
Rib	Calibration daily	0.57	0.33	0.64	0.62	10.7	0.63
	Calibration monthly	0.81	0.64	0.84	0.83	9.1	0.41
	Validation daily	0.17	0.07	0.63	0.60	7.4	0.61
	Validation monthly	0.69	0.52	0.75	0.74	8.5	0.51
Gumara	Calibration daily	0.93	1.32	0.68	0.66	-14.4	0.58
	Calibration monthly	0.87	0.73	0.83	0.82	5.1	0.43
	Validation daily	0.85	1.06	0.67	0.67	13.5	0.58
	Validation monthly	0.79	1.00	0.80	0.79	12.1	0.46

The slope and intercept of the best-fit regression line on the scatter plot of monthly flow calibration and validation (Figure 5-18 for Rib and 5-19 for Gumara) pointed out the deviation between observations and simulations.

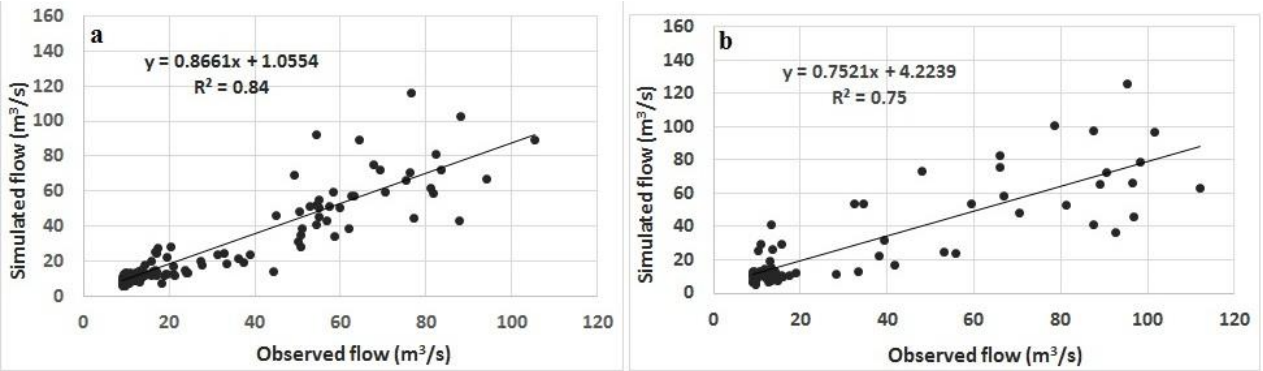

Figure 5-18 Regression best fit line of observed versus simulated monthly flow calibration (a) and validation (b), Rib

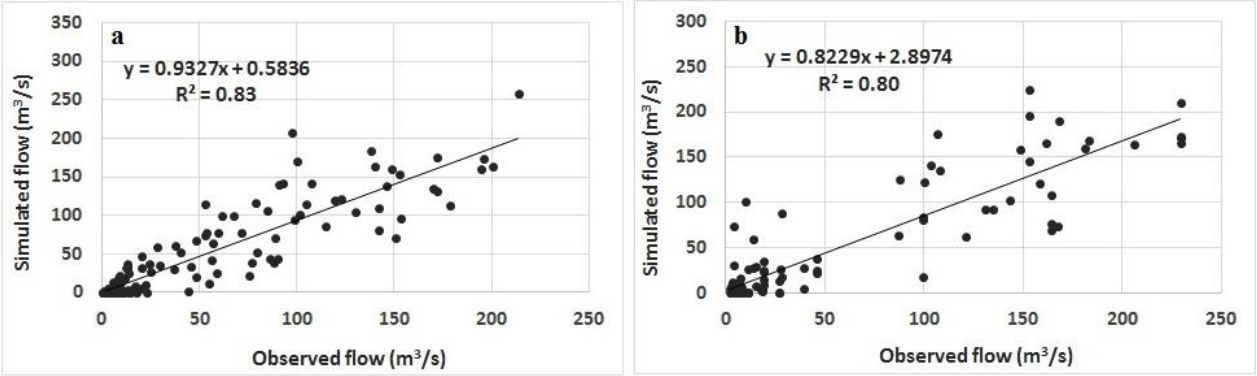

Figure 5-19 Regression best fit line of observed versus simulated monthly flow calibration (a) and validation (b), Gumara

5.3.5 Sediment calibration and validation

As shown in Table 5-13, the calibration and validation performance evaluation statistics respectively were, R^2 (0.74, 0.61), NSE (0.72, 0.60), PBIAS (18.8, 18.7%), and RSR (0.53, 0.64) for Rib and R^2 (0.76, 0.73), NSE (0.73, 0.71), PBIAS (7.0, 5.9 %), and RSR (0.51, 0.52) for Gumara. The calibration and validation of R^2 model performance evaluations of both watersheds were within the 'Very Good' rating scale except the validation value of Rib which was within the 'Good' performance range (Moriasi et al., 2007). The NSE and RSR performance values were within the 'Good' rating scale (Moriasi et al., 2007; Boskidis et al., 2012) as it is presented in Table 5-13.

The PBIAS performance value of calibration and validation of Rib (18.8, 18.7) and Gumara (7.0, 5.9) were within the rating scales of 'Good' and 'Very Good' respectively (Moriasi et al., 2007) (Table 5-11). The p-factor value of sediment calibration and validation for Rib and Gumara respectively were (0.62, 0.47) and (0.38, 0.31). The calibration and validation R-factor values of Rib and Gumara were (1.2, 0.46) and (0.81 and 0.66) in their order. The results showed that SUFI-2 has better goodness of fit of R-factor (thickness of the 95PPU) of sediment yield (Table 5-13).

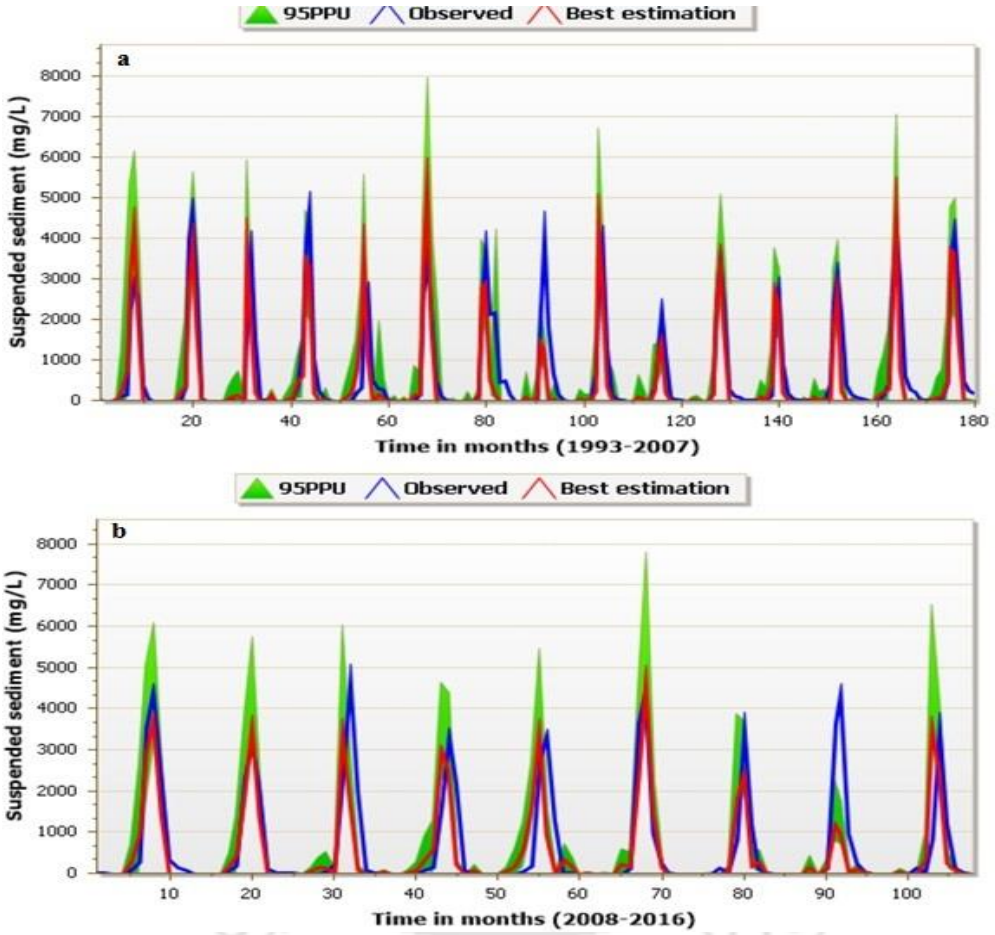

Figure 5-20 Observed versus simulated and 95PPU of Rib sediment calibration (a) and validation (b)

The fitted values of parameters and their upper and lower bounds of sediment yield (Table 5-9 for Rib and 5-10 for Gumara) were the final calibrated SWAT model parameter values of the watershed. The calibrated parameter ranges were used to validate the model by making a complete iteration.

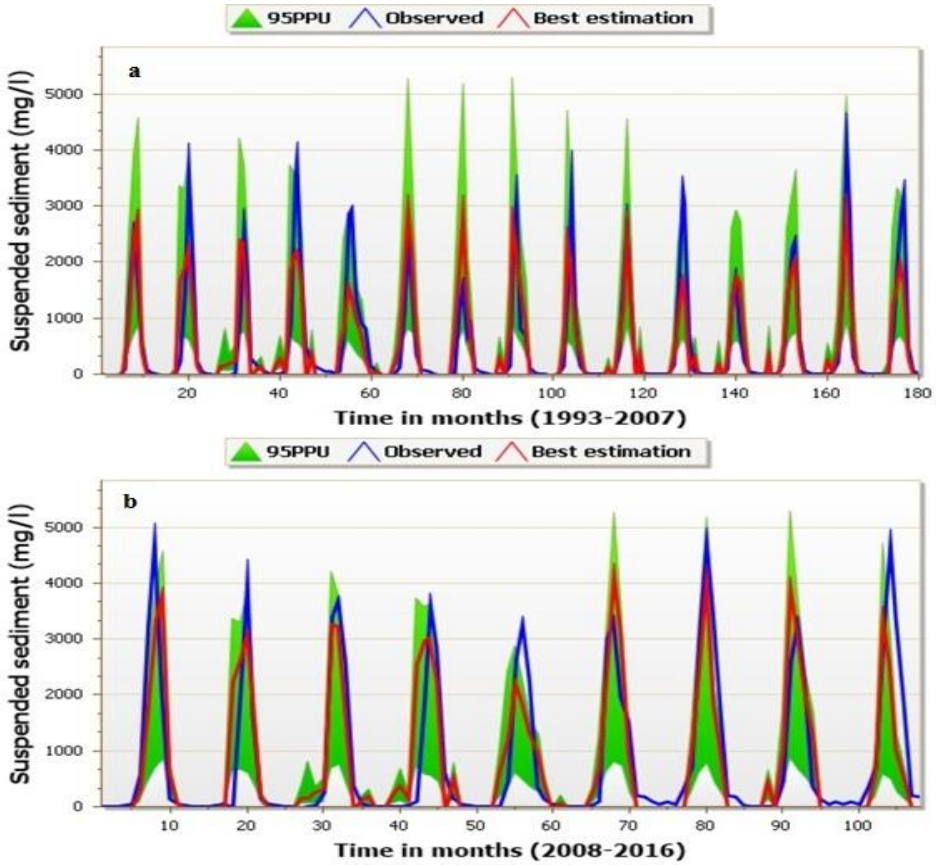

Figure 5-21 Observed versus simulated and 95PPU of Gumara sediment calibration (a) and validation (b)

Figure 5-20 & 5-21 shows measured, best-simulated sediment yield, and 95% model prediction uncertainty band and it describes the deviation between the observations and SWAT simulations for visual comparison for Rib and Gumara respectively. From the figures one can understand the deviation between observations and SWAT simulations.

Table 5-13 Sediment calibration and validation statistics of Rib and Gumara

	Components	p-factor	r-factor	R^2	NSE	PBIAS	RSR
Rib	Calibration	0.62	1.2	0.74	0.72	18.8	0.53
	Validation	0.47	0.46	0.61	0.60	18.7	0.64
Gumara	Calibration	0.38	0.81	0.76	0.73	7.0	0.51
	Validation	0.31	0.66	0.73	0.71	5.9	0.52

The slope and intercept on the regression best fit line of monthly sediment calibration and validation (Figure 5-22 for Rib and 5-23 for Gumara) pointed out the deviation between observations and simulations.

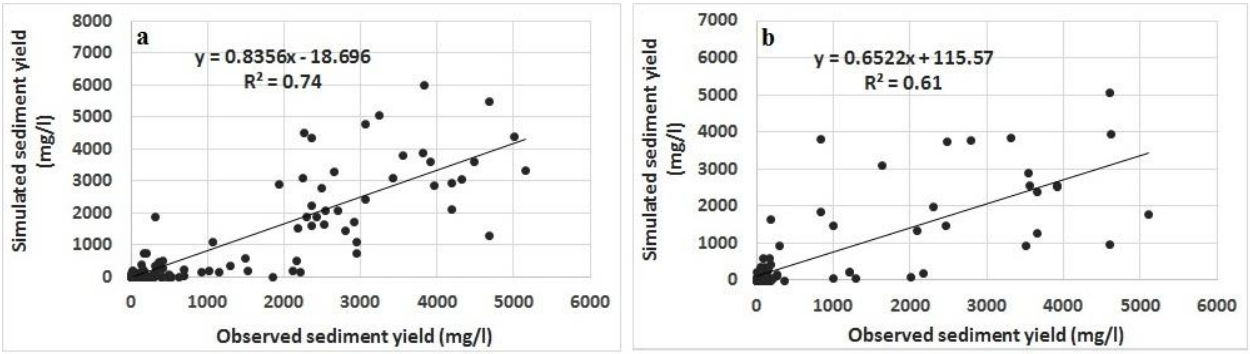

Figure 5-22 Regression best fit line of observed versus simulated monthly sediment calibration (a) and validation (b), Rib

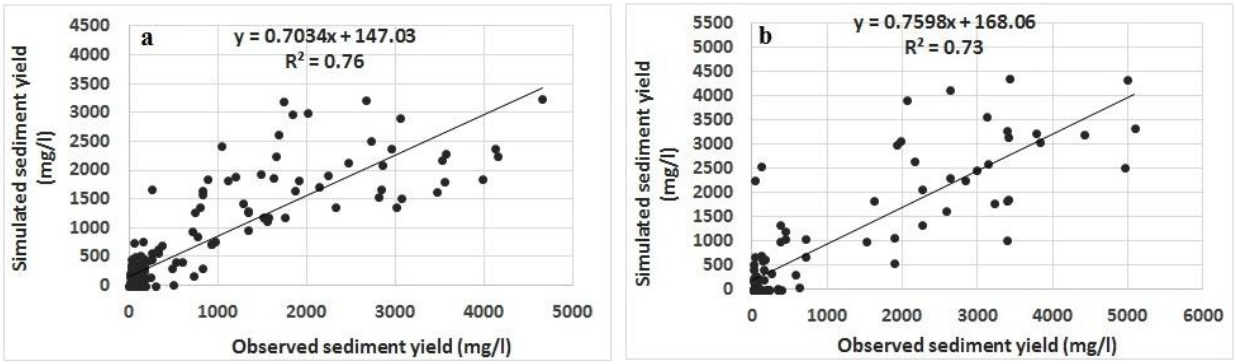

Figure 5-23 Regression best fit line of observed versus simulated monthly sediment calibration (a) and validation (b), Gumara

The time series plots of simulated versus measured and the performance evaluation statistics values of R^2, NES, RSR, PBIAS and the P-factor and R-factor of the calibration and validation indicated the presence of reasonable agreement between measured and simulated stream flow and sediment yield in the watersheds and the result indicated that the SWAT model with the SUFI-2 calibration procedure simulate satisfactorily the streamflow and sediment yield of the watersheds.

5.4 Conclusion

Assessing ArcSWAT model for its ability to simulate water balance components in general and streamflow and sediment yield in particular, employing various performance efficiency criteria such as R2, NSE, RSR, PBIAS, R-factor, and P-factor, provide insight into how one can successfully generate valuable information in watersheds where there is little available data. The result of this study suggested that SWAT hydrological model could be a useful tool, which once calibrated effectively, can produce meaningful predictions of catchment hydrology to aid watershed management decisions. This study provided a better understanding of SWAT model setup and hydrologic processes of the catchments.

In the study SWAT, a continuous in time, long-term, process-based watershed scale model, in combination with the GIS interface and SWAT CUP-SUFI-2 calibration procedure was applied to quantify daily and monthly streamflow, and monthly sediment yield at Rib and Gumara watersheds. Stream gauge station analyzed data and information were used for the ArcSWAT model setup. Flow and sediment yield calibration, uncertainty analysis, and validation were performed with SWAT CUP-SUFI-2 parameter optimization procedure. Even though, the study results showed the existence of an agreement between observations and model predictions of streamflow and sediment yield at the watershed outlet within the performance ratings of recommended statistics, SWAT under-predicted peak flow and sediment loads in calibration and validation periods. The limitations of this study were related to data resulted from the inconsistent measurement of flow and sediment. The calibrated model provides important information to apply the model in other ungauged watersheds of similar topography, land use, soil, climate, and management for the purpose of soil erosion assessments, scenario analyses, and implementation of the best management in Ethiopian highlands.

Chapter 6 : Assessment of the Impact of Agricultural Management Scenarios on Sediment Yield in Rib and Gumara Watersheds

6.1 Introduction

Land and soil resource degradation are major problems in Ethiopia. Rugged terrain, over-cultivation, and improper management of land make the rate of soil erosion and land degradation very high in Ethiopia (Hurni et al., 2005). The area of this study is part of Northwest Ethiopia where there is a high soils loss. The watersheds are among the populated areas in the region which causes deforestation and expansion of residential areas and agricultural lands. The frequent LULC changes and lack of land use management strategies have a great impact on the water balance of the watersheds by changing the magnitude and pattern of the components of streamflow and soil detachment and removal.

The Lake Tana (mouth of Rib and Gumara rivers) is the source of livelihood for a large number of people through fishing and tourism, and it plays a crucial role in balancing the surrounding ecosystem (Hurni et al., 2015; National Planning Commission, 2015). Because of its multi-dimensional use, it is registered as a Biosphere Reserves by UNESCO since 2015 (Bires and Raj, 2019). However, the lake is threatening by siltation due to environmental degradation (Awulachew et al., 2008). Soil erosion declines the agricultural production of the watersheds and sediment from the upstream has been accumulated into the Lake Tana (Dile et al., 2013). Lack of researches related to erosion and its management hinders development activities in the study watersheds. Therefore, the management of erosion needs watershed-scale modeling to quantify sediment yield at sub-watershed levels by considering hydrological processes, topography, weather conditions, soils, and management practices (Easton et al., 2010; Römkens et al., 2002). Studies of the impact of management practices on soil erosion (Römkens et al., 2002) enable to prioritize watersheds to implement appropriate soil and water conservation (SWC) strategies. Implementing management practices minimizes pollution and improves the quality of water (Bracmort et al., 2006). The implementation of selected management practices retards soil erosion and sediment transport especially in agriculture dominated watersheds. Identifying erosion susceptible sites using appropriate watershed-scale models is a fundamental input for planners and resource managers to implement site-specific land management measures in the watersheds (Sefelnasr, 2013).

Because of the complex nature of the soil erosion process, a variety of spatial and distributed models have been developed at different spatial scales (Pandey et al., 2016). These models play an important contribution in understanding the effect of management practices on sediment and agro-chemical yields in watersheds. SWAT model was examined in the analysis of runoff processes and water balance simulation in catchment scales (Melaku et al., 2018; Setegn et al., 2010; Addis et al., 2016; Ayele et al., 2017). The SWAT enables to estimate the effect of land management methods on hydrology and soil erosion and it is capable of identifying best management options in catchments (Arnold et al., 2012; Neitsch et al., 2011). The SWAT predicts the impact of management practice on water, sediment, and agro-chemical yields in watersheds having different soils and land use over time (Neitsch et al., 2011; Sefelnasr, 2013). The impact of agricultural management practices on sediment reduction was simulated with the SWAT model (Bracmort et al., 2006; Vaché et al., 2002; Santhi et al., 2006; Demissie et al., 2013). The impact of management practices on sediment processes is represented by modifying selected SWAT parameters (Bracmort et al., 2006). Selection and application of best management practice (BMPs) and their parameters are area specific (Abdelwahab et al., 2014).

The study area has limited physical soil and water conservation measures such cut-off drain, water way, check dams and gully treatment through biological and physical methods. The reasons raised by agricultural experts for the limited erosion and sediment management efficiency of the conservation structures found in the watershed were intentional action of farmers in avoiding structures since their land is occupied by physical measures, inconvenience for ploughing and grazing, and inappropriate spacing between structures. In addition, the conservation structures are not fully conducted in all parts of the watershed.

6.2 Materials and Methods

6.2.1 Agricultural management practices

The calibrated SWAT model was used to assess the impact of agricultural management scenarios on sediment yield. Based on the watersheds existing condition of sediment yield, agricultural management scenarios were determined. In the study, four scenarios were selected and the values of their parameters have been assigned on the basis of local research experience in the Ethiopian highlands (Hurni, 1985; Herweg and Ludi, 1999; Gebremichael et al., 2005; Addis et al., 2016; Nigussie et al., 2017; Sultan et al., 2017; Melaku et al., 2018).

The scenarios selected for simulation were part of Ethiopian soil and water management guideline and can be implemented with local resources of the study area (Hurni et al., 2015; National Planning Commission, 2015). The agricultural managements practices selected were grass filter strips and soil bunds. The function of the filter strip is to trap sediment by filtering the runoff in a plot of land (Bracmort et al., 2006; Mekonnen et al., 2016). The capacity of filter strips in reducing erosion and sediment depends on the strip width (FILTERW). Grass strips with 1m width and spaced at a vertical interval of 1 m could substitute physical conservation structures (Hurni et al., 2015). In this study, the grass filter strip with strip (FILTERW) width of 1m (scenario 1) and 5m (scenario 2) were introduced along the contour on agricultural HRUs, all slope classes and soil types, and the other parameters were kept as they were in the watershed existing condition (Hurni, 1985; Herweg and Ludi, 1999; Addis et al., 2016; Kassawmar et al., 2018). Agricultural management scenarios were presented in Table 6-1 for Rib and Table 6-2 for Gumara.

Table 6-1 Management scenarios and their parameters, Rib

Scenario	Description	Parameter	Calibrated	Modified
Baseline 0	Existing condition	**	**	**
Filter strips Scenario 1	Grass filter strips along the contour	FILTERW	0	1m
Filter strips Scenario 2	Grass filter strip along the contour	FILTERW	0	5m
Soil bunds Scenario 3	Soil bund along the contour	SLSUBBSN	*d*	10m
		CN2	*d*	59
		USLE_P	0.42	0.32
Soil bunds Scenario 4	Soil bund along the contour	SLSUBBSN	*d*	0.5*d*
		CN2	*d*	59
		USLE_P	0.42	0.32

Table 6-2 Management scenarios and their parameters, Gumara

Scenario	Description	Parameter	Calibrated	Modified
Scenario-0	Existing condition	**	**	**
Filter strips Scenario 1	Grass filter strip along the contour	FILTERW	0	1m
Filter strips Scenario 2	Grass filter strip along the contour	FILTERW	0	5m
Soil bunds Scenario 3	soil bund along the contour	SLSUBBSN	*d*	10m
		CN2	*d*	59
		USLE P	0.56	0.32
Soil bunds Scenario 4	Soil bund along the contour	SLSUBBSN	*d*	0.50d
		CN2	*d*	59
		USLE P	0.56	0.32

*Note: FILTERW: width of the strip, CN2: curve number, USLE_P: support factor of USLE, SLSUBBSN: average length of slope, d: calibrated value of parameters, **parameter values under the existing conditions.*

Soil bunds have a function to reduce surface flow, sheet erosion, and slope length (Addis et al., 2016; Bracmort et al., 2006; Nyssen et al., 2007). Soil bunds which are implemented along the contour have the capability to minimize rill erosion by 38% to 74% (Addis et al., 2016; Jemberu et al., 2018; Melaku et al., 2018). The impacts of soil bunds scenarios on erosion were analyzed on agricultural HRUs and in all soil and slope classes. The impacts of soil bunds on sediment yield are represented by parameters of average slope length (SLSUBBSN), Curve Number (CN2), and USLE practice factor (USLE_P). Spacing between continuous soil bunds on the ground is indicated by SLSUBBSN (Herweg and Ludi, 1999; Kassawmar et al., 2018). The SLSUBBSN value was assigned in the SWAT model depending on the slope values of the input topographic data (DEM). In this study the SLSUBBSN is reduced to 10m for soil bund scenario 3 and reduced by 50% for soil bund scenario 4. Considering the local experiences, USLE_P value of 0.32 was assigned (Nyssen et al., 2007; Sultan et al., 2017; Kassawmar et al., 2018). The CN2 value of 59 was assigned referred from SWAT manual for the contoured and terraced conditions (Neitsch et al., 2005).

6.3 Results and Discussion

6.3.1 Agricultural management scenarios and their impact on sediment yield

The watershed sediment classes were categorized into low (0–10), moderate (10–20), high (20–30), very high (30–50) and sever (>50) t $ha^{-1}yr^{-1}$. Sediment yield distribution and erosion affected areas of the watersheds are represented in Figure 6-1(a) Rib and (b) Gumara. In scenario 0, the basin existing conditions which corresponds to the current land management practices was considered. In the existing condition, the average sediment yield values of the watersheds were 23.6 t ha^{-1} $yr^{-}1$ for Rib and 57.6 t ha^{-1} $yr^{-}1$ for Gumara. The result of this study is in line with (Vanmaercke et al., 2010) which was reported as the annual sediment is between 5–66 t ha^{-1} yr^{-1} in the Highlands of Ethiopian.

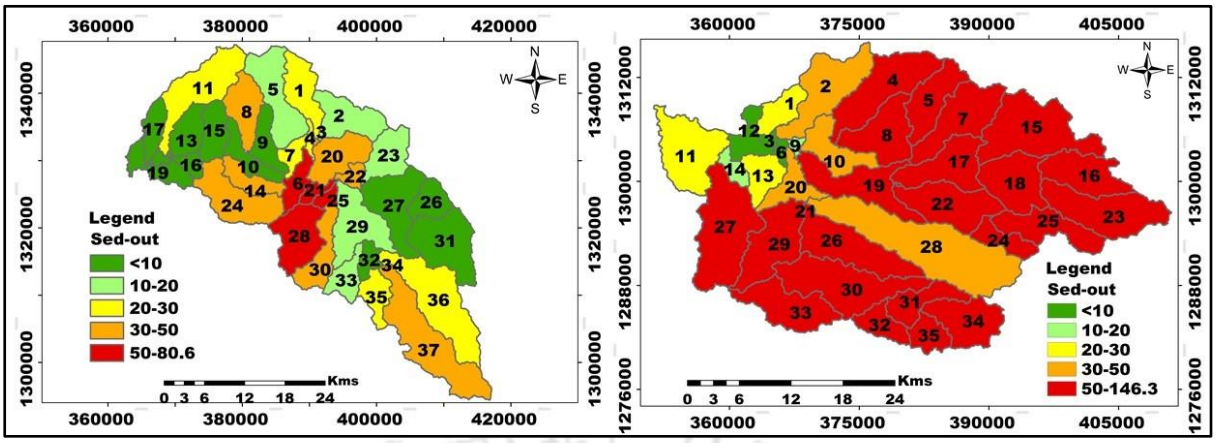

Figure 6-1 Map of sediment yield classes of sub-watersheds of Rib (a) and Gumara (b)

In scenario 0 the sediment yield of Rib ranges between 1.2 t ha^{-1} yr^{-1} (sub-watershed 19) to 80.6 t ha^{-1} yr^{-1} (sub-watershed 28) (Figure 6-1a). Sub-watersheds 9, 10, 12, 13, 15, 16, 17, 18, 19, 26, 27, 31, 32 and 34 are within the low range of sediment yield (<10 t ha^{-1} yr^{-1}) and sub-watersheds 2, 5, 23, 29 and 33 are within the moderate level of sediment class (10–20 t $ha^{-}1$ yr^{-1}). The sub-watersheds 1, 4, 7, 11, 35, and 36 were found within the high (20–30 t ha^{-1} yr^{-1}) sediment yield levels. Sub-watersheds 3, 8, 14, 20, 22, 24, 30, 37 were found within very high (30–50 t ha^{-1}) and 6, 21, 25, 28 were in the severe (>50 t ha^{-1}) sediment yield classes (Figure 6-1a). In Gumara, Sub-watersheds 3, 6, and 12 are found in the low range of sediment yield and 9 and 14 are found within the moderate sediment class. Sub-watersheds 1, 11 and 13 are found in the high sediment yield class. Sub-watersheds 2, 10 and 28 are experiencing very high sediment loss whereas sub-watersheds 4, 5, 7, 8, 15, 16, 17, 18, 19, 21, 22, 23, 24, 25, 26, 27, 29, 30, 31, 32, 33, 34, 35 are within the severe sediment yield category in Gumara (Figure 6-1b). High erosion and sediment yield were observed in the cultivated lands and low erosion was observed in the mixed forests and shrublands. The result showed that sediment yield is high in areas where the topography is rugged and relatively low in sub-watersheds found in the lower part of the watershed. According to the spatial variability of sediment source and sediment yield identified in the watersheds as represented in Figure 6-1, management practice scenarios (Table 6-1 for Rib and 6-2 for Gumara) were developed and simulated in SWAT model for identifying their effects on sediment yield production in sub-watershed scales. The average sediment yield with grass strip scenario 1 (FILTERW width of 1m) and grass strip scenario 2 (FILTERW width of 5m) were 16.5 and 12.0 t ha^{-1} yr^{-1} respectively in Rib. There were 30% and 49% average reduction in sediment yield in grass strip scenario 1 and grass strip scenario 2 respectively

from the base period. The average sediment yield in filter strip scenario 1 and filter strip scenario 2 are 36.7 and 23.9 t ha^{-1} yr^{-1} respectively in Gumara. There were 47% and 58.5% average reduction of sediment yield with the implementation of filter strip scenario 1 and filter strip scenario 2 respectively in the Gumara compared with the base period. The lowest and highest sediment yield in grass filter strip scenario 1 and 2 were 1.0, 56.3 t ha^{-1} yr^{-1} and 0.7, 41.4 t $ha^{-}1$ yr^{-1} in sub-watersheds 19 and 28 respectively in Rib (Figure 6-2a scenario 1 and 6-2b scenario 2). The lowest and highest sediment yield in grass strip scenario 1 and grass strip scenario 2 were 1.0, 92.9 t ha^{-1} yr^{-1} and 0.7, 60.2 t $ha^{-}1$ yr^{-1} in sub-watersheds 21 and 24 respectively in Gumara (Figure 6-3a scenario 1 and 6-3b scenario 2). The result showed that there is a significant decrease in sediment yield with the introduction of grass strips in the two scenarios. The high reduction is observed in the case of grass strip scenario 2 than scenario 1 in all agricultural lands, soils, and slope classes. Figure 6-2 and Figure 6-3 represents sediment yield classes of grass filter strip scenarios per sub-watershed levels in Rib and Gumara respectively.

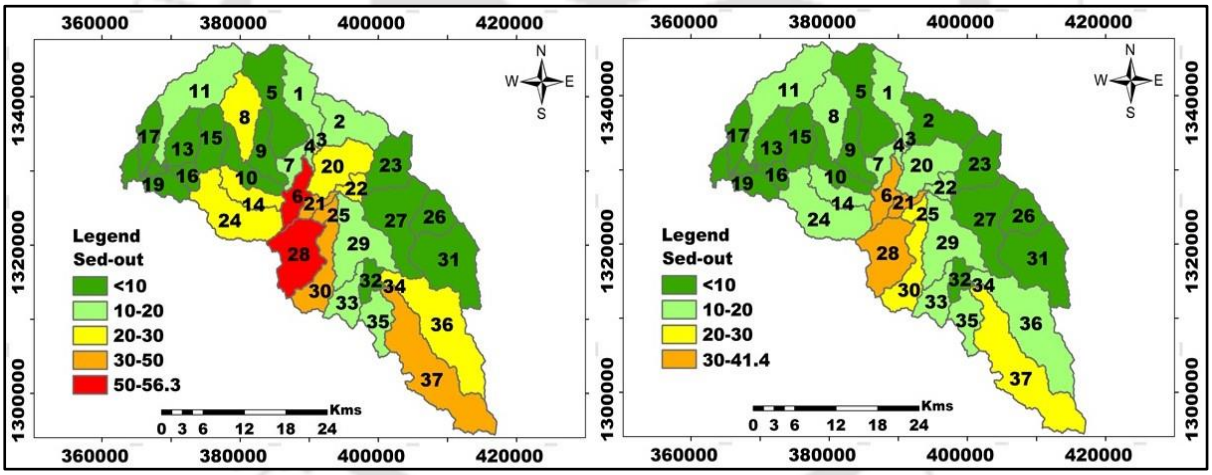

Figure 6-2 Sediment yield map of filter strip scenario 1 (a) and filter strip scenario 2 (b) of Rib

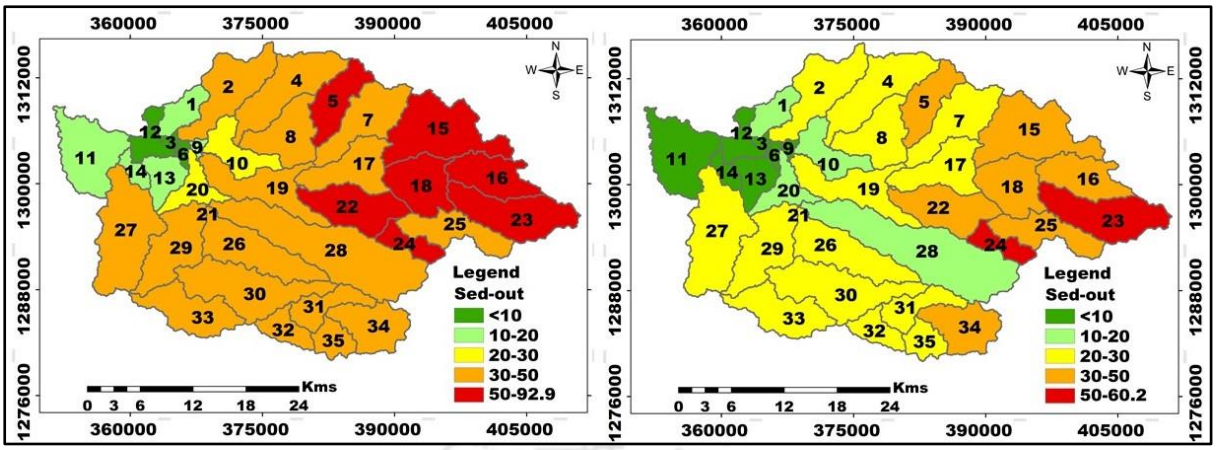

Figure 6-3 Sediment yield map of filter strip scenario1 (a) and scenario 2(b), Gumara

In Rib, sediment yield value of soil bund scenario 3 and scenario 4 ranges between 0.1–23.3 and 0.2–23.4 t ha^{-1} yr^{-1} respectively (Figure 6-4a scenario 3 and 6-4b scenario 4). The average sediment value of scenario 3 was 5.2 t ha^{-1} yr^{-1} and scenario 4 was 5.5 t ha^{-1} yr^{-1} compared to the base period of 23.3 t ha^{-1} yr^{-1}. The lowest and highest reduction of sediment yield was 71 % and 92 % in scenario 3, and 70.9 % and 84 % in scenario 4 in Rib.

In Gumara, sediment yield value of soil bund scenario 3 and scenario 4 ranges between 0.3–25.9 and 0.4–27.7 t ha^{-1} yr^{-1} respectively (Figure 6-5a scenario 3 and 6-5b scenario 4). The average sediment yield value of scenario 3 was 9.3 t ha^{-1} yr^{-1} and scenario 4 was 10.6 t ha^{-1} yr^{-1} compared to the base period of 57.6 t ha^{-1} yr^{-1} in Gumara. The lowest and highest reduction of sediment yield was 82.3% and 82.4% in scenario 3, and 76.5% and 81% in scenario 4 in Gumara. The effectiveness of each management practice in reducing sediment per hectare in each sub-watershed is represented in Table 6.3. The impact each management practice has on sediment yield reduction showed a broader spatial variation.

When filter strip and soil bund scenarios were compared, soil bunds have a high capacity in reducing sediment than the grass strips. The grass filter strip scenario1 and soil bund scenario 3 average sediment reductions capacity by 29.7 and 77.9 % and 36.3 and 83.5 % for Rib and Gumara respectively are comparable with Demissie et al. (2013) in the Gibe basin, Ethiopia. They reported that the performance of grass strips and soil bunds in sediment reduction is 35% and 82% respectively.

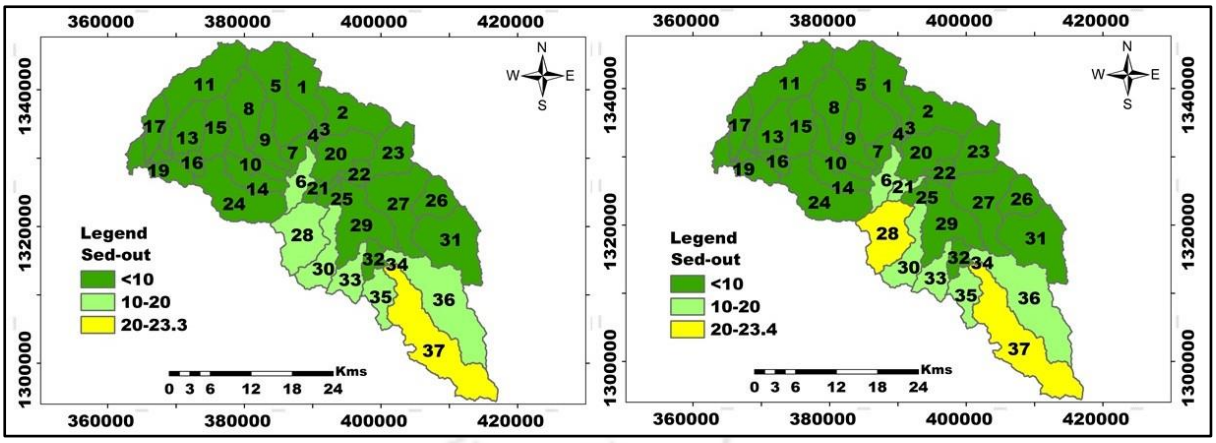

Figure 6-4 Sediment yield map of stone bund scenario 3 (a) and scenario 4 (b) of Rib

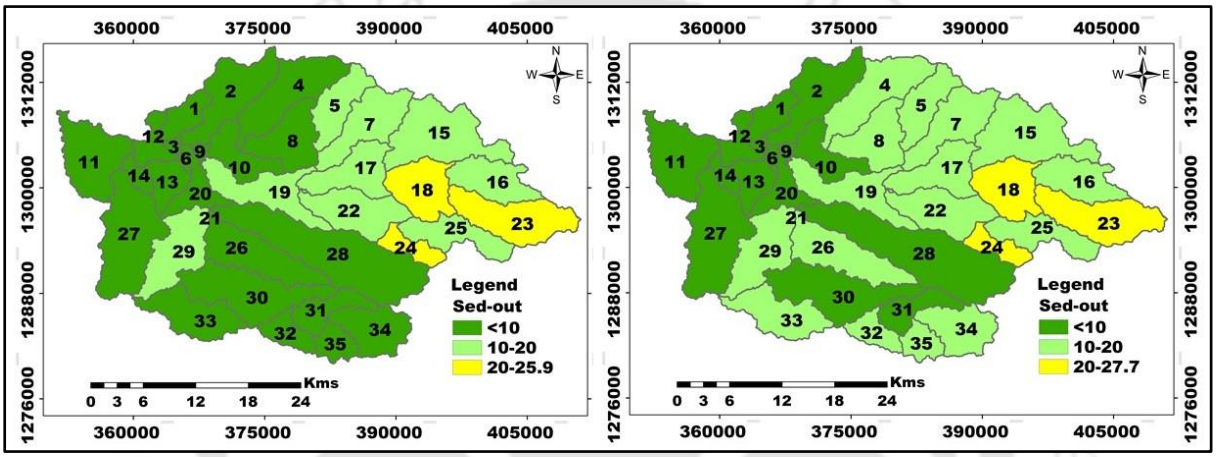

Figure 6-5 Sediment yield map of stone bund scenario 3 (a) and scenario 4 (b) of Gumara

Table 6-3 BMPs and sediment reduction per ha in Rib and Gumara

Sub basin	Base	Scenarios Rib				Base	Scenarios Gumara			
		1	2	3	4		1	2	3	4
1	20.2	15.8	13.0	8.5	8.5	29.6	18.9	12.3	4.2	5.3
2	18.2	12.1	8.4	2.0	2.1	48.1	30.7	20.1	8.2	9.9
3	38.5	24.4	15.7	0.7	1.0	5.8	3.7	2.4	1.0	1.3
4	28.1	17.8	11.5	0.5	0.9	57.1	36.4	23.7	8.4	10.1
5	11.8	8.4	6.3	2.9	2.9	87.1	55.6	36.2	15.4	16.1
6	80.5	53.3	36.7	12.2	13.0	9.4	6.0	3.9	1.4	2.0
7	26.2	16.6	10.7	1.0	1.5	60.6	38.7	25.3	12.0	12.8
8	35.8	22.7	14.7	1.9	2.7	64.8	41.3	26.9	9.1	11.2
9	5.8	3.7	2.4	0.1	0.2	16.9	10.7	7.0	2.3	3.0
10	8.7	6.2	4.6	2.3	2.4	35.2	22.6	14.8	4.8	6.4
11	25.2	17.5	12.7	4.7	4.8	20.8	13.2	8.6	3.1	3.8
12	1.4	1.1	0.8	0.5	0.5	7.5	4.8	3.2	1.4	1.8
13	7.5	5.1	3.7	1.5	1.6	22.7	14.4	9.3	3.8	4.3
14	37.3	24.9	17.3	5.3	6.0	17.0	10.8	7.0	2.5	3.1
15	7.3	4.8	3.3	0.8	0.9	93.3	59.4	38.7	14.1	16.4
16	4.7	3.2	2.2	0.6	0.6	104.9	66.8	43.4	17.0	19.0
17	3.7	2.3	1.5	0.1	0.1	65.9	42.1	27.5	12.7	13.1
18	1.6	1.3	1.0	0.7	0.7	105.9	67.5	44.1	20.5	20.6
19	1.2	0.9	0.7	0.3	0.4	59.9	38.2	24.9	10.0	11.1
20	31.6	20.0	12.9	1.4	1.9	40.9	26.0	16.8	6.0	7.1
21	71.1	47.1	32.4	10.0	11.2	1.7	1.1	0.7	0.3	0.4
22	34.7	23.9	17.4	7.5	7.9	93.0	59.2	38.6	17.1	17.3
23	12.4	9.9	8.3	6.1	6.1	141.7	90.8	59.7	25.9	27.7
24	32.3	21.3	14.5	3.3	3.9	146..3	92.9	60.2	24.9	26.3
25	59.9	37.9	24.4	4.1	5.2	73.9	47.8	31.7	15.3	15.8
26	4.6	2.9	1.9	0.3	0.3	65.0	41.2	26.6	9.7	11.1
27	7.1	4.5	2.9	0.5	0.6	57.0	36.1	23.3	8.6	9.8
28	80.6	56.3	41.4	19.1	20.0	48.2	30.7	20.0	7.1	8.5
29	19.6	14.1	10.8	5.6	6.0	63.2	40.0	25.8	10.4	11.2
30	42.7	31.0	23.9	12.9	13.8	57.3	36.3	23.4	6.8	9.4
31	5.2	4.3	3.7	2.8	2.8	50.4	31.9	20.6	5.5	8.2
32	7.4	6.2	5.5	4.3	4.3	58.8	37.2	24.0	9.6	10.9
33	15.4	13.8	12.7	11.2	11.3	65.6	41.6	27.0	8.6	10.8
34	5.0	4.8	4.7	4.5	4.5	74.2	47.0	30.3	8.8	12.0
35	20.8	17.2	15.0	11.7	11.9	66.9	42.3	27.3	9.8	11.4
36	25.1	21.9	19.9	16.9	17.1	----	----	----	----	----
37	34.7	30.1	27.3	23.3	23.4	-----	-----	----	-----	----

6.4 Conclusion

The SWAT has been implemented to assess the effect of AMPs on sediment reduction. Hot spots of erosion were identified in sub-watershed levels which are fundamental information for catchment management planning for erosion and sediment reduction. The result showed that grass filter strip and soil bund scenarios significantly reduced sediment yield at the sub-watershed levels. A significant portion of the watershed was covered by croplands and steep

slopes. High sediment reduction could be achieved by implementing grass filter strips at lower slopes and stone bunds at higher slopes of the sub-watershed. The result indicated that

a notable reduction of erosion and sediment could be obtained by implementing management practices in croplands in sub-watershed levels. This study provides fundamental information for decision-makers to prioritize areas of intervention. More effective AMPs should be investigated in order to reduce erosion and sediment outputs from the watershed for enhanced agricultural productivity. The procedures of this study could be implemented to other similar watersheds of the area for impact assessment of management practices on erosion and sedimentation to implement site-specific management strategies.

Chapter 7 : Estimate the Soil Loss and Sediment Yield of Anjeb Watershed

7.1 Introduction

In many parts of the world in general and in Ethiopia in particular, soil erosion affects the stability of ecosystems (Gebrehiwot et al., 2014; Haregeweyn et al., 2015) and frequently causing irreversible land degradation. Soil erosion has shown accelerating trends in the 20th century around the globe (Singh and Panda, 2017). FAO reported that the global annual water triggered soil erosion is estimated at about 20–30 gigatonnes per year (FAO, 2015). Diyabalanage et al. (2017) added that the global annual water and wind-driven soil erosion is estimated at around 75 billion tons. In tropical regions, the leading cause of land degradation by water is anthropogenic activities (Diyabalanage et al., 2017). Inhibition of erosion and sedimentation are significant since they have a direct effect on soil fertility and the quality of water (Wijesundara et al., 2018). Soil erosion declines the crop yields to 17% that enhances the usage of chemical fertilizers, which through time results for land relinquishment (Singh and Panda, 2017). Therefore, the catastrophic problem of soil erosion needs to be minimized considerably (Dissanayake et al., 2019).

On-site and off-site problems of basins can be related to the variety of soil erosion processes. On-site effects are related to land degradation and loss of agricultural productivity and off-site effects are mainly related to sedimentation of reservoirs (Balthazar et al., 2013; Garzanti et al., 2006; Haregeweyn et al., 2015) and loss in water storage capacity. The annual loss of storage capacity of the world's reservoirs due to sediment deposition is around 0.5–1% (World Commission on Dams, 2000), and reservoirs may lose the majority of their capacity in the next 25–30 years. A number of hydropower and irrigation reservoirs in Ethiopia (e.g, Legedadi, Abasamuel, Angerib, Borkena, Tekeze, and Gilgel Gibie I) have been affected by the problem of siltation. It is reported that their size is reducing and the water quality is deteriorating which impends the intended use and the life span of these reservoirs (Wolancho, 2012). By clogging irrigation channels, sedimentation raises water conveyances maintenance costs and create a negative impact on downstream agriculture (MoWR, 1998; Morgan, 2005).

The reduction of sediment volume delivered to the reservoirs can be achieved by reducing soil erosion as well as by minimizing the sediment delivery from the hillslopes to the rivers. Quantifying spatially distributed sediment yield and precise identification of sediment source and erosion vulnerable areas are significant for watershed conservation prioritization and

reduction of the socio-economic and environmental cost because of sedimentation on various irrigation and hydropower reservoirs (Hurni et al., 2015). Erosion and sediment yield information is, therefore, a crucial issue in detecting the source of pollution (Hua et al., 2012), comprehensive control and management of watersheds as well as in the design and maintenance of hydro structures such as dams and reservoirs (Yang et al., 2006). Knowledge of the quantitative and spatial distribution of erosion is required to control sediment load and has important implications for the study of off-site and on-site environmental impacts because of sediment deposition.

A physically distributed component is developed and incorporated with the RUSLE to assess soil loss from landscapes. Soil loss per grid cell of an area can be quantified by employing RUSLE (Van Remortel et al., 2004). The focus of USLE is on cropland inter-rill and rill erosion considering the impacts of topography, climate, and others (Dissanayake et al., 2019) but has limitations to estimate gully erosion (Wischmeier and Smith, 1978; Jain et al., 2001). The USLE was improved to RUSLE (Renard et al., 1997). RUSLE has a special advantage over USLE since it incorporates process-based and empirical characteristics (Yoder et al., 2004). Sediment yield in a watershed could be predicted with RUSLE having data inputs from GIS and RS (Bera, 2017). GIS allows more accurate outputs for the RUSLE in small watersheds, even though it is exposed to limited data availability (Pandey et al., 2007). Soil particles detached from the ground by raindrop impacts are transported to the rivers that augment the sediment load and sediment delivery ratio (SDR) of basins (Beskow et al., 2009).

The RUSLE methodology is chosen in this study because it has adequate data requirements and compatible with GIS (González-Bonorino et al., 2003). The spatial layers of RUSLE model inputs can be overplayed and processed in GIS (Cowen, 1993). The spatial distribution of sediment yield along stream channels was estimated with a sediment delivery model. In previous years' significant number of erosion assessment methods used plot scale observations to extrapolate catchment or landscape erosion rates (Grunblatt et al., 1992; Mantel and Van Engelen, 1999). Recent advances in GIS, remote sensing, and DEM have promoted the application of spatial models of erosion and sediment distribution at catchment scales (Nearing et al., 1989). As the spatial gross soil loss is measured with RUSLE, the amount of eroded and transported soil in a watershed could be estimated using observations of sediment deposits from measurement points or outlets and sediment rating curve methods.

Sediment delivery in watersheds could be estimated with SDR approach (Verstraeten and Poesen, 2002). The SDR estimates the amount of sediment that could be transported to the stream networks from the drainage area above (Renard et al., 1991). It is a fraction of upslope gross erosion and is considered as an index of sediment conveyance efficiency in watersheds (Richards, 1993). SDR enables to estimate sediment transport in watersheds where there are inadequate sediment yield observations. The Anjeb watershed is among Ethiopian critical watersheds that experience lack of sediment data. Hence, the amount of sediment accumulating in the channels from the upstream of the watershed has not yet quantified which is fundamental for the selection and implementation of appropriate watershed management practices in the watershed.

Previous studies related to erosion and sediment processes employing any modeling framework have not conducted in the Anjeb watershed. The practices of crop cultivation in all parts of the watershed coupling with low vegetation cover increase soil erosion in the watershed. Therefore, to plan and implement watershed-level management interventions and to minimize the sediment load, studying soil loss and sedimentation processes of the watershed is a critical issue. The objectives of this research were: (1) Estimation of the spatial pattern of soil erosion using RUSLE in GIS environment for conservation prioritization; (2) Estimating the spatial SDR of the watershed; and (3) Estimating sediment yield and mapping its spatial distribution along the channels of the watershed.

7.2 Materials and Methods

7.2.1 Description of the study area

Anjeb watershed with its size of 1165 hectares is situated in Amhara Region, East Gojjam Zone, Gonchia Siso Enessie and Enarji-Enawga districts (Figure 7-1). It is almost 160 kilometers far southwest from the Regional capital, Bahir Dar, and is about 320 km far North of Addis Ababa, capital of Ethiopia. The watershed is part of the North Western Highlands of Ethiopia. The source of river Anjeb is the foot of Choke Mountain Range, one of the highest mountain ranges of Ethiopia with its peak of about 4000m amsl. The river Anjeb is the tributary of The Blue Nile River. Agricultural practice (crop cultivation) is common in all parts of the watershed and there is a low amount of vegetation cover that reduces the detachment and transport of sediments in the watershed. Figure 7-1 shows the location of the study area. The mean annual rainfall of the area is 1449 mm and much of it occurs in June, July, August, and September. The highest rainfall occurs in July and the lowest in February.

The mean annual air temperature of the area is 16.5 °C. The main land-use and land cover (LULC) types of the watershed include cultivation of crops, grazing, plantation, and wasteland.

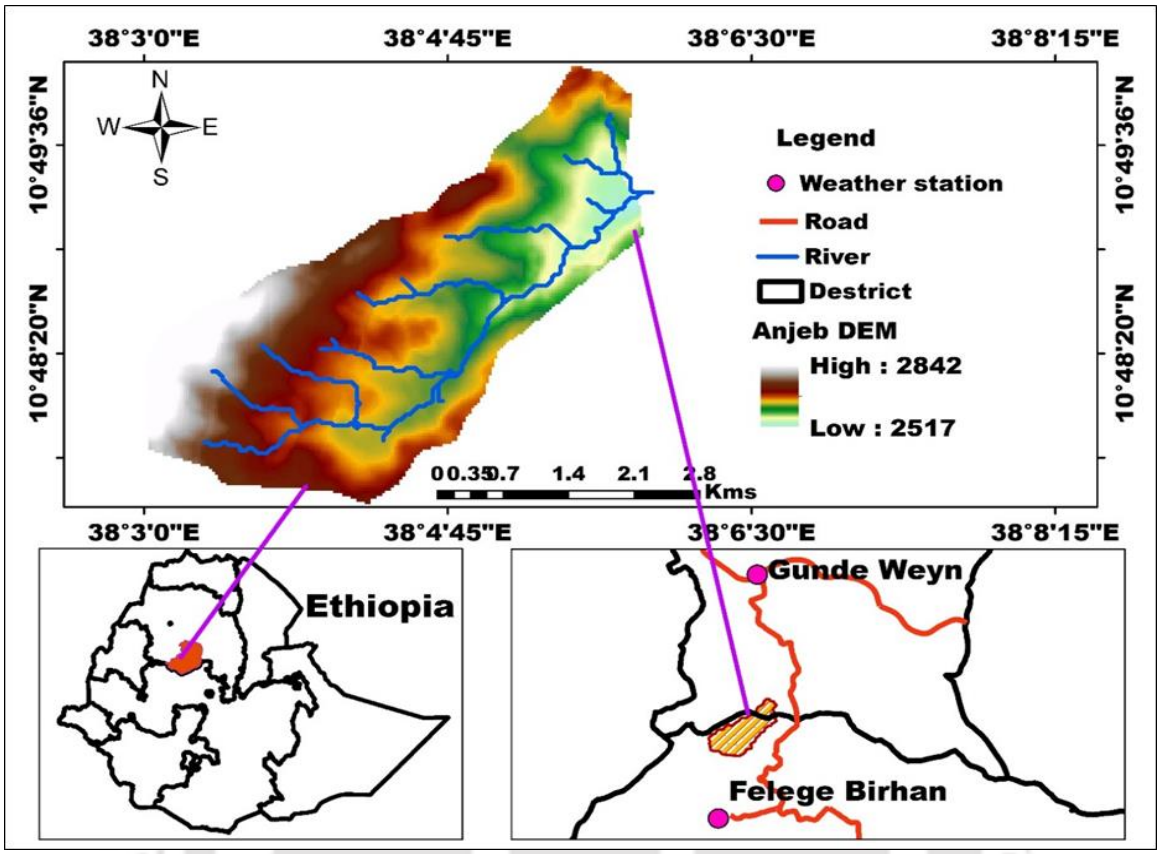

Figure 7-1 Location map of Anjeb watershed

7.2.2 The RUSLE parameters of soil loss estimation

Renard et al. (1991) developed the RUSLE for watershed-scale applications. The fundamental parameters required for the RUSLE model to estimate mean annual soil loss were the land cover (C-factor), land management practices (P-factor), rainfall erosivity (R-factor), the slope steepness (LS-factor), and the soil erodibility (K-factor). These parameters were integrated with GIS overlay analysis for the estimation of grid-based soil loss. The RUSLE model is chosen in this study because it is spatially distributed and compatible with ArcGIS. The RUSLE is represented in equation 7.1.

$$A = R * K * LS * C * P \qquad (7.1)$$

Where A is annual soil loss (t $ha^{-1}yr^{-1}$), R, rainfall-runoff erosivity factor (MJ mm ha^{-1} $h^{-1}yr^{-1}$), K, soil erodibility factor (t $ha^{-1}yr^{-1}$), LS, slope length and steepness factor, C, cover management factor, and P is the support practice factor. The diagrammatic representation of

the methodological flow is presented in Figure 7-2.

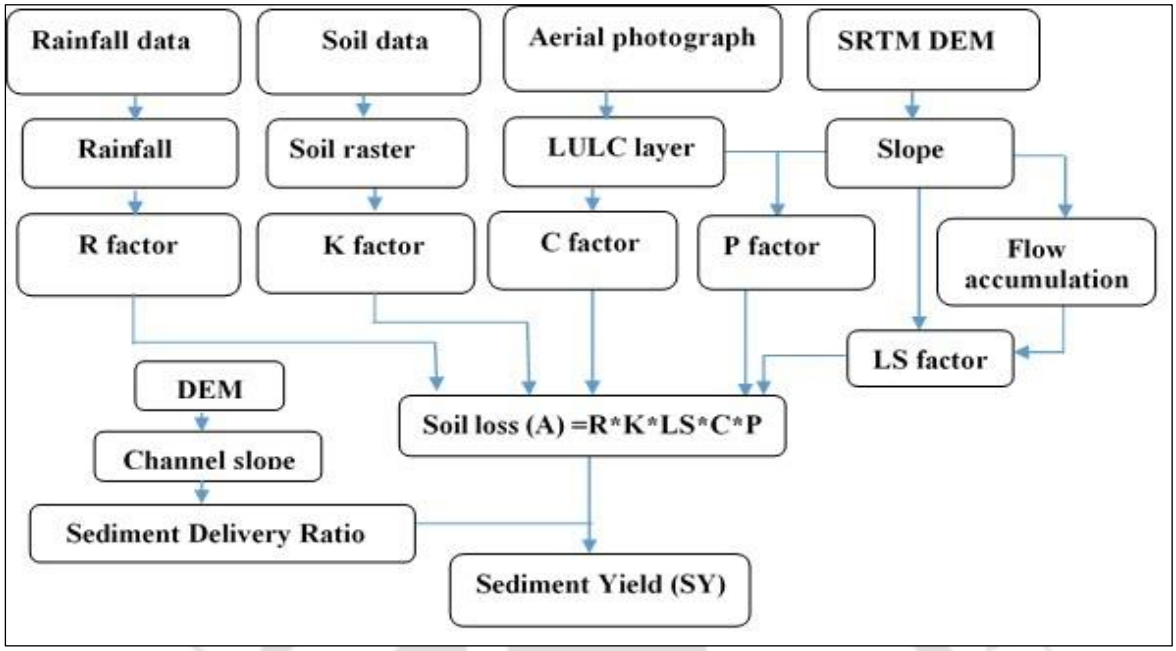

Figure 7-2 Schematic representation of soil erosion and sediment yield modeling

7.2.3 Determining RUSLE parameter values

7.2.3.1 Slope length-steepness (LS) factor

The topographic effect on rill and sheet erosion in an area is accounted by the LS-factor. The LS represents the ratio of anticipated soil loss compared to the loss from the standard plot of 22.13 m and a 9 percent slope (Wischmeier and Smith, 1978; Shinde et al., 2011). The slope for LS-factor computation for the study watershed was analyzed from the SRTM-DEM of 30m resolution obtained from the USGS database achieves (https://earthexplorer.usgs.gov/). As it is shown in Table 7-1 and Figure 7-3a, much of the watershed is found within 5-10 % and 10-20 % slope classes which cover 27.6 % and 50.5 % of the watershed. The area coverage of the slope classes of the watershed is presented in Table 7-1.

Table 7-1 Slope classes of the watershed based on FAO classification

Slope class %	Description	Area (ha)	% watershed area
0–5	Flat	124	10.3
5–10	Gently sloping	331	27.6
10–20	Sloping	606	50.5
20–30	Strongly sloping	134	11.2
30–41.3	Steep	6	0.5

Several studies indicated that slope length has a determining effect on soil erosion and others argue that the upslope contributing area is a better representation of the effect of topography for soil loss. Studies by (Desmet and Govers, 1996; Simms et al., 2003) indicated that slope length should be substituted by the upslope contributing area. The advanced LS-factor computation method (equation 7.2) based on the upslope contributing area suggested by (Desmet and Govers, 1996; Simms et al., 2003) was used for this study to derive the LS-factor of the watershed.

$$LS = Power\left(\left[Flowaccumulation\right] \times cellsize / 22.13\right)^{n} \times Power\left(\sin\left(\left[slope\right] \times 0.01745\right) / 0.09\right)^{m} \qquad (7.2)$$

Where LS, is slope length-steepness factor, *m* and *n* are exponents; *m* = 0.6 (a range between 0.4 and 0.6) and *n* = 1.3 (a range between 1.0 and 1.3). The LS factor of the watershed ranges between 0.0–12.9. The slope and the LS-factor of the watershed are represented in Figure 7-3a and 3b respectively.

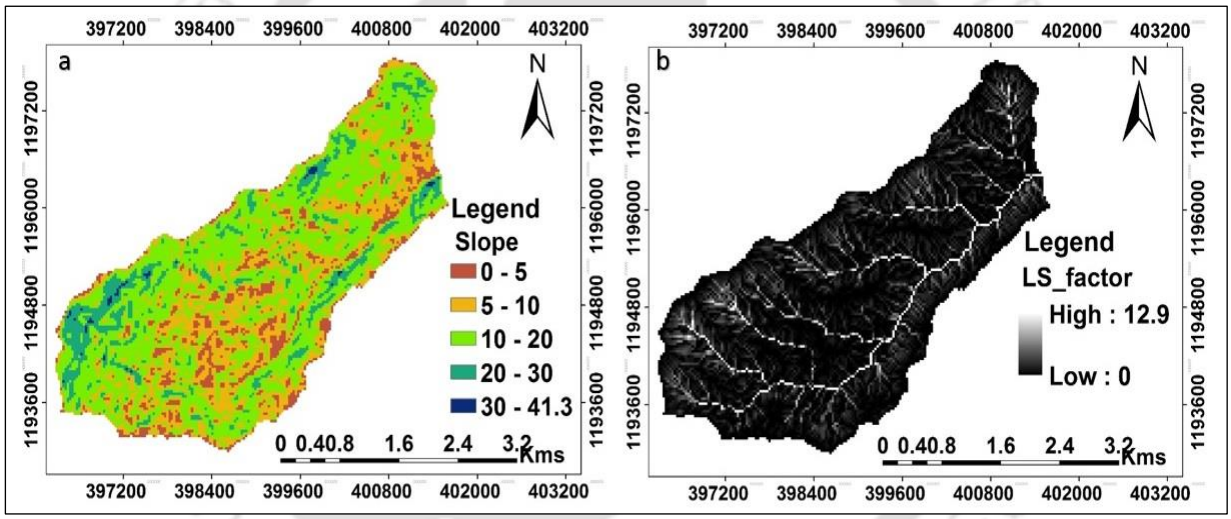

Figure 7-3 Slope (a) and LS map (b) of the watershed

7.2.3.2 Rain fall erosivity (R) factor

The Rainfall erosivity or R-factor is defined as the measured yearly total separate storm erosion index values, EI30, where E is the total storm kinematic energy and I30 is the maximum rainfall intensity in 30-minutes. Renard et al. (1991) stated that the numerical value R in RUSLE is needed to quantify the effect of raindrop impact. Because of scarcity in the record of maximum rainfall intensity in 30-minutes in the study area, the R-factor in this study was computed based on the method developed by Hurni (1985) for Ethiopian Highlands using average yearly rainfall data (equation 7.4). The spatial rainfall layer (Figure 7-4a) of the watershed was prepared using an interpolation method of Inverse Distance

Weighting (IDW) in ArcGIS from the rainfall of 30 years (1986-2015) of Felege Behran and Gunde Woyin stations. The IDW has been one of the most accurate methods in estimating spatial rainfall. In IDW the amount of rainfall to be estimated at station *x* is given by equation 7.3.

$$r_x = \frac{\sum_{i=1}^{n}\left(\frac{r_i}{D_i^b}\right)}{\sum_{i=1}^{n}\left(\frac{1}{D_i^b}\right)} \qquad 7.3$$

where r_x is rainfall to be estimated using the nearby station, r_i is a rainfall of the nearby stations, *D* is the distance between the index station and the ungauged location and *a* weight *b* is the inverse square of the distance. The rainfall of the watershed ranges between 1390 mm to 1449 mm (Figure 7-4a). The R-factor was calculated in the ArcGIS raster calculator using equation 7.4.

$$R = -8.12 + (0.562 \times P) \qquad (7.4)$$

Where R is the erosivity of the rainfall and P is the average yearly rainfall (the spatial layer of rainfall derived from IDW interpolation). The R-factor of the watershed ranges between 789.7–822.6 MJ mm ha^{-1} h^{-1} yr^{-1} (Figure 7-4b).

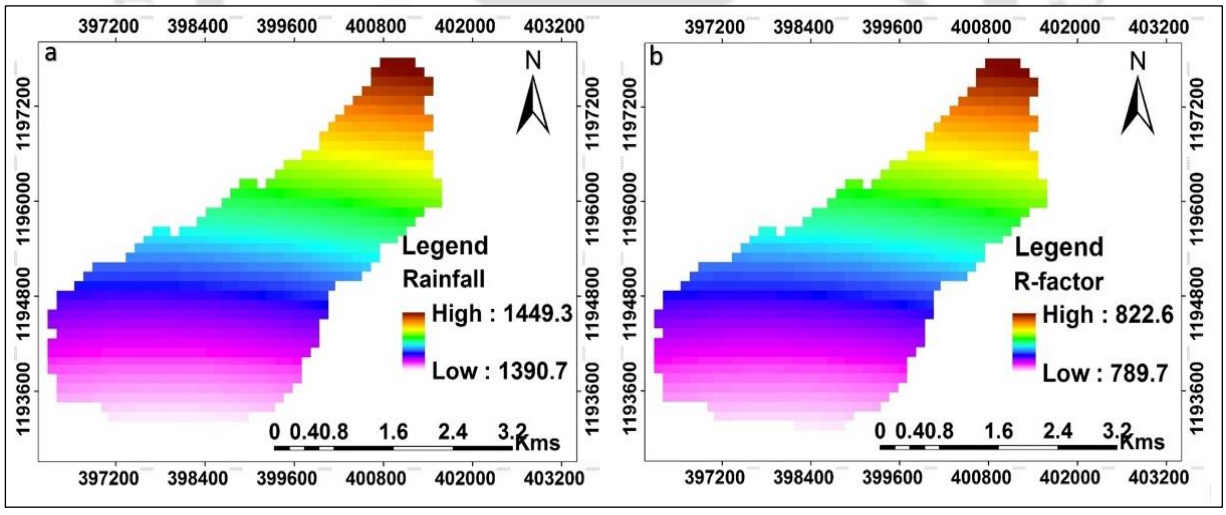

Figure 7-4 Rainfall distribution (a) and R-factor (b) map of the watershed

7.2.3.3 Soil erodability (K) factor

The K-factor is the vulnerability of particles of the soil for erosion because of the impact of rainfall and runoff (Renard et al., 1997). Different approaches were followed by authors to define the K-factor of soils (Renard et al., 1997). The availability of soil data in an area

governs the choice of methods to determine the K-factor values. The soil type data of the study watershed was acquired from the Ministry of Water Resources (MoWR) (1998).

The soil types of the study watershed are Eutric Nitosol, Eutric Verisil, and Haplic Alisol (Table 7-2). Because of limited data on soil properties, the soil colours were chosen to determine K-factor values as recommended by Hurni (1985) and Helldén (1987).

Table 7-2 Soil types, colours and K-factor values

Soil type	Soil colour	Area (ha)	K-value
Eutric Nitosol	Yellow	14.0	0.3
Eutric Nitosol	Red	31.5	0.25
Haplic Alisol	Brown	32.8	0.2
Eutric Verisol	Brown	685.9	0.2
Haplic Alisol	Yellow	199.2	0.3
Eutric Verisil	Yellow	110.5	0.3
Eutric Vertisol	Black	68.8	0.15
Haplic Alisol	Black	10.3	0.15
Water	Water	12.0	0

The soil colours were identified from soil samples taken from the field using Auger holes attached with GPS. The soil colours were differentiated using Munsell Colour (1994). The GPS points were exported in ArcGIS and through digitizing a soil colour map was prepared (Figure 7-5a). The K-factor value was assigned to each soil colour and erodibility map was prepared (Figure 7-5b). The K-factor value ranges between 0.0 and 0.3 t h MJ^{-1} mm^{-1} (Table 7-2 and Figure 7-5b).

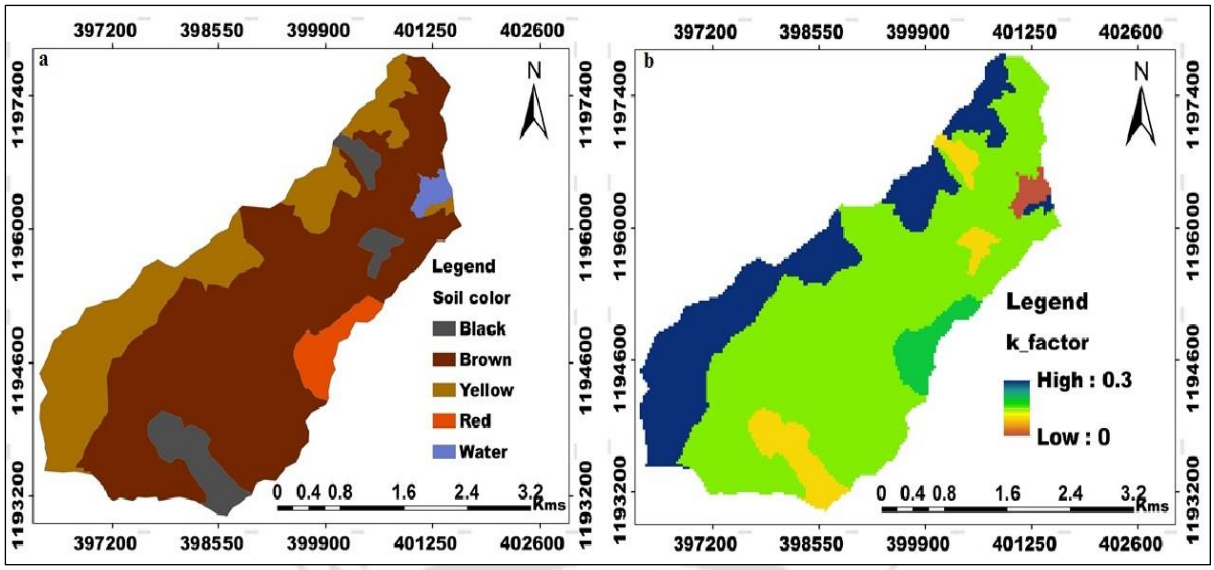

Figure 7-5 Soil colour (a) and K-factor (b) map of the watershed

7.2.3.4 Land use and land cover and management factor (C)

The C-factor describes the effect of LULC types on soil loss (Renard et al. 1997). Soil erosion and transportation is affected by the land feature cover and the land use of an area. The LULC data has been prepared to determine the c-factor value. The LULC data of the watershed is prepared from a high-resolution aerial photograph. Currently, the availability of data from remote sensing makes it easier to produce LULC of an area that can be suited for the soil loss estimation on a watershed-scale.

To prepare LULC of the study watershed, it was difficult to differentiate areas covered by crops and plantations, and extremely grazed lands (grazing lands) and wastelands from agricultural fields which were not presently covered by crops using satellite images since they have similar spectral reflectance values. Hence, in this study 0.25m high-resolution aerial photograph was used to digitize areas covered by crops, wastelands and grazing lands. The areas of plantations and agricultural fields which were not covered by crops were differentiated through the classification of the aerial photograph. Through the ArcGIS operation of 'merge', LULC types prepared through classification and digitizing were combined together, and the LULC raster layer was prepared. Agriculture /crop cultivation, plantation (eucalyptus), grazing, wasteland and waterbody are the LULC types of the watershed (Table 7-3 and Figure 7-6a).

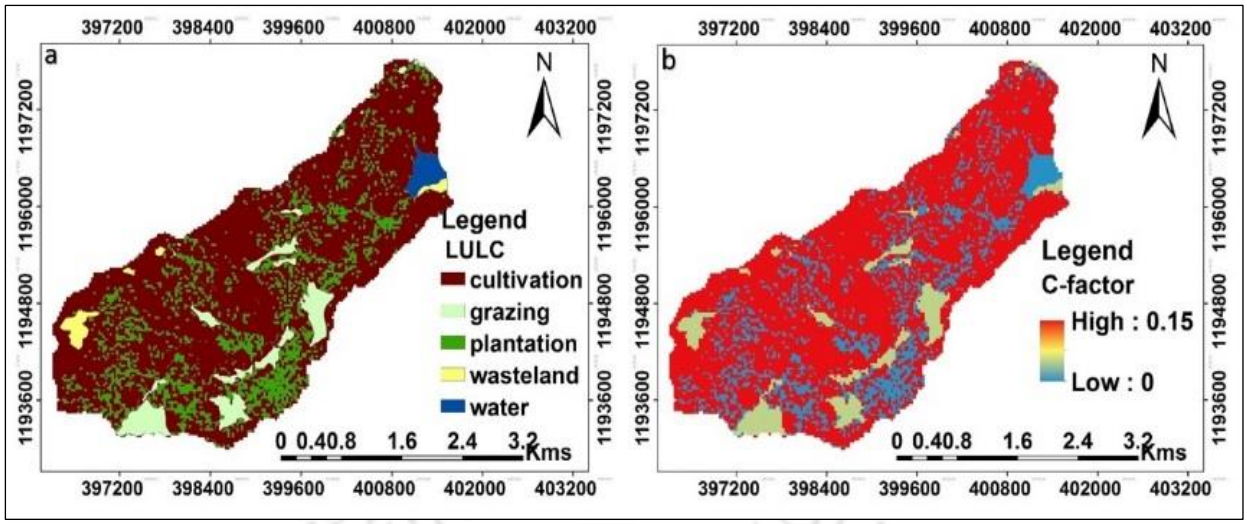

Figure 7-6 LULC (a) and C-factor (b) map of the watershed

Much of the watershed was covered by agriculture/crop cultivation and eucalyptus plantation which accounted for 72.7 % and 18.2 % of the watershed respectively (Table 7-3). The C-value was assigned to each LULC according to the proposal of Hurni (1985) to the Highlands of Ethiopia (Table 7-3 and Figure 7-6b). The value of waterbody is assigned based on the recommendation of (Ban et al., 2016).

Table 7-3 LULC and C-factor value of the watershed

Land use and cover	Area(ha)	% coverage	C- value
Plantation/forest	218.5	18.12	0.001
Cultivation/cereals	874	72.67	0.15
Bare land/wasteland	16.6	1.38	0.05
Grass land/degraded	76.1	6.33	0.05
Water	17.4	1.45	0

7.2.3.5 Support practice (P-factor)

The P-factor is the ratio of soil loss with a particular support practice to the corresponding loss with up and down slope cultivation (Wischmeier and Smith, 1978). This factor considers local erosion management control practices which reduce the eroding power of rainfall and runoff by their impact on drainage patterns (Kim, 2006). In a shortage of data on management practice, the P-factor was determined from combinations of slope and land use data (Wischmeier and Smith, 1978; Bewket and Teferi, 2009) and is widely accepted and

applicable for areas with varying slopes. Hence, to assign the value of P-factor the watershed was grouped into cultivated land and other land uses as recommended by Wischmeier and Smith (1978). Further, the cultivated lands were categorized according to slope classes, since management practices are depending on slopes.

Table 7-4 Land use, slopes and P-factor values

Land use type	Slope (%)	(P) factor	Area(ha)	% cover
Agricultural land	0–5	0.11	74	6.2
	5–10	0.12	239	20.0
	10–20	0.14	487	40.8
	20–30	0.22	92	7.7
	30–41.3	0.31	3	0.3
Other land	All	1	299	25.0

The LULC and slope raster layers of the watershed were overplayed in ArcGIS to create a layer of agricultural fields with varying slope classes, and P-factor was allocated for the corresponding slope class (Wischmeier and Smith, 1978; Bewket and Teferi, 2009, Tessema et al., 2020) (Table 7-4 & Figure 7-7). A value of 1 is assigned for non-agricultural land uses.

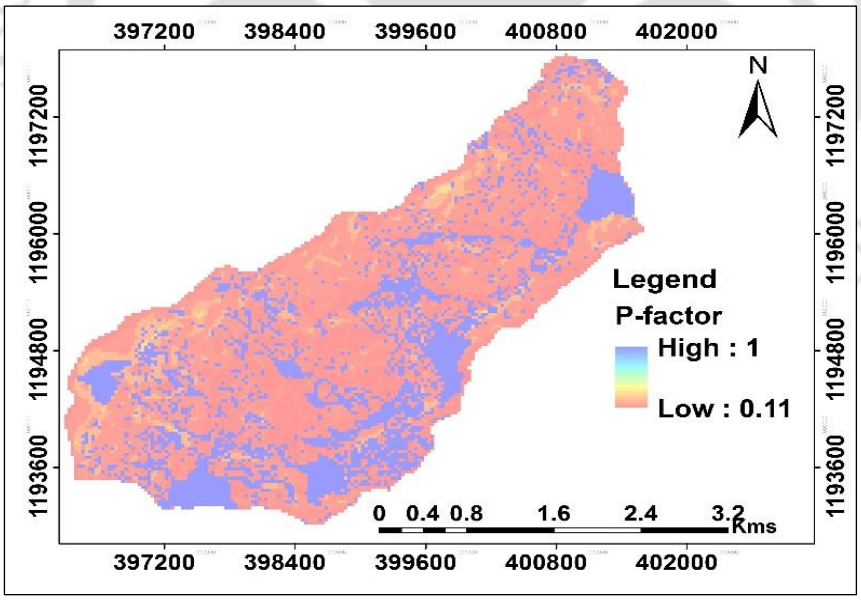

Figure 7-7 P-factor map of the watershed

7.2.4 Spatial Sediment Delivery Ratio (SDR)

There are a few methods to calculate the amount of eroded soil, namely, sediment rating curve, measurement of sediment deposit, and other empirical methods. During a rainfall

event, only some of the eroded soil is routed to the watershed channels and the outlet. The ratio between the watershed sediment yield at the outlet to the total soil erosion over the watershed is described as SDR (Maidment, 1993). Sediment yield models are often based on an empirical lumped approach (Verstraeten and Poesen, 2002), and a typical lumped concept is the SDR. It is a measure of sediment transport efficiency which accounts for the amount of sediment actually transported from the eroding sources to the catchment channels and outlet compared to the total amount of soil detached and eroded above the channels or the outlet point. The SDR could be determined with empirical methods using catchment area (Renfro, 1975; Kamaludin et al., 2013); and slope (Williams and Berndt, 1972; Onyando et al., 2005; Gelagay, 2016; Swarnkar et al., 2018).

Topographic characteristics affect the SDR of basins. Landscapes with short and steep slopes supply more sediment than long and flat slopes. In this study, SDR was determined from stream channel slopes of the watershed using equation 7.5.

$$SDR = 0.627\ SLP^{0.403} \qquad (7.5)$$

where SLP is the slope of stream channels in percent. The slope of stream channels was prepared from DEM using an ArcGIS interface HEC-GeoHMS tool. After terrain and basin processing on DEM, the average slope of each cell along the flow path of streams were calculated using HEC-GeoHMS (Figure 7-8). In calculating SDR, each cell in the flow path is considered as the outlet of its upstream catchment. The channel slope values of the watershed vary between 0.009-0.09 as it is represented in Figure 7-8.

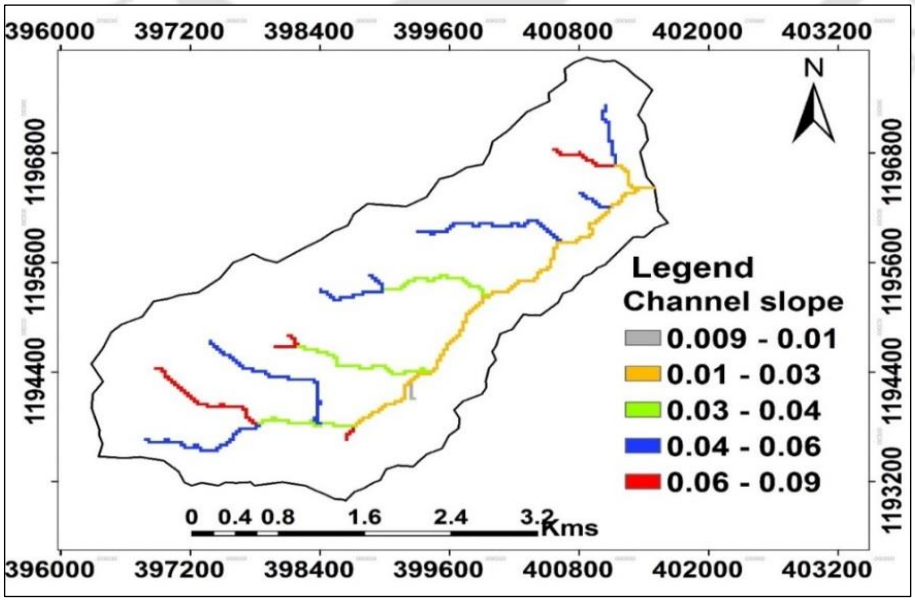

Figure 7-8 Channel slope of the watershed

7.2.5 Sediment Yield (SY)

The SY is the sediment load at the last point of the slope length, in the channels, at the outlet or sediment basins. It is the sediment load normalized for the drainage area and is the net result of erosion and deposition processes within a watershed. Mutua and Klik (2006) stated that sediment yield is typically unavailable as a direct measurement in a watershed lacking adequately recorded sediment data. They suggested the accurate estimation of SDR coupling with spatial soil loss is an important and effective approach in predicting sediment yield. In this study, sediment yield is computed by superimposing the soil loss and SDR layers of the watershed using equation 7-6.

$$SY = \sum_{i=1}^{n} SDR * E \qquad (7.6)$$

where SDR is the fraction of soil erosion delivered to the *ith* grid cell of the nearby channel or outlet, *SY* is the sediment yield, *E* is the soil erosion of the *ith* grid cell and *n* is the total grid cells.

7.3 Result and Discussion

7.3.1 Soil loss

The RUSLE soil loss parameters were super superimposed in ArcGIS 10.2 and the soil loss rate of each grid cell was computed with equation 7.1. The annual soil loss of the watershed ranges from 0 to 195 t $ha^{-1}yr^{-1}$ and the average annual rate of soil loss of the watershed was 17.3 t ha^{-1} $yr^{-1.}$ Based on the result found, the watershed has been categorized into six classes of erosion: slight (0–5), moderate (5–10), high (10–15), very high (15–30), sever (30–50), and very severe (>50) t $ha^{-1}yr^{-1}$ (Table 7-5 and Figure7-9). The average soil loss of sever and very sever classes accounted for 40t $ha^{-1}yr^{-1}$ and 132.5 t $ha^{-1}yr^{-1}$ and covered 5.8% and 7.1% of the watershed area respectively. It can be understood that a total of 13% of the watershed was under the severe erosion condition (both sever and very sever classes). Part of the watershed under the sever soil loss condition is located in the stepper slopes and much of it is in the upper part of the watershed where the main river originates. The average loss in the high and very high erosion classes were 12.5 and 22.5 t $ha^{-1}yr^{-1}$ sequentially. The proportion of the watershed found in the high erosion class (both very high and high) is about 17.6%. A significant part of the watershed, 11.3%, has been within the moderate classes of erosion which has an average loss of 7.5 t $ha^{-1}yr^{-1}$. Greater than 50% of the watershed was under the slight (average loss of 2.5 t $ha^{-1}yr^{-1}$) erosion classes and it covers from gentle to flat slopes of the watershed (Table 7-5). The total annual soil loss was estimated as 20125.5 t yr^{-1}. The

result indicated that a large amount of soil loss (54.6%) has come from a small section of the watershed (very sever class) which constitutes only 7.1% of the watershed area.

Table 7-5 Soil loss and erosion-risk classes of the watershed

Soil loss t $ha^{-1}yr^{-1}$	Average soil loss t $ha^{-1}yr^{-1}$	Erosion risk class	Area (ha)	Area %	Total soil loss t y^{-1}	Soil loss %
0–5	2.5	Slight	678	58.2	1695	8.4
5–10	7.5	Moderate	132	11.3	990	4.9
10–15	12.5	High	85	7.3	1062.5	5.3
15–30	22.5	V. high	120	10.3	2700	13.4
30–50	40	Severe	67	5.8	2680	13.3
>50	132.5	V. severe	83	7.1	10997.5	54.6
Total			1165	100	20125.5	100

Research outputs on erosion rates in Ethiopian Highland watersheds were reported as, 30.6 t ha^{-1} yr^{-1} in Jabitehinan District (Amsalu and Mengaw, 2014), 9.63 t $ha^{-1}yr^{-1}$ in Medego watershed (Brhane and Mekonen, 2009), 47.4 t $ha^{-1}yr^{-1}$ in Koga watershed (Gelagay and Minale, 2016), and 49 t $ha^{-1}yr^{-1}$ in Dembecha District (Zerihun et al., 2018). The average soil loss and the area size of Anjeb watershed are smaller than the studies indicated above except Medego watershed (Brhane and Mekonen, 2009) which had a soil loss of 9.63 t $ha^{-1}yr^{-1}$. Medego and Anjeb watersheds have a comparable size with 1091.5 and 1165 hectares respectively but Anjeb had a higher amount of average soil loss (17.3 t $ha^{-1}y^{-1}$) than Medego watershed (9.63 t $ha^{-1}yr^{-1}$). Overall the result of this study lies in between the previous works conducted in the Northwest Highlands of the country.

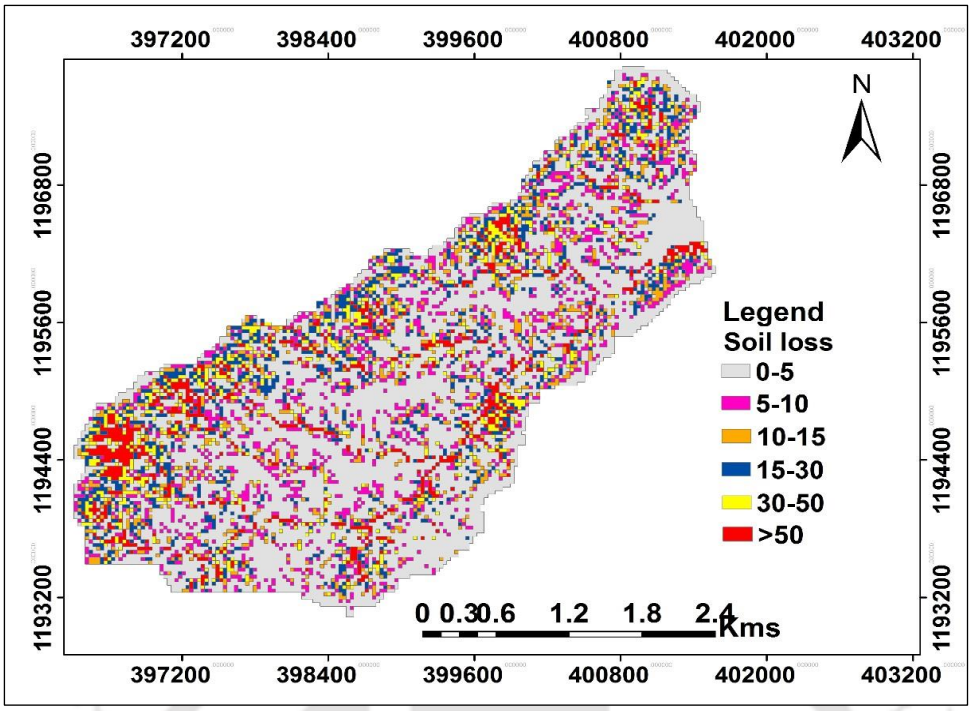

Figure 7-9 Soil loss map of the watershed

7.3.2 Sediment delivery ratio (SDR)

The SDR value of a raster grid cell measures its upstream sediment delivery capability (Lu et al. 2006). A spatial grid of SDR was generated for channels in the watershed employing equation 5. The result showed that the SDR value ranges between 0.03–0.214. Higher SDR values (>0.2) were observed along the higher channel slopes between 0.06-0.09. An intermediate amount of SDR values (0.15–0.2) were observed within the channel slope classes between 0.03-0.06 and SDR values (0.03–0.15) were found mainly along the main channel with slopes between 0.009-0.03 (Figure 7-10). As it is observed from Table 7-6, on average SDR values of 0.19 and 0.125 cover more area of the channels (43.9%, 20.5%) respectively. The lowest SDR value (0.065) constitutes 8% of the lowest channel area in the watershed (Table 7-6).

Table 7-6 Channel SDR value and the area coverage

SDR value	Average SDR	Area (ha)	area %
0.03–0.1	0.065	5.2	8.1
0.1–0.15	0.125	13.1	20.5
0.15–0.17	0.16	8.5	13.3
0.17–0.2	0.185	28.1	43.9
>0.2	0.21	9.1	14.2

On average, the sediment delivery capacity is about 0.122. This indicates that a mean of 12.2% of the eroded soil materials could be delivered to the channels and 87.8 % of the eroded materials are trapped and deposit before getting into the channel networks. The average SDR value of Anjeb watershed is a little higher than other studies 5.2 % (Lu et al., 2006); and 8 % (da Silva et al., 2014).

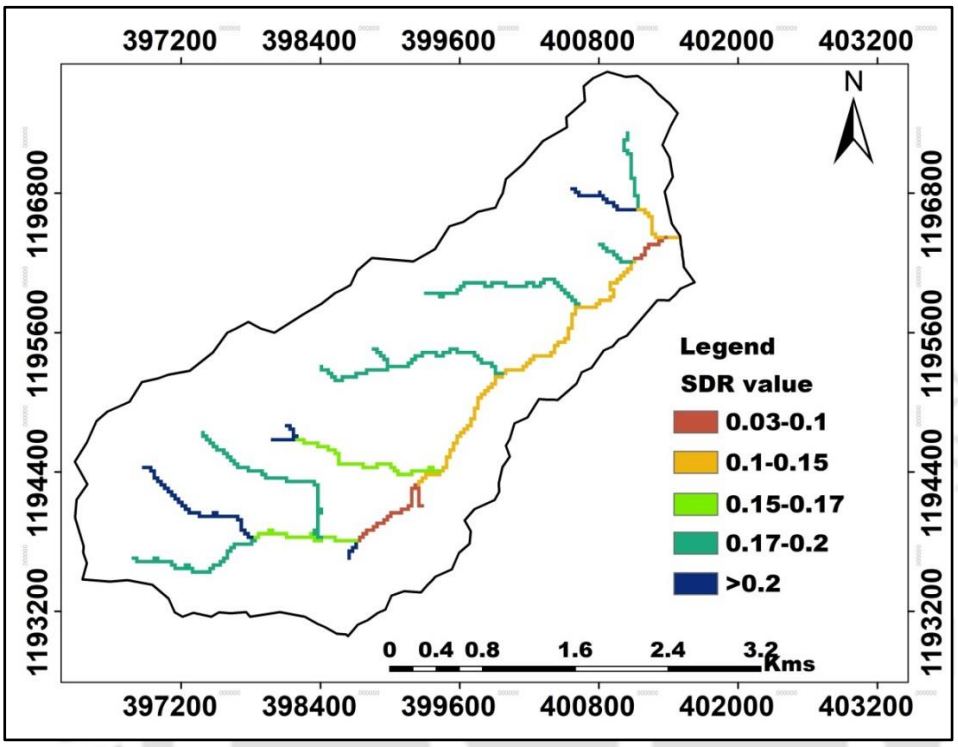

Figure 7-10 The SDR map of the watershed

7.3.3 Estimating sediment yield

The sediment delivered in the channel grid cells and the outlet was estimated with superimposing the soil loss and SDR raster layers as represented in equation 7.6. In order to uncover the severity of sediment yield, it has categorized into six classes, namely, low (0–5), moderate (5–10), high (10–15), very high (15–30), severe (30–50) and very severe (>50) t $ha^{-1}yr^{-1}$ (Table 7-7). The very severe sediment class which covered 17% of the area of the channels has a mean sediment yield of 157 t $ha^{-1}yr^{-1}$ and a total of 1727 tons of sediment in the watershed was from this channel section. Sever and very high sediment classes each covered 9.4% of the channels (total 18.8%) and their mean sediment yield were about 40 t $ha^{-1}yr^{-1}$ and 22.5 t $ha^{-1}yr^{-1}$ respectively. A low amount of sediment was from the low category of sediment classes that covers over 50% of the channels (Table 7-7).

Table 7-7 Sediment delivered to the channels

Range of SY t ha^{-1} yr^{-1}	Average SY t ha^{-1} yr^{-1}	SY classes	Area (ha)	Area %	Annual SY tone
0–5	2.5	Low	34	53.1	85
5–10	7.5	Moderate	4	6.3	30
10–15	12.5	High	3	4.7	37.5
15–30	22.5	Very high	6	9.4	135
30–50	40	Severe	6	9.4	240
>50	157	V. severe	11	17.2	1727
Total			64	100	2254.5

From a total of 20125.5 t yr^{-1} of eroded soil over the whole watershed 2254.5 t yr^{-1} of sediment load has been brought and deposited along the channels which cover 64 hectares or 5.5 % of the area of the watershed. Almost 12.2 % of the total soil loss has been transported and deposited to the channels. The map of sediment yield is presented in Figure 7-11. The sediment yield at the outlet grid cell is a product of total soil loss from the entire watershed and the SDR value of the grid cell. The sediment yield at the point of the outlet was estimated 2012.5 t yr^{-1}. The high sediment yield in the watershed is because of the cultivation of very steep slopes without implementing soil and water conservation practices.

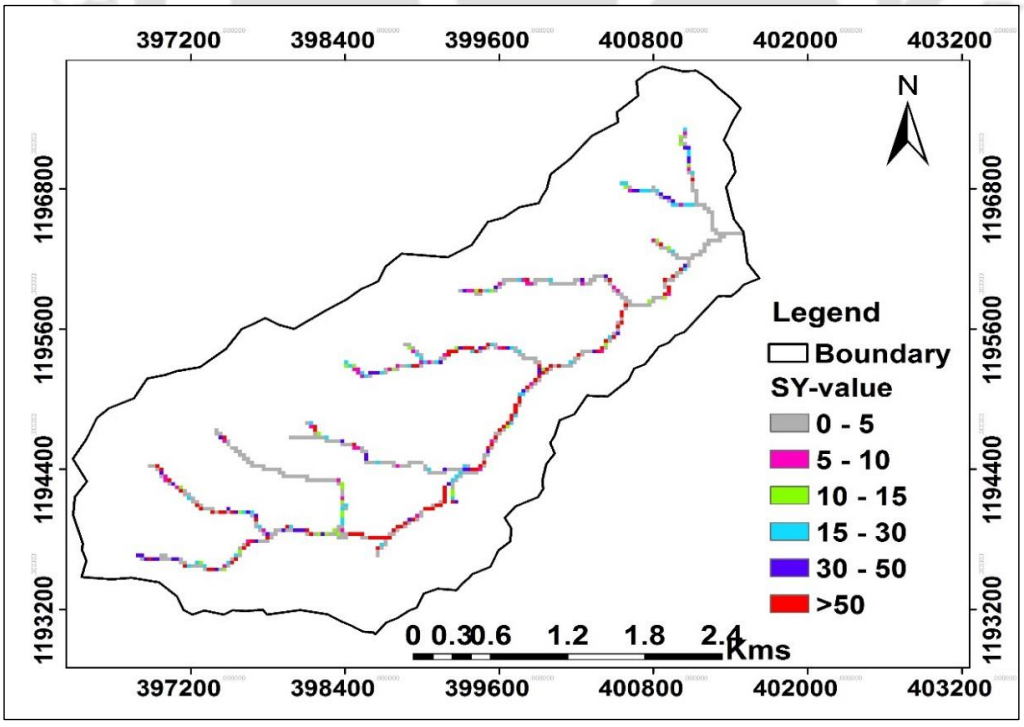

Figure 7-11 Sediment yield to channels in the watershed

7.4 Conclusion

Anjeb watershed situated in the middle of Northwest Ethiopian Highlands is an agriculture dominated (mainly crop cultivation) area. Basic datasets were organized and analyzed for estimating soil loss, SDR, and sediment yield. The result revealed that the spatial data processing efficiency of GIS integrating with RUSLE is capable of quantifying soil loss, SDR, and sediment yield of the Anjeb watershed. Topography, LULC, support practices, and soil factors were found to be determinant for soil loss and sediment yield assessment in the watershed. The watershed was categorized into six classes of erosion: slight (0–5 t $ha^{-1}yr^{-1}$), moderate (5–10 t $ha^{-1}yr^{-1}$), high (10–15 t $ha^{-1}yr^{-1}$), very high (15-30 t $ha^{-1}yr^{-1}$), sever (30-50 t $ha^{-1}yr^{-1}$) and very severe (>50 t $ha^{-1}yr^{-1}$). Soil loss ranges between 0 to 195 t $ha^{-1}yr^{-1}$ and the average soil loss was 17.3 t $ha^{-1}yr^{-1}$.

The average SDR value of 0.122 indicated that a significant proportion of the gross soil loss (12.2%) has been delivered into the channel networks. The average sediment yield ranges between 2.5 to 157 t $ha^{-1}yr^{-1}$. From a total of 20125.5 tons of soil eroded in the watershed 2254.5 tons of sediment was deposited to the stream channels per year and the sediment yield at the point of the outlet was estimated to 2012.5 t yr^{-1}. From the field survey, it is understood that the causes of high soil erosion and sediment yield are the cultivation of steep slopes without or little implementation of appropriate conservation practices and lack of vegetation covers. Based on our study, we recommend the local decision-makers and land managers to design and construct conservation measures suitable for the land use and adaptable to the slope to reduce the soil loss and increase productivity of the land. The model could be adapted to similar studies in the area following appropriate adjustments and this study could be a source of information for related researches that will be conducted in the area.

Chapter 8 : Investigate the Impacts of LULC and Climate Change Scenarios on Hydrology and Sediment Yield in Rib and Gumara Watersheds

8.1 Introduction

Studies about runoff and sediment transport using timely data of hydrology, topography, and predicted LULC and climate at watershed and catchment levels could be essential tools to design and implement catchment level resource management systems. The alteration of rainfall-runoff and evaporation balances in watersheds could be because of LULC change due to anthropogenic activities (Sahin and Mall, 1996; Kassa, 2009). The availability of water is challenged by the variability of climate conditions, which is the current problem in the Nile basin, where the study watershed is located. Even though studies have conducted on changes in hydrological processes due to climate and land-use changes globally (Li et al., 2009; Mango et al., 2011), it is limited in Africa, especially in Ethiopia. Impacts of climate and land-use changes in hydrology and sediments vary spatially and should be studied at a local-scale (Wang et al., 2013).

In climate change impact studies, the outputs of GCMs are sources of information for future climatic conditions. In addition, land use information is essential in watershed hydrology, erosion, and sediment studies since it significantly affects hydrological processes of surface runoff, evapotranspiration, groundwater, streamflow, and sediment load (Nie et al., 2011). A LULC change predicted data for hydrology and sediment studies is not common in Ethiopia in particular and Africa in general. Some of the study reports about watershed hydrology in Ethiopia mainly focus on either the use of climate change or LULC data only. Most impact studies rely on historic LULC data so that it limits to estimate the separate as well as combined possible future impact of the changing land use and climate.

Some studies were conducted related to hydrological processes either using climate or LULC data in the Blue Nile Basin of Ethiopia. Welde and Gebremariam (2017) reported that there has been an increase in mean annual streamflow with a range 129.2 to 137.7 m^3/s in Tekeze Dam watershed due to LULC changes. Setegn et al. (2011) analyzed the impact of climate change on groundwater and streamflow in Lake Tana Basin and the result revealed that there have been increases in temperature, and inconsistency in rainfall projections. They recommend a thorough investigation of the combined effect of climate and LULC changes on hydrological processes in the region. In the study of the impact of historic rainfall and LULC

on streamflow in upper Gilgel Abbay, Rientjes et al. (2011) reported that there has been a decreasing trend in rainfall and an increasing trend of LULC change that highly affected the streamflow. A study on the impact of climate change on streamflow hydrology in Gilgel Beles and Main Belese watersheds by Worqlul et al. (2018) using Hadley center climate model (HadCM3) output with A2 and B2 emission scenarios revealed that the minimum and maximum temperatures increase by 3.6^{o}C and 2.4^{o}C respectively at the end of the 21st century which might result for 64% and 19% increase and decrease in streamflow in wet and dry seasons respectively.

The above studies conducted on the impact of climate change over Blue Nile River Basin were based on the previous version of IPCC Assessment Report 4 (AR4) emission scenarios and recently the motive is emphasizing on current IPCC Assessment Report 5 (AR5) scenarios. GCM products based on the scenarios of RCP of the AR5 are expected to have better predictive performance over Blue Nile basin. Therefore, the objectives of this study were (1) assess the impacts of future climate changes on the watershed hydrology and sediment yield of the watersheds; (2) assess the combined impacts future LULC and climate changes on the watershed hydrology and sediment yield of the watersheds.

8.2 Materials and Methods

8.2.1 Land use land cover data

Landsat satellite images of 1984, 2003 and 2016 of the study watersheds were classified and their respective land use and land cover maps were prepared. The LULC maps were used to prepare the land use demands of the watersheds to predict the LULC scenario map of 2049.

8.2.2 Dyna-CLUE land use model

The LULC scenarios of the watersheds were predicted with the Dyna-CLUE land use model. The 1984 LULC data was used as a base to calibrate the Dyna-CLUE model and the classified and simulated maps of 2016 were used to validate the model for the 2049 LULC scenario predictions.

8.2.3 Climate model (GCM/RCM) data

High spatial resolution (50 km by 50 km) REMO RCM climate data from the driving model of ECHAM5 with the IPPC AR4 SRES A1B and RACMO22T RCM climate data from the driving model of HadGEM2-ES in CORDEX-Africa with AR5 RCP scenarios (RCP 2.6,

RCP 4.5 and RCP 8.5) were used to predict the future precipitation and maximum and minimum temperature of the watersheds from 2025 until 2099 with time slices of 2030s, 2060s and 2090s.

8.2.4 RCM/GCM data bias correction

The regional climate models with IPCC AR4 SRES A1B and AR5 RCP scenarios (RCP 2.6, RCP 4.5 and RCP 8.5) were bias corrected with the delta-change method. The delta-change additive and multiplicative methods were implemented to correct temperature and precipitation respectively.

8.2.5 SWAT model

SWAT model was calibrated and validated with the LULC, weather, soil and topographic data of the watersheds. The calibrated SWAT model was used to predict the hydrology and sediment yield of the watersheds using the projected LULC and climate data. The hydrology and sediment yield of the watersheds were estimated using the base LULC and the predicted climate and predicted LULC and predicted climate to differentiate the impact of LULC and climate changes.

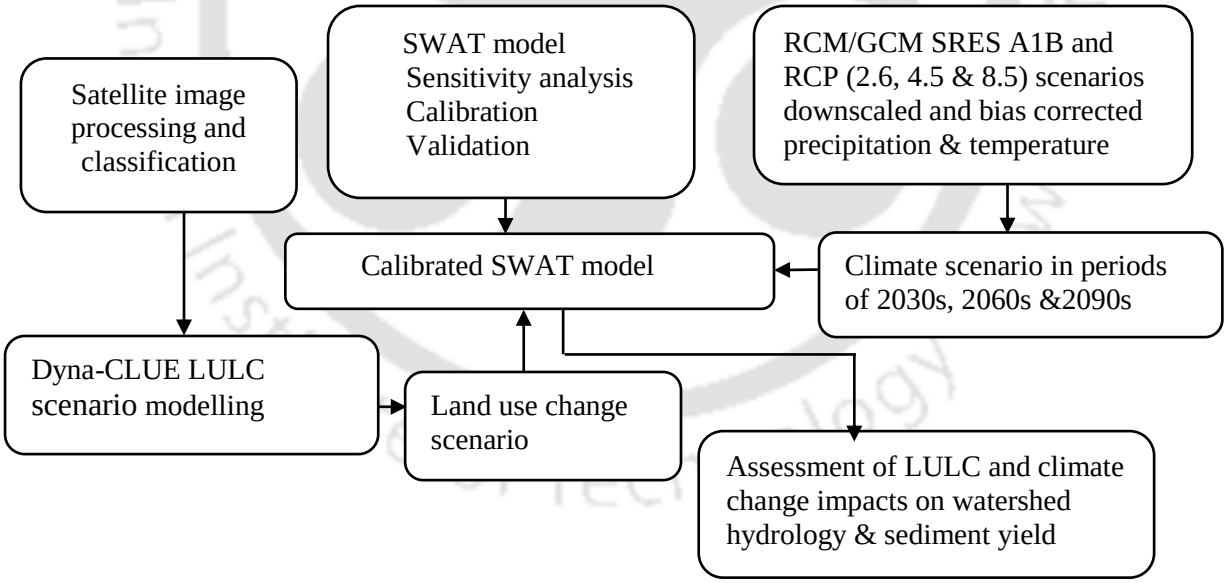

Figure 8-1 Schematic representation of impacts of LULC and climate change on hydrology

8.3 Results and Discussions

8.3.1 Impact of LULC and climate changes on hydrological components and sediment yield in Rib watershed

Understanding the catchment response to LULC changes are important for water resources management measures (Nie et al., 2011; Gyamfi et al., 2016). The 2016 and the predicted 2049 LULC and the predicted climate from 2025 to 2099 were used to show their impact on the hydrology of the watersheds. The impact of predicted LULC and climate and base LULC and predicted climate were analyzed. The hydrological components of surface runoff, lateral flow, groundwater flow, total water yield (WYLD), evapotranspiration (ET), and sediment yield on annual and monthly basis were assessed.

Generally, surface runoff will show a consistent decrease in A1B scenario simulations on both predicted LULC and climate and in the base LULC and predicted climate scenarios compared with the base period. Surface runoff shows is a little lower reduction in the predicted LULC and climate scenario than the base LULC and predicted climate scenario. Surface runoff decreasing values in A1B of the predicted LULC and climate and the base LULC and predicted climate scenarios in the time slices of the 2030s and 2090s respectively were 5.6%, 39.6% and 10.2%, 42.7% in Rib (Figure 8-2, Table 8-3). Surface runoff will show an increasing trend with a range between 0.3 to 28.7% in the RCPs predicted LULC and climate scenario compared with the baseline. It varies between -4.1% to 23.5% in the base LULC and predicated climate scenario. Lower increase of surface runoff will be observed in the 2060s of RCP 2.6, 4.5 and 8.5 with values of 0.3%, 7.2%, 7.3 % and -4.1%, 2.6%, 2.7% in the predicted LULC and climate and base LULC and predicted climate scenarios respectively (Table 8-3). It will also show lower increase in the 2030s of the RCP2.6 with values of 4.6% and 0.1% in the predicted LULC and climate and base LULC and predicted climate scenarios respectively. The highest increase will be observed in the 2030s scenario of RCP 8.5 with an increase of 28.7% and 23.5% in the predicted LULC and climate and base LULC and predicted climate scenarios respectively (Figure 8-2, Table 8-3). The 2090s of RCP 2.6, 4.5 and 8.5 scenarios will show significant increase in surface runoff with value of 12.5%, 15.5% and 15.5 % in the predicted LULC and climate scenario (Figure 8-2c). The results showed that higher surface runoff is observed in the predicted LULC and climate than the base LULC and predicted climate scenario simulations. This indicated that LULC change has a significant impact on the hydrologic response of watersheds.

Lateral flow and groundwater flow will show a decreasing trend in all the SRES A1B scenario time slices. The decreasing values in the predicted LULC and climate and the base LULC and predicted climate scenarios in the time slices of the 2030s and 2090s respectively will be, lateral flow (16.7%, 35.4%, and 9.2%, 31%), groundwater flow (21.9%, 53.3%, and 20.6%, 52.5%)(Figure 8-2, Table 8-3). These values indicated that lateral flow and groundwater flow will show a higher decrease in the predicted LULC and climate scenario than the base LULC and predicted climate scenario.

There will be a decrease in lateral flow and groundwater flow with a range between 3.7% to 13.6% and 7.1% to 22.4% in the 2030s and 2090s of the RCP 8.5 scenario respectively in the predicted LULC and climate scenario. The change in lateral flow in the base LULC and climate scenario varies between 3.5% to -7% in the 2030s and 2090s of the RCPs respectively. Groundwater flow will show a decrease between 6.7% to 23.5% in the 2030s and 2090s of the RCPs in the base LULC and predicted climate scenario. The decrease and increase in lateral flow and groundwater flow will occur in the RCP of 2030s and 2090s. Lateral flow will show a higher decrease in the predicted LULC and climate scenario than the base LULC and predicted scenario. Groundwater flow will show almost the same amount of reduction in the predicted LULC and climate and base LULC and predicted climate scenarios.

The total water yield (WYLD) will show a decreasing trend in all the SRES A1B scenario time slices. Its decreeing values in the predicted LULC and climate and the base LULC and predicted climate scenarios in the 2030s and 2090s time slices ranges between 15.6% to 46.9%, and 15.9% to 47.3% respectively. Total WYLD will show a higher decrease in the base LULC and predicted climate scenario. The change of variation in total WYLD ranges between -9.5 to 5.6 and -9.9 to 5.3% in the 2060s and 2030s of the RCP4.5 and 8.5 in the predicted LULC and climate scenario and base LULC and predicted climate scenario respectively. The range of variation in total WYLD is almost the same in the two scenarios. It will show an increase only in the 2030s of the RCP8.5 but in the other scenarios it shows a decreasing trend.

Table 8-1 Average annual hydrologic components in the predicted LULC and climate scenario compared to the baseline period, Rib

Scenario/hydrologic components		Surface runoff (mm)	Lateral flow(mm)	Groundwater flow (mm)	Total WYLD (mm)	ET (mm)	Sediment yield (t/ha)
Base (1993-2016)		232.8	43.1	330	624.4	474.3	21.6
	2030s	219.7	35.9	257.7	527	515.8	15.2
SRES	2060s	199.2	35.6	245.3	494.1	520.2	14
A1B	2090s	140.4	27.8	154	331.4	505.2	21.2
	2030s	243.6	39.1	277.5	575.9	549.9	22.3
RCP 2.6	2060s	233.5	39.1	279	567.4	546.6	18.8
	2090s	261.8	41.1	296.7	616.3	562.4	21.2
	2030s	265.8	40.1	285.0	606.9	560.9	30.2
RCP 4.5	2060s	249.6	38.2	262.2	564.8	551.8	22.9
	2090s	269	40.6	286.6	612.2	563.2	24.7
	2030s	299.5	41.5	301.4	659.3	547	33.4
RCP 8.5	2060s	249.7	38.8	266.8	570.4	559.9	24.9
	2090s	269	37.2	245.5	565.8	550.8	60.2

Table 8-2 Average annual hydrologic components in the base LULC and predicted climate scenario compared to the baseline period, Rib

Scenario/hydrologic components		Surface runoff (mm)	Lateral flow (mm)	Groundwater flow (mm)	Total WYLD (mm)	ET (mm)	Sediment yield (t/ha)
Base (1993-2016)		232.8	43.1	330	624.4	474.3	21.6
	2030s	208.9	39.1	262.0	524.9	518	11.7
SRES	2060s	189.9	38	249.3	491.4	522.9	10.8
A1B	2090s	133.3	29.7	156.8	329.3	507.3	17.3
	2030s	233.1	41.9	282.7	573.6	552.1	17.8
RCP 2.6	2060s	223.3	41.8	283.9	565	549	14.9
	2090s	250.9	44	302.5	614.3	564.3	17
	2030s	254.9	43	290.7	604.9	562.8	24.9
RCP 4.5	2060s	238.9	41	267.2	562.3	554.3	18.2
	2090s	257.7	43.6	292.4	610	565.4	19.6
	2030s	287.5	44.6	307.9	657.2	549.1	27.2
RCP 8.5	2060s	239	41.6	272.2	568.1	562.1	19.9
	2090s	258.7	40.1	252.4	565.6	551	53.6

There will be an increasing trend of ET in the predicted LULC and climate and the base LULC and predicted climate scenarios in the 2090s and 2060s time slices of A1B respectively with values of 6.5%, 9.7%, and 7%, 10.2%. The ET will show an increase between 15.2% to 18.7% and 15.8% to 19.2% in the 2030s and 2090s of the RCP8.5 and 4.5 in the predicted LULC and climate and base LULC and predicted climate scenarios respectively. The increase in ET is a little higher in the base LULC and predicted climate scenario. A little higher value of ET in the base LULC and predicted climate scenario might

be due to the decrease in precipitation and removal of vegetation in the scenario.

Table 8-3 Percentage (%) change of average hydrologic components in base and future LULC and future climate scenario, Rib

Scenario		Surface runoff		Lateral flow		Groundwater		Total WYLD		ET		Sediment	
		LULC		LULC		LULC		LULC		LULC		LULC	
		Base	Future	Base	Future	Base	Future	Base	Future	Base	Future	Base	Future
SRES A1B	2030s	-10.2	-5.6	-9.2	-16.7	-20.6	-21.9	-15.9	-15.6	9.2	8.7	-45.8	-29.6
	2060s	-18.4	-14.4	-11.8	-17.4	-24.5	-25.7	-21.3	-20.9	10.2	9.7	-50.0	-35.2
	2090s	-42.7	-39.6	-31.0	-35.4	-52.5	-53.3	-47.3	-46.9	7.0	6.5	-19.9	-1.9
RCP 2.6	2030s	0.1	4.6	-2.7	-9.2	-14.3	-15.9	-8.1	-7.8	16.4	15.9	-17.6	3.2
	2060s	-4.1	0.3	-3.0	-9.2	-14.0	-15.5	-9.5	-9.1	15.7	15.2	-31.0	-13.0
	2090s	7.8	12.5	2.0	-4.6	-8.3	-10.1	-1.6	-1.3	19.0	18.6	-21.3	-1.9
RCP 4.5	2030s	9.5	14.2	-0.2	-6.9	-11.9	-13.6	-3.1	-2.8	18.7	18.3	15.3	39.8
	2060s	2.6	7.2	-4.8	-11.3	-19.0	-20.6	-9.9	-9.5	16.9	16.3	-15.7	6.0
	2090s	10.7	15.5	1.1	-5.8	-11.4	-13.2	-2.3	-2.0	19.2	18.7	-9.3	14.4
RCP 8.5	2030s	23.5	28.7	3.5	-3.7	-6.7	-7.1	5.3	5.6	15.8	15.3	25.9	54.6
	2060s	2.7	7.3	-3.5	-9.9	-17.5	-19.2	-9.0	-8.6	18.5	18.0	-7.9	15.3
	2090s	11.1	15.5	-7.0	-13.6	-23.5	-22.4	-9.4	-9.4	16.2	16.1	64.0	82.0

Sediment yield will show decreasing trend on both predicted LULC and climate and the base LULC and predicted climate scenarios in the 2090s and 2060s time slices of A1B with values of 1.9%, 35.2%, and 19.9%, 50% respectively, with a higher decrease in the base LULC and predicted climate of the A1B scenario. Sediment yield will show a reduction by 1.9% and 13% only in the 2060s and 2090s of the RCP4.5 in the predicted LULC and climate scenario and it will show an increasing trend in other RCPs and time slices. It will vary with a range of -13% to 82% in the predicted LULC and climate scenario. The highest increase in sediment yield will be observed in the 2090s of the RCP8.5 which is 82% (Figure 8-2, Table 8-3).

In the base LULC and predicted climate scenario sediment yield will show increasing and decreasing fluctuations. It will show an increase in the 2030s of the RCP4.5 and 2030s and 2090s of the RCP8.5 with 15.3%, 25.9%, and 64% respectively. In the other scenarios, it will show a decrease with a range between 7.9% and 31%. Generally, sediment yield will show a higher increase in the predicted LULC and climate scenario. This might be attributed to the increasing situation of LULC conversion mainly the expansion of cultivated lands.

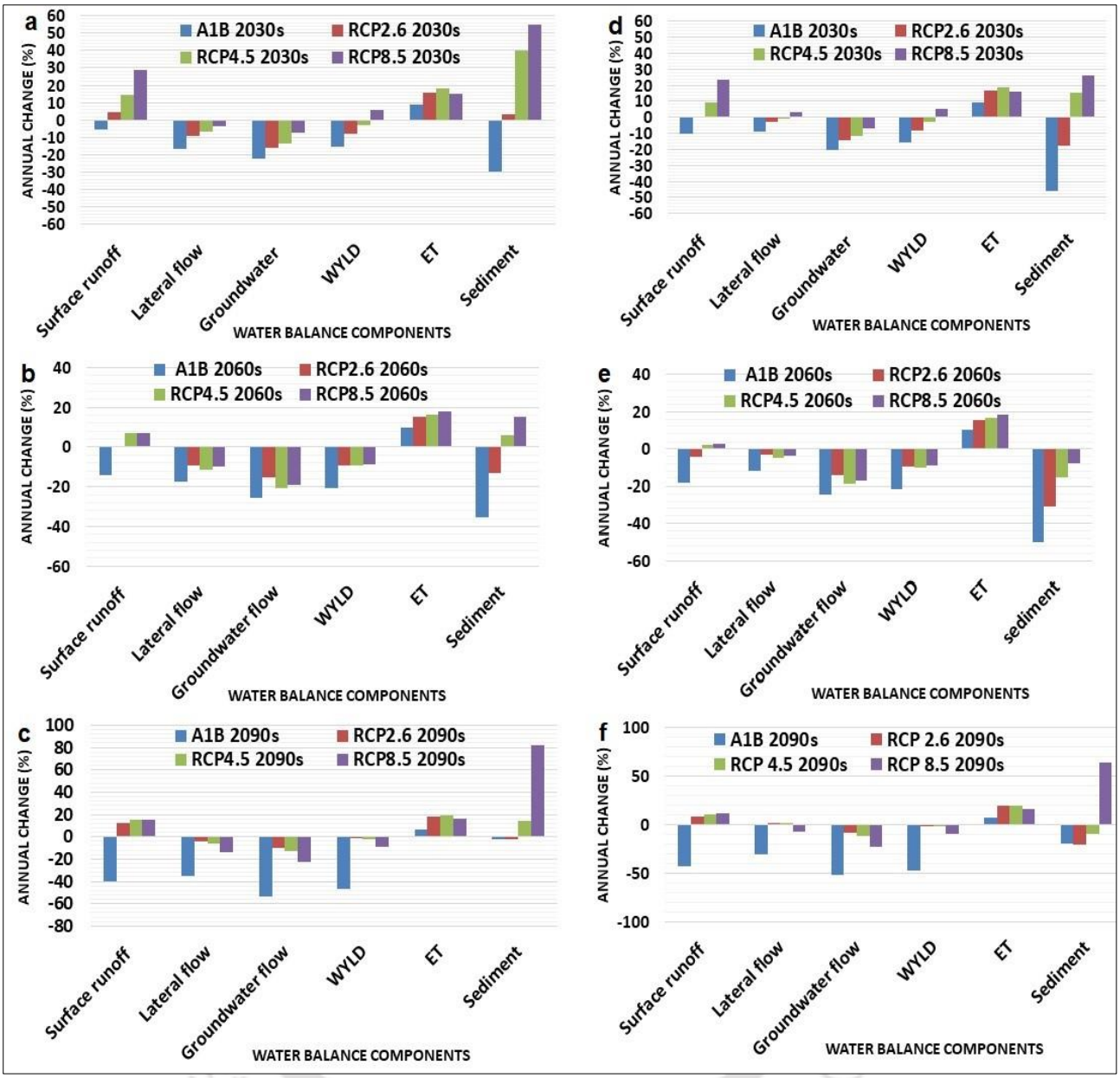

Figure 8-2 Percentage (%) change of annual average hydrologic components in predicted LULC and climate scenario (a, b & c) and base LULC and predicted climate scenario (d, e & f) in the 2030s, 2060s and 2090s time slices of A1B and RCP scenarios, Rib

8.3.2 Hydrologic components with predicted LULC and climate scenario in monthly basis, Rib

As it is observed from the Figure 8-3, surface runoff peaks in July (summer) in the base period. In the predicted scenarios, its peak shifted to August. In January, February, March, April, and May the base period surface runoff is higher than the future scenario periods. In

July, August, November, and December in the 2060s and 2090s of the A1B scenario surface runoff will be increasing. In the 2030s of the A1B scenario and 2090s of RCP scenarios high surface runoff will be observed in the Kiremt (summer) months. In all RCP scenarios surface runoff increases in the Bega (winter) seasons (October November, December, January, and February) (Figure 8-3)

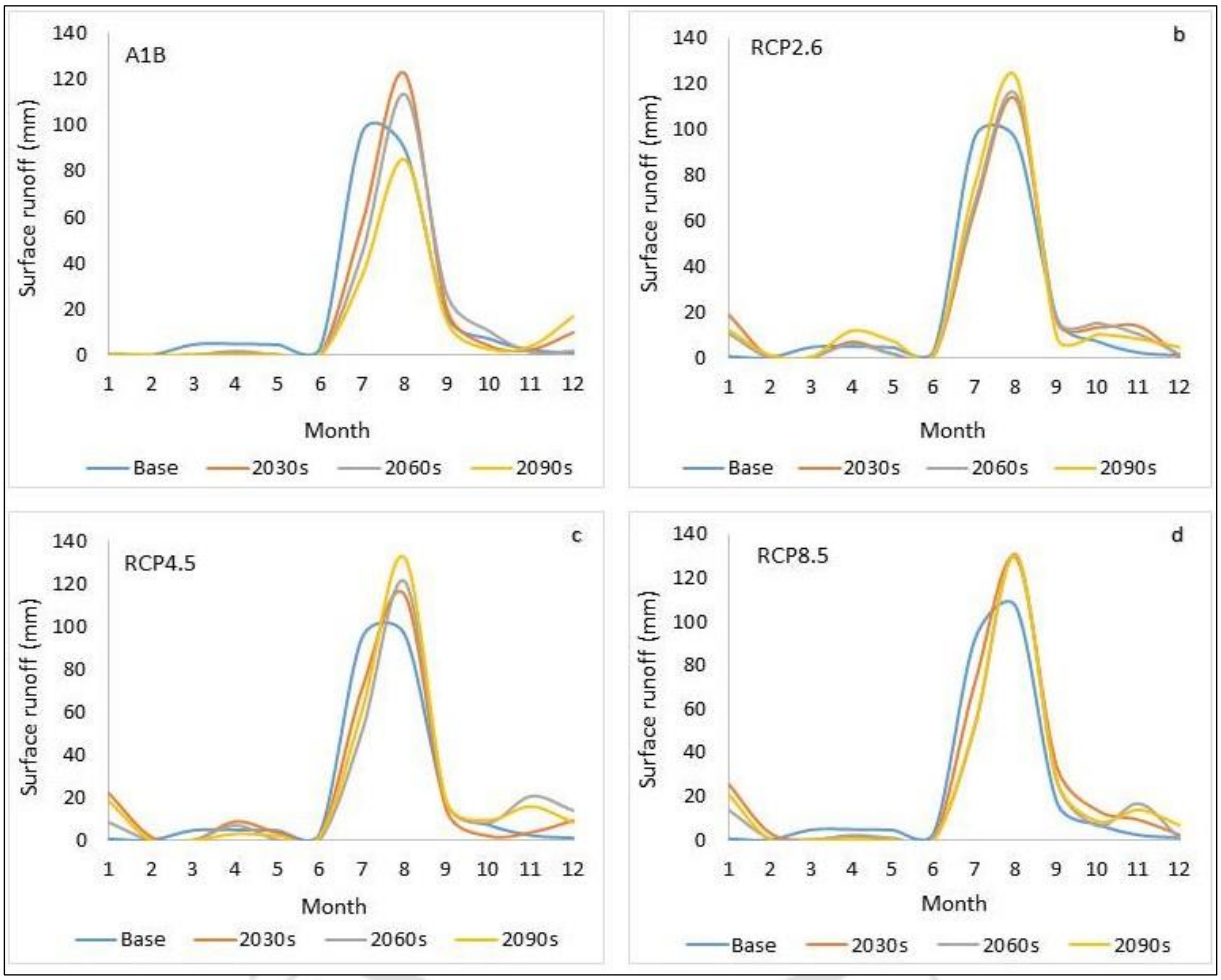

Figure 8-3 Surface runoff in the A1B (a), RCP2.6 (b), RCP4.5 (c) and RCP8.5 (d) scenarios

A high decrease and variation in lateral flow will be observed in the A1B scenarios. The highest decrease will be shown in the 2090s of the A1B scenario. In all RCP scenarios and time-slices, an increase in lateral flow will be observed in Bega (winter) months of October, November, December, January, and February compared to the base period. No significant variation is observed in the Kiremt (summer) months of August and September (Figure 8-4)

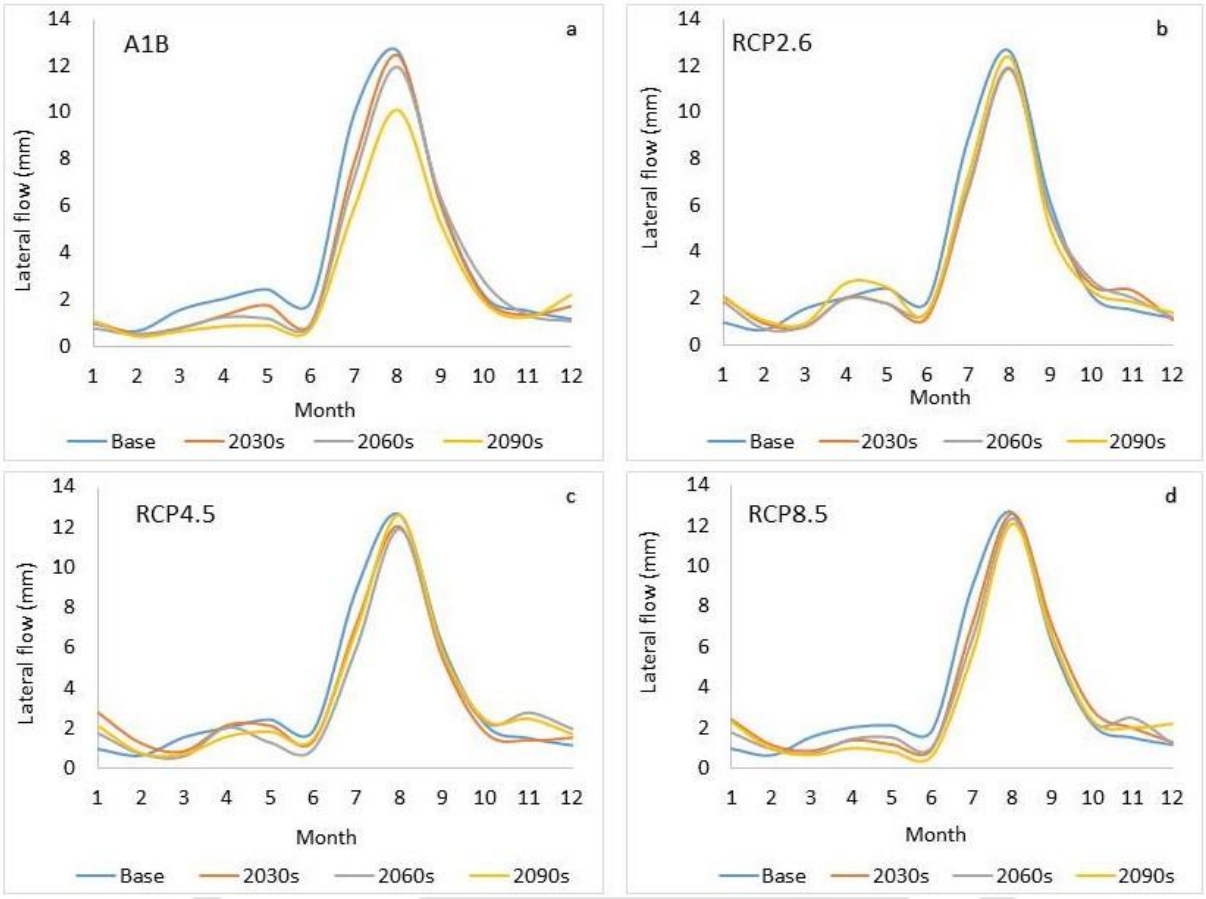

Figure 8-4 Lateral flow during A1B (a), RCP2.6 (b), RCP4.5 (c) and RCP8.5 (d) scenarios

As it is indicated in the Figure 8-5, water yield will show a general decrease in A1B and RCP scenarios. The highest decrease will be observed in the A1B scenario followed by RCP8.5. There will be an increase in the Bega (winter) months of November, December, January, and February in the RCP scenarios. August will show an increase in the 2090s of the RCP2.6 and 4.5 scenarios.

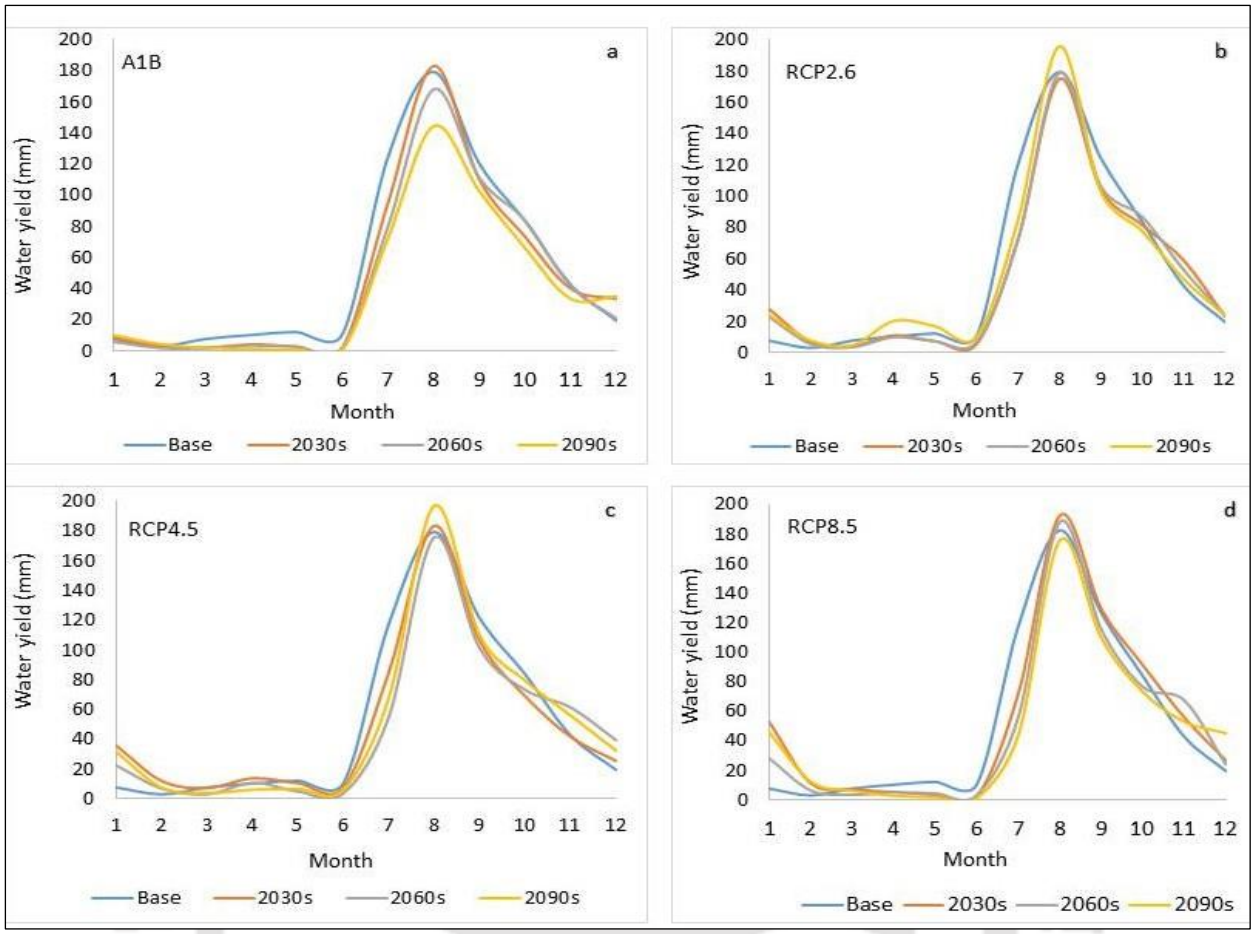

Figure 8-5 Total water yield during A1B (a), RCP2.6 (b), RCP4.5 (c) and RCP8.5 (d) scenarios

In most months evapotranspiration shows an increase. In March, April, and May (Belg season) and in June there will be a decrease in evapotranspiration in A1B scenarios. In the other months of A1B scenario, an increase in evapotranspiration will be observed. Except in May and June, in the other months of RCP 2.6 and 4.5 scenarios evapotranspiration will show increasing with the highest increase in the Bega (winter). Except May and June, other months will show an increase of evapotranspiration in the RCP 8.5 scenario with the highest increase in the 2090s (Figure 8-6).

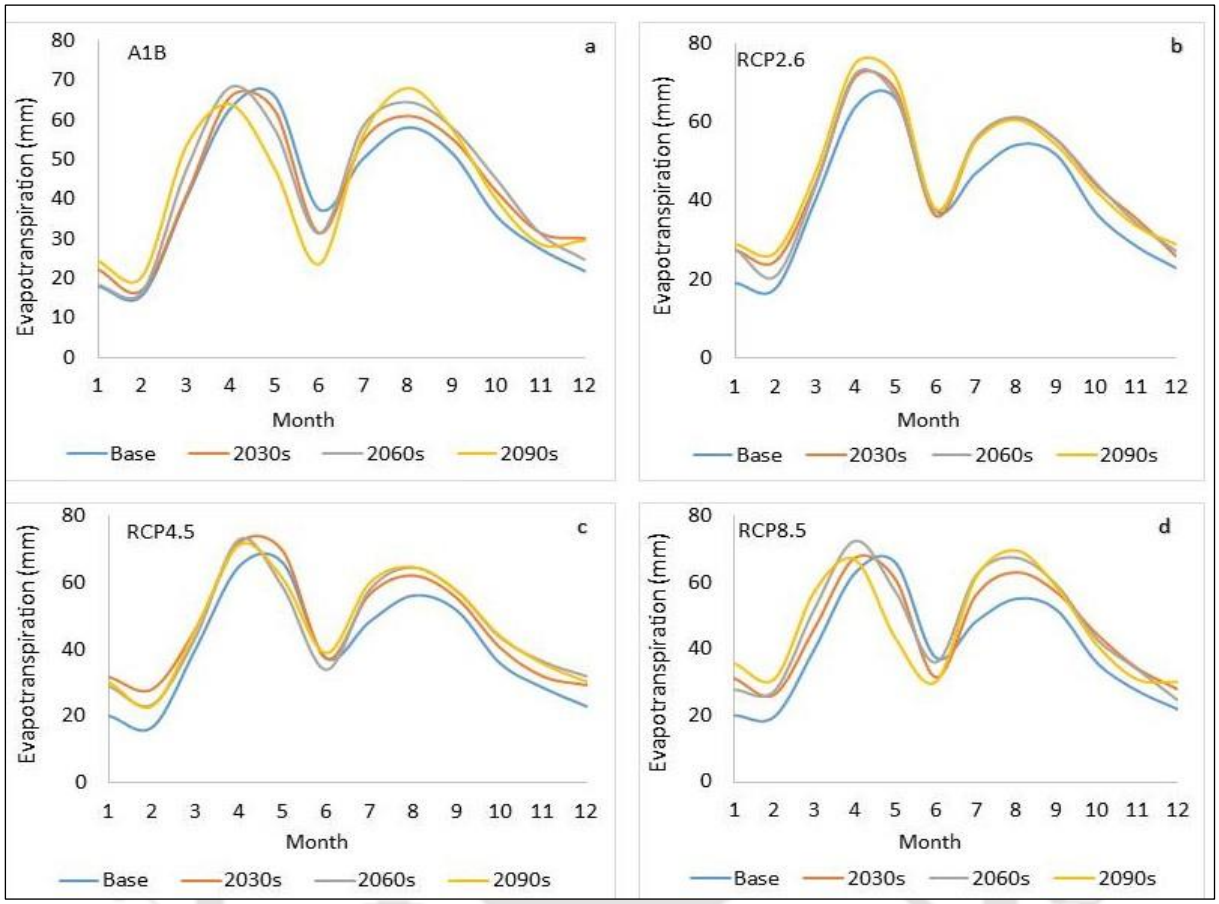

Figure 8-6 Evapotranspiration A1B (a), RCP26 (b), RCP45 (c) and RCP85 (d) scenarios

8.3.3 Impact of LULC and climate changes on the hydrological components and sediment yield in Gumara

Surface runoff shows a consistent decrease in A1B scenario simulations in the predicted LULC and climate and base LULC and predicted climate scenarios. The decrease in surface runoff in the predicted LULC and climate and the base LULC and predicted climate scenarios do not have a significant difference. It's decreasing values in the predicted LULC and climate and the base LULC and predicted climate scenarios in the 2030s and 2090s respectively will be 18.4%, 33.3% and 19%, 33.6% (Figure 8-7, Table 8-6). Surface runoff decreases in all RCP scenarios except in the 2030s of the RCP8.5 with an increase of 3.7%. Surface runoff will show a range of variation between 3.7% to -35.1% in the RCPs predicted LULC and climate scenario and -8% to -37.9% in base LULC and predicated climate scenario compared with the baseline. The highest decrease will be observed in the 2090s of the RCP 8.5 scenario with a decrease of 35.1% and 37.9% in the predicted LULC and climate and base LULC and predicted climate scenarios respectively (Figure 8-7). Relatively higher decrease in surface

runoff will be observed in the base LULC and predicted climate scenarios than the predicted LULC and climate scenarios of the RCPs (Figure 8-7, Table 8-6). A little higher surface runoff value in the predicted LULC and climate scenario might be related with the removal of vegetation due to LULC change in the watershed.

Lateral flow and groundwater flow will show a decreasing trend in all time slices of A1B scenario. The decreasing values in the predicted LULC and climate and base LULC and predicted climate scenarios in the 2030s and 2090s respectively will be; lateral flow 6.9%, 19.3%, and 4.7%, 17.8%, groundwater flow 11.8%, 38.6%, and 10.0%, 37.3%. From the result, it is understood that lateral flow and groundwater flow will show a little lower value in the predicted LULC and climate scenario than the base LULC and predicted climate scenario. The decrease in lateral flow and groundwater flow in the predicted LULC and climate scenario than the base LULC and climate scenario is related to the LULC change mainly vegetation removal. The removal of vegetation reduces the lateral flow and groundwater flow through seepage in the root systems. Vegetation reduces the velocity of runoff and gives time for lateral and groundwater flow through percolation and infiltration.

There is a decrease in lateral flow with a range between 6.7% to 23.7% and 7.6% to 25% in the 2030s and 2090s of the RCP 8.5 in the predicted LULC and climate and base LULC and predicted climate scenarios respectively (Figure 8-7, Table 8-6). There is a little higher decrease in lateral flow in the predicted LULC and climate scenario. Groundwater flow showed a decrease between 14.8% to 47.8% and 17.4% to 50.9% in the 2030s and 2090s of the RCP in the predicted LULC and climate and base LULC and predicted climate scenarios respectively. Groundwater flow will show a higher decrease in the base LULC and predicted climate scenario. The higher and lower decrease in lateral flow and groundwater flow will be occurring in the 2030s and 2090s of the RCP scenarios.

Total WYLD will show a decreasing trend in all time slices of the SRES A1B scenario. It's decreeing values in the predicted LULC and climate and the base LULC and predicted climate scenarios in the 2030s and 2090s time-slices will be 15.5%, 34%, and 15.1%, 33.6% respectively. The decrease in total water yield is not show a significant variation between predicted LULC and climate and the base LULC and predicted climate in the A1B scenario. Water yield will show a decrease in all the RCP scenarios. The lowest and highest decrease will be in the 2030s and 2090s of the RCP8.5 scenario. The decrease in total WYLD ranges

between 3.1% to 38.3% and 7.2 to 41.2% in the 2030s and 2090s of the RCP8.5 in the predicted LULC and climate and base LULC and predicted climate scenarios respectively. The higher reduction of total WYLD will be shown in the base LULC and climate change scenario.

Table 8-4 Average annual hydrologic components in the predicted LULC and climate scenario compared to the baseline period, Gumara

Scenario/hydrologic components		Surface runoff (mm)	Lateral flow (mm)	Groundwater flow (mm)	Total WYLD (mm)	ET (mm)	Sediment yield (t/ha)
Base (1993-2016)		526	59.6	267.3	868.4	556.3	71.6
SRES A1B	2030s	429	55.5	235.8	734.1	588.2	66.8
	2060s	373.3	53.5	218.2	657.8	589.2	82.81
	2090s	351	48.1	164.2	573.4	602.5	123.1
RCP 2.6	2030s	469	53.9	209.6	744.9	585.5	79.75
	2060s	489.1	54.9	220.0	777	581.4	78.3
	2090s	442.1	53.2	204.8	712.3	580.3	59.6
RCP 4.5	2030s	449.5	53	204.2	718.9	576.1	64.3
	2060s	419	50.4	180.4	660.7	578.9	89.6
	2090s	439.1	52.2	194.9	697.9	583.4	86
RCP 8.5	2030s	545.2	55.6	227.6	841.8	573.6	91.4
	2060s	455	51.8	189.8	708.1	589.3	121
	2090s	341.6	45.5	139.4	535.5	572.1	132

Table 8-5 Average annual hydrologic components in the base LULC and predicted climate scenario compared to the baseline period, Gumara

Scenario/hydrologic components		Surface runoff (mm)	Lateral flow (mm)	Groundwater flow (mm)	Total WYLD (mm)	ET (mm)	Sediment yield (t/ha)
Base (1993-2016)		526	59.6	267.3	868.4	556.3	71.6
SRES A1B	2030s	426	56.8	240.5	737.2	585.1	71.3
	2060s	371.1	54.6	222.4	661.2	585.8	84.8
	2090s	349.22	48.99	167.7	576.19	599.7	108
RCP 2.6	2030s	460.3	53.7	205.5	731.7	567.1	73.1
	2060s	483.9	54.8	215.7	767.2	564.6	75.2
	2090s	433.3	53.2	200.1	698.6	567	60.4
RCP 4.5	2030s	436.3	52.9	199.8	700.8	560.8	62
	2060s	410.4	50.1	177.1	648.5	561.1	77.6
	2090s	436.1	52.1	191.0	690.6	568.4	75.2
RCP 8.5	2030s	517.2	55.1	220.8	806	555.6	83.2
	2060s	437.8	51.2	183.4	683.6	571.9	112
	2090s	326.5	44.7	131.1	510.9	560.3	121

There will be an increasing trend of ET in the predicted LULC and climate and the base LULC and predicted climate scenarios in the 2030s and 2090s time slices of A1B scenario

with values of 5.7%, 8.3%, and 5.2%, 7.8% respectively. The ET is higher in the predicted LULC and climate scenario. The ET will show an increase in all RCP scenarios except the 2030s of the RCP8.5 in the base LULC and predicted climate scenario. The lower and higher increase in ET will be in the 2090s and 2060s of the RCP8.5 with values of 2.8% and 5.9% respectively in the predicted LULC and climate scenario. In the base LULC and predicted climate scenario the change of ET varies between -0.1% to 2.8% in the 2030s and 2060s of the RCP8.5 scenario respectively. The increase in ET is higher in the predicted LULC and predicted climate scenario (Figure 8-7, Table 8-6). This increase in ET in the predicted LULC and climate scenario might be due to the increase in temperatures.

Table 8-6 Percentage (%) change of average hydrologic components in base and future LULC and future climate scenario, Gumara

Scenario		Surface runoff		Lateral flow		Groundwater		Total WYLD		ET		Sediment	
		LULC		LULC		LULC		LULC		LULC		LULC	
		Base	Future	Base	Future	Base	Future	Base	Future	Base	Future	Base	Future
SRES A1B	2030s	-19.0	-18.4	-4.7	-6.9	-10.0	-11.8	-15.1	-15.5	5.18	5.7	-0.4	-6.7
	2060s	-29.4	-29.0	-8.4	-10.2	-16.8	-18.4	-23.9	-24.3	5.3	5.9	18.4	15.7
	2090s	-33.6	-33.3	-17.8	-19.3	-37.3	-38.6	-33.6	-34.0	7.8	8.3	50.8	71.9
RCP 2.6	2030s	-12.5	-10.8	-9.9	-9.6	-23.1	-21.6	-15.7	-14.2	1.94	5.2	2.1	11.4
	2060s	-8.0	-7.0	-8.1	-7.9	-19.3	-17.7	-11.7	-10.5	1.49	4.5	5.0	9.4
	2090s	-17.6	-16.0	-10.7	-10.7	-25.1	-23.4	-19.6	-18.0	1.92	4.3	-15.6	-16.8
RCP 4.5	2030s	-17.1	-14.5	-11.2	-11.1	-25.3	-23.6	-19.3	-17.2	0.81	3.6	-13.4	-10.2
	2060s	-22.0	-20.3	-15.9	-15.4	-33.7	-32.5	-25.3	-23.9	0.86	4.1	8.4	25.1
	2090s	-17.1	-16.5	-12.6	-12.4	-28.6	-27.1	-20.5	-19.6	2.18	4.9	5.0	20.1
RCP 8.5	2030s	-1.7	3.7	-7.6	-6.7	-17.4	-14.8	-7.2	-3.1	-0.1	3.1	16.2	27.6
	2060s	-16.8	-13.5	-14.1	-13.1	-31.4	-29.0	-21.3	-18.5	2.8	5.9	56.4	68.0
	2090s	-37.9	-35.1	-25.0	-23.7	-50.9	-47.8	-41.2	-38.3	0.72	2.8	69.0	84.3

Sediment yield will show a decrease in the 2030s of the A1B scenario. In the 2060s and 2090s time slices on both predicted LULC and climate and the base LULC and predicted climate scenarios it will increase with values of 15.7%, 71.9%, and 18.4%, 50.8% respectively. There will be a higher increase of sediment yield in the predicted LULC and climate scenario. Sediment yield will decrease by 16.8%, 13.4% and 10.2%, 15.6% only in the 2090s of the RCP2.6 and 2030s of the RCP4.5 in the predicted LULC and climate and base LULC and climate scenarios respectively. It has shown an increasing trend in other

RCPs and time slices on both scenarios. It will vary between -16.8% to 84.3% and -15.6% to 69.0 in the predicted LULC and climate and base LULC and predicted climate scenarios respectively. The highest increase in sediment yield will be observed in the 2030s, 2060s and 2090s of the RCP8.5 with values 27.6%, 68%, 84.3% and 16.2%, 56.4%, 69% in the predicted LULC and climate and base LULC and predicted climate scenarios respectively (Table 8-6). Generally, sediment yield will show a higher increase in the predicted LULC and climate scenario. This might be attributed to the increasing situation of LULC conversion mainly the expansion of cultivated lands.

In a decrease of surface runoff, there has been an increase in sediment yield which might be due to the accelerated expansion of intensively cultivated lands in the steeper slopes. In the watershed, intensively cultivated land has increased from 9.4% and 9.3% during 1984–2003 and 2003–2016 respectively to nearly 21% during 2016–20149 which plays a significant role in the increase of sediment yield even if there has been a decrease in surface runoff. There has been a great loss of vegetation which strongly related to the expansion of cultivation lands especially in the higher slopes and escarpments where cultivation is prohibited. About 15–30% and >30% slopes cover 35.3% and 12% of the watershed respectively which are the very sites of erosion and sediments in the watershed. In the study area, remnant vegetation covers have been observed in the steeper slopes and escarpments which are not suitable for cultivation, but currently and in the future trends, because of shortage of lands and decreasing land productivity, these areas are turning to crop fields. This condition results in a high increase of erosion and sediment yield with the available rainfall/surface runoff. Various studies in the highlands of Ethiopia have shown that soil erosion and sediment yield have been accelerating at steep slopes where there has been expansion of cultivated lands.

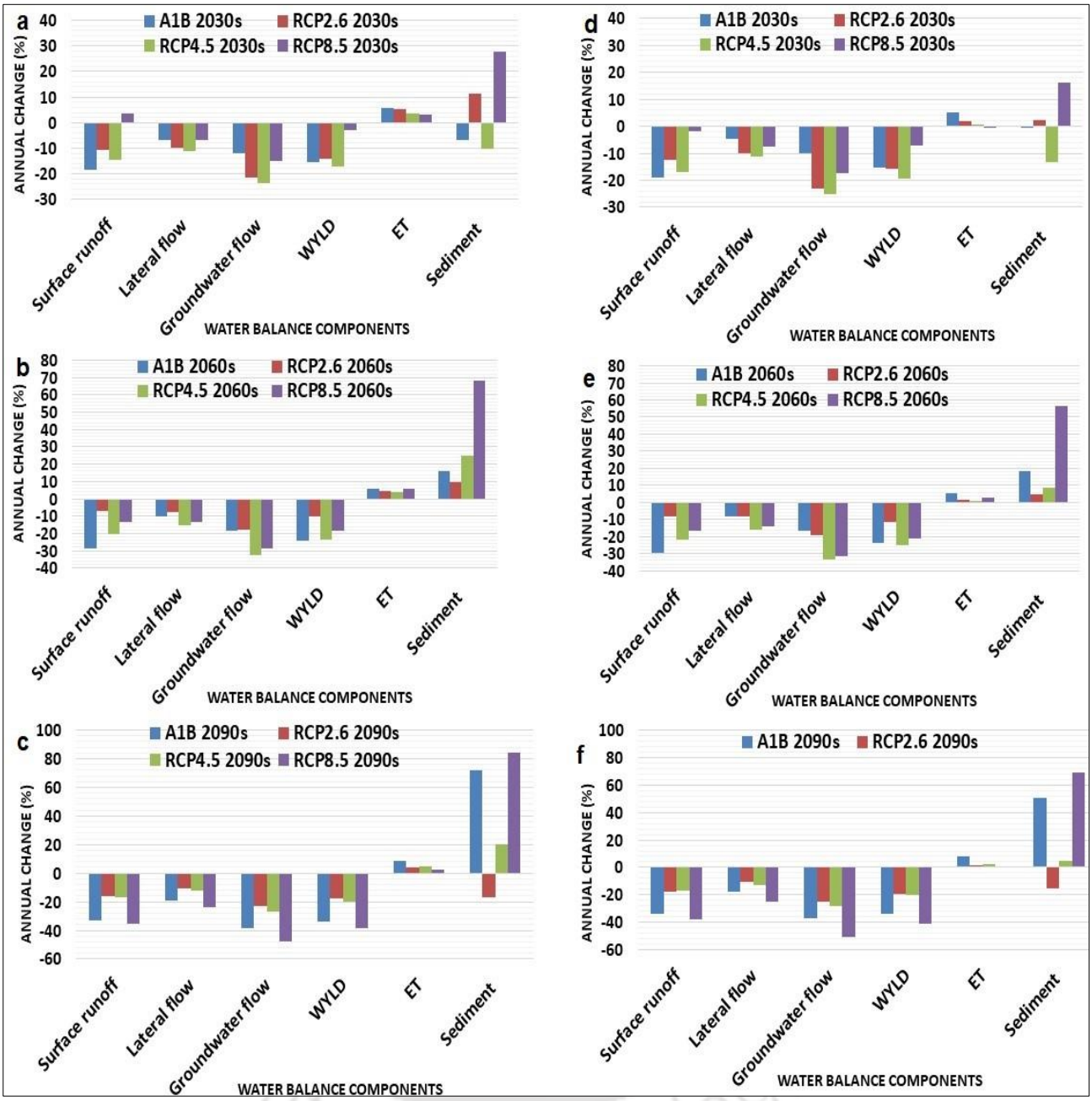

Figure 8-7 Percentage (%) change of annual average hydrologic components in predicted LULC and climate scenario (a, b & c) and base LULC and predicted climate scenario (d, e & f) in the 2030s, 2060s and 2090s time slices of A1B and RCP scenarios, Gumara

8.3.4 Hydrologic components with predicted LULC and climate scenario on monthly basis, Gumara

In May, June, and July the base period surface runoff is higher than the predictions. In August, the 2030s A1B scenario surface runoff will be higher than other periods. August

shows its lowest surface runoff in the 2090s of the A1B scenario compared to other scenarios. High surface runoff in the A1B scenario is predicted in the 2030s. The RCP2.6 and 4.5 will show a little higher surface runoff in August. There will be an increasing trend of surface runoff in the Bega (winter) months of October, November, and December in all scenario periods. In all scenarios (A1B and RCPs) no significant variation in surface runoff in January, February, March, and May (Figure 8-8)

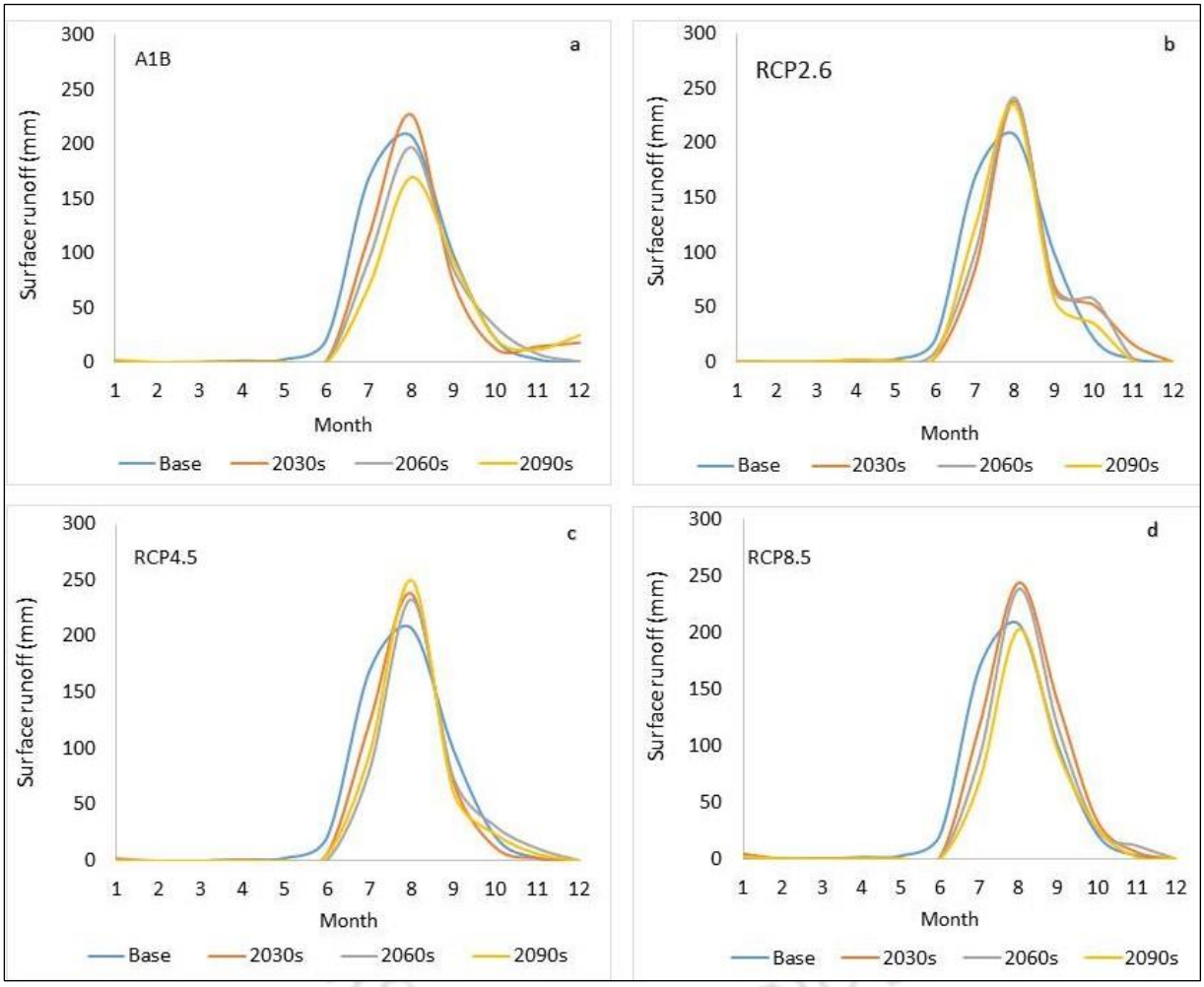

Figure 8-8 Surface runoff during A1B (a), RCP2.6 (b), RCP4.5 (c) and RCP8.5 (d) scenarios

In all scenario periods and months, lateral flow will have decreasing trends compared to the base period (Figure 8-9). Significant decreasing variation in lateral flow will occur in 2030s, 2060s, and 2090s of the A1B scenario in June, July, August, September (summer months) with the highest decrease in the 2090s. The 2060s of the RCP4.5 scenario will show a relatively higher decrease than other periods in July, August, and September (summer). A clear variation in all months between scenarios will be shown in RCP8.5, with a high variation in June, July, August, September, and October. The decreasing order of lateral flow

from the highest to lowest in all months in the RCP8.5 is 2030s, 2060s, and 2090s.

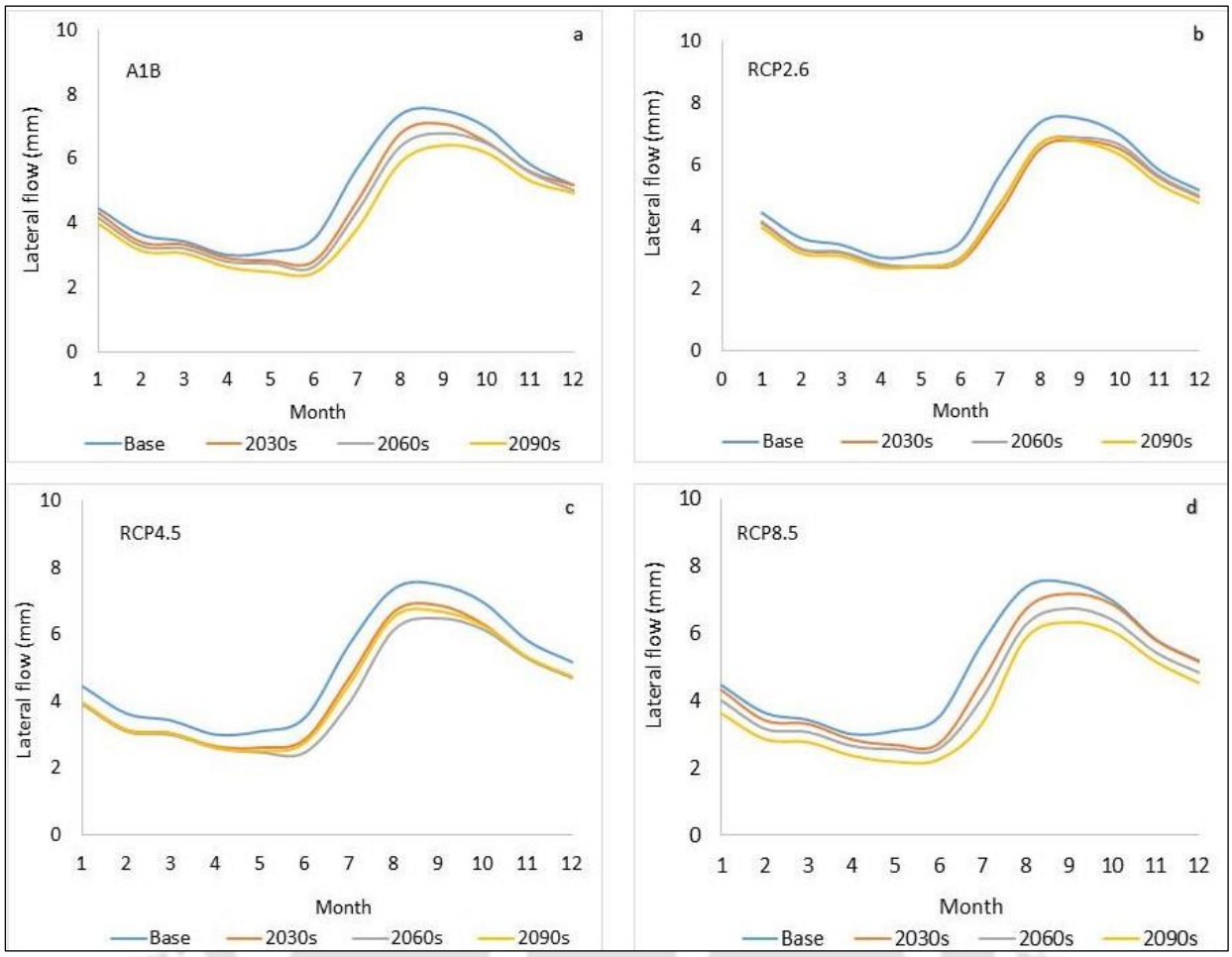

Figure 8-9 Lateral flow in A1B (a), RCP2.6 (b), RCP4.5 (c) and RCP8.5 (d) scenarios

As it is indicated in the Figure 8-10, water yield shows a general decrease in A1B and RCP scenarios. The highest decrease especially in summer months will be observed in the A1B scenario. The summer months will show a significant decrease in the 2060s and 2090s of the A1B scenario. There will be an increase in the Bega (winter) months of October of November, December, and January especially in A1B and in the RCP2.6 scenarios. August will show a little increase in the 2030s and the 2090s of the RCP4.5 scenario. The summer months of June, July, and September will show a decreeing trend in the A1B, RCP2.6 and 4.5 scenarios. Generally, August will not show significant variation except the 2090s of the A1B and RCP8.5 scenarios.

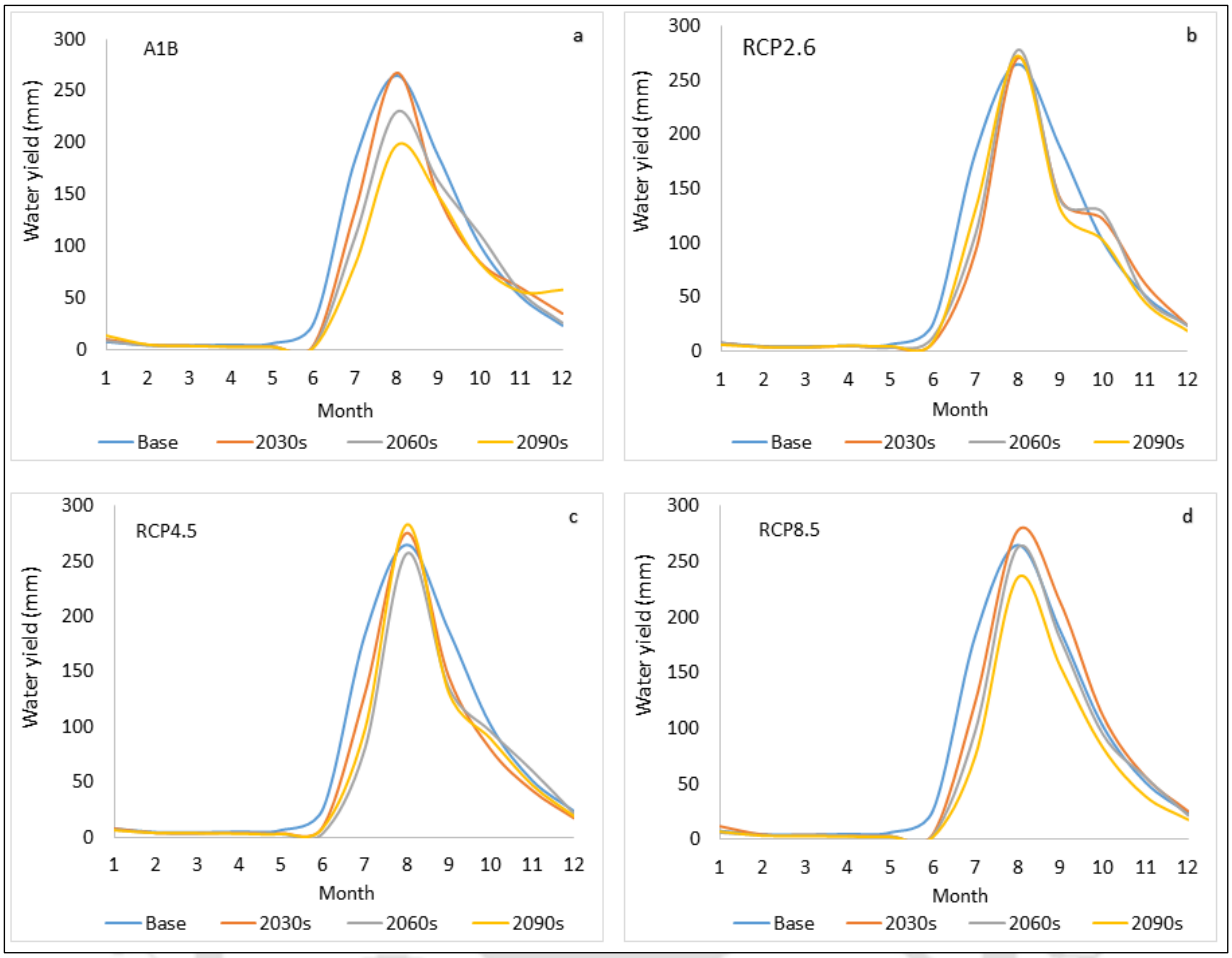

Figure 8-10 Water yield in A1B (a), RCP2.6 (b), RCP4.5 (c) and RCP8.5 (d) scenarios

In most months evapotranspiration shows an increase. In May of the Belg season and June of the summer season, there will be a decrease in evapotranspiration in all scenarios. A significant increase will be in the A1B followed by RCP8.5 scenarios. In July, August and September there will be a clear increasing trend in all RCP scenarios with great variability in the RCP8.5 scenario. In October November and December, the variation will not be significant except the A1B scenario periods. There will be a visible increase in January and February (Bega) in all scenarios with the highest in A1B scenario (Figure 8-11).

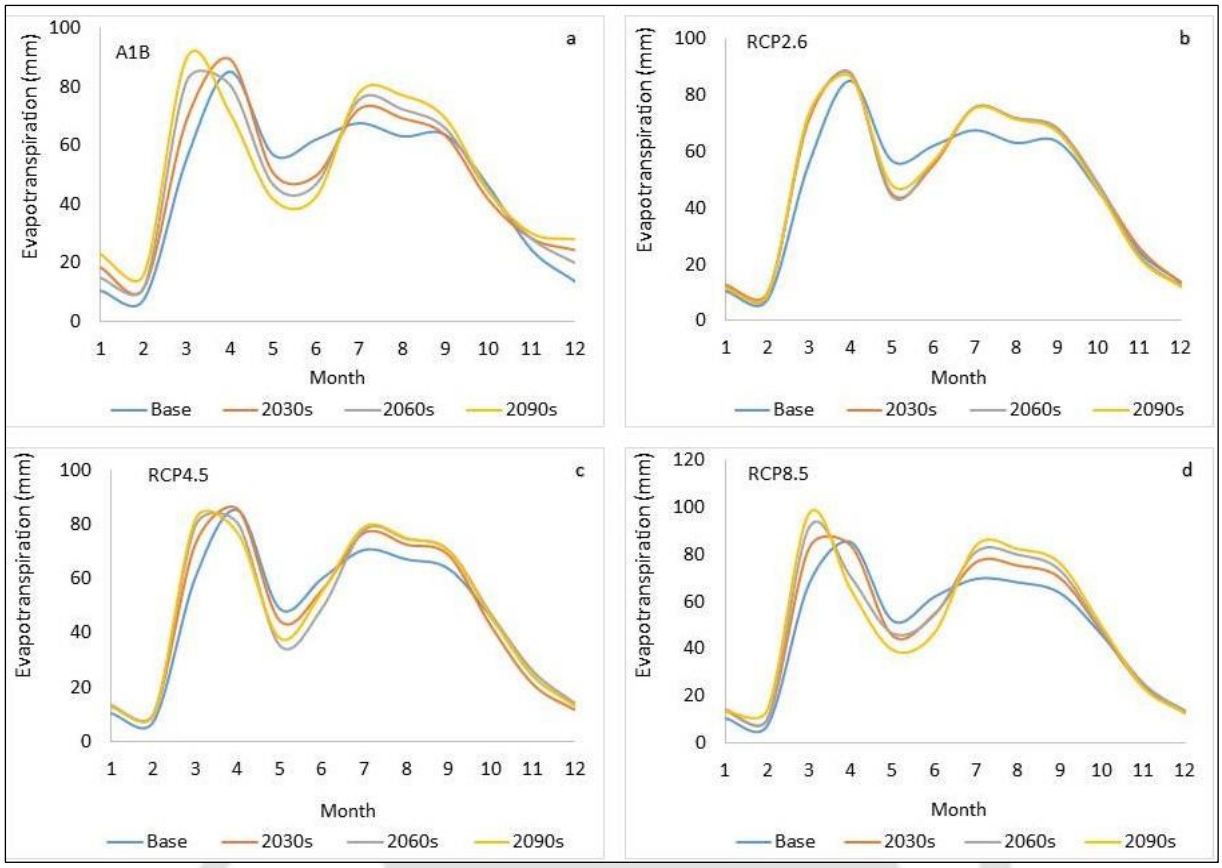

Figure 8-11 Evapotranspiration in A1B (a), RCP26 (b), RCP45 (c) and RCP85 (d) scenarios

8.4 Repercussions of the research on soil and water management/roles of practitioners

Based on the results of this study, soil, and water conservation practitioners are recommended to design and implement appropriate watershed management practices to mitigate erosion to boost land productivity. Since the past four decades, the Ethiopian governments have been launching and practicing soil conservation practices but due to various reasons, the practices were not successful (Shiferaw and Holden, 1999; Herweg and Ludi, 1999; Hengsdijk et al., 2005). Different reasons have been raised by the immediate practitioners (farmers) and agriculture extension experts (land managers). Among others, the ineffectiveness of the conservation measures, unsustainability of structures, poor quality structures, intentional removal of structures by farmers themselves are the reasons that made government campaigns on soil and water conservation unsuccessful (Shiferaw and Holden, 1999; Hengsdijk et al., 2005). The conservation measures that have been practicing also lack local adaptability and were not research-based depending on the hydrological characteristics of watersheds. In this regard in most parts of the country including Rib and Gumara watersheds, soil bunds, waterways, afforestation, and some biological measures in gully areas were

practicing (El-Swaify and Hurni, 1996). An important issue regarding stone bunds is their spacing along the contour. In many cases, the implementation of stone bunds did not consider their spacing along the slope to properly reduce erosion from crop fields. The design and implementation of land management activities have to be research-based and consider their capability in reducing runoff and soil erosion depending on the slope and cover of the areas where the management activities are implementing. In this study, the soil erosion hot spots and amount of sediment yield per sub-watershed levels were identified and discussed in chapter six. This study revealed that because of the expansion of crop fields with the expense of vegetation covers there has been an increase in erosion and sediment yield, especially in Gumara watershed. Therefore, appropriate soil and water conservation measures need to be constructed to reduce erosion and increase land productivity. In this regard, filter strips having a width of 1m and 5m and soil/stone bunds with a slope length of 10m and 50% reduction along the contour in agricultural fields were assessed. Filter strip with 5m width showed a significant decrease in sediment yield whereas no significant variation between soil/stone bund spacing of 10m and 50% reduction. Therefore, the local farmers and land managers need to practice filter trips in lower slopes and soil/stone bunds in the steeper slopes of the watersheds. The climate prediction showed a decrease in rainfall which has an impact on groundwater recharge for streamflow. The LULC prediction also showed a decrease in vegetation covers which has an impact on an increase in sediment yield. Therefore, the land management practitioners have to appreciate vegetation cover, especially on hilly and steep slope areas to reduce surface runoff and sediment yield for better environmental management and agricultural productivity.

8.5 Conclusion

The predicted climate showed that there will be a decrease in rainfall and an increase in temperature in both watersheds. The future LULC scenario showed an increase in cultivation land with the expense of vegetation in both watersheds. The decrease of vegetation in Rib results for an increase in surface runoff the RCP scenarios. The increasing values of surface runoff are higher in the predicted LULC and climate and base LULC and predicted climate scenarios. There will be a general decrease in lateral flow, groundwater flow, and total water yield in A1B and RCP scenarios with the highest decrease in the A1B scenario. Lateral flow and groundwater flow will show a higher decrease in the predicted LULC and climate scenario than the base LULC and predicted climate scenario. The decrease in total water yield is not show a significant variation between the predicted LULC and climate and the

base LULC and predicted climate scenarios. There will be an increasing trend in ET in A1B and RCP scenarios with a higher increase in the RCPs. Sediment yield will show an increase except in the 2060s and 2090s of the RCP2.6 and A1B scenarios. A significant decrease will occur in the A1B scenario. Generally, sediment yield will show a higher increase in the predicted LULC and climate scenario.

In Gumara surface runoff will show a consistent decrease in A1B scenario simulations in the predicted LULC and climate and base LULC and predicted climate scenarios. Surface runoff decreases in all RCP scenarios except in the 2030s of the RCP8.5. The decrease in surface runoff in the predicted LULC and climate and the base LULC and predicted climate scenarios do not show a significant difference. The decrease in surface runoff might be attributed to the decreasing trend of precipitation in all RCP scenarios. Lateral flow and groundwater flow show a decreasing trend in all time slices of the A1B and RCP scenarios of the watershed. Lateral flow and groundwater flow will show a little lower value in the predicted LULC and climate scenario than the base LULC and predicted climate scenario. The decrease in lateral flow and groundwater flow in the predicted LULC and climate scenario than the base LULC and climate scenario is related to the LULC change mainly vegetation removal.

Total WYLD will show a decreasing trend in A1B and RCPs scenarios. The decrease in total water yield will not show a significant variation between predicted LULC and climate and the base LULC and predicted climate scenarios in A1B, but a higher decrease will be shown in the base LULC and climate change scenario in the RCPs. In general, there will be an increase in ET in A1B and RCPs. The increase in ET is higher in the predicted LULC and climate scenario in the RCPs. Generally, sediment yield will show a higher increase in the predicted LULC and climate scenario. This might be attributed to the increasing situation of LULC conversion mainly the expansion of cultivated lands. The increase in sediment through the future periods is generally due to the increase of cultivated land and the decrease of forest and shrublands. Reports from the Ethiopian Highlands indicated that the increase of sediment yield is attributed to an increase in crop cultivation. From this study it is found that both the changing LULC and climate have significant impact on the hydrological response of the watersheds. Instead of using only climate change data in watershed impact studies, we suggest to incorporate the LULC change scenarios to acquire a comprehensive picture of the hydrological response.

Chapter 9 : Conclusions and Recommendations

The study is designed to address the following research themes

1. **Predicting and analysis of the future LULC change scenario of Rib and Gumara watersheds**

The Dyna-CLUE model was employed to predict the LULC of the watersheds. Important LULC driving factors were identified and the logit regression was used to select relevant factors from the list of expected driving factors. For the LULC prediction future demand of each LULC was determined using extrapolation of trends of the recent past using the historical LULCs of the watersheds. The conversion sequences of the LULCs of the area were determined using the historical trends of the LULC conversion, expert opinions, and knowledge and experience of aged people in the localities. The resistance of conversion or conversion elasticity of land-uses was also defined on the basis of the expert opinions. The Dyna-CLUE model having the inputs of demand, conversion elasticity, conversion matrix or conversion sequences, and the base map was used to predict the future LULC of the watersheds. The capability of the model in predicting the LULC of the watersheds was assessed with the ROC statistics and validation between simulated and reality maps of the areas. The result showed that the model was capable of predicting the LULC scenarios of the watersheds with a reasonable level of accuracies of Kappa, KLocation, and KHisto values of Rib 0.734, 0.762, 0.963 and Gumara 0.730, 0.751, 0.971 respectively. The result indicated that a large increase will be observed in cultivated lands and a gradual and low increase in plantation and urban LULCs. There will be a decrease in shrubland and mixed forests in all time periods and both watersheds. The accelerated increase in cultivated lands and a decrease of vegetation might have an impact on the increase of the sediment yield of the watersheds.

2. **Predicting future climate change of Rib and Gumara watersheds**

The climate changes in the watersheds were predicted employing the RCM/GCM data outputs from REMO-ECHAM5 with AR4 IPCC SRES A1B scenario and RACMO22T-HadGEM2-ES in the CORDEX-Africa domain with AR5 IPCC RCPs (2.6, 4.5, and 8.5) scenarios. The precipitation and temperature time series RCM model data outputs were bias-corrected using the delta change method to reduce the anomalies between the historic and the predictions. The predicted climate showed that there will be a general decrease in precipitation and an increase in temperature in both watersheds. In terms of seasonal

precipitation, the highest decrease will be observed in the Belg season (March, April, and May) and the highest increase in the Bega especially in the months of January and February. In both watersheds, there will be a slight shift in high rainfall from the month of July to August. A higher decrease in precipitation is observed in the SRES A1B scenarios than the RCPs. Compared to the baseline period there will be a decrease of mean annual precipitation by 5.1%, 6.6%, and 27.7% in Rib and 4.6%, 5.2%, and 24.6% in Gumara in the 2030s, 2060s, and 2090s of the A1B scenario respectively. The range of decrease in precipitation is between 0.8% in the 2030s to 16.7% in the 2090s of the RCP8.5 scenario in Rib watershed. In Gumara the variation in precipitation will be between 1.4% in the RCP2.6 scenario of the 2060s to 18.8% in the RCP8.5 scenario in the 2090s. The increasing variation in maximum and minimum temperatures respectively will be between 1.3°C, 1.3°C in the 2030s to 4.1°, 3.82°C in the 2090s in the A1B scenario in Rib and 1.3°C, 1.3°C in the 2030s, to 4.2°C, 3.84°C in the 2090s respectively in Gumara. Generally, the result indicated that the highest increase in temperature will be recorded in the 2090s of the RCP8.5 scenario and the lower increase will be in the 2030s of the RCP2.6 scenario in both watersheds.

3. Evaluation of the ArcSWAT model in simulating watershed hydrology and sediment yield in Rib and Gumara watersheds

ArcSWAT model with SWAT CUP-SUFI-2 calibration procedure was employed to evaluate its performance in predicting watershed hydrology and sediment discharge of the watersheds. The assessment of the SWAT hydrological model in simulating water balance components especially streamflow and sediment yield using recommended model efficiency evaluation criteria gave a valuable input of hydrologists about generating useful information in data-scarce watersheds. In the study model efficiency criteria of R^2, NSE, RSR, PBIAS, R-factor, and P-factor were used to measure the agreement between measured and predicted streamflow and sediment values in calibration and validation periods. The results indicated that the simulated watershed outputs of calibration and validation were consistent with measured values. The model performance is well in both calibration and validation periods. The monthly calibration and validation statistics of Rib flow respectively were R^2 (0.84, 0.75), NSE (0.83, 0.74), PBIAS (0.9%, 8.5%), and RSR (0.41, 0.51). The monthly calibration and validation values of Gumara respectively were R^2 (0.83, 0.80), NSE (0.82, 0.79), PBIAS (5.1%, 12.1%), and RSR (0.43 0.46). The monthly sediment calibration and validation performance evaluation statistics respectively of Rib were R^2 (0.74, 0.61), NSE (0.72, 0.60),

PBIAS (18.8, 18.7%), and RSR (0.53, 0.64) and Gunara were R^2 (0.76, 0.73), NSE (0.73, 0.71), PBIAS (7.0, 5.9 %), and RSR (0.51, 0.52). The model predicted flow and sediment yield of the watersheds satisfactorily as per the recommended performance evaluation criteria. From the statistical indices, it can be concluded that the ArcSWAT model has satisfactory performance in predicting the watersheds streamflow and sediment which once calibrated effectively the model can provide valuable predictions to aid in management decisions in the watersheds.

4. Assessment of the impact of agricultural management scenarios on sediment yield in Rib and Gumara Watersheds

The calibrated SWAT model has been used to assess the effect of agricultural management practices on sediment reductions. The sediment statuses of the watersheds during the current condition were analyzed and management practice scenarios were developed to simulate their impact in reducing sediment yield. Based on that grass filter strip scenario with FILTREW width of 1m (scenario 1) and 5m (scenario 2) and soil bund scenario of reduced SLSUBBSN (slope length) parameter to 10m (scenario 3) and 50% (scenario 4) of the watersheds were simulated. The other soil bund determining parameters of CN2 and USLE_P factor were installed to 59 and 0.32 by considering the local experiences. It is found that on average 30%, 48.7%, and 47%, 58.5 % sediment reduction were obtained with the implementation of grass filter strip scenarios 1 & 2 in Rib and Gumara respectively. The result showed that there is a significant decrease in sediment yield with the introduction of grass strips. There was a decrease in sediment yield by 77.9%, 76.6%, and 83.8 %, 81.5 % in soil bund scenarios 3 & 4 in Rib and Gumara respectively. Soil bund scenarios have a high capacity in reducing sediment than the grass strips. There was no significant difference between soil bund scenarios, so implementing soil bund scenario 4 provides a wider space (slope length) for practicing agricultural activities than scenario 3. The result showed that agricultural management practices especially soil bund scenarios significantly reduced sediment yield at the sub-watershed levels. The result indicated that a notable reduction of erosion and sediment could be obtained by implementing management practices in croplands in sub-watershed levels. This study provides fundamental information for decision-makers to prioritize areas of interventions.

5. Assessment of soil loss and sediment yield in Anjeb watershed

Important data inputs were analyzed to estimate soil loss, SDR, and sediment yield of the

Anjeb watershed. The RUSLE parameters of rainfall erosivity (R-factor), soil erodibility (K-factor), topography (LS-factor), cover management (C-factor) and the support practice (P-factor) were prepared and spatial soil loss was calculated in a GIS raster calculator. The slope of the channels was calculated using an ArcGIS extension and analysis tool, HEC-Geo HMS to analyze the SDR along the channels. The spatial sediment yield of the watershed was prepared by superimposing the spatial soil loss and the SDR layers of the watershed. The result revealed that the spatial data processing efficiency of GIS integrating with RUSLE is capable of quantifying soil loss, SDR, and sediment yield of the watershed. The soil loss ranges between 0 to 195 t $ha^{-1}yr^{-1}$ and the average annual soil loss was 17.3 t ha^{-1} yr^{-1}. A total of 13% of the watershed was under the severe and very severe erosion and located in the stepper slopes. The total annual soil loss of the watershed was estimated as 20125.5 t yr^{-1}. The SDR value ranges between 0.03–0.214. On average, the sediment delivery capacity is about 0.122 which indicated a mean of 12.2% of the eroded soil materials could be delivered to the channels and the remaining are trapped and deposit before getting into the channel networks. From a total of 20125.5 t yr^{-1} of eroded soil over the watershed 2254.5 t yr^{-1} of sediment has been deposited along the channels. The sediment yield at the point of the outlet was estimated 2012.5 t yr^{-1}.

6. Impact of LULC and climate change scenarios on hydrology and sediment yield in Rib and Gumara watersheds

With an input of the predicted LULC and climate scenario to the calibrated SWAT model, the hydrologic components and sediment yield of the watersheds were predicted. The impacts of predicted LULC and climate (combined impact) and base LULC and predicted climate on the hydrologic components of surface runoff, groundwater flow, lateral flow, total water yield, ET, and sediment yield of the watersheds were compared. The result showed that there will be a decrease in surface runoff in A1B and an increase in the RCPs in the predicted LULC and climate and base LULC and predicted climate scenarios in Rib. The increasing surface runoff is higher in the predicted LULC and climate than base LULC and predicted climate scenarios in the RCPs. There will be a general decrease in lateral flow, groundwater flow, and total water yield in A1B and RCP scenarios with the highest decrease in the A1B scenario. Lateral flow and groundwater flow will show a higher decrease in the predicted LULC and climate than the base LULC and predicted climate scenarios which will be attributed to the removal of the vegetation covers. Total WYLD will show a decreasing trend with small

variation between the predicted LULC and climate and the base LULC and predicted climate scenarios. There was an increasing trend in ET in A1B and RCP scenarios with a higher increase in the RCPs. Sediment yield will show an increase except for the 2060s and 2090s of the RCP2.6 and A1B scenarios. Significant decreases will occur in the A1B scenarios. Generally, sediment yield will show a higher increase in the predicted LULC and climate scenario in Rib.

In Gumara surface runoff will have a decreasing trend in A1B scenario simulations. Surface runoff will show some increase in the 2030s of the RCP8.5 and decrease in all other RCP scenarios and this might be due to the decreasing trend of precipitation. Surface runoff will not show much difference in the predicted LULC and climate and base LULC and predicted climate scenarios. Lateral flow and groundwater flow will show a decrease in A1B and RCP scenarios with a little higher value in the predicted LULC and climate than the base LULC and predicted climate scenarios. Generally, sediment yield will show an increase in the RCP scenarios with a higher increase in the predicted LULC and climate scenario in Gumara. This might be related to the expansion of cultivated lands. Reports from the Ethiopian Highlands indicated that the increase of sediment yield is attributed to an increase in crop cultivation. From this study, it is found that the changing LULC and climate have a significant impact on the hydrological response of the watersheds with a greater impact from the changing climate.

7. **Recommendation**

The study revealed that the watersheds have been affected by serious soil erosion (upstream) and sedimentation (downstream) mainly due to continual LULC change especially the expansion of croplands and loss of vegetative covers. The nature of the topography (large area cover of steep slopes), expansion of crop fields to steep slopes, a significant decrease in vegetation, and lack of soil conservation works are the fundamental factors of land degradation in the areas. The climate prediction has shown that there will be a decrease in precipitation and an increase in temperature that will alter the hydrological cycle and sediment conditions of the watersheds. Therefore, development programs (soil and water management activities) that will be conducted have to consider the existing and future LULC and climatic conditions of the areas. This study provides fundamental information for decision-makers to prioritize areas of intervention and to design short and long-term watershed level resource management activities depending on the changing land use and

climate conditions. The findings of the study reveal that filter strips with 5m width and soil/stone bunds having a slope length of 10m and 50% reduction showed a significant decrease in erosion and sediment yield, hence we recommend the local farmers and land managers implement these practices, especially in agricultural land use. Regional and local government authorities and landowners have to designed and implement afforestation and reforestation land management programs, especially in steep slopes to minimize land degradation and augment groundwater recharge. We also recommend agricultural research centers focus on producing crop varieties that will adapt to the changing climate for a better yield. To find out the best results, to better understand the present and cope with future conditions, further studies incorporating varieties of land use and climate prediction models need to be conducted. Lastly, we recommend that in watershed impact studies, researchers have to incorporate the LULC change scenarios in addition to the climate changes to acquire a comprehensive picture of the hydrologic response of watersheds.

References

Abbaspour, K.C., Rouholahnejad, E., Vaghefi, S., Srinivasan, R., Yang, H., Kløve, B. (2015). A continental-scale hydrology and water quality model for Europe: Calibration and uncertainty of a high-resolution large- scale SWAT model. *Journal of Hydrology*, 524, 733-752.

Abbaspour, K.C. et al., (2007). "Modelling Hydrology and Water Quality in the Pre Alpine/Alpine Thur Watershed Using SWAT". *Journal of Hydrology*, 333, 413-430.

Abdelwahab, O.M., Bingner, R.L., Milillo, F., Gentile, F. (2014). Effectiveness of alternative management scenarios on the sediment load in a Mediterranean agricultural watershed. *Journal of Agricultural Engineering*, 45(3), 125-136.

Abdo, K.S., Fiseha, B.M., Rientjes, T.H.M., Gieske, A.S.M., Haile, A. T. (2009). Assessment of climate change impacts on the hydrology of Gilgel Abay catchment in Lake Tana basin, Ethiopia. Hydrological Processes: *An International Journal*, 23(26), 3661-3669.

Abtew, W., Melesse, A.M. (2014). The Nile River Basin. In Melesse, A.M., Abtew W., Setegn S.G. (Eds.), Nile River Basin: Eco-hydrological Challenges, Climate Change and Hydro-politics, (pp. 7–21).

Addis, H.K., Strohmeier, S., Ziadat, F., Melaku, N.D., Klik, A. (2016). Modeling streamflow and sediment using SWAT in Ethiopian Highlands. *International Journal of Agricultural and Biological Engineering*, *9*(5), 51-66.

Agarwal, C. (2002). A review and assessment of land-use change models: dynamics of space, time, and human choice (Vol. 297). US Department of Agriculture, Forest Service, Northeastern Research Station.

Alemseged, T.H., Tom, R. (2015). Evaluation of regional climate model simulations of rainfall over the Upper Blue Nile basin. *Atmospheric research*, *161*, 57-64.

Amsalu, T., Mengaw, A. (2014). GIS based soil loss estimation using RUSLE model: the case of Jabitehinan woreda, ANRS, Ethiopia. *Natural Resources*, 5, 616-626.

Andréasson, J., Bergström, S., Carlsson, B., Graham, L. P., Lindström, G. (2004). Hydrological change–climate change impact simulations for Sweden. *AMBIO: A Journal of the Human Environment*, *33*(4), 228-235.

Arnold, J.G., Moriasi, D.N., Gassman, P.W., Abbaspour, K.C., White, M.J., Srinivasan, R., Kannan, N. (2012). SWAT: Model use, calibration, and validation. Transactions of the ASABE, 55(4), 1491-1508.

Arnold, J.G., Srinivasan, R., Muttiah, R.S., Williams, J. R. (1998). Large area hydrologic modeling and assessment part I: model development I. *Journal of the American Water Resources Association*, 34(1),73-89.

Arsanjani, J.J., Helbich, M., Kainz, W., Boloorani, A.D. (2013). Integration of logistic regression, Markov chain and cellular automata models to simulate urban expansion. *International* Journal *of Applied Earth Observation and Geoinformation*, 21265-275.

Awulachew, S.B., McCartney, M., Steenhuis, T.S., Ahmed, A.A. (2008). A review of hydrology, sediment and water resource use in the Blue Nile Basin. International Water Management Institute (IWMI), Colombo, Sri Lanka, p.81.

Ayele, G.T., Teshale, E.Z., Yu, B., Rutherfurd, I.D., Jeong, J. (2017). Streamflow and sediment yield prediction for watershed prioritization in the Upper Blue Nile River Basin, Ethiopia. *Water*, 9(10), 782.

Balthazar, V., Vanacker, V., Girma, A., Poesen, J., Golla, S. (2013). Human impact on sediment fluxes within the Blue Nile and Atbara River basins. *Geomorphology*,180, 231–241.

Ban, K. J., Yu, I., Jeong, A. (2016). Estimation of Soil Erosion Using RUSLE Model and GIS Techniques for Conservation Planning from Kulekhani Reservoir Catchment. *Journal of the Korean Society of Hazard Mitigation*,16(3),323-330.

Bates, B., Kundzewicz, Z., Wu, S. (2008). Climate change and water. Technical Paper Intergovernmental Panel on Climate Change IPCC Secretary: 210. doi: 10.1016/j.jmb.2010.08.039

Bauwens, A., Sohier, C., Degre´, A. (2011). Hydrological response to climate change in the Lesse and the Vesdre catchments: contribution of a physically based model (Wallonia, Belgium). *Hydrology and Earth System Sciences*, 15 (6), 1745–1756.

Bera A. (2017). Assessment of soil loss by universal soil loss equation (USLE) model using GIS techniques: a case study of Gumti River Basin, Tripura, India. *Modeling Earth Systems and Environmen*, 3(1), 29.

Beskow S., Mello C.R., Norton L.D., Cur N., Viola M.N., Avanzi J.C. (2009). Soil erosion prediction in the Grande River Basin, Brazil using distributed modeling. *Catena*, 79,49–59.

Beven, K., Binley, A. (1992). The future of distributed models: model calibration and uncertainty prediction, Hydrol. Process, 6, 279-298,

Bewket, W., Teferi, E. (2009). Assessment of soil erosion hazard and prioritization for treatment at the watershed level: case study in the Chemoga watershed, Blue Nile basin, Ethiopia. *Land Degradation and Development*, 20(6), 609-622.

Bicknell, B.R., Imhoff, J.C., Kittle, Jr, J.L., Jobes, T.H., Donigian, Jr, A.S. (2001). Hydrological Simulation Program– Fortran (HSPF): User's manual for release 12, U.S. Environment Protection Agency, Athens, Ga.

Bires, Z., Raj, S. (2019). Determinants of environmental conservation in Lake Tana Biosphere Reserve, Ethiopia. *Heliyon* 5(7) e01997.

BoEPLAU, (2015). Tana sub-basin integrated land use planning and environmental impact study project. Technical report: land use land cover and change detection. Bahir Dar, Ethiopia.

Boskidis, I., Gikas, G., Sylaios, G., Tsihruntzis, V.A. (2012). "Hydrologic and water quality modelling of lower Nestos river basin." *Water resources management*, 26(10), 3023-3051.

Bosshard, T., Kotlarski, S., Ewen, T., Schär, C. (2011). Spectral representation of the annual cycle in the climate change signal. *Hydrology and Earth System Sciences*, *15*(9), 2777-2788.

Bosshart, U., (1997). Catchment Discharge and Suspended Sediment Transport as Indicators of Physical Soil and Water Conservation in the Mayketin Catchment, Afdeyu Research Unit. A Case Study in the Northern Highlands of Eritrea. Bern, SCRP, Research Report 39, pp 137.

Boyer, C., Chaumont, D., Chartier, I., Roy, A.G. (2010). Impact of climate change on the hydrology of St. Lawrence tributaries. *Journal of hydrology*, 384(1-2), 65-83.

Bracmort, K.S., Arabi, M., Frankenberger, J.R., Engel, B.A., Arnold, J.G. (2006). Modeling long-term water quality impact of structural BMPs. *Transactions of the ASABE*, 49(2), 367-374.

Braimoh, A.K., Vlek, P.L.G. (2005). Land-cover change trajectories in Northern Ghana. *Environmental Management*, 36(3)**,**356-373.

Brands, S., Herrera, S., Fernández, J., & Gutiérrez, J. M. (2013). How well do CMIP5 Earth System Models simulate present climate conditions in Europe and Africa? *Climate dynamics*, *41*(3-4), 803-817.

Brhane, G., Mekonen, K. (2009). Estimating soil loss using Universal Soil Loss Equation (USLE) for soil conservation planning at Medego watershed, Northern Ethiopia. *Journal of American Science*, 5(1), 58-69.

Carter, T.R., Hulme, M., Lal, M. (1999). IPCC-TGCIA Guidelines on the use of scenario data for climate impact and adaptation assessment, version I. IPCC, Task Group on Scenarios for Impact Assessment.

Castella, J.C., Verburg, P.H. (2007). Combination of process-oriented and pattern-oriented models of land-use change in a mountain area of Vietnam. *Ecological modelling*, 202**,** 410-420.

Cebecauer, T., Hofierka, J. (2008). The consequences of land-cover changes on soil erosion distribution in Slovakia. G*eomorphology*, 98, 187–198.

Collier, P., Conway, G., Venables, T. (2008). Climate change and Africa. Oxford Review of Economic Policy, 24, 337–353.

Congalton, R.G., Green, K. (1999). Assessing the accuracy of remotely sensed data: principles and practices. Boca Raton: Lewis Publishers.

Conway, D., Schipper, E.L.F. (2011). Adaptation to climate change in Africa: Challenges and opportunities identified from Ethiopia. *Global Environmental Change*, 21(1), 227-237.

Conway, T.M., Lathrop, R.G.J. (2005). Modeling the ecological consequences of land-use policies in an urbanizing region. *Environmental Management*, 35:278-291.

Cowen. J. (1993). A proposed method for calculating the LS factor for the USLE in a grid-based environment: Proceedings of the thirteenth annual ESRI user conference, pp. 65 - 74.

CSA (2017). Projected population of Ethiopia. Addis Ababa, Ethiopia.

da Silva, R.M., Santos, C.A., Silva, A.M. (2014). Predicting soil erosion and sediment yield in the Tapacurá catchment, Brazil. *Journal of Urban and Environmental Engineering*, 8(1),75 82

Demissie, T.A., Saathof, F., Seleshi, Y., Gebissa, A. (2013). Evaluating the Effectiveness of Best Management Practices in Gilgel Gibe Basin Watershed-Ethiopia. *Journal of Civil Engineering and Architecture*, 7(10), 1240.

Desmet, P.J.J., Govers, G. (1996). A GIS procedure for automatically calculating the USLE LS factor on topographically complex landscape units. *Journal of soil and water conservation*, 51(5), 427-433.

Dessu, S.B., Melesse, A.M. (2012). "Modelling the rainfall-runoff process of the Mara River basin using the Soil and Water Assessment Tool." *Hydrological Processes*, 26 (26),4038-4049

Dibaba,W.T., Demissie, T.A., Miegel, K. (2020). Drivers and implications of land use/land cover dynamics in finchaa catchment, Northwestern Ethiopia. *Land*, 9, 113.

Dietzel, C., Clarke, K.C. (2007). Toward optimal calibration of the SLEUTH land use change model. *Transactions in GIS*, 11:29–45.

Dile, Y., Berndtsson, R., Setegn, S. (2013). "Hydrological Response to Climate Change for Gilgel Abay River, in the Lake Tana Basin - Upper Blue Nile Basin of Ethiopia." *PLoS ONE*, 8(10),12-17

Dissanayake, D.M.S.L.B., Morimoto, T., Ranagalage, M. (2019). Accessing the soil erosion rate based on RUSLE model for sustainable land use management: A case study of the Kotmale watershed, Sri Lanka. *Modelling Earth Systems and Environment*, 5(1):291-306

Diyabalanage, S., Samarakoon, K.K., Adikari, S.B., Hewawasam, T. (2017). Impact of soil and water conservation measures on soil erosion rate and sediment yields in a tropical watershed in the Central Highlands of Sri Lanka. *Applied Geography*, 79,103–114.

Duan, Z., Xianfeng, S.,Liu, J. (2009). Application of SWAT for sediment yield estimation in a mountainous agricultural basin. In International Conference on Geoinformatics, pp.1-5. IEEE.

Easton, Z.M., Fuka, D.R., White, E.D., Collick, A.S., Biruk, Ashagre, B., McCartney, M., Awulachew, S.B., Ahmed, A.A., Steenhuis, T.S. (2010). A multi basin SWAT model analysis of runoff and sedimentation in the Blue Nile, Ethiopia. *Hydrology and Earth System Sciences*, 14(10), 1827–1841.

Elirehema, Y. (2001). Soil water erosion modeling in selected watersheds in Southern Spain. Enschede, IFA, ITC.

El-Swaify, S. A., Hurni, H. (1996). Transboundary effects of soil erosion and conservation in the Nile basin. Basin. New Delhi, Oxford and IBH Pub. Land Husbandry, 1(1-2), 7-21.

Endris, H.S., Lennard, C., Hewitson, B., Dosio, A., Nikulin, G., Panitz, H.J. (2016). Teleconnection responses in multi-GCM driven CORDEX RCMs over Eastern Africa. *Climate dynamics*, *46*(9-10), 2821-2846.

ENMA (2007). Climate Change National Adaptation Programme of Action (NAPA) of Ethiopia. p 1–73.

Erdoğan, N., Nurlu, E., Erdem, Ü. (2011). Modelling land use changes in Karaburun by using CLUE-s. *A|Z ITU Journal of the Faculty of Architecture*, 8(2), 91-102.

FAO (2015). Global soil status, processes and trends. Status of the World's Soil Resources (SWSR)—Main Report of the Food and Agriculture Organization, New York, United Nations.

FAO (1998). "Digital Soil Map of the World (DSMW)." http://www.fao.org/soils-portal/soil-survey/soil-maps-nd-databases/faounesco-soil-map-of-the world/en/. Accessed 15 April 2019.

FAO (1984). Ethiopian Highland Reclamation Study (EHRS); Final Report; FAO: Rome, Italy, Volume 1, pp. 37–46.

Faramarzi, M., Abbaspour, K.C., Vaghefi, S.A., Farzaneh, M.R., Zehnder, A.J., Srinivasan, R.,Yang, H. (2013). Modeling impacts of climate change on freshwater availability in Africa. *Journal of Hydrology*, 480:85–101.

Funk, C., Senay, G., Asfaw, A., Verdin, J., Rowland, J., Michaelsen, J., Eilerts, G., Korecha, D., Choularton, R. (2005). Recent drought tendencies in Ethiopia and equatorial-subtropical eastern Africa. FEWS Report 1: 13.

Garzanti, E., Andò, S., Vezzoli, G., Megid, A.A.A., El Kammar, A. (2006). Petrology of Nile River sands (Ethiopia and Sudan): sediment budgets and erosion patterns. *Earth and Planetary Science Letters*, 252: 327–341.

Gbobaniyi, E., Sarr, A., Sylla, M.B., Diallo, I., Lennard, C., Dosio, A., Dhiédiou, A., Kamga, A., Klutse, N.A.B., Hewitson, B., Nikulin, G., Lamptey, B. (2014). Climatology, annual cycle and interannual variability of precipitation and temperature in CORDEX simulations over West Africa. *International Journal of Climatology*, 34:2241–2257.

Gebreegziabher, T., Nyssen, J., Govaerts, B., Getnet, F., Behailu, M., Haile, M., Deckers, J. (2008). Contour furrows for in situ soil and water conservation, Tigray, northern Ethiopia. *Soil & Tillage Research*, 103: 257–264.

Gebrehiwot, S.G., Bewket, W., Gärdenäs, A.I., Bishop, K. (2014). Forest cover change over four decades in the Blue Nile Basin, Ethiopia: comparison of three watersheds. *Regional Environmental Change*, 14: 253–266.

Gebremichael, D., Nyssen, J., Poesen, J., Deckers, J., Haile, M., Govers, G., Moeyersons, J. (2005). Effectiveness of stone bunds in controlling soil erosion on cropland in the Tigray Highlands, northern Ethiopia. *Soil Use and Management*, 21(3), 287-297

Gelagay, H.S. (2016). RUSLE and SDR Model Based Sediment Yield Assessment in a GIS and Remote Sensing Environment; A Case Study of Koga Watershed, Upper Blue Nile Basin, Ethiopia. *Hydrology: Current Research*, 7, 239.

Gelagay, H.S., Minale, A.S. (2016). Soil loss estimation using GIS and Remote sensing techniques: A case of Koga watershed, North-western Ethiopia. *International Soil and Water Conservation Research*, 4(2),126-136.

Gete., Z, Hurni, H. (2001) Implications of Land Use and Land Cover Dynamics for Mountain Resource Degradation in the Northwestern Ethiopian Highlands. *Journal of Mountain Research and Development* 21: 184-191.

Glysson, G.D. (1987). "Sediment-transport curves." No. 87-218. US Geological Survey, Reston VA.

González-Bonorino, G., Osterkamp, W.R., Colombo, Piñol, F. (2003). An averaging procedure for applying the Revised Universal Soil Loss Equation (RUSLE) to disturbed mountain watersheds. G*eogaceta*, 33: 43-46.

Graham, L.P., Andréasson, J., Carlsson, B. (2007). Assessing climate change impacts on hydrology from an ensemble of regional climate models, model scales and linking methods–a case study on the Lule River basin. *Climatic Change*, 81(1), 293-307.

Green, W.H., Ampt, G.A. (1911). Studies in soil physics. Part I. The flow of air and water through soils. *Journal of Agricultural Science*, 4:1–24.

Grunblatt, J., Ottichilo, W.K., Sinange, R.K. (1992). A GIS approach to desertification assessment and mapping. *Journal of Arid Environments*, 23(1): 81-102.

Guan, D., Li, H., Inohae, T., Su, W., Nagaie, T., Hokao, K. (2011). Modeling urban land use change by the integration of cellular automaton and Markov model. *Ecological Modelling*, 222, 3761–3772.

Gupta, H.V., Sorooshian, S., Yapo, P.O. (1999). "Status of automatic calibration for hydrologic models: Comparison with multilevel expert calibration." *Journal of hydrologic engineering*, 4, 16054.

Gyamfi, C., Ndambuki, J.M., Salim, R.W. (2016). Hydrological responses to land use/cover changes in the Olifants Basin, South Africa. *Water*, 8, 588.

Hagen, A. (2003). Fuzzy set approach to assessing similarity of categorical maps. *International Journal of Geographical Information Science*, 17:235-49.

Hansen, J., Ruedy, R., Sato, M., Lo, K. (2010). Global surface temperature change. Reviews in Geophysics, 48, RG4004.

Haregeweyn, N., Tsunekawa, A., Nyssen, J., Poesen, J., Tsubo, M., Meshesha, D.T., Tegegne, F. (2015). "Soil erosion and conservation in Ethiopia: a review." *Progress in Physical Geography*, 39(6), 750-774.

Haregeweyn, N., Meshesha, D.T., Tsunekawa, A., Tsubo, M. (2012). Dynamics and hotspots of soil erosion and management scenarios of the Central Rift Valley of Ethiopia**.** *International Journal of Sediments Research*, 27, 84-99

Haregeweyn, N., Poesen, J., Nyssen, J., De Wit, J., Haile, M., Govers, G., Deckers, S. (2006). Reservoirs in Tigray (Northern Ethiopia): characteristics and sediment deposition problems. *Land Degradation & Development*, 17(2), 211-230.

Hattermann, F.F. (2011). Re-Thinking Water Storage in Subsaharan Africa, report on generation of regional climate scenarios.

Helldén, U. (1987). An assessment of woody biomass, community forests, land use and soil erosion in Ethiopia. A feasibility study on the use of remote sensing and GIS analysis for planning purposes in developing countries. Lund University.

Hengsdijk, H., Meijerink, G.W., Mosugu, M.E. (2005). Modeling the effect of three soil and water conservation practices in Tigray, Ethiopia. *Agriculture, Ecosystems & Environment*. 105: 29-40.

Herweg, K., Ludi, E. (1999). The performance of selected soil and water conservation measures—case studies from Ethiopia and Eritrea. *Catena*, 36(1-2), 99-114

Hewitson, B.C., Daron, J., Crane, R.G., Zermoglio, M.F., Jack, C. (2014). Interrogating empirical-statistical downscaling. *Climatic change*, *122*(4), 539-554.

Hewitt, R., Escobar, F. (2011). The territorial dynamics of fast-growing regions: Unsustainable land use change and future policy challenges in Madrid, Spain. *Applied Geography*, 31:650-667.

Houessou, L.G., Teka, O., Imorou, I.T., Lykke, A.M., and Sinsin, B. (2013). Land Use and Land-Cover Change at "W" Biosphere Reserve and Its Surroundings Areas in Benin Republic (West Africa). *Environment and Natural Resources Research*, 3(2):87-101.

Hua, L., He X., Yuan, Y., Nan, H. (2012). Assessment of runoff and sediment yields using the AnnAGNPS model in a three-gorge watershed of China. *International Journal of Environmental Research and Public Health*, 9 (5): 1887-1907.

Hulme, M., Carter, T.R. (1999). Representing uncertainty in climate change scenarios and impact studies, 11- 37. In Carter, T.R., Hulme, M., Viner, D (eds.), Representing uncertainty in climate change scenarios and impact studies - ECLAT-2 Workshop Report, Climatic Research Unit, Norwich, UK.

Hurni, K., Zeleke, G., Kassie, M., Tegegne, B., Kassawmar, T., Teferi, E., Moges, A., Tadesse, D., Ahmed, M., Degu, Y., Kebebew, Z., Hodel, E., Amdihun, A., Mekuriaw, A., Debele, B., Deichert, G., Hurni, H. (2015). Soil degradation and sustainable land management in the rainfed agricultural areas of Ethiopia: An assessment of the economic implications. Water and Land Resource Centre, Ethiopia and University of Bern, Switzerland

Hurni, H., Tato, K., Zeleke, G. (2005). The implications of changes in population, land use, and land management for surface runoff in the upper Nile Basin Area of Ethiopia. *Mountain Research and Development*, 25, 147–154.

Hurni, H. (1989). "Soil for the Future." Environmental Research for Development Cooperation. Uni Press, University of Berne, Berne, pp. 42-46.

Hurni, H. (1985). "Soil Conservation Manual for Ethiopia." Field Guide for Conservation Implementation; Ministry of Agriculture: Addis Ababa, Ethiopia.

IPCC (2001). Climate Change 2001: Synthesis Report. A Contribution of Working Groups I, II, and III to the Third Assessment Report of the Intergovernmental Panel on Climate Change, Watson, R.T. and the Core Writing Team (eds.). Cambridge University Press, Cambridge, United Kingdom, and New York, NY, USA, 398 pp.

IPCC (2014). Climate Change 2014: Synthesis Report. Contribution of Working Groups I, II and III to the Fifth Assessment Report of the Intergovernmental Panel on Climate Change Pachauri, R.K., Meyer, L.A. (eds.). IPCC, Geneva, Switzerland, 151 pp.

IPCC (2007). Climate Change 2007: Synthesis Report. Contribution of Working Groups I, II and III to the Fourth Assessment Report of the Intergovernmental Panel on Climate Change. Pachauri, R.K., Reisinger, A. (eds.). IPCC, Geneva, Switzerland, 104 pp.

Irwin, E.G., Geoghegan, J. (2001). Theory, data, methods: developing spatially explicit economic models of land use change. *Agriculture, Ecosystems & Environment*, 85(1–3):7–24

Ito, A. (2007). Simulated impacts of climate and land-cover change on soil erosion and implication for the carbon cycle, 1901 to 2100. *Geophysical Research Letters*, 34, L09403.

Jain, S.K., Kumar, S., Varghese, J. (2001). Estimation of soil erosion for a Himalayan watershed using GIS technique. *Water Resources Management*, *15*(1), 41-54.

James, L.D., Burges, S.J. (1982). Selection, calibration, and testing of hydrologic models. In: Haan, C.T., Johnson, H.P., Brakensiek, D.L.(Eds) Hydrologic modeling of Small Watersheds. American Society of Agricultural and Biological Engineers. St. Joseph, Mich, pp.437-472

Jemberu, W., Baartman, J.E., Fleskens, L., Ritsema, C.J. (2018). Participatory assessment of soil erosion severity and performance of mitigation measures using stakeholder workshops in Koga catchment, Ethiopia. *Journal of environmental management*, *207*, 230-242.

Jordan, G., van Rompaey, A., Szilassi, P., Csillag, G., Mannaerts, C., Woldai, T. (2005). Historical land use changes and their impact on sediment fluxes in the Balaton basin (Hungary). *Agriculture Ecosystems and Environment*, 108, 119–133.

Kamaludin, H., Lihan, T., Rahman, Z.A., Mustapha, M.A., Idris, W.M.R., Rahim, S.A. (2013). Integration of remote sensing, RUSLE and GIS to model potential soil loss and sediment yield. *Hydrology and Earth System Sciences*, 10, 4567–4596.

Kassa, T. (2009). Watershed Hydrological Responses to Changes in Land Use and Land Cover, and Management Practices at Hare Watershed, Ethiopia. Doctoral Dissertation, University of Siegen, Research Institute for water and Environment, Siegen, Germany.

Kassa, T., Foerch, G. (2007). Impacts of Land use/cover dynamics on streamflow: The case of Hare watershed, Ethiopia. In the proceedings of the 4th International SWAT2005 Conference, Delft, The Netherlands, 4–6 July.

Kassawmar, T., Gessesse, G. D., Zeleke, G., Subhatu, A. (2018). Assessing the soil erosion control efficiency of land management practices implemented through free community labor mobilization in Ethiopia. *International Soil and Water Conservation Research*, *6*(2), 87–98.

Kebede, S., Travi, Y., Alemayehu, T., Marc, V. (2006). Water balance of Lake Tana and its sensitivity to fluctuations in rainfall, Blue Nile basin, Ethiopia. *Journal of hydrology*, 316(1-4), 233-247.

Kennedy, J., Eberhart, R. (1995). Particle swarm optimization. In Proceedings of ICNN'95-International Conference on Neural Networks (Vol. 4, pp. 1942-1948). IEEE.

Kim, H.S. (2006). Soil erosion modeling using RUSLE and GIS on the Imha watershed, South Korea. Dissertation, Colorado State University.

Knisel, W.G. (1980). CREAMS: A Field-Scale Model for Chemicals, Runoff and Erosion for Agricultural Management Systems. US Department of Agriculture, Conservation Research Report 26.

Kotlarski, S., Keuler, K., Christensen, O.B., Colette, A., Déqué, M., Gobiet, A., Goergen, K., Jacob, D., Lüthi, D., van Meijgaard, E., et al. (2014**).** Regional climate modeling on European scales: A joint standard evaluation of the EURO CORDEX RCM ensemble. *Geoscientific Model Development*, 7, 1297–1333.

Lambin, E.F., Rounsevell, M.D.A., Geist, H.J. (2000). Are agricultural land use models able to predict changes in land-use intensity? *Agriculture, Ecosystems & Environment*, 82:321–331

Lambin, E.F. (1997). Modelling and monitoring land-cover change processes in tropical regions. *Progress in Physical Geography*, 21, 375e393.

Landis, J.R., Koch, G.G. (1977). The measurement of observer agreement for categorical data. *Biometrics*, 33(1)**,**159-174.

Legates, D.R., McCabe, G.J. (1999**). "**Evaluating the use of "goodness-of-fit" measures in hydrologic and hydroclimatic model validation." *Water Resources Research*, 35(10), 233-241.

Lillesand, T.M., Kiefer, R.M. (2004). Remote Sensing and Image Interpretation (Fifth Edition). *Geographical Journal*, 146 (3).

Lima, M.L., Romanelli, A., Massone, H.E. (2015). Assessing groundwater pollution hazard changes under different socio-economic and environmental scenarios in an agricultural watershed. *Science of the Total Environment*, 530:333–346.

Li, W., Wu, C., Zang, S. (2014). Modeling urban land use conversion of Daqing City, China: a comparative analysis of ''top-down'' and ''bottom-up'' approaches. *Stochastic Environmental Research and Risk Assessment*, 28(4):817–828

Li, Y., Chen, B.M., Wang, Z.G., Peng, S.L. (2011). Effects of temperature change on water discharge, and sediment and nutrient loading in the lower Pearl River basin based on SWAT modeling, Hydrological Science Journal, 56, 68–83.

Li, Z., Liu, W Z., Zhang, X.C., Zheng, F.L. (2009). Impacts of land use change and climate variability on hydrology in an agricultural catchment on the Loess Plateau of China. *Journal of Hydrology*, 377, 35–42.

Lin, P.Y., Nien-Ming Hong, N.M., Pei-Jung, Wu, P.J., Lin, C.J. (2007). Modeling and assessing land-use and hydrological processes to future land-use and climate change scenarios in watershed land-use planning. *Environmental Geology*, 53:623–634.

Lioubimtseva E. (2005). Environmental changes in arid Central Asia inferred from remote sensing data and ground observations. *Arid Ecosystems*, 11(26–27):64–72.

Loukas, A., Sidiropoulos, P., Mylopoulos, N. (2015). Assessment of the effect of climate variability and change and human intervention in the lake Karla aquifer. *European Water*, 49:19–31

Lu, H., Moran, C.J., Prosser, I.P. (2006). Modelling sediment delivery ratio over the Murray Darling Basin. *Environmental Modelling & Software*, 21, 1297-1308

Luck, M., Landis, M., Gassert, F. (2015). Aqueduct Water Stress Projections: Decadal Projectons of Water Supply and Demand Using CMP5 GCMs; Technical Note; World Resources Institute: Washington, DC, USA, pp. 1–20

Luo, M., Liu, T., Meng, F., Duan, Y., Frankl, A., Bao, A., De Maeyer, P. (2018). Comparing Bias Correction Methods Used in Downscaling Precipitation and Temperature from Regional Climate Models: A Case Study from the Kaidu River Basin in Western China. *Water*, 10, 1046.

Maidment, D.R. (1993). Handbook of hydrology. New York: McGraw-Hill. V. 9780070, p. 397323.

Mandrekar, J. N. (2010). Receiver operating characteristic curve in diagnostic test assessment. *Journal of Thoracic Oncology*, 5, 1315-1316.

Mango, L., Melesse, A., McClain, M.E., Gann, D., Setegn, S.G. (2011). "Land use and climate change impacts on the hydrology of the upper Mara River Basin, Kenya: results of a modelling study to support better resource management." *Hydrology and Earth System Sciences*, 15(7), 2245–2258.

Mantel, S., Van Engelen, V.W.P. (1999). Assessment of the impact of water erosion on productivity of maize in Kenya: an integrated modelling approach. *Land Degradation and Development*, 10(6): 577-592.

Mekonnen, M., Keesstra, S. D., Ritsema, C. J., Stroosnijder, L., Baartman, J. E. (2016). Sediment trapping with indigenous grass species showing differences in plant traits in northwest Ethiopia. *Catena*, *147*, 755-763.

Melaku, N.D., Renschler, C.S., Flagler, J., Bayu, W., Klik, A. (2018). Integrated impact assessment of soil and water conservation structures on runoff and sediment yield through measurements and modeling in the Northern Ethiopian highlands. *Catena*, *169*, 140-150.

Middelkoop, H., Daamen, K., Gellens, D., Grabs, W., Kwadijk, J. C., Lang, H., Wilke, K. (2001). Impact of climate change on hydrological regimes and water resources management in the Rhine basin. *Climatic change*, 49(1-2), 105-128.

Miller, T., Peterson, J., Lenhart, C., Nomura, Y. (2012). The Agricultural BMP Handbook for Minnesota.

Millington, J. D. A., Perry, G. L. W., Romero-Calcerrada, R. (2007). Regression Techniques for Examining Land Use/Cover Change: A Case Study of a Mediterranean Landscape. Ecosystems, Vol. 10, No. 4, p. 562–578.

Moore, K., Pierson, D., Pettersson, K., Schneiderman, E., Samuelsson, P. (2007). Effects of warmer world scenarios on hydrologic inputs to Lake Mälaren, Sweden and implications for nutrient loads. In European Large Lakes Ecosystem changes and their ecological and socioeconomic impacts (pp. 191-199). Springer, Dordrecht.

Morgan, R.P.C. (2005). Soil Erosion and Conservation, 3rd edition, Blackwell, USA

Morgan, R.P.C., Quinton, J.N., Smith, R.E., Govers, G., Poesen, J.W.A., Auerswald, K., Chisci, G., Torri, D., Styczen, M.E. (1998). The European Soil Erosion Model (EUROSEM): a Dynamic Approach for Predicting Sediment Transport from fields and small catchments. *Earth Surface Processes and Landforms*, 23, 527–544.

Morgan, R.P.C. (1995). Soil erosion and conservation. Longman, London.

Moriasi, D.N., Arnold, J.G., Van Liew, M.W., Bingner, R.L., Harmel, R.D., Veitch, T.L. (2007). "Model evaluation guidelines for systematic quantification of accuracy in watershed simulations." *Transactions of the ASABE*, 50 (3), 885–900.

MoWR (1998). "Abbay river basin integrated development master plan project. Phase 2: Data collection—site investigation survey and analysis".

Mullan, D., Favis-Mortlock, D., Fealy, R. (2012). Addressing key limitations associated with medelling soil erosion under the impacts of future climate change. *Agricultural and Forest Meteorology*, 156, 18–30.

Munsell Color (1994). Munsell Soil Color Charts. Macbeth Division of Kollmorgen Instruments Corporation, New Windsor, USA.

Murphy, J. (1999). 'An Evaluation of Statistical and Dynamical Techniques for Downscaling Local Climate, Journal of Climate, 12, 2256–2284.

Murray-Rust, D., Brown, C., van Vliet, J., Alam, S.J., Robinson, D.T., Verburg, P.H., Rounsevell, M. (2014). Combining agent functional types, capitals and services to model land use dynamics. *Environmental Modelling & Software*, 59,187-201.

Mutua, B.M., Klik, A. (2006). Estimating Spatial Sediment Delivery Ratio on a Large Rural Catchment. *Journal of Spatial Hydrology*, 6(1), 64-80.

Nadew, B., Chaniyalew, E., Tsegaye, T. (2018). Runoff Sediment Yield Modeling and Development of Management Intervention Scenarios, Case Study of Guder Watershed, Blue Nile Basin, Ethiopia. *Hydrology of Current Research*, 9, 306.

National Planning Commission (2015). Growth and transformation plan II (GTP II) (2015/16-2019/20). Addis Ababa, Ethiopia.

Nearing, M.A., Jetten, V., Baffaut, C., Cerdan, O., Couturier, A., Hernandez, M., Le Bissonnais, Y., Nichols, M.H., Nunes, J.P., Renschler, C.S., Souchère, V., van Oost, K. (2005). Modeling response of soil erosion and runoff to changes in precipitation and cover. *Catena*, 61, 131–154.

Nearing, M.A., Foster, G.R., Lane, L.J., Finkner, S.C. (1989). A process based soil erosion model for USDA water erosion prediction project technology. *American Society of Agricultural and Biological Engineers*, St. Joseph, Michigan.

Neitsch, S.L., Arnold, J.G., Kiniry, J.R., Williams, J.R. (2011). SWAT Theoretical documentation version 2009. Texas Water Resources Institute Technical Report. A and M University system, Texas, USA.

Neitsch, S.L., Arnold, J.G., Kiniry, J.R., Williams, J.R. (2005). Soil and water assessment tool theoretical documentation version 2005. Grassland, Soil and Water Research Laboratory; Agricultural Research Service 808 East Blackland Road; Temple, Texas 76502; USA.

New, M., Hewitson, B., Stephenson, D.B. (2006). Evidence of trends in daily climate extremes over southern and West Africa. *Journal of Geophysical Research: Atmospheres*, 111, –11.

Nie, W.M., Yuan, Y.P., Kepner, W., Nash, M.S., Jackson, M., Erickson, C. (2011). Assessing impacts of landuse changes on hydrology for the upper San Pedro watershed. *Journal of Hydrology*, 407, 105–114.

Nigussie, Z., Tsunekawa, A., Haregeweyn, N., Adgo, E., Nohmi, M., Tsubo, M., Abele, S. (2017). Factors affecting small-scale farmers' land allocation and tree density decisions in an acacia decurrens-based taungya system in Fagita Lekoma District, North-Western Ethiopia. *Small-scale Forestry*, 16(2), 219-233.

Nikulin, G., Jones, C., Giorgi, F., Asrar, G., Büchner, M., Cerezo-Mota, R., van Meijgaard, E. (2012). Precipitation climatology in an ensemble of CORDEX-Africa regional climate simulations. *Journal of Climate*, 25(18), 6057-6078.

Nunes, J.P., Seixa, J., Keizer, J.J. (2013). Modeling the response of within-storm runoff and erosion dynamics to climate change in two Metiterranean watersheds: a multimodel, multi-scale approach to scenario design and analyses. *Catena*, 102, 27–39.

Nyenje, P.M., Batelaan, O. (2009), "Estimating the effects of climate change on groundwater recharge and base flow in the upper Ssezibwa catchment, Uganda". *Hydrological Sciences Journal*, 54 (4), 713-726

Nyssen, J., Poesen, J., Gebremichael, D., Vancampenhout, K., D'aes, M., Yihdego, G., Deckers, J. (2007). Interdisciplinary on-site evaluation of stone bunds to control soil erosion on cropland in Northern Ethiopia. *Soil and Tillage Research*, 94(1), 151–163.

Onyando, J.O., Kisoyan, P., Chemelil, M.C. (2005). Estimation of potential soil erosion for river perkerra catchment in Kenya. *Water Resource Management*, 19(2),133-143.

Pandey, A., Himanshu, S.K., Mishra, S.K., Singh, V.P. (2016). Physically based soil erosion and sediment yield models revisited. *Catena*, 147, 595–620.

Pandey, A., Chowdary, V.M., Mal, B.C. (2007). Identification of critical erosion prone areas in the small agricultural watershed using USLE, GIS and remote sensing. Water Resource Management, 21(4):729–746.

Panitz, H.J., Dosio, A., Büchner, M., Lüthi, D., Keuler, K. (2014). COSMO-CLM (CCLM) climate simulations over CORDEXAfrica domain: analysis of the ERA-interim driven simulations at 0.44° and 0.22° resolution. *Climate Dynamics*, 42:3015–3038.

Pilesjoe, P. (1992). "GIS and remote sensing for soil erosion studies in semi-arid environments estimation of soil erosion parameters at different scales." University of Lund, Lude.

Pontius, Jr.G.R., Schneider, C.L. (2001). Land-cover change model validation by an ROC method for the Ipswich watershed, Massachusetts, USA. *Agriculture, Ecosystems & Environment*, 85, 239–248.

Pontius, Jr.R.G. (2000). Quantification error versus location error in comparison of categorical maps. *Photogrammetric Engineering & Remote Sensing*, 66, 1011–1016.

Preuschmann, S. (2012). Regional surface albedo characteristics-analysis of albedo data and application to land-cover changes for a regional climate model (Doctoral dissertation, Hamburg University Hamburg).

Raes, D., Kafiriti, E.M., Wellens, J., Deckers, J., Maertens, A., Mugogo, S., Dondeyne, K., Descheemaeker, K. (2007). Can soil bunds increase the production of rain-fed lowland rice in south eastern Tanzania? *Agricultural Water Management*, 89: 229–235.

Ramaswamy, V. et al. (2001). Radiative forcing of climate change. In: Climate Change 2001: The Scientific Basis. Contribution of Working Group I to the Third Assessment Report of the Intergovernmental Panel on Climate Change, Houghton, J.T., et al. (eds.). Cambridge University Press, Cambridge, United Kingdom and New York, NY, USA, pp. 349–416.

Rawat, J.S., Kumar, M. (2015). Monitoring land use/cover change using remote sensing and GIS techniques: a case study of Hawalbagh block, district Almora, Uttarakhand, India. *Egyptian Journal of Remote Sensing and Space Sciences*, 18(1), 77–84.

Renard, K.G., Foster, G.R., Weesies, G.A., McCool, D.K., Yoder, D.C. (1997). Predicting rainfall erosion losses: a guide to conservation planning with the revised universal soil loss equation (RUSLE) US. Department of Agriculture, Agricultural Handbook 703, Washington, DC, p 404

Renard, K.G., Foster, G.R., Weesies, G.A., Porter, J.P. (1991). RUSLE: Revised universal soil loss equation. *Journal of soil and Water Conservation*, 46(1), 30-33.

Renfro, W.G. (1975). Use of erosion equation and sediment delivery ratios for predicting sediment yield. In: Present and Prospective Technology for Predicting Sediment Yields and Sources. US Dept. Agric, Publ. ARS-S-40, 33-45.

Riahi, K., Rao, S., Krey, V., Cho, C., Chirkov, V., Fischer, G., Kindermann, G., Nakicenovic, N., Rafaj, P. (2011). RCP 8.5 a scenario of comparatively high greenhouse gas emissions. *Climate Change*, 109,33 57.

Richards, K. (1993). Sediment delivery and the drainage network. In: Beven K, Kirkby M.J (eds) Channel Network Hydrology. John Wiley, New York, USA, pp 221-254

Rientjes, T.H., Haile, A.T., Kebede, E., Mannaerts, C.M., Habib, E., Steenhuis, T.S. (2011). Changes in land cover, rainfall and stream flow in Upper Gilgel Abbay catchment, Blue Nile basin-Ethiopia. Hydrology and Earth System Sciences, 15:1979–1989.

Roeckner, E., Arpe, K., Bengtsson, L., Christoph, M., Claussen, M., Dümenil, L., Schulzweida, U. (1996). The atmospheric general circulation model ECHAM-4: Model description and simulation of present-day climate.

Römkens, M.J.M., Helming, K., Prasad, S.N. (2002). Soil erosion under different rainfall intensities, surface roughness, and soil water regimes. *Catena*, 46(2–3), 103–123.

Ruelland, D., Levavasseur, F., Tribotte, A. (2010). Patterns and dynamics of land cover changes since the 1960s over three experimental areas in Mali. *International Journal of Applied Earth Observation and Geoinformation*, 12, 11e17.

Rykiel, E.J. (1996). Testing ecological models: the meaning of validation. *Ecological Modelling*, 90(3), 229-244.

Sahin, V., Hall, M.J. (1996). The effects of afforestation and deforestation on water yields. *Journal of Hydrology*, 178, 293–309.

Santhi, C., Srinivasan, R., Arnold, J.G., Williams, J.R. (2006). A modeling approach to evaluate the impacts of water quality management plans implemented in a watershed in Texas. *Environmental Modelling Software*, 21(8), 1141-1157.

Schaldach, R., Priess, J. A. (2008). Integrated models of the land system: a review of modelling approaches on the regional to global scale. *Living Reviews in Landscape Research*, 2(1), 1863e7329.

Schmidli, J., Goodess, C.M., Frei, C., Haylock, M.R., Hundecha, Y., Ribalaygua, J., Schmith, T. (2007). Statistical and dynamical downscaling of precipitation: An evaluation and comparison of scenarios for the European Alps. *Journal of Geophysical Research Atmosphers*, 112, 1–20.

Schwierz, C., Davies, H. C., Appenzeller, C., Liniger, M. A., Müller, W., Stocker, T. F., & Yoshimori, M. (2006). Challenges posed by and approach to the study of seasonal-to-decadal climate variability. *Climate chang*e, 79:31–63.

SCS (1972). "National engineering handbook, section 4, Hydrology.

Sefelnasr A. (2013) Hotspot delineation in the Eastern Nile, Abbay/Blue Nile Basin, as a criterion for the optimal risk assessment and watershed management of the basin. In Proceedings of Basic and Applied Sciences. Hurghada, Egypt, pp. 493–505

Setegn, S.G., Rayner, D., Melesse, A.M., Dargahi, B., Srinivasan, R. (2011). Impact of climate change on the hydroclimatology of Lake Tana Basin, Ethiopia. Water Resource Research, 47, W04511.

Setegn, S.G., Dargahi, B., Srinivasan, R., Melesse, A.M. (2010). Modeling of sediment yield from Anjeni-gauged watershed, Ethiopia using swat model. *Journal of the American Water Resources Association*, 46(3), 514-526.

Shabalova, M.V., Van Deursen, W.P.A., Buishand, T.A. (2003). Assessing future discharge of the river Rhine using regional climate model integrations and a hydrological model. *Climate research*, 23(3), 233-246.

Shawul, A.A., Chakma, S., Melesse, A.M. (2019). The response of water balance components to land cover change based on hydrologic modeling and partial least squares regression (PLSR) analysis in the Upper Awash Basin. *Journal of Hydrology: Regional Studies*, 26, 1–19.

Shawul, A.A., Alamirew, T., Melesse, A.M., Chakma, S. (2016). Climate change impact on the hydrology of Weyib River watershed, bale mountainous area, Ethiopia. In: Landscape Dynamics, Soils and Hydrological Processes in Varied Climates. Springer International Publishing, p 587-613.

Shiferaw, B., Holden, S. (2001). Farm-level benefits to investments for mitigating land degradation: empirical evidence from Ethiopia. *Environment and Development Economics*, 6, 335–358.

Shiferaw, B., Holden, S. (1999). Soil erosion and smallholders' conservation decisions in the highlands of Ethiopia. *World Development*, 27: 739–752.

Shinde, V., Sharma, A., Tiwari, K.N., Singh, M. (2011). Quantitative determination of soil erosion and prioritization of micro-watersheds using remote sensing and GIS. *Journal of Indian Society of Remote Sensing*, 39(2): 181-192.

Shrestha, S., Htut, A.Y. (2016). Modelling the potential impacts of climate change on hydrology of the Bago River Basin, Myanmar. *International Journal of River Basin Management*, 14, 287–297.

Simms, A.D., Woodroffe, C.D., Jones, B.G., (2003). Application of RUSLE for erosion management in a coastal catchment, southern NSW, In Proceedings of MODSIM 2003: International Congress on Modelling and Simulation, volume 2, Integrative Modelling of Biophysical, Social and Economic Systems for Resource Managment Solutions, Townsville, Queensland, 14-17 July 2003, 678-683.

Singh, G., Panda, R.K. (2017). Grid-cell based assessment of soil erosion potential for identification of critical erosion prone areas using USLE, GIS and remote sensing: A case study in the Kapgari watershed, India. *International Soil and Water Conservation Research*, 5(3), 202-211.

Siyuan, W., Jingshi, L., Cunjian, Y. (2007). Temporal change in the landscape erosion pattern in the Yellow River Basin, China. *International Journal of Geographical Information Science*, 21, 1077–1092.

Sohl, T.L., Sayler, K.L., Drummond, M.A., Loveland, T.R. (2007). The FORE-SCE model: a practical approach for projecting land cover change using scenario-based modeling. *Journal of Land Use Science*, 2:103–126.

Solomon, S., Qin, D., Manning, M., Averyt, K., Marquis, M. (2007). Climate Change 2007: The Physical Science Basis. Contributions of Working Group I to the Fourth Assessment Report of the Intergovernmental Panel on Climate Change. Cambridge University Press, Cambridge.

Sonneveld, B.G., Keyzer, M.A., Stroosnijder, L. (2011). Evaluating quantitative and qualitative models: An application for nationwide water erosion assessment in Ethiopia. *Environmental modelling & software*, 26(10), 1161-1170.

Steegen, A., Govers, G., Takken, I., Nachtergaele, J., Merckx, R. (2001). Factors controlling sediment and phosphorus export from two Belgian agricultural catchments. *Journal of Environmental Quality*, 30(4), 1249-1258.

Sultan, D., Tsunekawa, A., Haregeweyn, N., Adgo, E., Tsubo, M., Meshesha, D. T., Ebabu, K. (2017). Analyzing the runoff response to soil and water conservation measures in a tropical humid Ethiopian highland. *Physical Geography*, 38(5), 423-447.

Swarnkar, S., Malini, A., Tripathi, S., Sinha, R. (2018). Assessment of uncertainties in soil erosion and sediment yield estimates at ungauged basins: an application to the Garra River basin, India. *Hydrology and Earth System Sciences*, 22(4), 2471.

Switanek, M.B., Troch, P.A., Castro, C.L., Leuprecht, A., Chang, H.I., Mukherjee, R., Demaria, E.M.C. (2017). Scaled distribution mapping: A bias correction method that preserves raw climate model projected changes. *Hydrology and Earth System Sciences*, 21, 2649–2666.

Syvitski, J.P., Morehead, M.D., Bahr, D.B., Mulder, T. (2000). Estimating fluvial sediment transport: The rating parameters. *Water resources research*, 36(9), 2747-2760.

Tang, L., Yang, D., Hu, H., Gao, B. (2011). Detecting the effect of land-use change on streamflow, sediment and nutrient losses by distributed hydrological simulation. *Journal of Hydrology*, *409*(1-2):172-182.

Taylor, K.E., Stouffer, R.J., Meehl, G.A. (2012). An overview of CMIP5 and the experiment design. *Bulletin of the American Meteorological Society*, 93(4), 485-498.

Tebaldi, C., Hayhoe, K., Arblaster, J.M., Meehl, G.A. (2006). Going to the extremes: An inter-comparison of model-simulated historical and future changes in extreme events. *Climatic Change*, 79, 185–211.

Teferi, E., Bewket, W., Uhlenbrook, S., Wenninger, J. (2013). Understanding recent land use and land cover dynamics in the source region of the Upper Blue Nile, Ethiopia: spatially explicit statistical modeling of systematic transitions. *Agriculture. Ecosystems & Environment*, 165, 98e117.

Tessema, Y.M., Jasińska, J., Yadeta, L.T., Świtoniak, M., Puchałka, R., Gebregeorgis, E.G. (2020). Soil Loss Estimation for Conservation Planning in the Welmel Watershed of the Genale Dawa Basin, Ethiopia. *Agronomy*, 10(6), 777.

Theobald, D.M., Hobbs, N.T. (2002). A framework for evaluating land use planning alternatives: protecting biodiversity on private land. *Conservation Ecology*, 6(1).

Thoeun, H.C. (2015**).** Observed and projected changes in temperature and rainfall in Cambodia. *Weather and Climate Extremes*, 7, 61–71.

Thomson, A., Calvin, K., Smith, S.J., Kyle, P., Volke, A., Patel, P., Delgado, A.S., Bond-Lamberty, B., Wise, M., Clarke, L., Edmonds, J. (2011). RCP4.5: a pathway for stabilization of radiative forcing by 2100. *Climate Change*, 109:77-94.

Tizora, P., Le Roux, A., Mans, G., Cooper, A.K. (2018). Adapting the Dyna-CLUE model for simulating land use and land cover change in the Western Cape Province. *South African Journal of Geomatics*, 7(2), 190-203.

Tomer, M.D., Schilling, K.E. (2009). A simple approach to distinguish land-use and climate-change effects on watershed hydrology. *Journal of Hydrology*, 376, 24–33.

Troeh, F.R., Hobbs, J.A., Donahue, R.L. (2004). Soil and Water Conservation for Productivity and Environmental Proteciton, Helba, S. (Ed.) (4th ed.). New Jersey: Pearson Education.

Tsighe, Z. (1995). The political economy of land degradation in Ethiopia. *Northeast African Studies*, 2(2), 71-98.

Tu, J. (2009). Combined impact of climate and land use changes on streamflow and water quality in eastern Massachusetts, USA. Journal of Hydrology, 379, 268–283.

Unganai, L.S. (1996). Historic and future climatic change in Zimbabwe. *Climate Research* 6:137–145.

Vaché, K.B., Eilers, J.M., Santelmann, M.V. (2002). Water quality modeling of alternative agricultural scenarios in the us corn belt I. *Journal of the American Water Resources Association*, 38(3), 773-787.

Van Griensven, A., Meixner, T. (2006). Methods to quantify and identify the sources of uncertainty for river basin water quality models. *Water Science and Technology*, 53(1), 51-59.

Vanmaercke, M., Zenebe, A., Poesen, J., Nyssen, J., Verstraeten, G., Deckers, J. (2010). Sediment dynamics and the role of flash floods in sediment export from medium-sized catchments: a case study from the semi-arid tropical highlands in northern Ethiopia. *Journal of Soils and Sediments*, 10(4), 611-627.

Van Remortel, R.D., Maichle, R.W., Hickey, R.J. (2004). Computing the LS factor for the Revised Universal Soil Loss Equation through array-based slope processing of digital elevation data using a C++ executable. *Computers & geosciences*, 30(9-10), 1043-1053.

Van Rompaey, A., Bazzoffi, P., Jones, R. J. A., Montanarella, L. (2005). Modeling sediment yields in Italian catchments. G*eomorphology*, 65, 157–169.

Veldkamp, A., Lambin, E.F. (2001). Predicting land-use change. *Agriculture, Ecosystems & Environment*, 85, 1–6.

Veldkamp, A., Fresco, L.O. (1996). CLUE: a conceptual model to study the conversion of land use and its effects. *Ecological Modelling*, 85, 253–270.

Verburg, P.H. (2010). The Clue Modelling Framework. VU Amsterdam, Institute for Environmental Studies. Available: http://www.ivm.vu.nl/en/Images/Exercises_tcm234-284019.pdf (Accessed 23 January 2019).

Verburg, P.H., Overmars, K.P. (2009). Combining top-down and bottom-up dynamics in land use modeling: exploring the future of abandoned farmlands in Europe with the Dyna-CLUE model. *Landscape Ecology*, 24(9), 1167–1181.

Verburg, P.H., Veldkamp, A. (2004). Projecting land use transitions at forest fringes in the Philippines at two spatial scales. *Landscape Ecology*, 19,77–98.

Verburg, P.H., Soepboer, W., Veldkamp, A., Limpiada, R., Espaldon, V., Mastura, S.S. (2002). Modeling the spatial dynamics of regional land use: the CLUE-S model. *Environmental Management*, 30, 391-405.

Verstraeten, G., Poesen, J. (2002). Using sediment deposits in small ponds to quantify sediment yield from small catchments: possibilities and limitations. *Earth Surface Processes and Landforms*, 27(13), 1425-1439.

Visser, H., De Nijs, T. (2006). The map comparison kit. *Environmental Modelling & Software*, 21(3), 346-358.

Vlek, P., Tamene, L., Martius, C., Lamers, J., Drechsel, P., Ziadat, F.M., Le, Q.B., Mirzabaev, A., Nkonya, E.,Lynden, G.V., et al. (2017). Land Degradation and the Sustainable Development Goals: Threats and Potential Remedies; CIAT Publication No. 440; International Center for Tropical Agriculture (CIAT): Nairobi, Kenya.

Volosciuk, C., Maraun, D., Vrac, M., Widmann, M.A. (2017). Combined statistical bias correction and stochastic downscaling method for precipitation. *Hydrology and Earth System Sciences*, 21, 1693–1719.

Wale, A., Rientjes, T.H.M., Gieske, A.S.M., Getachew, H.A. (2009). Ungauged catchment contributions to Lake Tana's water balance. *Hydrological processes: an international journal*, *23*(26), 3682-3693.

Wang, G.Q., Zhang, J.Y., Xuan, Y.Q., Jin, J.L., Bao, Z.X., He, R.M., Liu, C.S., Liu, Y.L., Yan, X.L. (2013). Simulating the impact of climate change on runoff in a typical river catchment of the Loess Plateau, China. Journal of Hydrometeorology,14(5):1553–1561.

Wang, X., Williams, J.R., Gassman, P.W., Baffaut, C., Izaurralde, R.C., Jeong, J., Kiniry, J.R. (2012). EPIC and APEX: Model use, calibration, and validation. *Transactions of the ASABE*, 55(4):1447-1462.

Wear, D.N., Bolstad, P. (1998). Land-use change in southern Appalachian landscape: Spatial analysis and forecast evaluation. Ecosystems, 1, 575-594

Welde, K., Gebremariam, B. (2017). Effect of land use land cover dynamics on hydrological response of watershed: Case study of Tekeze Dam watershed, northern Ethiopia. *International Soil and Water Conservation Research*, *5*(1), 1-16.

Wijesundara, N.C., Abeysingha, N.S., Dissanayake, D.M.S.L.B. (2018). GIS-based soil loss estimation using RUSLE model: A case of Kirindi Oya river basin, Sri Lanka. *Modelling Earth Systems and Environment*, 4(1), 251-262.

Wilby, R.L., Dawson, C.W. (2007). Using SDSM version 4.1 SDSM 4.2; A decision support tool for the assessment of regional climate change impacts. User Manual. Leics: LE11 3TU, UK.

Wilcke, R.A.I., Mendlik, T., Gobiet, A. (2013). Multi-variable error correction of regional climate models. Climatic Change, 120, 871–887.

Williams, J.R., Berndt, H.D. (1977). Sediment yield prediction based on watershed hydrology. *American Society of Agricultural Engineers*, 20, 1100-l 104

Williams, J.R. (1995). The EPIC model. In: Singh, V.P. (Ed.), Computer Models of Watershed Hydrology. Water Resources Publisher, Colorado, pp. 909– 1000.

Williams, J.R. (1980). Spnm, a model for predicting sediment, phosphorus, and nitrogen yields from agricultural basins1. *Journal of the American Water Resources Association*, 16(5), 843-848.

Williams, J.R., Berndt, H.D. (1972). Sediment Yield Computed with Universal Equation. *Journal of Hydraulic Division*, A*SCE*, 98, 2087-2098.

Wischmeier, W.H., Smith, D.D. (1978). Predicting Rainfall Erosion Losses: A Guide to Conservation Planning. In: Series: Agriculture Handbook. USDA, Washington DC.

WMO (2016) GREENHOUSE GAS BULLETIN: The State of Greenhouse Gases in the Atmosphere Based on Global Observations through 2015: No. 12, WMO, SSN 2078-0796.

Wolancho, K.W. (2012). Watershed management: An option to sustain dam and reservoir function in Ethiopia. *Journal of Environmental Science and Technology*, 5(5), 262-273.

World Commission on Dams (WCD). (2000). Dams and development: A new framework for decision-making: The report of the world commission on dams. Earth scan.

Worqlul, A.W., Dile, Y.T., Ayana, E.K., Jeong, J., Adem, A.A., Gerik, T. (2018). Impact of climate change on streamflow hydrology in headwater catchments of the Upper Blue Nile Basin, Ethiopia. *Water*, 10(2), 120.

Yang, W., Andréasson, J., Graham, L.P., Olsson, J., Rosberg, J., Wetterhall, F. **(2010)** Distribution-based scaling to improve usability of regional climate model projections for hydrological climate change impacts studies. *Hydrology Research*, 41(3-4), 211–229.

Yang, C.T., Randle, T.J., Daraio, J. (2006). Erosion and reservoir sedimentation. In Erosion and sedimentation manual. U.S. Department of the Interior. Sedimentation and River Hydraulics Group, Denver, Colorado

Yang, D., Kanae, S., Oki, T., Koike, T., Musiake, K. (2003). Global potential soil erosion with reference to land use and climate changes. *Hydrological Processes*, 17, 2913–2928.

Yoder, D.C., Foster, G.R., Weesies, G.A., Renard, K.G., McCool, D.K., Lown, J.B. (2004). Evaluation of the RUSLE Soil Erosion Model. In: Thomas, D.L, Huffman, R.L. (eds) Agricultural non-point water quality models: Their use and application. University of Tennessee Agricultural Experiment Station: Southern Cooperative Series Bulletin, USA, pp 107–116.

Young, R.A., Onstad, C.A., Bosch, D.D., Anderson, W.P. (1989). AGNPS: A nonpoint-source pollution model for evaluating agricultural watersheds. *Journal of soil and water conservation*, 44(2), 168-173.

Zerihun, M., Mohammedyasin, M.S., Sewnet, D., Adem, A.A., Lakew, M. (2018). Assessment of soil erosion using RUSLE, GIS and remote sensing in NW Ethiopia. *Geoderma regional*, 12, 83 90.

Zhang, X.C. (2007). A comparison of explicit and implicit spatial downscaling of GCM output for soil erosion and crop production assessments. *Climate Change*, 84, 337–363.

Zhang, X.C., Nearing, M.A. (2005). Impact of climate change on soil erosion, runoff and wheat productivity in central Oklahoma. *Catena*, 61, 185–195.

Publications

Research articles published from this thesis work:

1. Ayalew, L. T., & Bharti, R. (2020). Modelling sediment yield of Rib watershed, Northwest Ethiopia. *ISH Journal of Hydraulic Engineering*, 1-12. https://doi.org/10.1080/09715010.2020.1797544
2. Tsegaye, L., & Bharti, R. (2021). Soil erosion and sediment yield assessment using RUSLE and GIS-based approach in Anjeb watershed, Northwest Ethiopia. SN Applied Sciences, 1-19. https://doi.org/10.1007/s42452-021-04564-x

Appendix

Appendix A: Appendix of Tables

The GCPs were collected from the field and accuracy assessments were conducted on classified images using the confusion or error matrix and the producer and user accuracy per category of LULCs is presented.

Appendix Table 1 Error matrix of Rib LULC classified images

		Reference 1984									
	1984	0	1	2	3	4	5	6	7	Row total	User accuracy
Classified 1984	0	145	---	1	---	3	---	1	---	150	96.7
	1	---	94	1	10		1	---	---	106	88.7
	2	4	7	66	2	2	---	---	---	81	81.5
	3	2	8	---	55	---	1	---	---	66	83.3
	4	11	1	6	---	33		---	---	51	64.7
	5	---	---	---	2	---	11	---	---	13	84.6
	6	1	---	---	---	---	---	7	---	8	87.5
	7	1	---	---	---	---	---	---	7	8	87.5
	Column total	164	110	74	69	38	13	8	7	483	
	Producer accuracy	88.4	85.5	89.2	79.7	86.8	84.6	87.5	100.0		
		Reference 2003									
		0	1	2	3	4	5	6	7	Row total	User accuracy
Classified 2003	0	105	---	6	3	10	1	1	1	127	82.7
	1	5	112	---	6	---	4	---	---	127	88.2
	2	6	5	66	---	5	---	---	---	82	80.5
	3	---	7	---	74	---	2	---	---	83	89.2
	4	7	---	5	---	89	---	1	---	102	87.3
	5	---	4	---	2	---	33	---	---	39	84.6
	6	1	---	---	---	---	---	10	---	11	90.9
	7	1	---	---	---	---	---	---	10	11	90.9
	Column total	125	128	77	85	104	40	12	11	582	
	Producer accuracy	84	87.5	85.7	87.1	85.6	82.5	83.3	90.9		
		Referenced 2016									
		0	1	2	3	4	5	6	7	Row total	User accuracy
Classified 2016	0	150	---	2	---	11	---	1	2	166	90.4
	1	---	76	1	4	1	3	---	---	85	89.4
	2	4	---	74	---	3	---	---	---	81	91.4
	3	1	5	---	36	---	3	---	---	45	80.0
	4	5	---	2	---	62	---	---	---	69	89.9
	5	---	1	---	1	---	23	---	---	25	92.0
	6	---	---	---	---	---	---	19	---	19	100.0
	7	1	---	---	---	---	---	---	9	10	90.0
	Column total	161	82	79	41	77	29	20	11	500	
	Producer accuracy	93.2	92.7	93.7	87.8	80.5	79.3	95.0	81.8		

Appendix Table 2 Error matrix of Gumara LULC classified images

		Referenced 1984									
		0	1	2	3	4	5	6	7	Row total	User accuracy
Classified 1984	0	129	3	---	---	16	---	1	2	151	0.85
	1	---	83	10	3	---	1	---	---	97	0.86
	2	4	2	63	---	4	---	---	---	73	0.86
	3	---	9	1	40	---	2	---	---	52	0.77
	4	17	---	---	---	102	---	---	---	119	0.86
	5	---	3	---	7	---	18	---	---	28	0.64
	6	---	---	---	---	---	---	9	---	9	1.00
	7	1	---	---	---	---	---	---	17	18	0.94
	Column total	151	100	74	50	122	21	10	19	547	
	Producer accuracy	0.85	0.83	0.85	0.80	0.84	0.86	0.90	0.89		
		Referenced 2003									
		0	1	2	3	4	5	6	7	Row total	User accuracy
Classified 2003	0	131	---	---	---	12	---	2	1	146.0	0.90
	1	1	71	6	4	1	2	---	---	85.0	0.84
	2	5	---	44	---	6	1	---	---	56.0	0.79
	3	1	10	2	29	---	---	---	---	42.0	0.69
	4	16	---	1	---	90	---	---	3	110.0	0.82
	5	---	4	---	2	---	21	---	---	27.0	0.78
	6	---	---	---	---	---	---	15	---	15.0	1.00
	7	2	---	---	---	---	---	------	22	24.0	0.92
	Column total	156	85	53	35	109	24	17	26	505	
	Producer accuracy	0.84	0.84	0.83	0.83	0.83	0.88	0.88	0.85		
		Referenced 2016									
		0	1	2	3	4	5	6	7	Row total	User accuracy
Classified 2016	0	154	2	1	---	7	---	---	---	164	0.94
	1	2	80	2	3	---	3	---	---	90	0.89
	2	4	3	67	---	5	---	---	---	79	0.85
	3	---	3	---	35	---	2	---	---	40	0.88
	4	10	1	3		88		1	1	104	0.85
	5	---	1	---	1	---	33	---	---	35	0.94
	6	1	---	---	---	---	---	18	---	19	0.95
	7	1	---	---	---	2	---	---	19	22	0.86
	Column total	172	90	73	39	102	38	19	20	553	
	Producer accuracy	0.90	0.89	0.92	0.90	0.86	0.87	0.95	0.95		

0, intensively cultivated; 1, shrub land; 2, grassland; 3, mixed forest; 4, moderately cultivated; 5, plantation; 6, urban and 7, waterbody

Appendix B: Appendix of figures

The LULC conversion of an area is initiated by driving factors or factors of change. In this study the dominant factors were identified and their grids of coverage were prepared using GIS analysis.

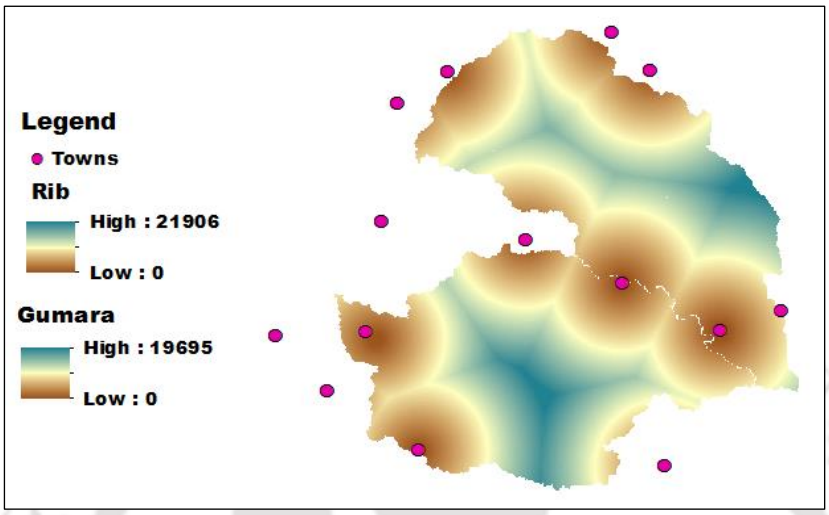

Appendix Figure 1 Distance from towns

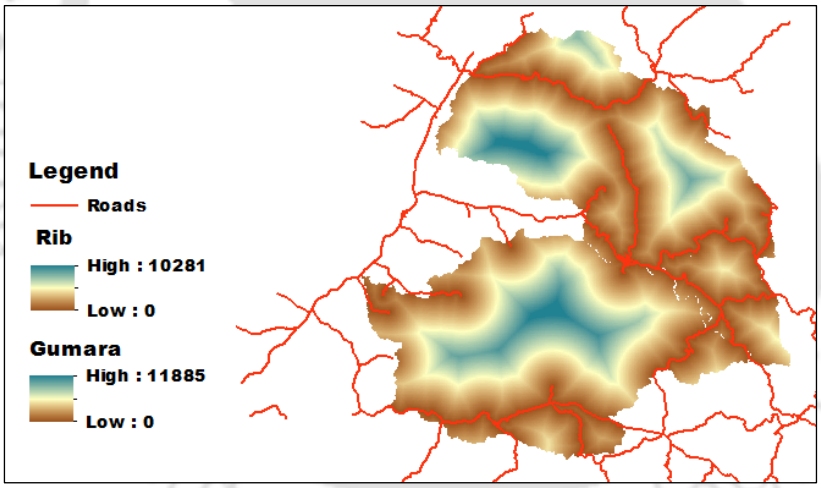

Appendix Figure 2 Distance from roads

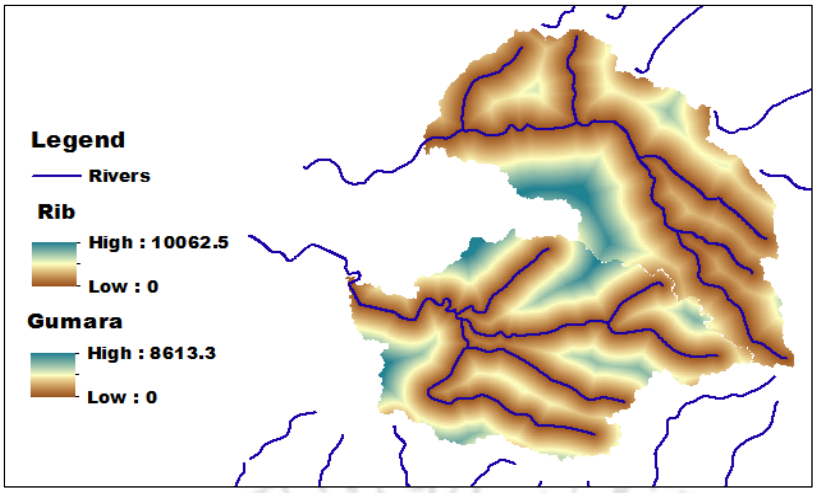

Appendix Figure 3 Distance from rivers (waterbody)

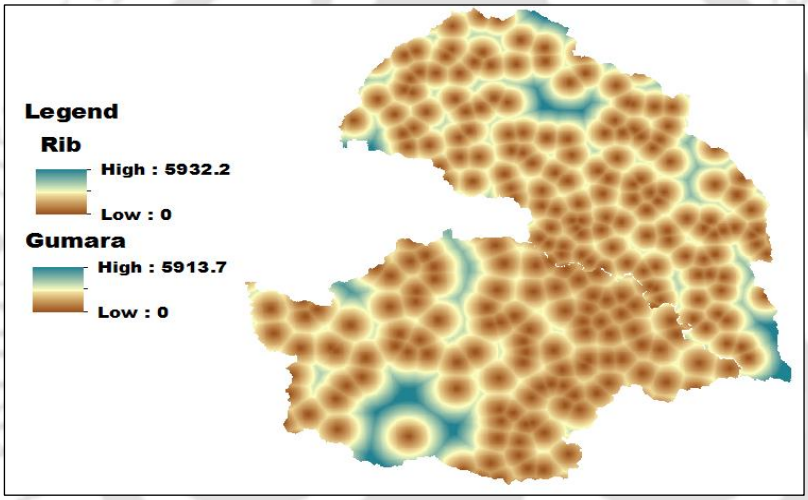

Appendix Figure 4 Distance from Churches

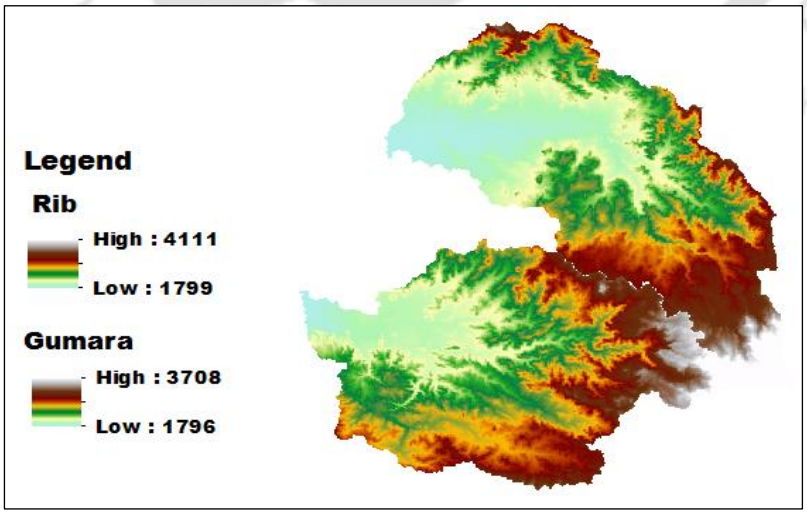

Appendix Figure 5 Elevation

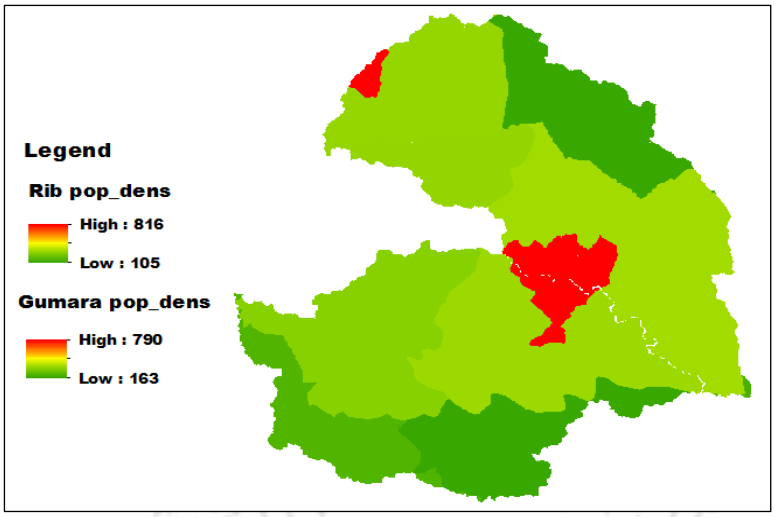

Appendix Figure 6 Population density

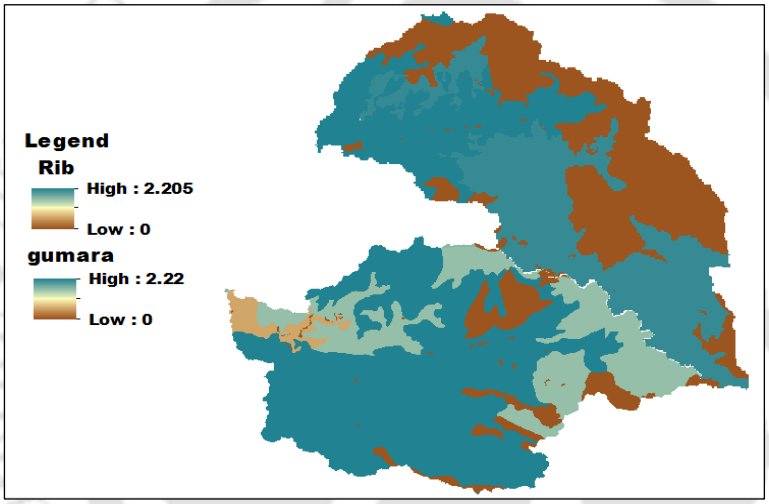

Appendix Figure 7 soil organic matter

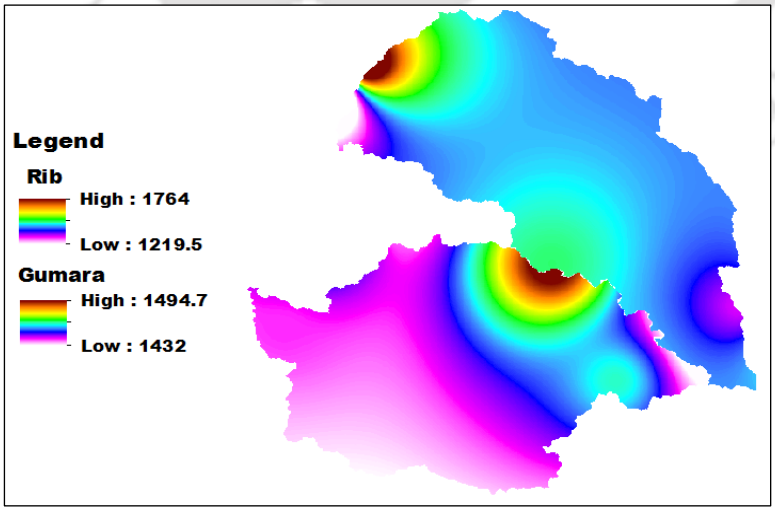

Appendix Figure 8 Rainfall distribution

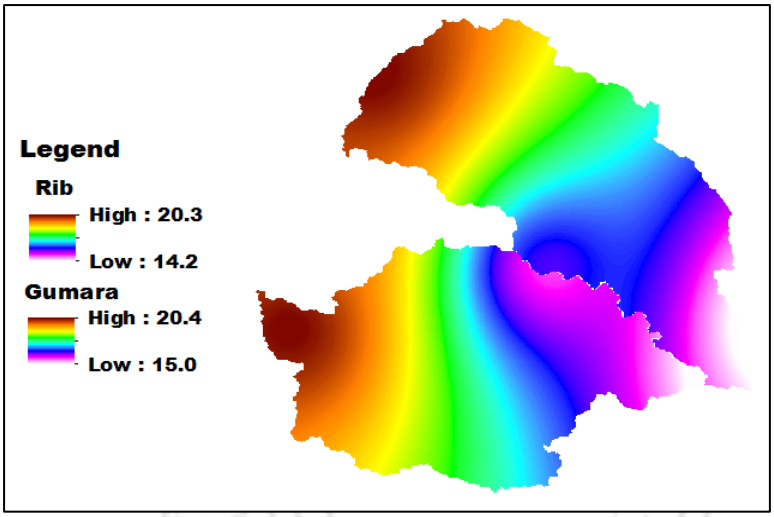

Appendix Figure 9 Temperature distribution

The driving factors determine the suitability of a grid cell for a specific land-use which could be analyzed by the binary logit model. The validity of the model in assigning a grid cell for a land-use has been checked by the receiver operating characteristics (ROC) curve.

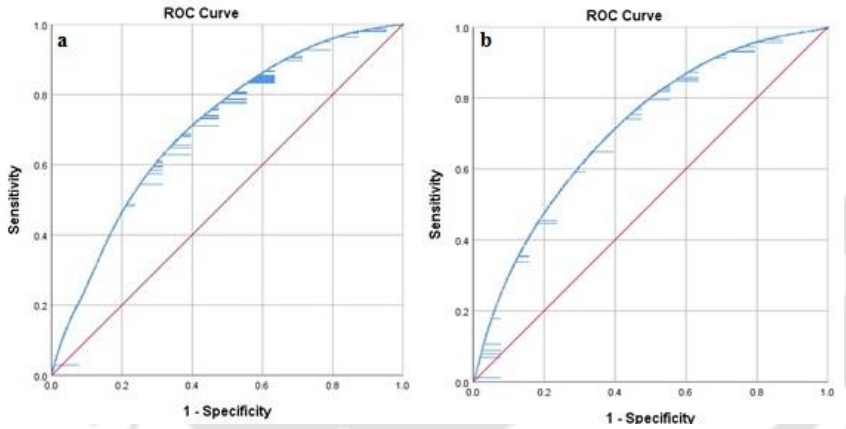

Appendix Figure 10 ROC curve of intensively cultivated land (a) Rib and (b) Gumara

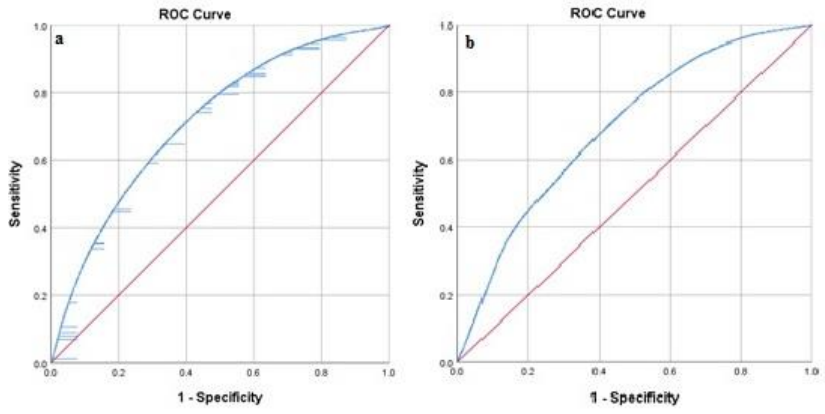

Appendix Figure 11 ROC curve of shrubland (a) Rib and (b) Gumara

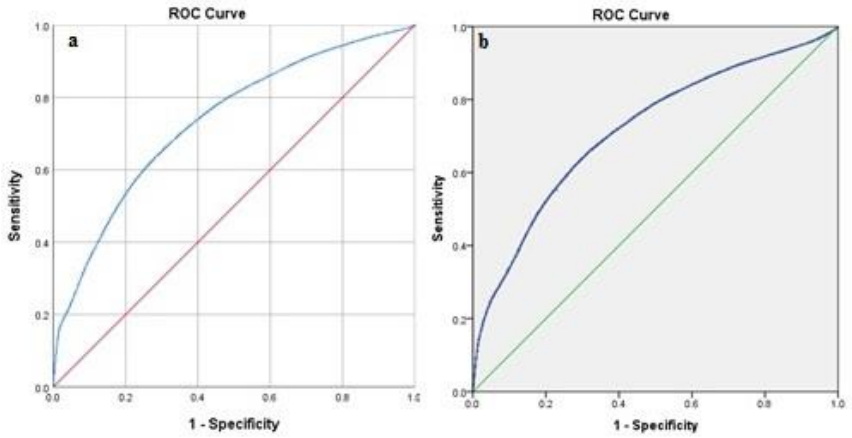

Appendix Figure 12 ROC curve of Grassland (a) Rib and (b) Gumara

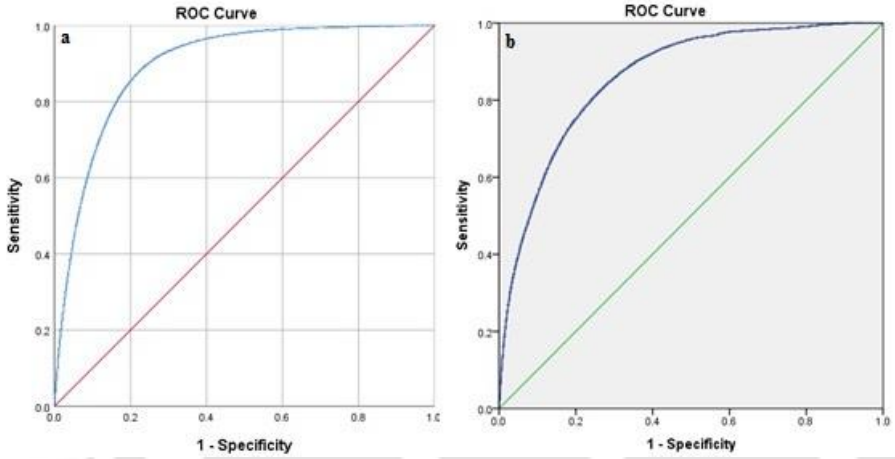

Appendix Figure 13 ROC curve of mixed forest (a) Rib and (b) Gumara

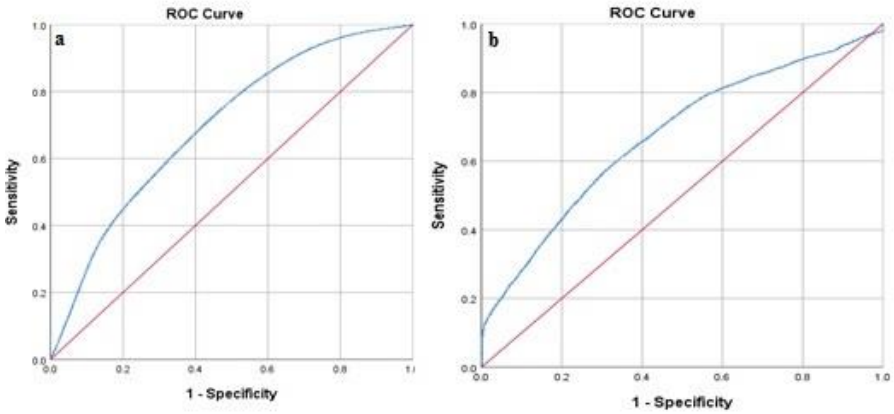

Appendix Figure 14 ROC curve of moderately cultivated (a) Rib and (b) Gumara

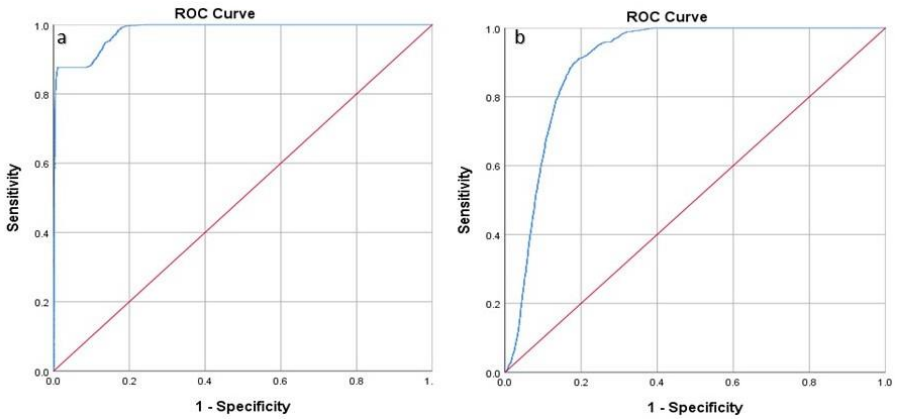

Appendix Figure 15 ROC curve of plantation (a) Rib and (b) Gumara

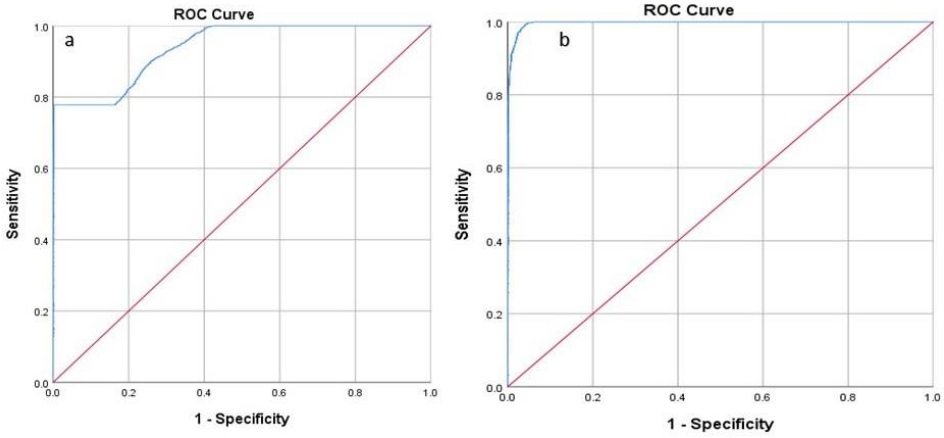

Appendix Figure 16 ROC curve of Urban (a) Rib and (b) Gumara

Homogeneity of the long-term annual rainfall of the meteorological stations was tested with Rainbow software with significance levels of 0.1, 0.05 and 0.01alpha levels.

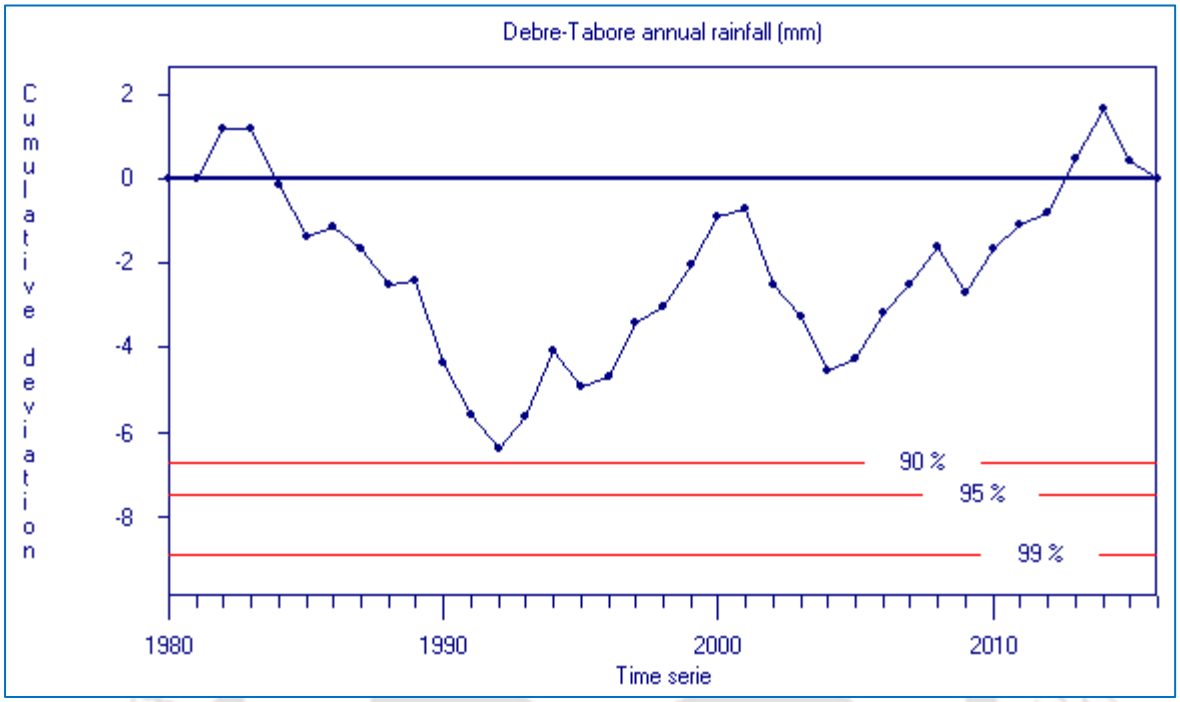

Appendix Figure 17 Homogeneity test of the annual rainfall of Deberetabore station (homogeneous)

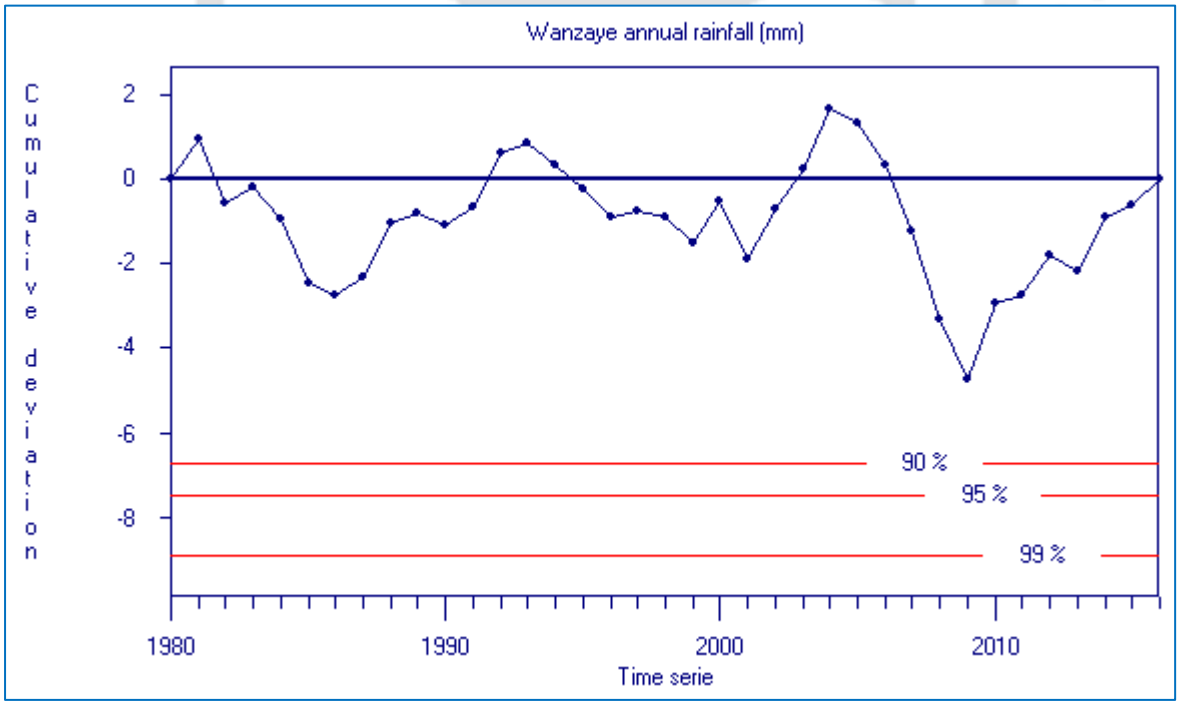

Appendix Figure 18 Homogeneity test of the annual rainfall of Wanzaye station (homogeneous)

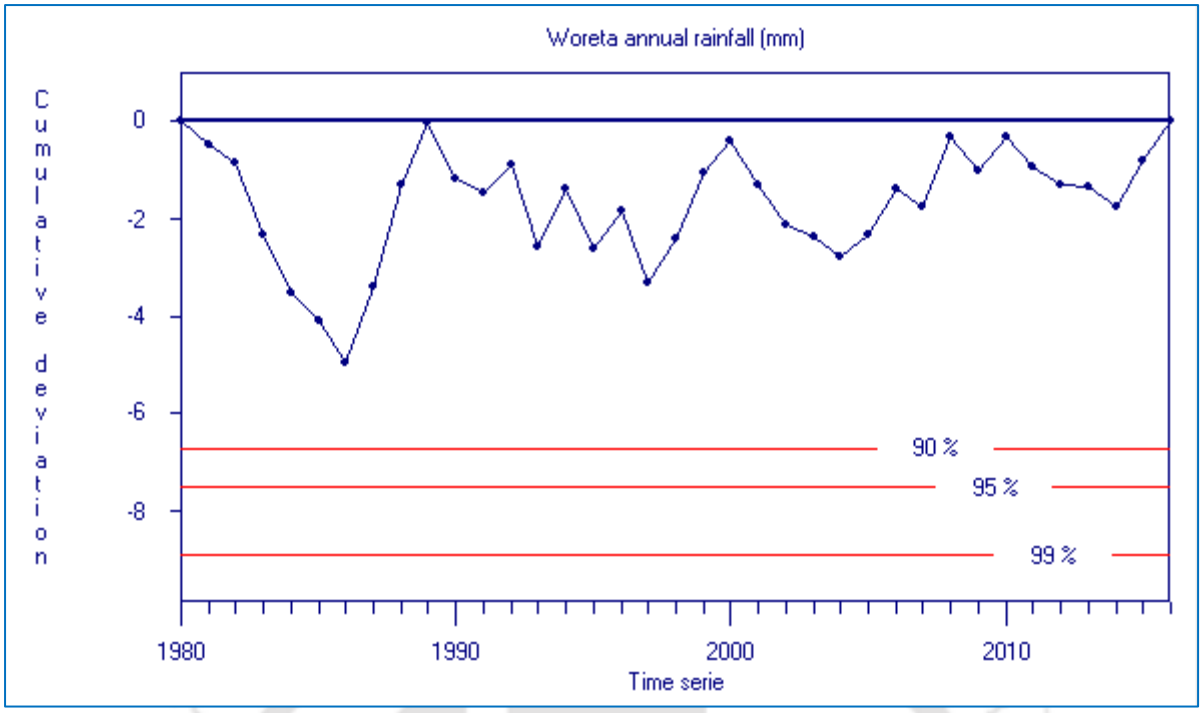

Appendix Figure 19 Homogeneity test of the annual rainfall of Woreta station (homogeneous)

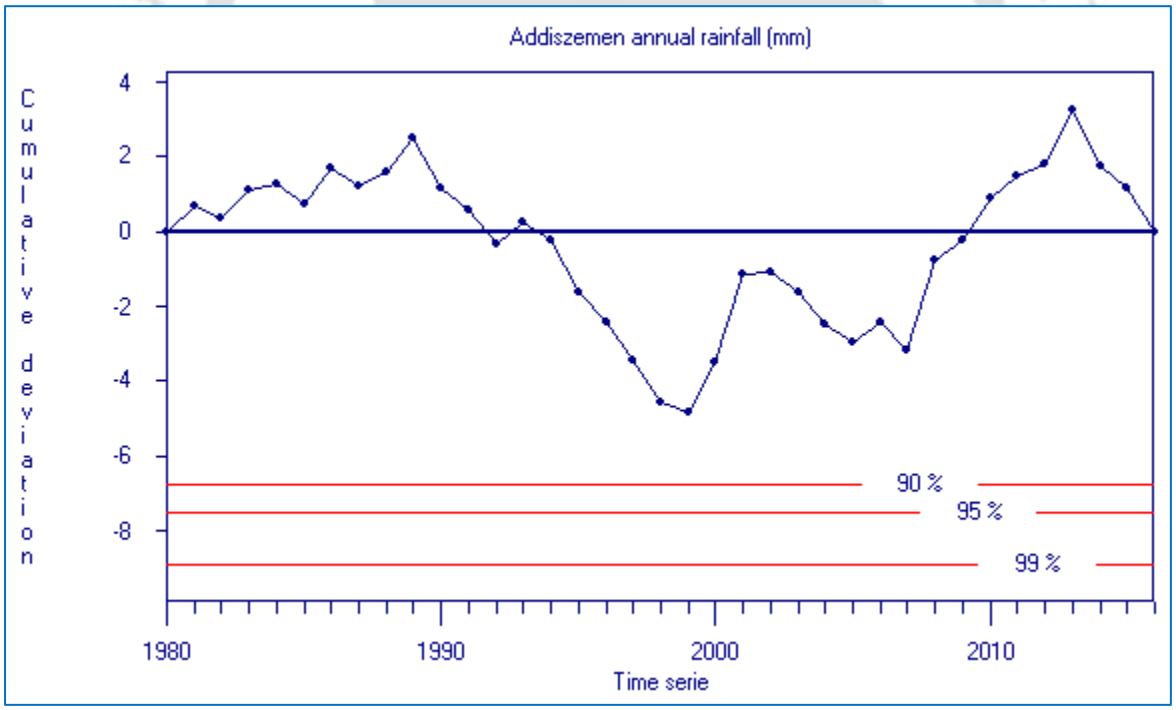

Appendix Figure 20 Homogeneity test of the annual rainfall of Addiszemen station (homogeneous)

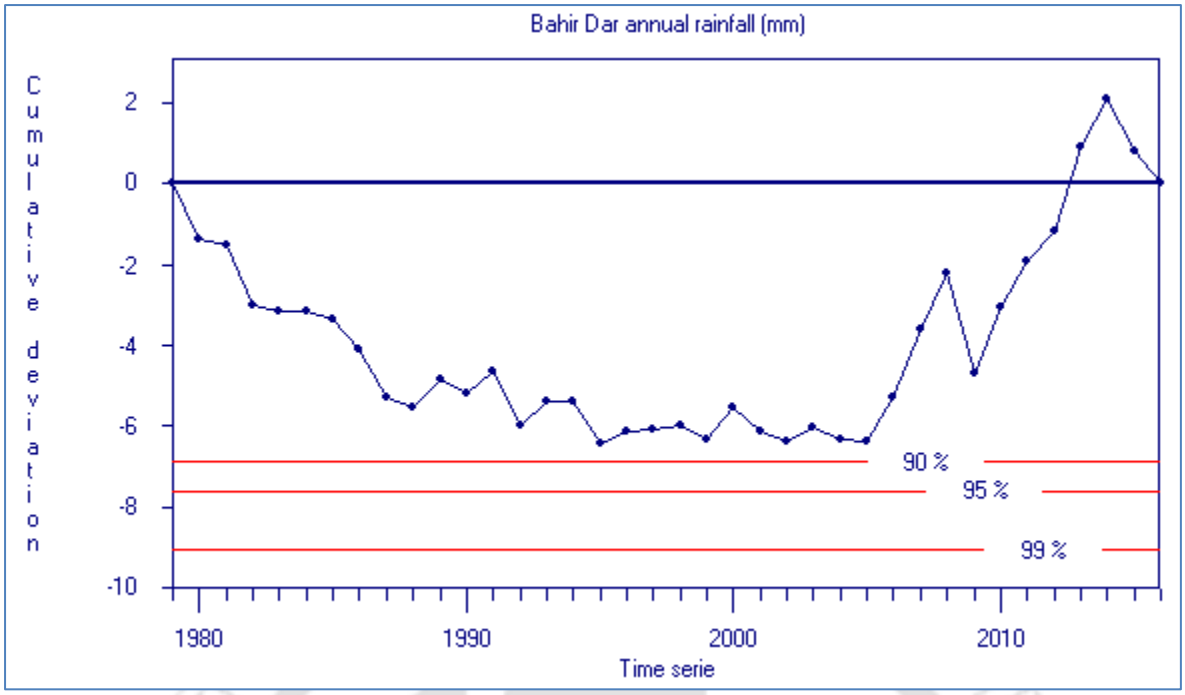

Appendix Figure 21 Homogeneity test of the annual rainfall of Bahir Dar station (homogeneous)

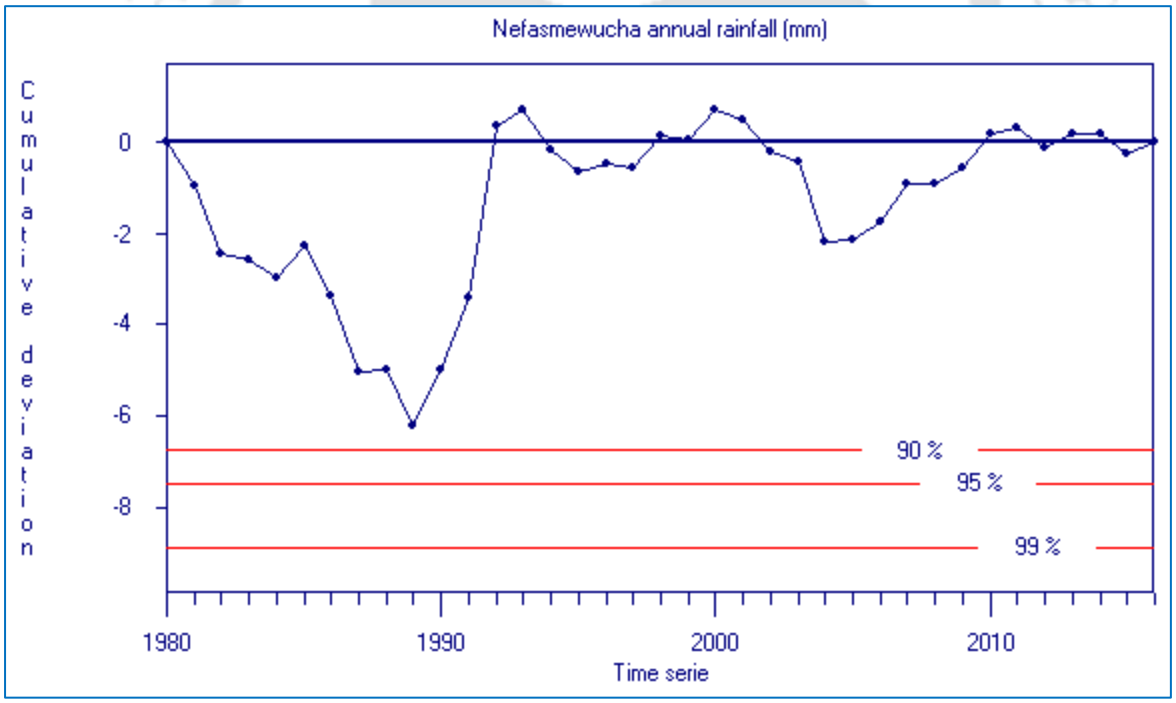

Appendix Figure 22 Homogeneity test of the annual rainfall of Nefasmewucha station (homogeneous)

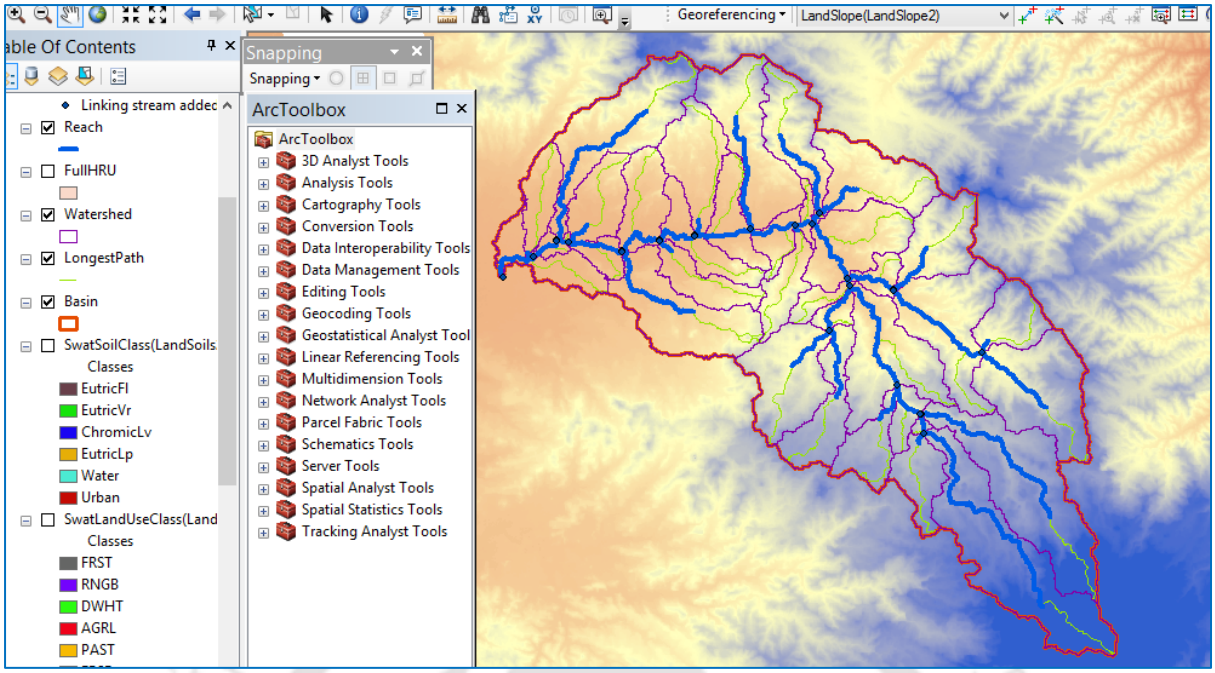

Appendix Figure 23 The illustration of the ArcSWAT model, Rib watershed

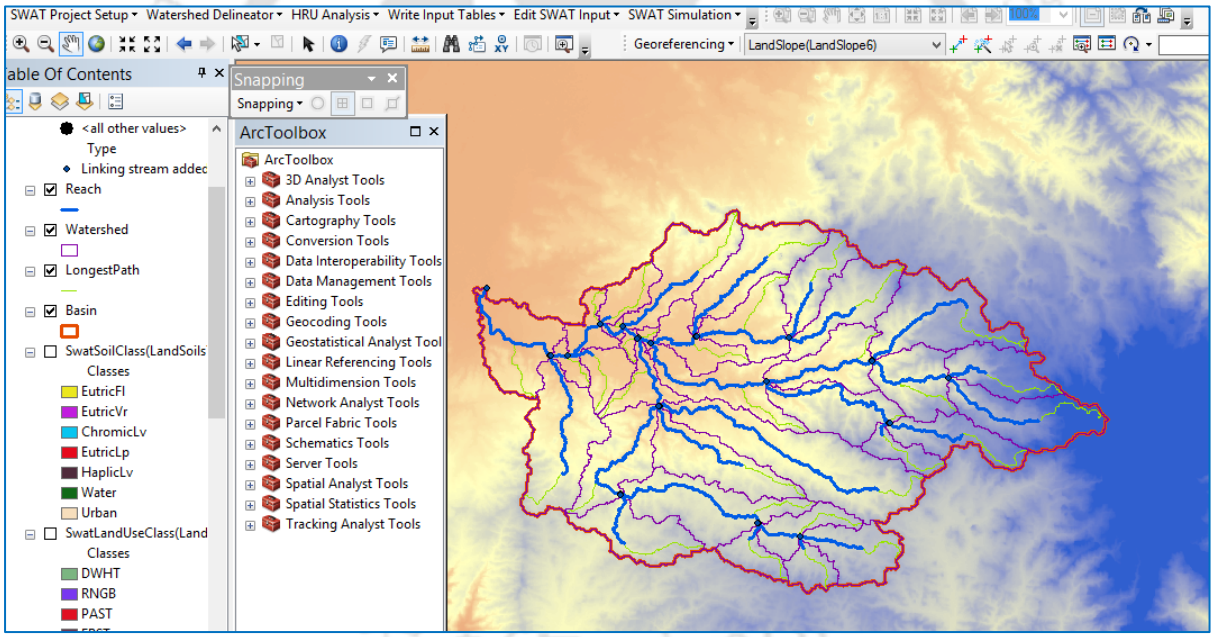

Appendix Figure 24 The illustration the ArcSWAT model, Gumara watershed

Appendix C: Appendix of photographs

Photographs taken from the study area during field observations were presented as the following

Appendix Figure 25 Section of Rib River at its lower course

Appendix Figure 26 Section of Gumara River at its lower course

Appendix Figure 27 A section of Anjeb watershed (a) and a large gulley (b)